

# **Design, Assembly and Triggering of Interlocked DNA Nanoarchitectures**

**DISSERTATION**

zur Erlangung des Doktorgrades (Dr. rer. nat.)  
der Mathematisch-Naturwissenschaftlichen Fakultät der Rheinischen  
Friedrich-Wilhelms-Universität Bonn

vorgelegt von  
**Dipl.-Chem. Finn Lohmann**  
aus Zweibrücken

**Bonn 2015**

Angefertigt mit der Genehmigung der Mathematisch-Naturwissenschaftlichen Fakultät  
der Rheinischen Friedrich-Wilhelms-Universität Bonn.

1. Gutachter: Prof. Dr. M. Famulok
2. Gutachter: Prof. Dr. G. Mayer

Tag der Promotion: 01.09.2015

Erscheinungsjahr: 2015

Die vorliegende Arbeit wurde am LIMES-Institut der Rheinischen Friedrich-Wilhelms-Universität Bonn in der Zeit von November 2010 bis 2015 unter der Leitung von Prof. Dr. Michael Famulok angefertigt.

Teile der vorliegenden Arbeit wurden vorab veröffentlicht:

- [i] **Lohmann, F.; Ackermann, D.; Famulok, M. Reversible light switch for macrocycle mobility in a DNA rotaxane. *J. Am. Chem. Soc.* 2012, 134, 11884-11887.**
- [ii] **Lohmann, F.; Valero, J.; Famulok, M. A novel family of structurally stable double stranded DNA catenanes. *Chem. Commun.* 2014, 50, 6091-6093.**
- [iii] **Lohmann, F.; Weigandt, J.; Valero, J.; Famulok, M. Logic gating by macrocycle displacement using a double-stranded DNA [3]rotaxane shuttle. *Angew. Chem. Int. Ed.* 2014, 53, 10372-10376.**
- [iiii] **Li, T.; Lohmann, F.; Famulok, M. Interlocked DNA nanostructures controlled by a reversible logic circuit. *Nat. Commun.* 2014, 5, 4940.**





<b>1</b>	<b>Abstract</b> .....	<b>1</b>
<b>2</b>	<b>Introduction</b> .....	<b>3</b>
<b>2.1</b>	<b>DNA Nanotechnology</b> .....	<b>3</b>
<b>2.2</b>	<b>Deoxyribonucleic Acid (DNA)</b> .....	<b>4</b>
2.2.1	Structure of DNA.....	4
2.2.2	Secondary Structures of DNA .....	7
2.2.3	Enzymatic DNA Synthesis .....	9
2.2.4	Solid Phase DNA Synthesis .....	10
2.2.5	Modifications of DNA.....	13
2.2.6	Switching Mechanisms of DNA Hybridization .....	19
<b>2.3</b>	<b>Structural DNA Nanotechnology</b> .....	<b>21</b>
<b>2.4</b>	<b>Dynamic DNA Nanotechnology</b> .....	<b>25</b>
<b>2.5</b>	<b>DNA Computing</b> .....	<b>27</b>
<b>2.6</b>	<b>Interlocked Molecules</b> .....	<b>31</b>
2.6.1	Molecular Catenanes .....	32
2.6.2	Molecular Rotaxanes .....	33
2.6.3	Rotaxane Based Molecular Devices.....	34
<b>2.7</b>	<b>Interlocked Assemblies Based on DNA</b> .....	<b>37</b>
<b>3</b>	<b>Aims of this Project</b> .....	<b>41</b>
<b>4</b>	<b>Results</b> .....	<b>45</b>
<b>4.1</b>	<b>Switching of Macrocycle Mobility in an Interlocked DNA Architecture</b> .....	<b>45</b>
4.1.1	Assembly and Characterization of DNA Rotaxanes for Switching Applications	45
4.1.2	Toe-hold Switch.....	50
4.1.3	pH Switch .....	54
4.1.4	Light switch.....	57
<b>4.2</b>	<b>A Molecular Shuttle Based on a ds DNA Rotaxane</b> .....	<b>68</b>
4.2.1	Assembly and Characterization of a non-Symmetric Shuttle System Containing one Ring- and one Spherical-stopper.....	69
4.2.2	Light Induced Translocation of a Shuttle-ring in a ds DNA Rotaxane.....	72
4.2.3	Toe-hold Induced Translocation of a Shuttle-ring in a ds DNA Rotaxane Containing one Ring- and one Origami-stopper.....	74
<b>4.3</b>	<b>Cascade Release Reaction in a [3]Pseudorotaxane Performing Logic AND Operation</b> .....	<b>81</b>
4.3.1	Assembly and Characterization of a [3]Pseudorotaxane .....	81

4.3.2	Input Dependent Cascade Release Reaction in a [3]Pseudorotaxane Performing AND Logic Operation.....	85
<b>4.4</b>	<b>Design, Assembly, Characterization and Triggering of ds DNA Catenanes.....</b>	<b>92</b>
4.4.1	Design, Assembly and Characterization of ds DNA Catenanes .....	92
4.4.2	Triggering of ds DNA Catenanes.....	99
4.4.3	A [3]Catenane as Framework for a Controllable DNAzyme.....	101
<b>5</b>	<b>Discussion and Outlook .....</b>	<b>104</b>
<b>6</b>	<b>Materials and Methods.....</b>	<b>109</b>
<b>6.1</b>	<b>Materials and Reagents .....</b>	<b>109</b>
<b>6.2</b>	<b>Buffer Systems .....</b>	<b>109</b>
<b>6.3</b>	<b>Equipment.....</b>	<b>110</b>
<b>6.4</b>	<b>Methods.....</b>	<b>111</b>
6.4.1	UV Absorption Spectroscopy .....	111
6.4.2	Absorption Spectroscopy of <i>cis/trans</i> -DMAB5-RO.....	112
6.4.3	Absorption Spectroscopy of AB and DMAB Modified DNA after Thermally Induced <i>cis to trans</i> Isomerization.....	112
6.4.4	DNA Melting Experiment.....	112
<b>6.5</b>	<b>Gel Electrophoresis .....</b>	<b>113</b>
6.5.1	Native Polyacrylamide Gel Electrophoresis (PAGE) .....	113
6.5.2	Agarose Gel Electrophoresis .....	113
<b>6.6</b>	<b>High Performance Liquid Chromatography (HPLC).....</b>	<b>114</b>
6.6.1	Reverse Phase HPLC.....	114
6.6.2	Weak Anion Exchange HPLC.....	114
<b>6.7</b>	<b>Fluorescence Measurements.....</b>	<b>114</b>
6.7.1	Fluorescence Quenching Experiments .....	114
6.7.2	Fluorescence Polarization (FP) Experiments .....	115
<b>6.8</b>	<b>Atomic Force Microscopy (AFM) .....</b>	<b>115</b>
6.8.1	Intermittent Contact Mode (AC Mode) .....	115
6.8.2	Contact Mode in Liquid (Hyperdrive™ Mode) .....	115
<b>6.9</b>	<b>Photo Induced Isomerization of AB and DMAB.....</b>	<b>116</b>
<b>6.10</b>	<b>Synthesis of AB and DMAB Phosphoramidite .....</b>	<b>116</b>
6.10.1	Synthesis of Ethyl-4-nitrosobenzoate .....	117
6.10.2	Synthesis of Ethyl-2',6'-dimethylazobenzene-4-carboxylate .....	118
6.10.3	Synthesis of 4-Carboxy-2',6'-dimethylazobenzene.....	118
6.10.4	Synthesis of 4-Carboxy-2',6'-dimethylazobenzene-D-threoninol.....	119



6.10.5	Synthesis of DMT Protected 4-Carboxy-2',6'-dimethylazobenzene-D-threoninol.....	120
6.10.6	Synthesis of DMT Protected 4-Carboxy-2',6'-dimethylazobenzene-D-threoninol-phosphoramidite.....	121
<b>6.11</b>	<b>Synthesis of AB and DMAB Modified ODNs .....</b>	<b>122</b>
<b>6.12</b>	<b>Assembly of DNA Nanostructures .....</b>	<b>122</b>
6.12.1	Assembly of Macrocycles and Ring Stoppers .....	123
6.12.2	Assembly of Spherical Stopper .....	123
6.12.3	Assembly of Origami Stopper.....	123
6.12.4	Assembly of [2]Rotaxane .....	124
6.12.5	Assembly of [3]Pseudorotaxane .....	125
6.12.6	Assembly of [2]Catenane .....	125
6.12.7	Assembly of [3]Pseudocatenane.....	126
<b>6.13</b>	<b>Switching of Macrocycle Mobility.....</b>	<b>126</b>
6.13.1	Toe-hold Mechanism .....	126
6.13.2	pH Induced Mechanism .....	127
6.13.3	Light Switching Mechanism.....	127
<b>6.14</b>	<b>Translocation of a Shuttle-ring.....</b>	<b>129</b>
6.14.1	Light Induced Translocation.....	129
6.14.2	Toe-hold Mechanism Induced Translocation.....	129
<b>6.15</b>	<b>Input Dependent Cascade Release Reaction in a [3]Pseudorotaxane .....</b>	<b>130</b>
<b>6.16</b>	<b>Pseudocatenane to Catenane Conversion .....</b>	<b>131</b>
<b>6.17</b>	<b>AFM Study with [3]Pseudocatenane, [3]Catenane and the Tetracyclic Structure .....</b>	<b>132</b>
<b>6.18</b>	<b>Three-Dimensional Models .....</b>	<b>132</b>
<b>7</b>	<b>Appendix.....</b>	<b>133</b>
7.1	List of Abbreviations .....	133
7.2	Supplementary Data .....	135
7.3	NMR Spectra .....	144
7.4	Tables.....	151
7.5	Acknowledgements.....	160
7.6	<i>Curriculum Vitae</i> Finn Lohmann.....	161
<b>8</b>	<b>Literature.....</b>	<b>162</b>



## 1 Abstract (English)

Interlocked molecular systems are well known in supramolecular chemistry and are widely used for various applications like sensors, molecular machines and logic gates. However, these systems present some drawbacks, as the synthesis is demanding and their handling in aqueous media and biocompatibility is rather problematic.

Due to Watson Crick base pairing rules, DNA is an optimal material for the self-assembly of highly ordered and complex nanoarchitectures. Furthermore, it is synthetically accessible, relatively stable, water-soluble and shows good biocompatibility.

Therefore, the study of novel DNA based interlocked systems is of interest for nanotechnology. Indeed, a DNA rotaxane reported by Famulok *et al.* gained great attention and the threading principle described in that work was used for the assembly of various interlocked DNA architectures.

In the present study, DNA rotaxanes were modified in order to precisely control and switch on and off the molecular motion of its mechanically trapped components. Such switching was utilized to create a molecular shuttle in which a macrocycle is translocated along an axle from one station towards another in a controlled fashion.

Another aim of this research was to design and assemble entirely new DNA based interlocked systems suitable for the introduction of diverse functions. In this context, a [3]pseudorotaxane was assembled and fully characterized by means of gel electrophoresis and Atomic Force Microscopy. Indeed, by introducing different triggers into this system, a logic AND gate could be created. Apart from the rotaxane structures, also novel catenane structures could be assembled and properly characterized, which were then used for several applications, such as the construction of complex logic gates or catalytic activity control in a DNAzyme based system.

The presented DNA based systems proved to be optimal frameworks for the introduction of highly controllable functionality and pave the way in order to build dynamic nanostructures and complex nanomachinery.

---

## Abstrakt (Deutsch)

Ineinander verzahnte Systeme sind in der supramolekularen Chemie gut bekannt und finden in verschiedenen Bereichen Anwendung, z.B. als Sensoren, als molekulare Maschinen und als Logikgatter. Allerdings weisen diese Systeme Nachteile auf, da die Synthese anspruchsvoll ist und die Handhabung in wässrigem Medium sowie die Biokompatibilität problematisch sind.

Dank der Watson Crick Regeln zur Basenpaarung ist DNA ein optimales Substrat für die Selbstassemblierung komplexer Nanoarchitekturen. Des Weiteren ist DNA synthetisch zugänglich, relativ stabil, wasserlöslich und sie weist eine hohe Biokompatibilität auf.

Daher ist die Erforschung DNA basierter, ineinander verzahnter Systeme von Interesse für die Nanotechnologie. In der Tat hat ein von Famulok *et al.* vorgestelltes DNA Rotaxan große Beachtung gefunden und das beschriebene *Threading*-Prinzip wurde für die Assemblierung verschiedener ineinander verzahnter DNA Architekturen verwendet.

In der vorliegenden Studie wurden DNA Rotaxane so modifiziert, dass eine präzise Kontrolle des Ein- und Ausschaltens der mechanisch verknüpften Komponenten möglich wurde. Diese Schaltung wurde genutzt, um ein molekulares Shuttle zu konstruieren, in welchem ein *Macrocycle* entlang einer Achse von einer Station zu einer anderen transloziert werden kann. Ein weiteres Ziel dieser Arbeit war das Design und die Assemblierung eines neuartigen, DNA basierten und ineinander verzahnten Systems, welches einfach funktionalisiert werden kann. In diesem Zusammenhang wurde ein [3]Pseudorotaxan assembliert und mittels Rasterkraftmikroskopie und Gel Elektrophorese charakterisiert. Durch die Einführung verschiedener Schaltungen konnte so ein UND-Gatter erschaffen werden. Zusätzlich zu den Rotaxan Strukturen wurden neuartige Catenan Strukturen assembliert und charakterisiert. Diese Strukturen fanden verschiedene Anwendungen, wie die Konstruktion von Logikgattern oder die Steuerung katalytischer Aktivität in einem DNAzyme basierten System.

Die präsentierten DNA basierten Systeme haben sich als ideale Gerüste für die Etablierung von kontrollierbarer Funktionalität erwiesen und ebnen den Weg für die Konstruktion von komplexen dynamischen Nanomaschinen.

## 2 Introduction

### 2.1 DNA Nanotechnology

With the sentence “There’s Plenty of Room at the Bottom”, R. P. Feynman introduced nanotechnology to the audience of the annual meeting of the American Physical Society in 1959,<sup>1</sup> and indeed, in the last decades, nanotechnology has found application in many areas such as computing, electronics, material science, cosmetics and medicine.

Nanotechnology is a scientific field covering materials and objects with dimensions smaller than 100 nm. This scale is colloquially called nanometer scale. Different from other materials, the physical and chemical properties like electric conductivity, magnetism and optic properties are not only based on the chemical composition but mainly on the size of such nanoparticles.<sup>2</sup>

There are two well-established methods in order to fabricate nanoparticles and manipulate these objects, the top-down and the bottom-up method. The top-down method is used more widely. The approach here is the deconstruction or miniaturization of larger structures into their smaller composite parts. The bottom-up method is a relatively new approach, in which the construction of nanostructures is performed by the assembly or self-assembly of their atoms or molecular components.<sup>3</sup> The bottom-up method offers the possibility to design nanostructures in a highly controlled and programmable fashion.

Building blocks suitable for the construction of nanostructures *via* the bottom-up method need to fulfill specific requirements. They have to self-assemble into bigger aggregates and the aggregation has to be controllable in order to program the features of the product. The accessibility of the substrates and the stability of the nanoassemblies are desirable, too. Deoxyribonucleic acid (DNA) fulfills all those requirements. The Watson-Crick base pairing rules allow predicting the formation of a DNA duplex out of the single-stranded (ss) oligodeoxynucleotides (ODNs).<sup>4</sup> Such DNA duplex can be equipped with sticky-ends, ss DNA overhangs, enabling the assembly with

---

complementary DNA fragments and thereby forming more complex structures. The sequences of the ODNs are crucial when designing DNA nanoassemblies. Certainly, the use of automated solid phase DNA synthesis paves the way to plan and synthesize any desired DNA sequence. Again, by taking advantage of the base pairing rules, different switching mechanism can be introduced into DNA nanostructures, which provide the possibility to implement function into such assemblies (see chapter 2.2.6). Furthermore, DNA is a relatively stable material, soluble in water and a great number of chemical modifications can be easily introduced, thus increasing the inherent complexity and properties of this molecule. In summary, DNA can be seen as a molecular analogue to children's building block such as Lego® or Duplo®.<sup>5</sup>

## **2.2 Deoxyribonucleic Acid (DNA)**

DNA is the carrier of genetic information of all living organisms on earth. The ability of DNA to self-replicate, mutate and encode information was crucial for the evolution and thereby the biodiversity. The discovery of the structure of DNA by Watson and Crick through x-ray analysis<sup>4</sup> and the determination of the DNA sequence of organism (e.g. Human Genome Project) were key steps for the understanding of life on a molecular level. Nevertheless, as mentioned above, the exceptional characteristics of the macromolecule DNA qualifies it as ideal building block for the bottom-up synthesis of nanostructures.

### **2.2.1 Structure of DNA**

DNA is an oligomeric macromolecule consisting of nucleotides. Nucleotides themselves are composed of the sugar deoxyribose, which is linked to a nucleobase at the 1'-position and to a phosphate. In the oligomeric form, the nucleotides are connected to each other *via* phosphodiester bonds between the 3'- and 5'-position of the deoxyribose. DNA can be composed by four different nucleobases, the pyrimidine derivatives thymine (T) and cytosine (C) and the purine derivatives adenine (A) and guanine (G). The generic structure of a nucleotide and a 4mer ODN displaying the four different nucleobases are shown in Figure 2.1.

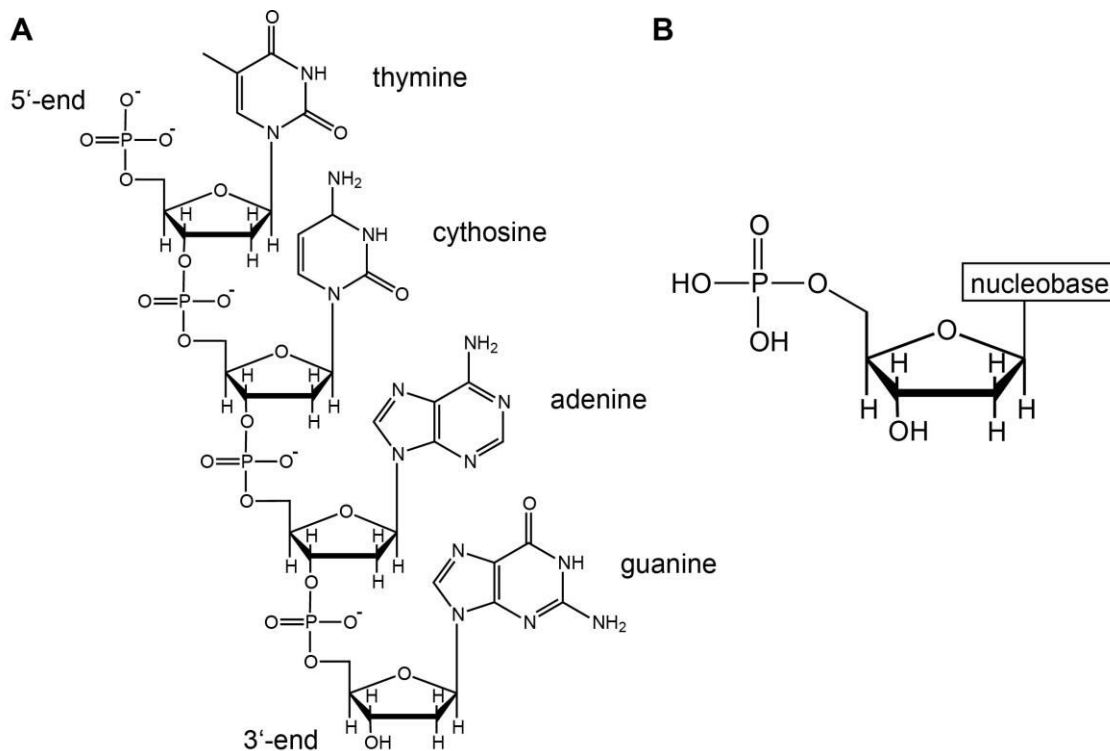


**Figure 2.1.** A) Chemical structure of a 4mer ODN containing the four different nucleobases T, C, A, and G. The 5'-end is phosphorylated. B) Generic structure of a single nucleotide.

Rules for the composition of DNA regarding the four different nucleobases (Chargaff's rules) reveal that the content of T is always equal to the content of A and the same for G and C.<sup>6</sup> This regularity could be explained when the structure of DNA was enlightened by x-ray analysis.<sup>4</sup> It was found that A and T as well as G and C form base pairs (bp) in a DNA duplex, which are promoted by hydrogen bonds through the amino group and the free electron pair of the carbonyl oxygen or the endocyclic amino group of the nucleobases. The chemical structures of the AT and GC base pairs given in Figure 2.2 elucidate how the hydrogen bonds are formed and that the AT pair is stabilized by two and the GC pair by three hydrogen bonds, which increases the stability of the latter. The specific base pairing leads to the hybridization of two complementary DNA strands to the antiparallel double stranded (ds) DNA duplex, as DNA is usually present in living cells.

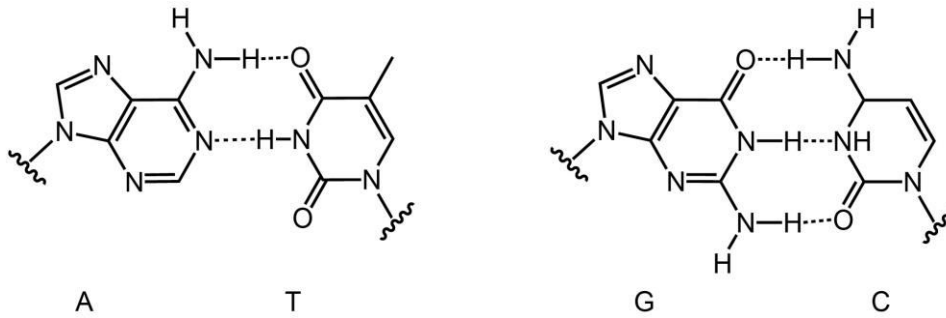


**Figure 2.2. Watson Crick base pairing.** The chemical structures of AT and GC base pairs displaying two and three hydrogen bonds respectively (dotted lines) are shown.

The helical DNA duplex (see Figure 2.3.A) presents unique geometrical and spatial characteristics, which are summarized in the table of Figure 2.3.B. The ds form of DNA is not only stabilized by the base pairing, but also by  $\pi$ -stacking, mediated through the planar and aromatic nucleobases, arranged parallel in the duplex and a hydrophobic effect, which makes the polar parts of the molecule (i.e. phosphodiester groups and the sugar bases) being exposed to the water, whereas the nucleobases are shielded within the duplex structure.

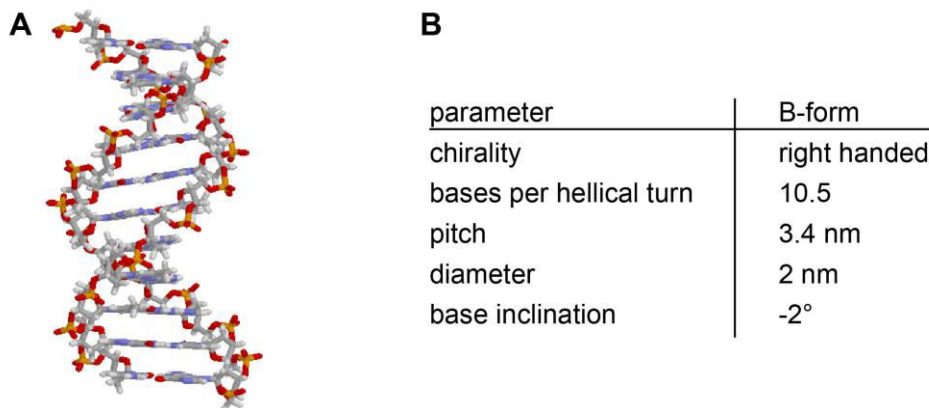


**Figure 2.3. A) Three-dimensional model of a B-form DNA duplex. B) Table summarizing the properties of the B-form DNA duplex.**

A DNA duplex can exist in different conformations; the B-form, as shown in Figure 2.3.A, is most commonly found in nature; the other forms are the A- and the Z-form. They differ in the direction of rotation, diameter, twist, pitch and ascent per base among others.



## 2.2.2 Secondary Structures of DNA

The base pairing in a DNA strand cannot only lead to the intermolecular formation of a duplex out of two strands (see Figure 2.4.A), but also an intramolecular duplex formation within one DNA strand is possible. The simplest secondary structure that a DNA strand can adopt is the so-called hairpin motif. Such motif consists of a stem region build from the complementary ends of a DNA sequence and a randomized sequence in between. The secondary structure of a stable hairpin is shown in Figure 2.4.B. DNA strands can also hybridize in a way that junctions are introduced into a DNA duplex (see Figure 2.4.C,D). Such a 4-way junction (called Holliday junction) was firstly reported by R. Holliday in 1964.<sup>7-8</sup> Since this junction contains sequence symmetry, the branching point can move in this junction. N. Seeman achieved the design of a stable 4-way junction showing no branch migration by using non-symmetric sequences (other than in the previously described Holliday junctions), also 3-way junctions can be designed this way.<sup>9-10</sup> The presented motifs can be utilized to build up higher order two- and three-dimensional architectures (see chapter 2.3).

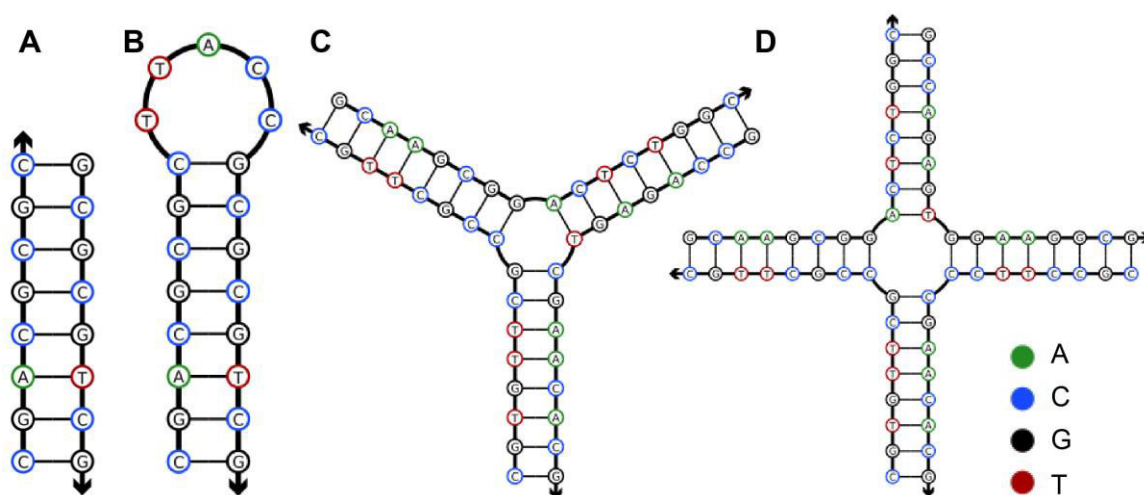


Figure 2.4. Secondary structures of A) a DNA duplex formed out of two separate ODNs, B) a DNA hairpin, C) a stable 3-way junction and D) a stable 4-way junction. The arrow indicates the 3'-end of the ODNs. The images were made with the open access DNA analysis program available on [www.nupak.org](http://www.nupak.org).<sup>9,11</sup>

A DNA duplex containing a randomized sequence is in principle a linear molecule, but the low rigidity of the macromolecule leads to a bending of the duplex. The degree of rigidity can be defined with the persistent length of the DNA that describes the length in

---

which the direction of the duplex axle correlates with the direction of the axle at the starting point.<sup>12</sup> Distinct sequences lead to an increase or decrease in rigidity,<sup>13</sup> or in some cases to a curvature of the duplex. The latter case was found for DNA sequences containing an A<sub>4-6</sub>-tract per helical turn (e.g. N<sub>5</sub>A<sub>5</sub>N<sub>5</sub>A<sub>6</sub>, N = randomized nucleobases). In an NMR study, a 12mer (GGCAAAAACGG/CCGTTTTTTGCC) DNA duplex containing one A<sub>6</sub>-tract has an overall axle bending of 19° and the bending provides an increased rigidity of the duplex.<sup>14</sup> The computational model of the DNA duplex calculated from NMR data given in Figure 2.5 shows such DNA duplex with the curvature of the axle indicated.



**Figure 2.5. Three-dimensional model of a DNA duplex containing an A<sub>6</sub>-tract. The grey line in the center of the duplex indicates the curvature. The third A of the A<sub>6</sub>-tract is highlighted in red. The image was taken and slightly modified from reference <sup>14</sup>.**

Under slightly acidic pH (4-6), protonated cytosines (C<sup>+</sup>) form base pairs with cytosines, which leads in sequences containing diverse C-tracts (stretches of two, three, or more cytosine in a row) to the formation of a four stranded structure other than the presented double stranded duplex.<sup>15</sup> The C<sup>+</sup>C base pair is stabilized by hydrogen bonds between two amino groups with the carbonyl oxygen and between the protonated and unprotonated endocyclic amino groups (see Figure 2.6.A). The C<sup>+</sup>C base pairs of the two duplexes are stacked in a zipper-like conformation in order to form the quadruplex structure (see Figure 2.6). Such quadruplex structures are called i-motif structures and the formation can occur either intramolecular but also intermolecularly between two three or four individual strands. Due to its pH sensitivity, the i-motif structure has been widely used to trigger dynamic processes in DNA devices (see chapter 2.2.6.2).

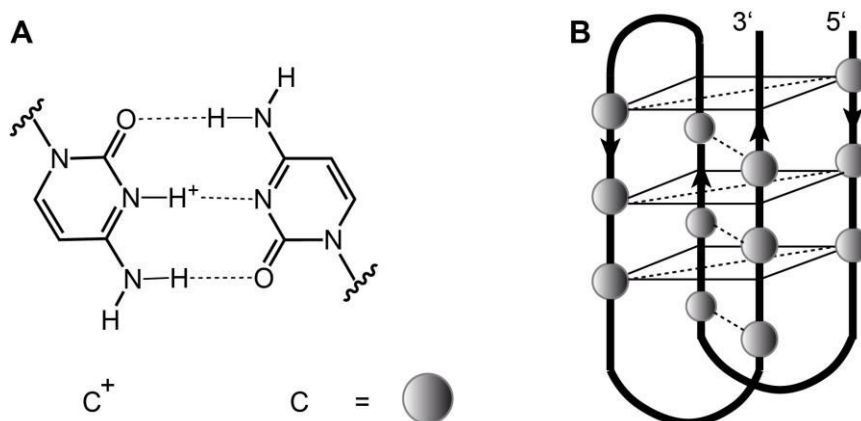


**Figure 2.6. A) Chemical structure of a C<sup>+</sup>C base pair. B) Secondary structure of an unimolecular i-motif quadruplex structure. The C<sup>+</sup>C base pairs are indicated with dotted lines.**

Similar to the i-motif, a quadruplex structure can be formed by G-rich DNA strands. These so-called G-quadruplex structures consist of potassium stabilized G<sub>4</sub>-tetrads held together *via* hydrogen bonds. These tetrads are orientated in parallel and thereby stabilize the four-stranded structure through stacking effects.

### 2.2.3 Enzymatic DNA Synthesis

Nucleic acids in nature are synthesized by the enzymes DNA- and RNA-polymerase. The precursors are always the nucleotide triphosphates; polymerases require a template strand in order to synthesize the complementary strand. The synthesis follows from the 5'- to the 3'-end. The covalent connection between two DNA fragments is performed by ligase enzymes. The ligation can occur by connecting blunt-ends or *via* sticky-end ligation (see Figure 2.7).

While the DNA used in this study was exclusively synthesized chemically (see 2.2.4) without the use of enzymes, DNA ligase was utilized to covalently join different DNA fragments.

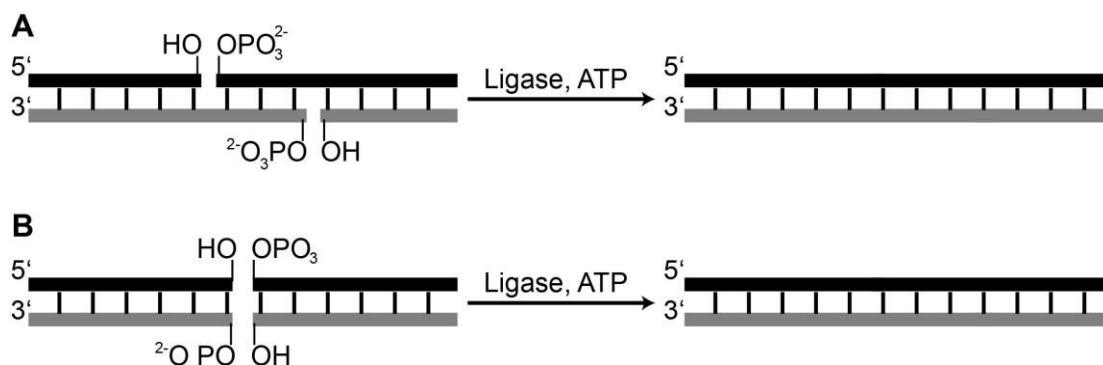


**Figure 2.7.** A) Scheme of the sticky-end mediated ligation. Note that 5'-ends are phosphorylated for successful ligation. B) Scheme of the blunt-end ligation.

### 2.2.4 Solid Phase DNA Synthesis

The first artificial dinucleotide was reported in 1955, using the phosphotriester method<sup>16</sup>. Performing the synthesis on solid phase prevents time- and yield-costly purification steps. The optimization of reaction conditions and the development of new activators and protecting groups improved the synthesis furthermore. Finally, by the invention of phosphoramidite building blocks, a highly efficient synthesis was developed. The phosphoramidite method<sup>17</sup> combined with solid phase synthesis enables the fabrication of ODNs with length up to 200 bases. The yield of each coupling step reaches up to 99.5 %.

The solid support, located in a column, usually consists of Controlled Pore Glass (CPG) and is linked to the 3'-terminal nucleotide. The 5'-hydroxyl group of the immobilized nucleotide as well as the 5'-hydroxyl group of the phosphoramidite building block is protected with the acid-labile dimethoxytrityl group (DMT) (temporary protecting group). Moreover, the exocyclic amino groups of the phosphoramidites have to be protected in order to prevent undesired side reactions. Therefore, the adenosine phosphoramidite is protected with benzoyl-, the guanine phosphoramidite with dimethylformamidino- and the cytosine phosphoramidite with an acetyl-protecting group (permanent protecting groups). Since thymine has no amino groups, no protecting group is required. Another difference of a phosphoramidite in comparison with a nucleotide is the activated phosphorous. The trivalent phosphorous is activated with an amidite group and the remaining free oxygen is protected with a cyanoethyl protecting

group. The chemical structure of a phosphoramidite and the four protected nucleobases are shown in Figure 2.8.

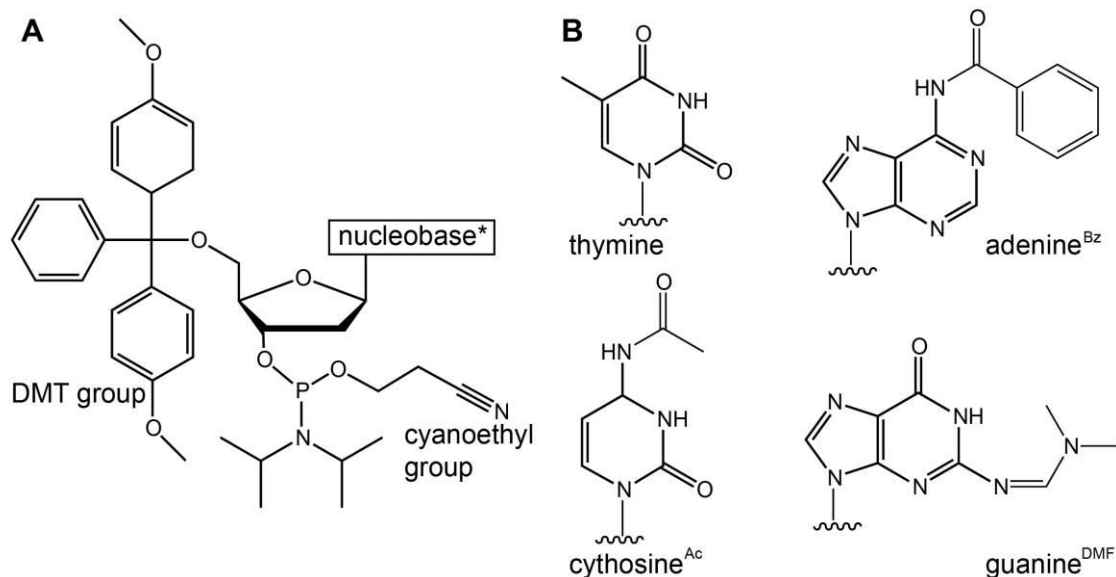


**Figure 2.8.** A) Generic structure of a nucleoside phosphoramidite with a dimethoxytrityl protecting group at the 5'-position and a cyanoethyl protecting group at the phosphite moiety. The attached nucleobases carry protecting groups as well (except for thymine, see Figure 2.8.B). B) Chemical structures of the protected nucleobases of the four deoxynucleosides (Bz = benzoyl-, Ac = acetyl- and DMF = dimethylformamidino-protecting group).

The synthesis is a completely automatized process; only the cleavage from the solid support and the deprotection of the functional groups is performed manually. The synthesis cycle is depicted in Figure 2.9.

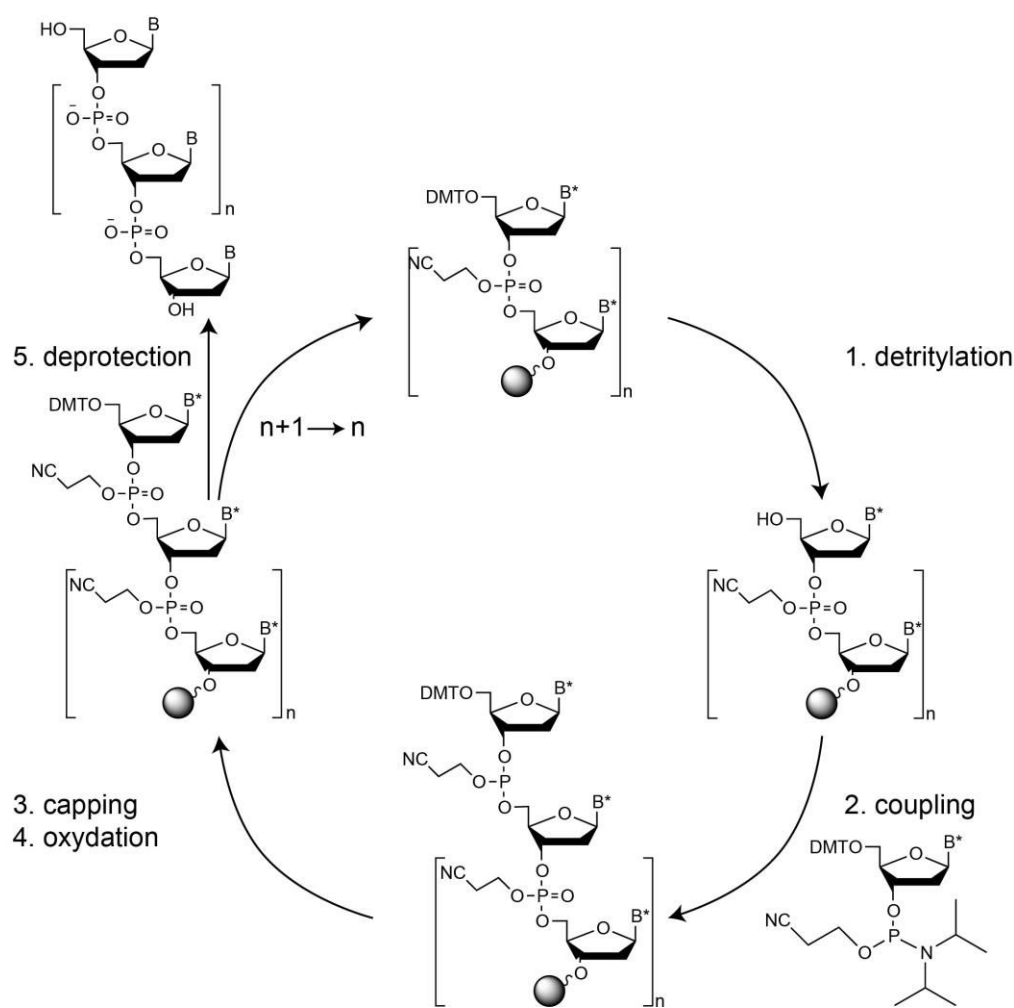


**Figure 2.9. Synthesis cycle for the DNA synthesis using the phosphoramidite method. All cycle steps 1-4. are indicated together with the final deprotection step. B\*/B = protected/unprotected base or T, respectively.**

Starting from the immobilized DMT protected nucleotide; the acid-labile DMT-group is removed by dichloroacetic acid (detritylation). In the next step, a phosphoramidite building block is added and activated with 5-thioethyl-1-H-tetrazol resulting in the tetrazolide. The coupling takes place with the 5'-hydroxyl group of the immobilized nucleotide under formation of phosphite triester (coupling). All unreacted hydroxyl groups are made to react with acetic anhydride in order to prevent them from further undesired reactions (capping). In the last step of the cycle, the phosphite triester is oxidized into the phosphate triester with an iodine/water/pyridine solution. Following, the cycle starts with the next round by alternate detritylation. When the synthesis is finished, the product can be cleaved from the solid support by ammonolysis. This also

removes all permanent protecting groups as well as the cyanoethyl group. The product is usually purified *via* High Performance Liquid Chromatography (HPLC), using reverse phase or ion exchange columns. The characterization is made by mass spectrometry.

### **2.2.5 Modifications of DNA**

DNA is used in biology, chemistry and related fields for a broad variety of applications, e.g. in polymerase chain reaction (PCR) in the forensic DNA analysis, in genetic studies, as specific binder (aptamers) or in the DNA nanotechnology. Especially in the latter two cases, chemical modification of the DNA increase the scope of the applications.

DNA contains diverse functional groups and can thereby easily be modified at different positions with a broad variety of active groups and molecules. Especially by using solid phase DNA synthesis, it is possible to first synthesize a customized phosphoramidite which then can be introduced into the desired DNA strand.

#### **2.2.5.1 Fluorophore- and Quencher-Modifications**

Fluorophores are molecules, which absorb light of a specific wavelength and after a short period of time emit light at a higher wavelength. Quenchers are molecules capable to absorb light of a specific wavelength without further emission of light. In the latter case, the photonic energy is transformed into thermal energy. The chemical structures and the emission and absorption spectra of a typical fluorophore/quencher pair (cyanine 3 (Cy3) and black hole quencher 2 (BHQ-2)), which is used in DNA nanotechnology, are given in Figure 2.10.

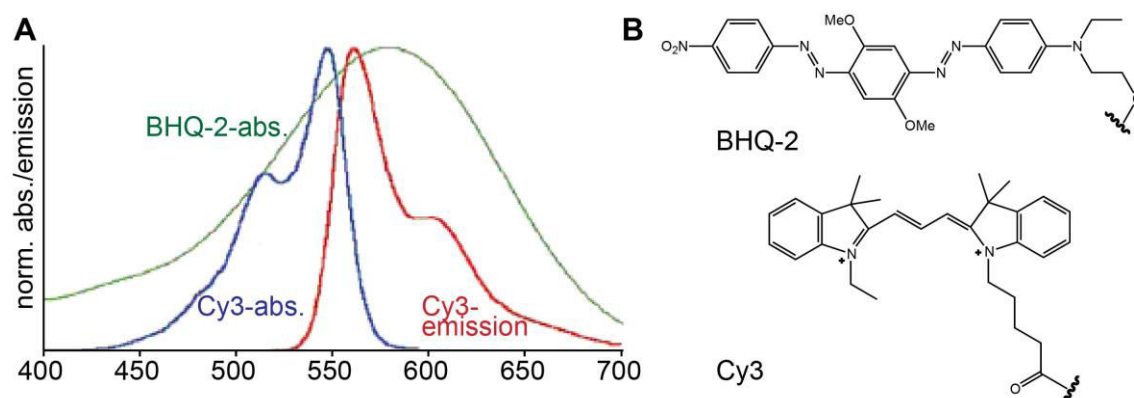


**Figure 2.10.** A) Absorption spectra of the quencher BHQ-2 and absorption/emission spectra of the fluorophore Cy3. Since BHQ-2 absorbs at the emission wavelength of Cy3, both together represent a fluorophore/quencher pair. B) Chemical structure of BHQ-2 and Cy3.

When a fluorophore is located in close proximity (up to 10 nm) to the corresponding quencher (absorbing light in the emission wavelength of the fluorophore), the fluorescence emission after the corresponding excitation of the fluorophore is reduced (fluorescence quenching, FQ). When a second fluorophore (absorbing in the emission wavelength of the first fluorophore) replaces the quencher, this one is excited by the first fluorophore. The fluorescence emission is then shifted towards a higher wavelength. This energy transfer is named Förster Resonance Energy Transfer (FRET).<sup>18</sup> Attachment of a fluorophore at the 5'-end of an ODN and the corresponding quencher at the 3'-end of a complementary ODN makes it possible to detect whether the ODNs are hybridized or not. The labeling of an ODN capable to form a hairpin structure (see Figure 2.4.B) with a fluorophore/quencher pair at the ends of this ODN makes it possible to detect whether the hairpin exists in its closed or open form. This feature is widely used for different applications, e.g. for the detection of transcription product, through the opening of a hairpin by hybridization with the transcribed ribonucleic acid (RNA). Thus, the transcription can be followed in real time by measuring the increase in fluorescence.

### 2.2.5.2 Azobenzene Modifications

One important goal in DNA nanotechnology is the implementation of mechanical motion into DNA assemblies. One widely used method to trigger DNA is by on- and off switching of the hybridization of complementary DNA strands. This can be achieved by the



external delivery of inputs, e.g. fuel DNA (see chapter 2.2.6.1) through strand displacement mechanisms, but also irradiation with light at specific wavelength can lead to the hybridization/dehybridization of a modified DNA duplex. One approach utilizes caged thymidine moieties introduced into an ODN. The cage modification consists of a 2-nitrophenylethyl group attached to the exocyclic oxygen (O4-position) of the thymine. The cage inhibits the hybridization of the modified ODN with its complementary ODN and furthermore the cage can be removed by UV irradiation. Taking advantage of this feature, it was possible to synthesis an inactive thrombin aptamer that could be activated simply by irradiation with UV light.<sup>19-21</sup> A disadvantage of this approach is the irreversibility of the process. Asanuma *et al.* overcame this problem by introducing azobenzene moieties into DNA strands and thereby achieved a reversible switching mechanism.<sup>22</sup>

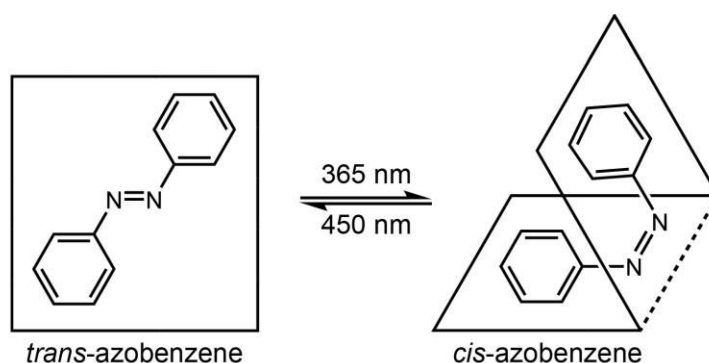


**Figure 2.11.** Light induced reversible *cis* to *trans* isomerization of azobenzene. While the *trans*-azobenzene is a planar molecule, the *cis*-azobenzene is nonplanar.

Azobenzene, firstly described in 1834,<sup>23</sup> consists of two benzene rings connected to each other *via* the so-called azo bond (-N=N-) and due to its strong light absorption properties it is used as dye in a variety of industries. One outstanding feature of azobenzene is its reversible photoisomerization of the planar *trans*- to the nonplanar *cis*-form. The *trans* to *cis* isomerization is induced by ultraviolet (UV, around 365 nm) irradiation; the *cis* to *trans* isomerization takes place after visible (vis, around 450 nm) light irradiation (see Figure 2.11). As a result of its distorted configuration and consequent decrease in the delocalized aromatic electron system, the *cis* form is less stable and thus, the *cis* to *trans* isomerization can also occur thermally.<sup>24</sup>

The light switchable property of azobenzene could be used to switch DNA hybridization on and off. Therefore, azobenzene moieties were introduced into DNA strands *via* solid phase DNA synthesis. The required azobenzene phosphoramidite (see Figure 2.12.B) was synthesized by coupling of azobenzene derivatives to D-threosinol, a reduction product of the amino acid threonine.<sup>25</sup> Threosinol functions as a structural analogue to deoxyribose, since it exhibits a primary and a secondary hydroxyl group corresponding to the 5'- and 3'-hydroxyl groups in the sugar molecule. Furthermore, the amino group can easily be modified *via* amide bond formation with carboxylic acid derivatives, as in the present case with the carboxyazobenzene. The reaction scheme for the synthesis of an azobenzene phosphoramidite derivative is given in Figure 4.12.

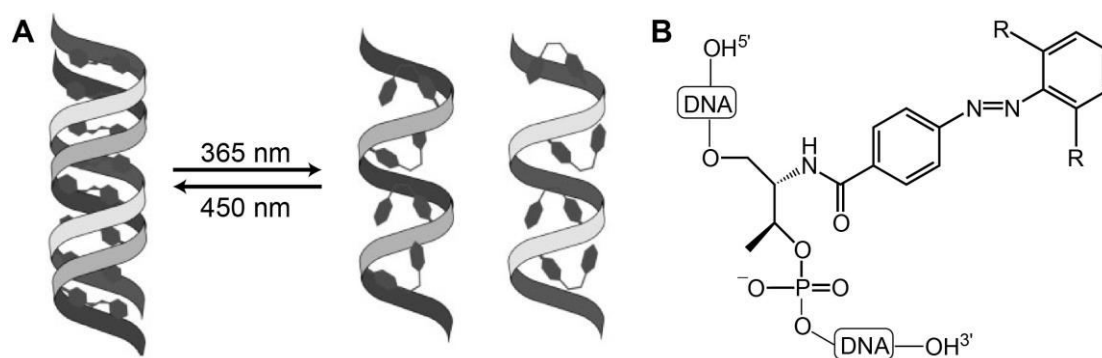


**Figure 2.12.** A) Scheme of the reversible light induced on/off switching of two azobenzene (AB) modified complementary ODNs. The *trans*-AB stabilizes the duplex (left) while the *cis*-AB leads to destabilization and subsequent dehybridization. The image was taken and slightly modified from reference <sup>26</sup> B) Chemical structure of an azobenzene moiety as it is incorporated into a DNA strand (-R = -H, azobenzene (AB); -R = -CH<sub>3</sub>, dimethylazobenzene (DMAB)).

The hybridization/dehybridization mechanism of this light switch is based on the planar/nonplanar nature of the aromatic azobenzene molecule. When the azobenzene, incorporated into an ODN exists in its planar *trans* form (after vis light irradiation), stabilization of the DNA duplex takes place, due to intercalation and increase of the  $\pi$ -stacking interaction. On the other hand, the nonplanar *cis*-azobenzene (after UV light irradiation) decreases the stability of the duplex due to steric hindrance and consequent decrease in  $\pi$ -stacking. An illustration of the on/off photoregulation of an azobenzene modified DNA duplex is shown in Figure 2.12.A.

Since the melting temperature of a duplex ( $T_m$ ) is an indicator for the stability of the double stranded form of DNA, melting curves of complementary ODNs containing azobenzene modifications were measured to investigate the efficiency of the photoregulation. It was found that the melting temperature of the duplex is decreased if the sample was irradiated with UV light before measuring. The destabilization could be reverted by vis light irradiation. The corresponding melting curves for the duplex formation of two complementary 8mer ODNs, one of which is carrying two azobenzene modifications, before and after irradiation, are shown in Figure 2.13.A. The decrease in the melting temperature for the duplex with the AB in the *cis* form (after UV irradiation) is obvious, although the hybridization could not be avoided entirely, since the  $T_m$  of the *cis* species is 22°C, indicating partial existence of ds DNA at room temperature (RT).<sup>22</sup>

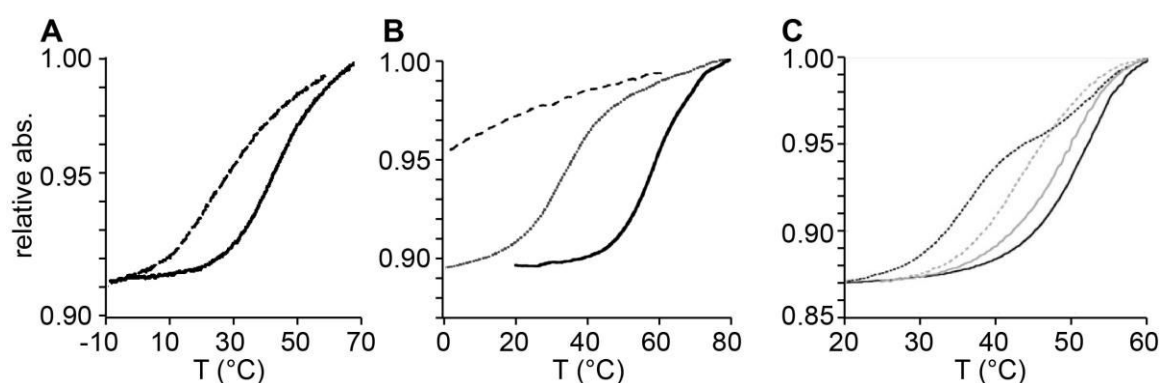


**Figure 2.13.** A) Melting curves of a DNA duplex containing two AB modifications in one strand (5'-GCYGAGTYCG/3'-CGCTCAGC) (Y = AB) before (solid line) and after UV irradiation (dashed line). B) Melting curves of a DNA duplex containing three AB modifications in one strand and four AB modifications in the complementary strand (5'-CGTYTAYGTYTCA/3'-GCYAAITYAAYGT, interstrand-wedged motif, cf. Figure 2.14) (Y = AB) before (solid line) and after UV irradiation (dashed line). As a reference, also the melting curve of the corresponding duplex without any modifications is shown (dotted line). C) Melting curves of a DNA duplex containing one DMAB modification in one strand (5'-GGTATCXGCAATC/3'-CCATAGCGTTAG) (X = DMAB) before (solid black line) and after UV irradiation (dashed black line). For comparison, the melting curves of the corresponding duplex carrying an AB modification instead of the DMAB modification before (solid grey line) and after UV irradiation (dashed grey line) are shown. The images were taken and slightly modified from references<sup>22,26-27</sup>.

In order to improve the switching efficiency, two approaches were followed. It is known that *trans* to *cis* isomerization of azobenzene does not occur in a quantitative fashion, thus the introduction of more azobenzene moieties into one DNA strand should not only increase the stabilizing or destabilizing effect of the *trans*- or the *cis*-form respectively, but also the chance to isomerize at least a certain percentage of the azobenzene

modifications into the *cis* form after UV light irradiation. Different sequence designs were tested (see Figure 2.14) and it was found that an increase of the amount of AB modifications could increase the switching efficiency. The melting curves of the duplex formation of two complementary 10mer ODNs, one of which is carrying three azobenzene the other four azobenzene modifications (interstrand-wedged motif), before and after irradiation with UV light were measured. It was found that in the *cis* form no  $T_m$  at all could be determined, because no duplex is formed even at low temperature. Whereas in the *trans* form, the  $T_m$  is strongly increased in comparison with an unmodified duplex with the same sequence. This result indicates that UV irradiation of a duplex, modified with AB in the interstrand-wedged motif, entirely switches the hybridization of the complementary ODNs off, while vis irradiation increases the duplex stability.<sup>26</sup>

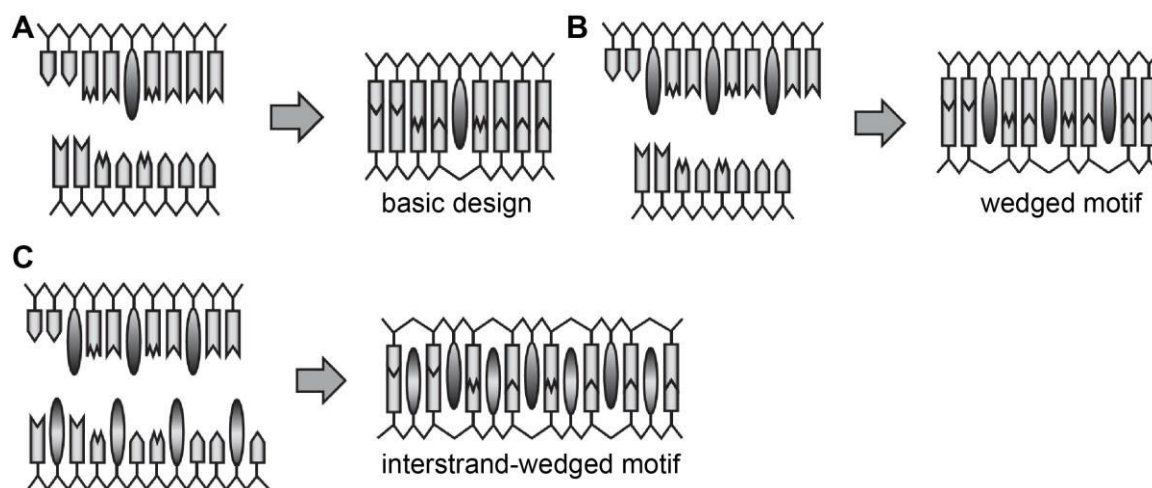


**Figure 2.14.** The sequence design of photo switchable complementary ODNs. A) In the basic design only one AB modification is inserted in one of the complementary DNA strands. B) The wedged motif has several AB modifications inserted in one of the complementary DNA strands. C) The interstrand-wedged motif includes AB modifications in both complementary DNA strands resulting in an alternating alignment of base pairs and AB modifications. The images were taken from reference<sup>28</sup>.

The second approach was to increase the switching efficiency of the azobenzene modification itself. Therefore, diverse azobenzene derivatives were incorporated into DNA strands and the switching efficiency of those were tested by means of  $T_m$  measurements.<sup>29</sup> Indeed, the switching efficiency was dramatically increased when using an azobenzene, carrying two methyl groups on the ortho position of the benzene ring far from the DNA backbone. The melting curves of the duplex formation of two

complementary 12mer ODNs, one of which is carrying one of those dimethylazobenzene (DMAB) modifications (see Figure 2.12.B) before and after UV irradiation are shown in Figure 2.13.C. Additionally, the melting curves of similar ODNs with an AB modification instead of the DMAB modification are shown. Evident from Figure 2.13.C, the stabilization and destabilization of the DMAB modified duplex before and after UV irradiation are tremendously increased.<sup>27</sup>

The methyl groups on the distal benzene ring not only increase the stabilizing and destabilizing effect when isomerized into the *trans*- and *cis*-form respectively but also the thermal stability of the *cis* form is increased by 10-fold longer half-life in comparison with the non-substituted azobenzene. The longer half-life was explained by the “steric hindrance between the unpaired electrons of the  $\pi$ -orbital of the nitrogen atom of the inversion center and the methyl group” and a resulting hindrance of the *cis* to *trans* isomerization.<sup>29</sup>

The presented azobenzene modifications are efficient tools for the introduction of functionality into DNA assemblies as shown in the following section.

### 2.2.6 Switching Mechanisms of DNA Hybridization

As already mentioned, switching mechanisms, which allow switching DNA hybridization on and off, are of great interest in order to build DNA machinery capable to perform controlled mechanical motion. In this chapter, the three switching mechanisms used in this study will be described. Since every switching mechanism displays advantages and disadvantages, the possibility to use diverse switching mechanisms is beneficial in order to establish systems widely usable under different conditions. Table 2.1 gives a summary of the pros and cons of the presented switching mechanisms.

	Toe-hold switch	pH switch	Light switch
trigger	fuel DNA	acid and base	light
input	external addition of ODNs	external addition of NaOH/HCl	no external input
accumulation of waste	waste DNA duplex	NaCl and H <sub>2</sub> O	no waste
dilution	yes	yes	no
biocompatibility	no hazardous impact	affect on acid/base sensitive systems	affect on light sensitive systems

**Table 2.1.** Summary of the characteristics of three different switching mechanisms used in DNA nanotechnology.

### 2.2.6.1 Switching DNA Hybridization with DNA Fuel

Switching DNA hybridization on and off due to addition of DNA fuel is a well-established method (toe-hold mechanism), which is used in a broad variety of applications.<sup>30</sup> The scheme depicted in Figure 2.15 illustrates the switching principle.

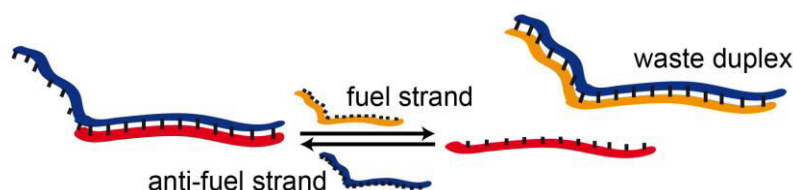


**Figure 2.15.** Scheme of the DNA fuel induced strand displacement mechanism. For more details, see text.

The red strand represents the DNA, which will be released from the complementary blue strand. Since the blue strand contains a single stranded (ss) overhang (toe-hold), strand displacement takes place when a fuel strand (yellow) entirely complementary to the blue strand is added. Because of the increased number of base pairs, the resulting duplex has lower free energy than the initial duplex and is thereby preferentially formed. The process can be reverted by adding additional blue strand (anti-fuel strand), the formed duplex from the yellow- and the blue-strand remains in the system (waste duplex).

### 2.2.6.2 Switching DNA Hybridization *via* pH Adjustment

The pH-induced switch is based on the formation of the i-motif structure (see chapter 2.2.2). The switching principle is shown in Figure 2.16. At neutral pH the C-rich ODN

(blue) hybridizes to its complementary strand (red), whereas at acidic pH the blue strand forms the i-motif structure, resulting in release of the red strand. Adjusting the pH back to neutral reverts this process.<sup>31</sup>

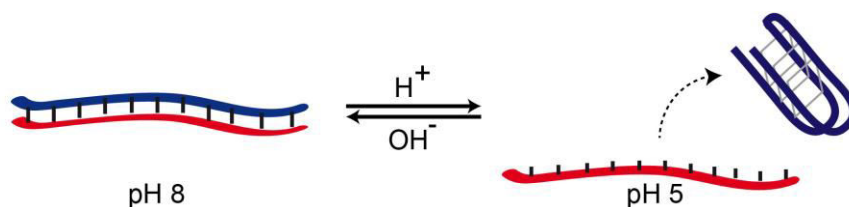


Figure 2.16. Scheme of the pH induced strand displacement mechanism. For more details, see text.

### 2.2.6.3 Switching DNA Hybridization *via* Light Irradiation

The light switch is based on two isomeric forms of azobenzene, the planar *trans* form and the non-planar *cis* form. The *trans* to *cis* isomerization is induced by UV (365 nm) irradiation while the *cis* to *trans* isomerization takes place either by vis (450 nm) irradiation or thermally. The switching principle is depicted in Figure 2.17. As illustrated, irradiation of a DNA duplex, containing an AB modified strand (blue) and the complementary strand (red) with UV light, leads to the isomerization of the AB into the *cis*-form and subsequent dehybridization. Irradiation with vis light reverts this process.

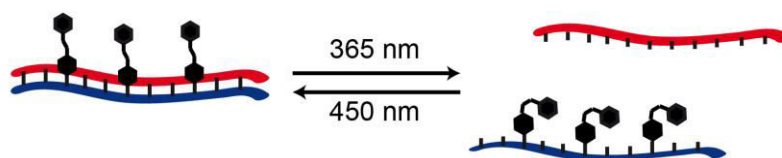
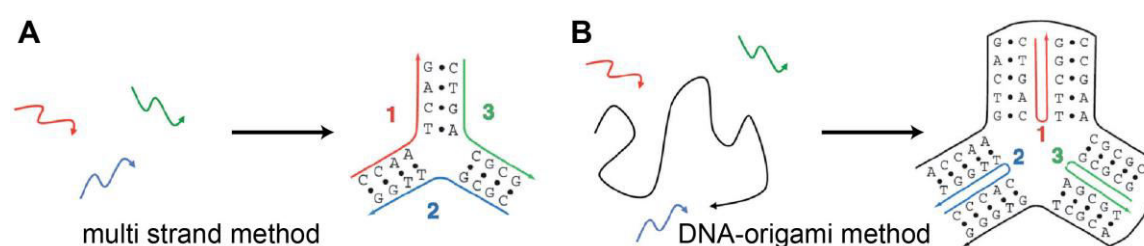


Figure 2.17. Scheme of the light induced strand displacement mechanism. For more details, see text.

## 2.3 Structural DNA Nanotechnology

DNA nanotechnology treats with the design, assembly, characterization and triggering of structures in the nanometer scale. The field of DNA nanotechnology was initiated by N. Seeman more than 30 years ago by using the fundamental Watson-Crick base pairing rules to build up higher order aggregates<sup>5,9</sup> and since then, developed into a scientific field covering the construction of two- and three-dimensional (3D) architectures,<sup>32-33</sup> nanotubes,<sup>34</sup> crystal lattices<sup>35</sup> (structural DNA nanotechnology) and the assembly of molecular machines<sup>36</sup> as well as devices suitable for DNA computing<sup>37</sup> (dynamic DNA

nanotechnology, see chapter 2.4). Two main strategies are used to assemble DNA structures in the nano scale, the multi strand method and the DNA origami method (see Figure 2.18). In the multi strand method, ODNs are designed in a way, that they hybridize into branched motifs (tiles), which can be joined by hybridization of sticky-ends to form bigger structures. In the origami method, a long scaffold strand is folded into the desired shape *via* hybridization with short staple strands.<sup>38</sup> Due to the similarity to the Japanese art of paper folding, these kinds of assemblies are called DNA-origami.



**Figure 2.18.** The two main principles for the fabrication of DNA objects. A) In the multi strand method, the ODNs are designed in a way that they hybridize into well-defined branches. Those branches can be connected *via* sticky-ends into more complex structures. B) In the DNA-origami method one long scaffold strand is formed *via* hybridization with many short staple strands into the desired shape. The images were taken and slightly modified from reference<sup>38</sup>.

The first complex DNA nanoarchitecture reported in literature has the connectivity of a cube. This assembly is constructed out of ten ODNs, which are stepwise assembled into the final structure. First two squares containing four 3-way junctions and four sticky-ends were assembled which were first ligated into a three-ring structure and finally into a cube-like structure (see Figure 2.19.A).<sup>33</sup> As a result a huge variety of diverse structures was assembled using the multi strand methodology (see Figure 2.18.A). A remarkable example within these structures is a DNA tetrahedron (see Figure 2.19.B), which can be assembled in a one-pot synthesis, giving remarkably high yields.<sup>39</sup> The fact that the junctions are flexible, leads to objects with less rigidity than suggested from the drawings of Figure 2.19.



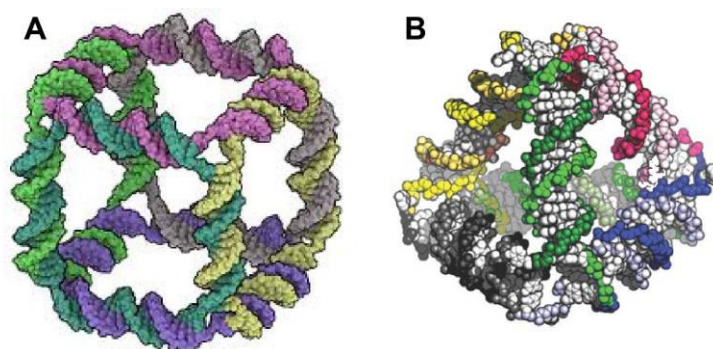


Figure 2.19. Three-dimensional model of A) a DNA cube and B) a DNA tetrahedron. The images were taken from reference <sup>33,39</sup>.

Apart from the assembly strategy using junctions and sticky-ends, the powerful methodology of DNA origami was introduced by P. Rothemund in 2006.<sup>32</sup> Here, DNA objects with any desired shape are assembled by folding a long viral DNA scaffold strand (approx. 7000 bases long) through hybridization with various short DNA staples (20-40 bases long). The staple strands hybridize to the scaffold strand at different positions, thus folding it into specific shapes (see Figure 2.18.B). The sequence of the scaffold strand is known, whereas the sequences of the staple strands are defined by a computer aided design in order to fold the scaffold strand into (almost) any desired two- or three-dimensional shape. Resulting from the multitude of antiparallel crossovers linking the helices within one structure, the assemblies are more rigid than the previously presented multistrand based structures.

The variety of assembled DNA origami structures ranges from two-dimensional structures like squares and smiley faces (see Figure 2.20.A)<sup>32</sup> to three-dimensional structures like boxes (see Figure 2.20.B)<sup>40</sup> and tubes.<sup>41</sup>

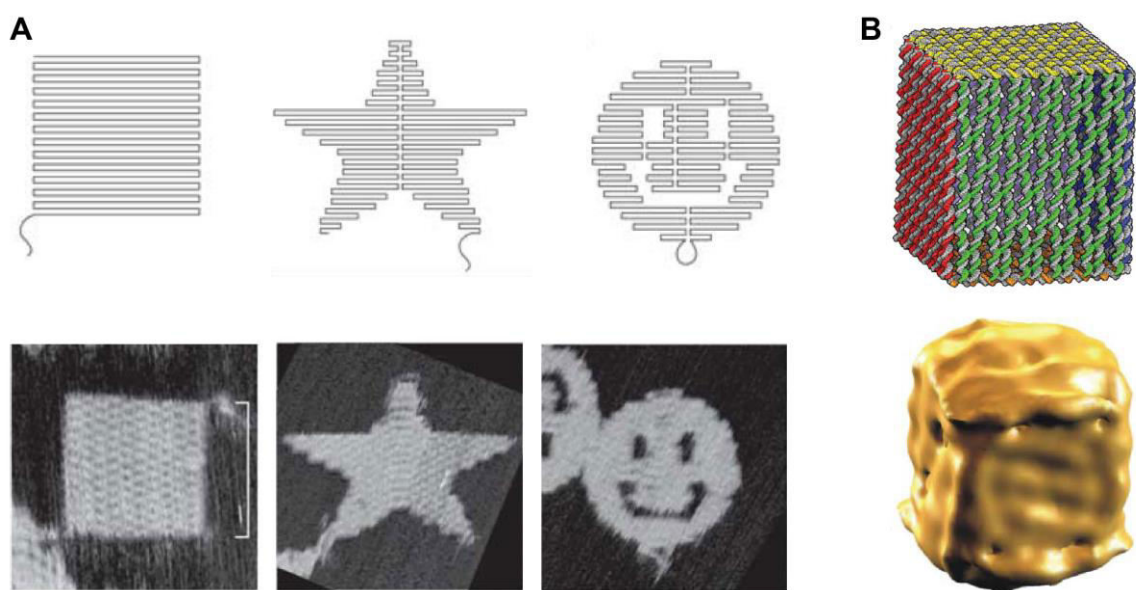


Figure 2.20. A) The folding path of the scaffold strand (upper panel) for the assembly of two-dimensional DNA origami square, star and smiley face and Atomic Force Microscopy (AFM) images of the same (lower panel). B) Three-dimensional representation of a DNA origami box (upper panel) and a surface representation of the assembly created from cryo-electron microscopic images (lower panel). The images were taken and slightly modified from reference <sup>32,40</sup>.

Since the first description of DNA origami assemblies, quite a number of different objects performing a broad variety of functions have been presented, and also alternative and improved assembly strategies were developed. Yin *et al.* reported the assembly of DNA origami structures without using a scaffold strand.<sup>42</sup> Instead, only synthetic short ODNs were used, each of which was binding to four neighboring ODNs through base pairing (the assembly scheme for such a DNA origami is given in Figure 4.26). In this way, a rectangle was assembled which serves as a “canvas” with 310 pixels (each ODN representing one pixel). Simply by excluding the corresponding ODNs, 107 distinct shapes could be synthesized. This method is particularly suitable when assemblies of different sizes are required, since there is no limitation caused by the 7000 bases long scaffold strand. Additionally, the modification of such DNA origami is straightforward, as the exclusion or exchange of single ODNs can easily be achieved. In a follow-up study, Yin *et al.* modified the mentioned rectangle origami in a way, that addition of diverse ODNs resulted in strand displacement and predictable reconfiguration of the origami into another shape.<sup>43</sup>

## 2.4 Dynamic DNA Nanotechnology

As previously commented, control of the hybridization of DNA strands can be easily achieved (cf. chapter 2.3). A step forward within the DNA nanotechnology was to build DNA machines capable of performing controlled mechanical motion or even produce work in a controlled fashion.<sup>44</sup> The general inputs used to trigger these systems are the already mentioned toe-hold, pH and light switches, but also alternative triggers based on ion strength<sup>45</sup> or DNA-protein interactions<sup>46</sup> were implemented.

The first example of such DNA device was a DNA tweezers, which can exist in an open and closed state, depending on the externally added input. The device consists of three ODNs. One long strand to which the other two are partially hybridized in a way that they have ss parts dangling at the ends of the long strand. The long strand has a ss part in the middle, serving as a hinge. When a fuel strand, complementary to the dangling parts of the device is added, the latter hybridize with this strand leading to a closed form of the tweezers. Since the fuel strand contains a toe-hold, it can be removed by adding an antifuel strand, resulting in the open state of the tweezers. The opening and closing of this DNA fuel driven device could be followed by FRET, due to fluorophores attached to the end of the long strand.<sup>47</sup> Following this design, similar devices were triggered by changes in pH<sup>48</sup> or light irradiation. For the light triggered tweezers, the fuel strand was modified with various AB modifications, allowing to set and reset the system simply by irradiation with vis- and UV-light respectively.<sup>49</sup> A more sophisticated device represents the so-called DNA walker. Such DNA walker is capable of moving along a predefined track without detaching. Usually, a DNA walker consists of a body with two or more legs, which hybridize to two anchoring sites on a track. Releasing one of the legs allows the walker to move one step further, while the second leg is still attached to the track. The first reported example was triggered by the addition of DNA fuel, in order to displace the corresponding legs from the track (see Figure 2.21.A).<sup>50</sup> By introducing restriction enzymes into a walker system, it was possible to transport a cargo (here a DNA fragment) along a track without stepping back, since the enzyme destroys the track by catalyzing the hydrolysis of the anchoring sites. The DNA cleavage depends on the state and position of the device (see Figure 2.21.B).<sup>51</sup>

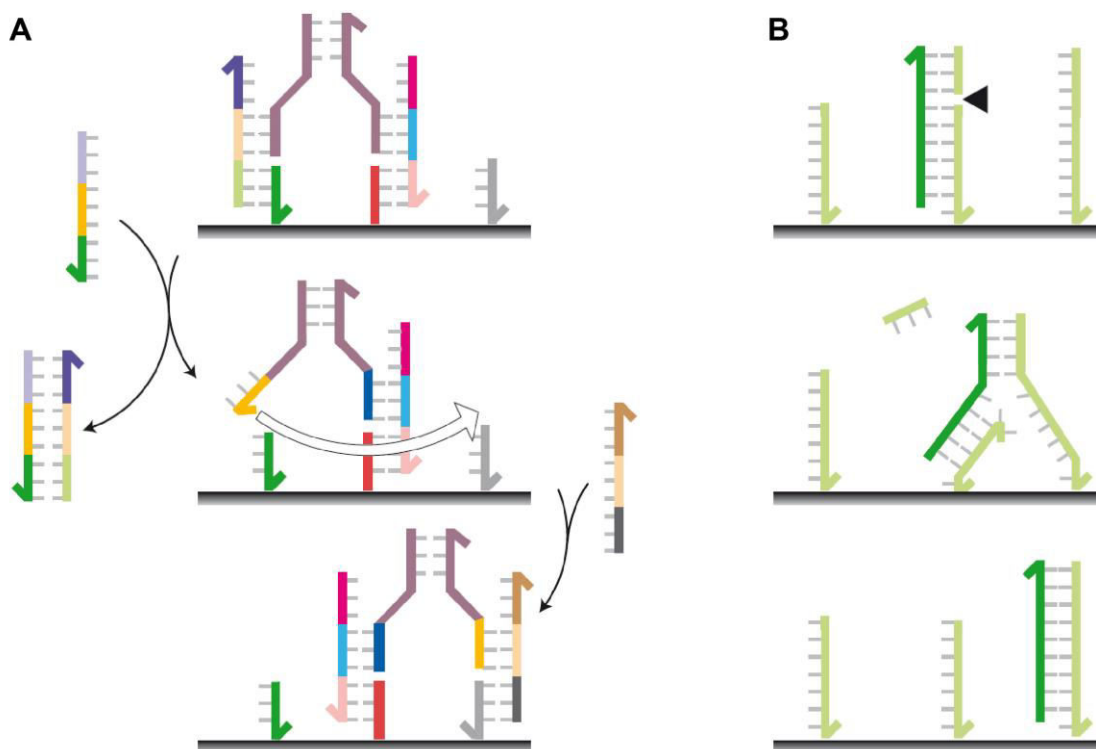
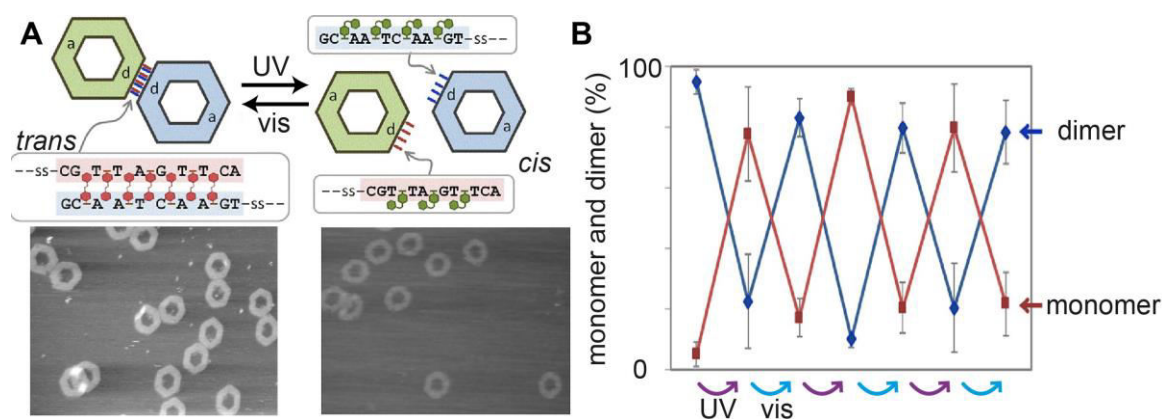


Figure 2.21. A) DNA walker fueled by strand displacement ODNs with two feet that steps along a track with different anchoring sites. Stepwise addition of two ODNs first releases the back foot from its anchoring site, which then binds it to the next anchoring site. Here, only the first step is shown. B) Autonomous movement of cargo driven by enzymatic hydrolysis of the track. Binding of the cargo (dark green) to the anchoring site induces enzymatic hydrolysis of the latter. The small fragment of the anchoring site is released, thereby leaving a part of the cargo single stranded. This single stranded part hybridizes to the next anchoring site and upon branch migration, the whole cargo steps further. The destruction of the track leads to an unidirectional movement of the cargo. The images were taken from reference <sup>36</sup>.

Recently, a DNA walker was reported, which can stride over a track consisting of two combined DNA origami structures. This is a step towards devices that can move over micrometer distances.<sup>52</sup>

By combining the DNA origami technique with the use of azobenzene modified DNA, Sugiyama *et al.* achieved a reversible light controlled assembly of hexagonal origamis into various unique patterns.<sup>53</sup>



**Figure 2.22.** A) Scheme illustrating the light controlled reversible switching of the azobenzene modified hexagonal origamis into dimeric structures (upper panel), together with AFM images of the dimers and monomers respectively (lower panel). B) Switching efficiency of the reversible switching. The percentages of dimers and monomers after consecutive switching with UV and vis light are given. The data was obtained from quantification of a gel shift assay. The images were taken and slightly modified from reference <sup>53</sup>.

In particular, hexagonal origamis were equipped with azobenzene-modified overhangs at one or two sites. When such origamis were mixed with similar origamis featuring complementary overhangs, dimers, chains and rings were formed. Irradiation with UV light resulted in the disassembly of the higher order structures into the monomeric hexagonal origamis. The scheme in Figure 2.22.A illustrates the switching principle for the reversible formation of the dimeric structure, together with AFM images displaying either the monomers or the dimers. The switching efficiency was evaluated by a gel shift assay, showing a nearly quantitative and highly reversible monomer to dimer conversion (see Figure 2.22.B). In a similar approach, Niemeyer *et al.* achieved a DNA origami nano chamber, which could be reversibly opened and closed and thereby might serve as a dynamic compartmentalization system.<sup>54</sup>

## 2.5 DNA Computing

DNA encodes the genetic information required for the development of all living organisms on earth. The data storage is mediated by the four different nucleobases of the biomolecule. This enormous capability to store data led to the idea, to use DNA in order to build DNA based bio computers.<sup>55</sup>

Indeed, in a pilot experiment it was possible to work out an instance of the directed Hamiltonian path problem (a classical problem in the mathematical field of graph

---

theory), by using the tools of molecular biology as operations and DNA as the data storage.<sup>56</sup> By the ordered hybridization of distinct ODNs from a mixture of designed ODNs, each of which representing specific information, followed by ligation, PCR and gel electrophoresis, a solution for the Hamiltonian path problem could be found.

Regarding the big experimental effort necessary for the operation and read out of a DNA computer, there is no industrial use of such devices, but if the molecular biology provides enhanced biochemical methods, DNA has the potential to serve as ideal candidate for the construction of alternative data storage and computing devices. Currently, the focus lies on the implementation of DNA logic gates, which are devices capable of performing Boolean function. Simplified, logic gates are the reason why a computer responds to the inputs given by the user with a distinct output. Hence, the availability of logic gates and logic circuits built with DNA is a key requirement for further developments.

The first examples of DNA logic gates reported in 2002 were based on DNAzymes, capable to cleave a certain DNA strand at one position. The cleavage leads to a separation of a FRET pair and thereby increases the fluorescence emission of the fluorescence donor. Furthermore, the DNAzymes could be either activated or inactivated by the addition of distinct input ODNs. This is explained by an activation/inactivation change of the secondary structure of the DNAzyme upon hybridization with the input ODN. Using these systems, entirely based on DNA (the input and the gate itself), it was possible to create YES-, NOT-, AND-, OR - and XOR-logic gates.<sup>57</sup> In Figure 2.23.A-C schemes for the first three gates are depicted together with their truth tables. The table of truth of a logic gate lists all the inputs and outputs in digital binary format (1 = yes, 0 = no). In the YES gate, cleavage and consequent increase in fluorescence was only detected after addition of the input ODN and *vice versa* for the NOT gate. In the case of the AND gate, only after addition of both input ODNs A and B an increase in fluorescence was observed upon hybridization and subsequent opening of two stem-loop motifs. In contrast to the open form, in the closed form the stem-loop motifs hamper the DNAzyme activity.

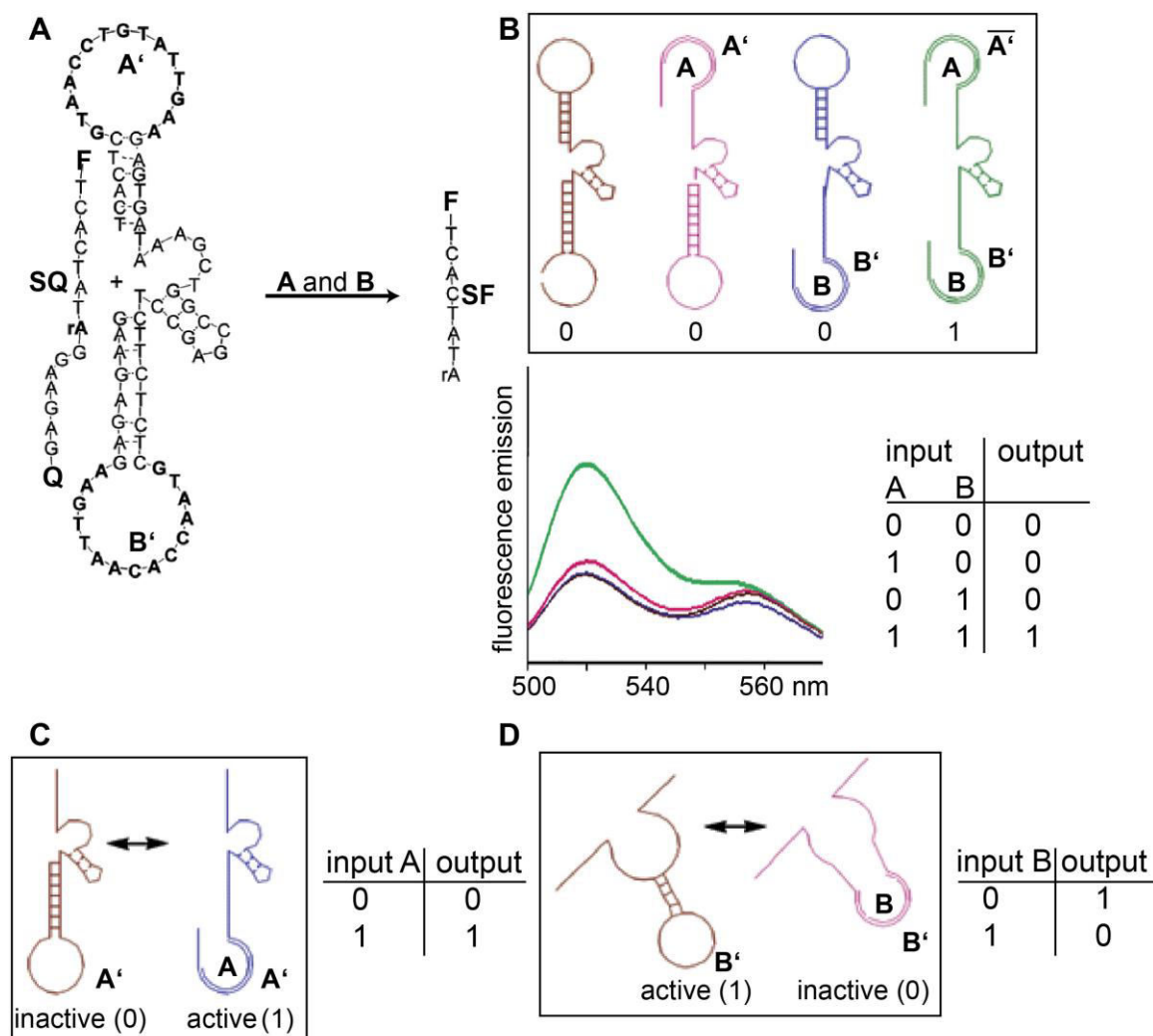
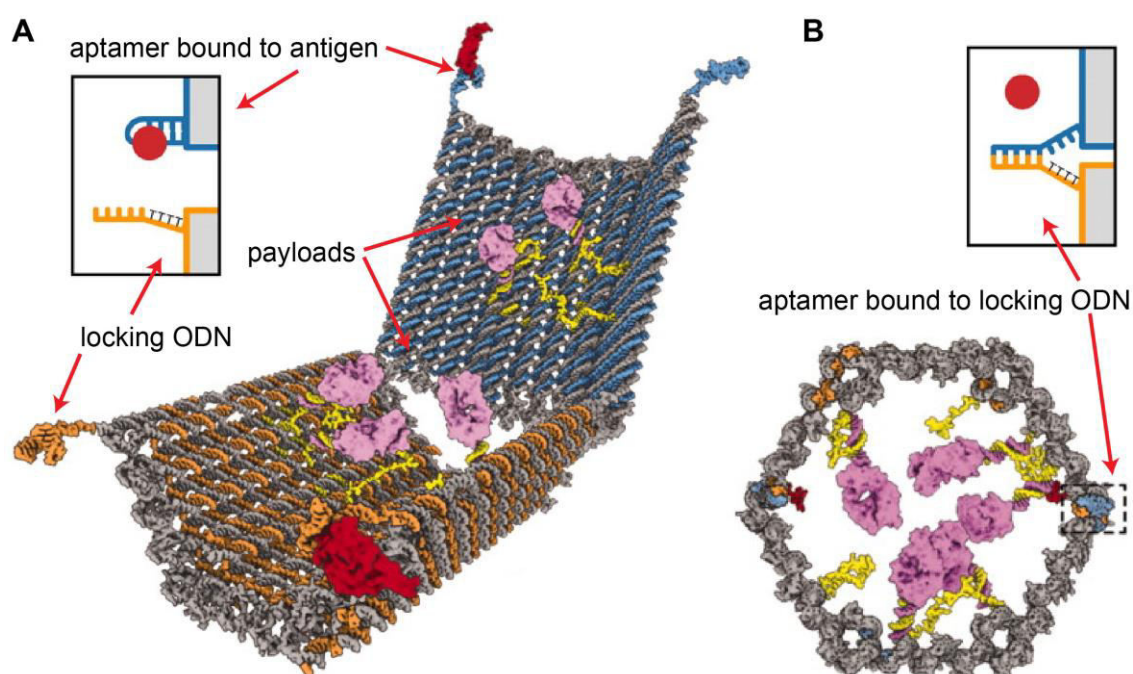


Figure 2.23. A) Secondary structure of a DNAzyme modified with two hairpin sequences A' and B' for the use as logic AND gate. The DNAzyme is inactive when one or both hairpins are formed, while the active form cleaves the fluorophore/quencher labeled ODN "SQ", resulting in the separation of the fluorophore/quencher pair and subsequent fluorescence emission. Each hairpin is opened upon addition of a distinct input ODN A or B. Hence, addition of input A and B activates the DNAzyme while only input A or B does not activate the DNAzyme. B) Scheme of the three inactive and the active states (upon addition of input A and B) of the DNAzyme (upper panel). The lower panel shows the fluorescence spectra measured before (brown) and after addition of input A (magenta), input B (blue) or both (green) and the resulting table of truth for this logic AND gate. C) Scheme of the active and inactive state of DNAzyme used as single input YES gate (left). Only after addition of input ODN A the DNAzyme is active resulting in increased fluorescence emission (data not shown). The resulting table of truth for this YES gate is shown on the right. D) Scheme of the active and inactive state of DNAzyme used as single input NOT gate (left). Addition of input B inactivates the DNAzyme resulting in decreased fluorescence emission (data not shown). The table of truth for this logic NOT gate is shown on the right. The images were taken and slightly modified from reference<sup>57</sup>.

To date, diverse DNA based logic gates has been employed, which are triggered upon pH changes<sup>58</sup>, light irradiation<sup>59</sup>, enzyme activity<sup>60</sup> and others<sup>61</sup>. Also whole logic circuits, in which the output of the first gate triggers the second, have been recently described as

well as reversible logic gates.<sup>62-63</sup> Since the output of the DNA based logic gates can serve as input for other gates, communication networks can be constructed and recognition and even analytical functions might be implemented.<sup>57</sup>

The benefit of combining different building blocks and techniques widely used in DNA nanotechnology and molecular biology was strikingly shown by Church *et al.*<sup>64</sup> Using the origami technique, a DNA container was constructed, which can be loaded with different kinds of payloads, such as gold nanoparticles but also the bioactive Fab' antibody fragment. Therefore, DNA linkers were attached to these cargoes, which are complementary to toe-hold sequences inside of the DNA container.



**Figure 2.24. Schematic view of the logic gated nanorobot for targeted transport of cargoes in its open (A) and closed form (B). The images were taken and slightly modified from reference <sup>64</sup>.**

Furthermore, the container is equipped with two locks, consisting of different aptamers that undergo a structural reorganization upon binding to specific antigens. Aptamers are ODNs that bind specific compounds, ranging from small molecules to proteins. Aptamers are routinely identified through the process of systematic evolution of ligands by exponential enrichment (SELEX).<sup>65</sup> The locks are located at the left and right front side of the container and in the unbound state, they partially hybridize to a complementary locking ODN on the other front side of the container, resulting in a closed state with the



payloads locked inside. Upon binding to their targets, the aptamers undergo a structural reorganization, leading to a dehybridization of the aptamer locks followed by the opening of the container and release of the cargo (see Figure 2.24). In particular, those locks were programmed to only respond when cells express two antigen stimuli simultaneously (representing an AND logic gate). This “nanorobot” represents a logic gated driven autonomous tool that can selectively deliver drugs *in vivo*.

## 2.6 Interlocked Molecules

Interlocked molecules consist of at least two molecules, which are held together not by covalent interactions, but through mechanical bonds.<sup>66-67</sup> The most well known examples are catenanes and rotaxanes. Additionally, diverse other interlocked architectures were synthesized in the past 50 years, like borromean rings, knots,<sup>68</sup> pretzelans<sup>69</sup> and daisy chains<sup>70</sup>. Since the first reported synthesis of a catenane in 1961 with yields ranging from low to marginal,<sup>71</sup> a notably development in the field of supramolecular chemistry has contributed to the improved assembly of these interlocked structures and nowadays, different catenanes and rotaxanes are synthesized in nearly quantitative yields. The accessibility of interlocked molecules opened up the possibility to use them in order to construct molecular devices. Catenanes and rotaxanes are ideal candidates for this purpose. The mechanical bond within these structures restricts the movement of the interlocked components to each other and thereby favors intramolecular *versus* intermolecular contacts (non-covalent interactions), as the effective local concentration of the interlocked components is higher than in the non-interlocked systems. The non-covalent interactions can be used to control the movements of the interlocked components.<sup>72</sup>

Owing to the versatility of interlocked architectures and states in which they can exist, different suggestions have been made regarding the nomenclature of those structures. In this work the IUPAC nomenclature will be used.<sup>73</sup> Hence, interlocked rotaxanes or catenanes in which the components are linked together *via* forces like hydrogen bonds or coulomb forces are called pseudorotaxanes or pseudocatenanes respectively. Rotaxanes or catenanes consisting of two or three subunits are called [2]- or [3]rotaxane

and [2]- or [3]catenane respectively. The ring structures are called macrocycles (if not stated otherwise), a rotaxane without any threaded macrocycle (only axle and stoppers) is called dumbbell.

### 2.6.1 Molecular Catenanes

A catenane (from the Latin word *catena*, meaning “chain”) consists of at least two macrocycles, which are interlocked to each other *via* mechanical bonds. Two different approaches are commonly used for the synthesis of catenanes. The statistical synthesis is based on a simple ring closing reaction, expecting that two rings in close proximity form an interlocked structure.<sup>71</sup> Since this method gives low yields, it is rarely used. The other approach is the template directed assembly. Due to hydrogen bonding, metal coordination, coulombic interaction,  $\pi$ - $\pi$ -stacking or hydrophobic forces, a supramolecular preorganization of one macrocycle (or an open macrocycle precursor) and an open macrocycle precursor takes place. In a mechanism called clipping, the open macrocycle is closed resulting in the catenane formation (cf. chapter 2.6.2 and see Figure 2.26).

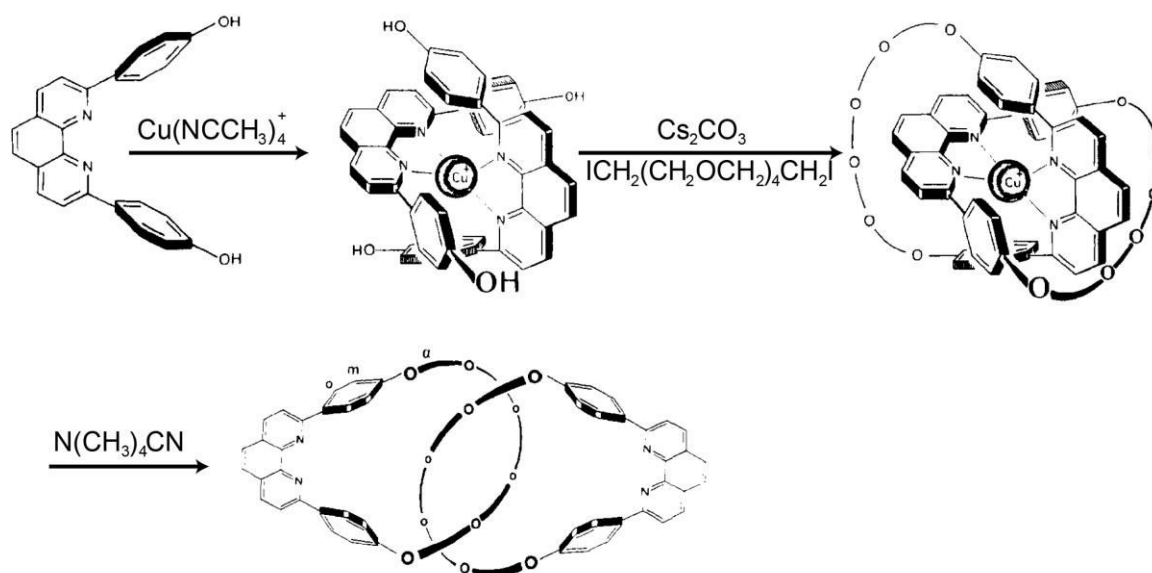


Figure 2.25. Synthesis route for the metal templated synthesis of a catenane reported by Sauvage *et al.* The image was taken and slightly modified from reference <sup>74</sup>.

An example of a catenane synthesized by using the template directed approach is shown in Figure 2.25, together with its synthesis route. The first step of the metal templated

synthesis is the complexation of two equiv. of 2,9-bisphenol-1,10-phenanthroline with 1,14-diiodo-3,6,9,12-tetraoxatetradecane in dimethylformamide in the presence of  $\text{Cs}_2\text{CO}_3$  yielding the metallocatenane (pseudocatenane). Demetallation with tetramethylammonium cyanide in acetonitrile-water leads to the catenane structure. The product formation was followed by NMR, mass spectrometry and crystal structure analysis.<sup>74-75</sup>

### 2.6.2 Molecular Rotaxanes

A rotaxane (from Latin *rota* and *axis*, meaning wheel and axle) consists of at least one macrocycle, which is threaded on a dumbbell shaped molecule. The macrocycle is mechanically trapped on the axle of the dumbbell due to bulky end-groups (stoppers). There are different ways to synthesize a rotaxane. The clipping mechanism is similar to the catenane synthesis. The open macrocycle precursor is threaded on the axle of the dumbbell *via* non-covalent interactions, followed by a ring closing reaction, which yields the rotaxane structure. The stoppering mechanism is similar but here, the closed ring is threaded on the axle of the dumbbell before the stoppers are linked to the axle, resulting in the formation of the rotaxane (see Figure 2.26). In the slippage mechanism, the macrocycle and the dumbbell are synthesized separately, before both are mixed. Upon heating, the macrocycle slips over the stopper of the axle by forming the rotaxane.<sup>72</sup>

One example of a molecular rotaxane assembled with template directed synthesis based on  $\pi$ -donor  $\pi$ -acceptor interactions is shown in Figure 2.27.

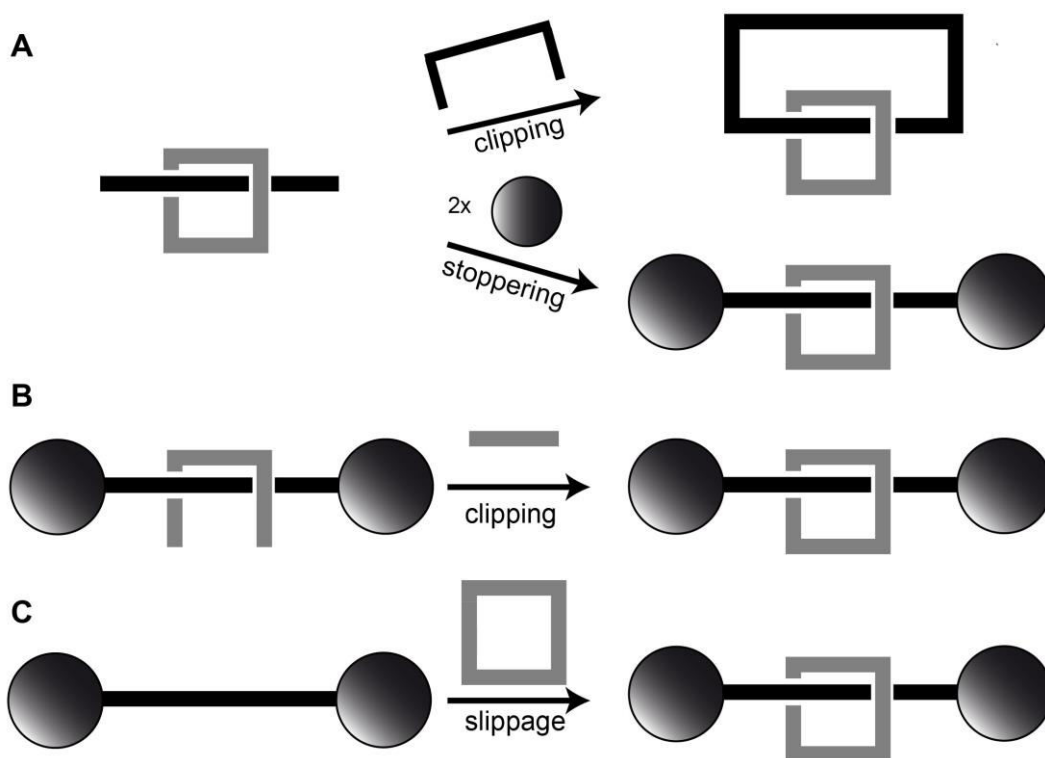


Figure 2.26. A) Scheme of the clipping mechanism for catenane synthesis (upper panel) and the stoppering mechanism for the rotaxane synthesis (lower panel). Both mechanisms start with a threaded ring, either on an open ring or an axle and subsequent ring closing reaction or attachment of stoppers. B) Scheme of the clipping mechanism for rotaxane synthesis. Here an open ring is threaded on a dumbbell and subsequently the rotaxane is synthesized in a macrocycle closing mechanism. C) Scheme of the slippage mechanism for rotaxane synthesis. Here, the synthesized ring and dumbbell are mixed and the rotaxane is formed *via* slippage of the macrocycle over the stopper.

### 2.6.3 Rotaxane Based Molecular Devices

One striking goal in nanotechnology is the assembly of nanodevices, which can serve as switches, which are capable of performing work, directed movement or transport of cargoes and signals. Molecular switches are promising devices for computing and nanoengineering. Since catenanes and rotaxanes can exist with stalled or moving macrocycles, both having entirely different properties, these assemblies are ideal candidates for this purpose.

When observing molecular motors in nature one can find devices consisting of a rotor within a stator. The ATP synthase represents such a device, powered by proton gradients and capable of synthesizing adenine triphosphate out of the corresponding diphosphate substrate. A rotaxane consisting of a macrocycle rotating around an axle features similar components.<sup>76</sup>

The transport of cargoes along a predefined track can be achieved when the rotaxane axle contains two different “stations”. The macrocycle can then serve as shuttle, capable of moving towards one or the other station. A relevant example of such system, called molecular shuttle, is presented in Figure 2.27.

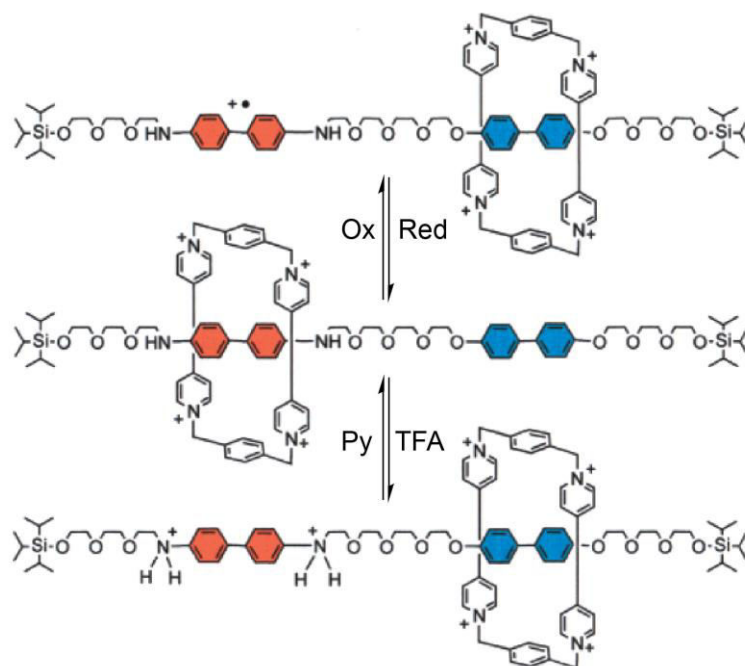


**Figure 2.27.** Molecular shuttle rotaxane presented by Stoddart *et al.* The cyclophane ring represents the macrocycle; the biphenol (blue) and a benzidine unit (red) within the polyether axle represent the stations. The isopropylsilyl groups prevent the macrocycle from dethreading. The macrocycle can be shuttled from one station towards the other *via* oxidation/reduction (Ox/Red) reactions or upon addition of base (Py = pyridine) or acid (TFA = trifluoroacetic acid). The image was taken and slightly modified from reference <sup>76</sup>.

The macrocycle consists of a cyclophane wheel with two paraquat building blocks. The stations are either a biphenol or a benzidine unit within a polyether chain of the rotaxane axle. Since the cationic cyclophane acts as a  $\pi$ -electron acceptor and the stations as  $\pi$ -electron donors, the templated threading of the macrocycle takes place upon attractive  $\pi$ -electron interaction. The macrocycle is preferentially located near the benzidine unit. Finally, the triisopropylsilyl groups serve as bulky stoppers, preventing the macrocycle from dethreading. By using NMR spectroscopy, it was possible to distinguish between the rotaxane with the macrocycle located on one or the other station. Furthermore, it was possible to shuttle the macrocycle position by triggering it with external stimuli. Both, protonation and oxidation transfer the macrocycle towards

---

the biphenol station due to electrostatic repulsion of the positively charged cyclophane ring, whereas addition of base or reduction revert this process, transferring the macrocycle back to the benzidine station.<sup>76-77</sup>

One main objective with mechanical interlocked molecules is to construct machines to generate controlled motion. Muscle tissue is a material relying on the organization of molecular machines (myosin) and filaments (actins) and is capable of producing force for locomotion and many other essential life processes. Daisy chain rotaxanes, composed of covalently linked, self-complementary ring-thread monomers, which are mechanically cross-threaded into oligomers, are excellent candidates for the fabrication of artificial muscles.

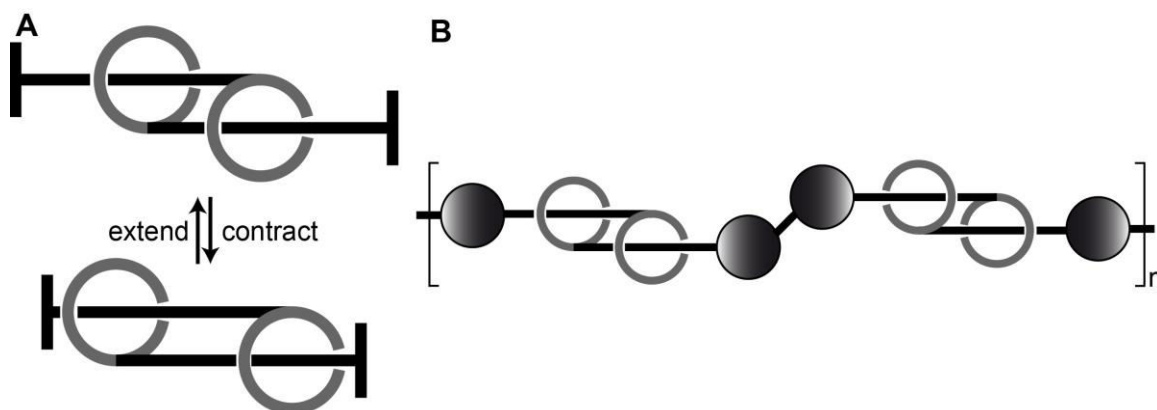


**Figure 2.28.** A) Schematic view of a daisy chain rotaxane in its extended and contracted state. B) Schematic view of an oligomeric daisy chain polyrotaxane.

The daisy chain rotaxane as shown in Figure 2.28.A is composed of two cyclic components, which can slide along the thread of its partner in one dimension.<sup>78</sup> Daisy chain rotaxanes that exist in two different states, an extended and a contracted state, have been described. The switching between the different states can be triggered with stimuli like protons,<sup>79</sup> light<sup>80</sup> or electrochemically<sup>81</sup>. Like in myofibrils, where thousands of sacromers are linked together in a linear array, it was possible to synthesize linear daisy chain rotaxane polymers (see Figure 2.28.B). These daisy chain based muscles might be utilized in diverse applications such as conductive polymers, sensors or robotics. In fluidic devices they could serve as valves or for the contraction and dilation of channels in order to control the flow of the liquid.

## 2.7 Interlocked Assemblies Based on DNA

The idea to combine the structural features and advantages of interlocked molecules with the unique properties of DNA (cf. chapter 2.2) has been recently explored in our research group, paving the way for the design and construction of new interlocked assemblies based on DNA. As a result, in 2010 a fully ds DNA rotaxane was reported by Famulok *et al.*

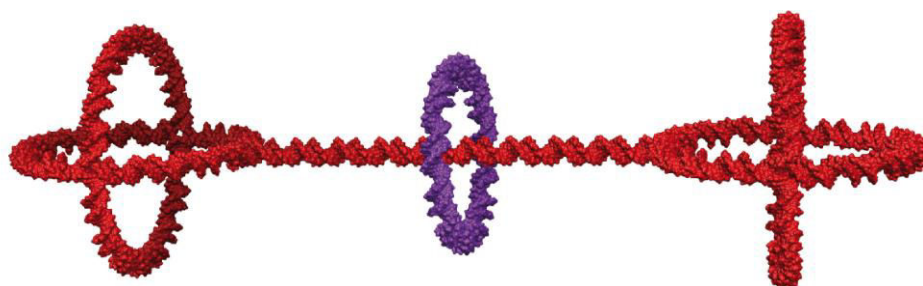


**Figure 2.29.** Molecular model of the ds DNA rotaxane presented by Famulok *et al.* The image was taken from reference <sup>82</sup>.

The threading of the macrocycle in this interlocked architecture is mediated by Watson-Crick base pairing. Therefore, the ds DNA macrocycle as well as the ds DNA axle exhibit complementary ss gap regions. Upon incubation, the macrocycle threads on the axle. The stoppers used in this assembly consist of two ds DNA rings linked together *via* two Holliday-junctions, thereby forming rigid spherical stoppers. The rings themselves are designed with a series of A<sub>5</sub>- and A<sub>6</sub> tracts separated by five randomized nucleotides. This results in the formation of rigid rings with a well-defined shape. Due to the sequence requirements (N<sub>5</sub>A<sub>5</sub>N<sub>5</sub>A<sub>6</sub>), all the rings display a multiple of 21 base pairs (105, 126 or 168 bp).<sup>83-84</sup> In order to induce proper threading, the gap of the macrocycle has to point towards the inner part of the ring. The right position for the gap can be estimated from a three-dimensional model of an A<sub>6</sub>-tract containing ODN (see Figure 2.5). For details of the assembly see chapter 4.1.1 and Figure 4.1. Once the pseudorotaxane is assembled a release oligo (RO), which replaces the macrocycle from the gap of the axle, is added resulting in the formation of the desired rotaxane structure with a mobile macrocycle interlocked. A molecular model of such rotaxane is shown in Figure 2.29. The assembly was confirmed both by gel electrophoresis and Atomic Force

Microscopy (AFM). An interesting feature of this structure was found when flexible and less bulky stoppers consisting of one single ring replaced the spherical stoppers. In these systems, macrocycle dethreading occurs even if the stopper is bigger than the size of the macrocycle (i.e. 168 bp stopper and 105 bp rings, respectively). By fine-tuning the sizes of the stopper and the macrocycle different kinetics for the dethreading were observed (see Figure 2.30). Besides, the relative rigidity of the circular components was supplemented by implementing a stiffened axle consisting of two parallel duplexes linked together *via* diverse paranemic crossovers.<sup>85-86</sup> For systems requiring a solid and robust framework, the enhanced rigidity of such axle can be beneficial.

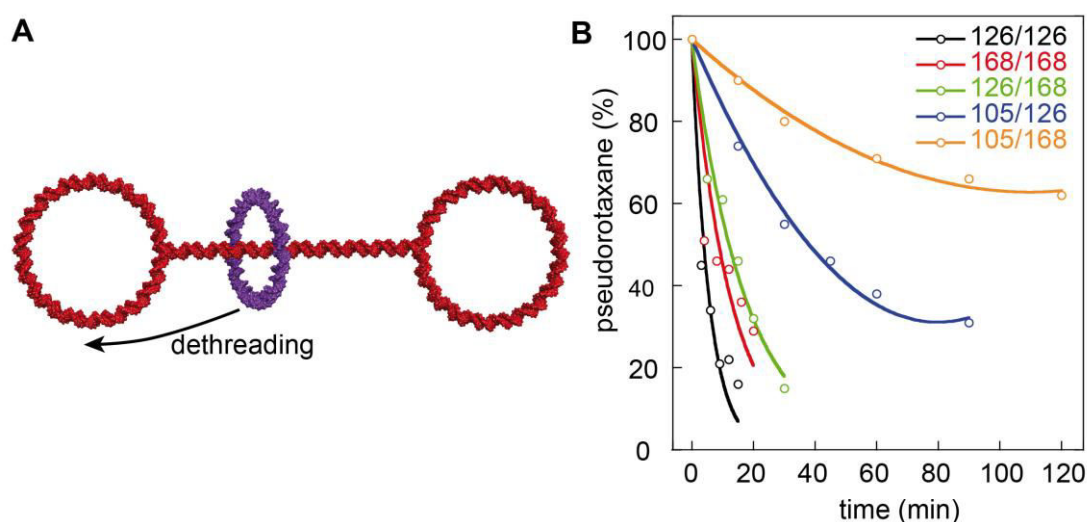
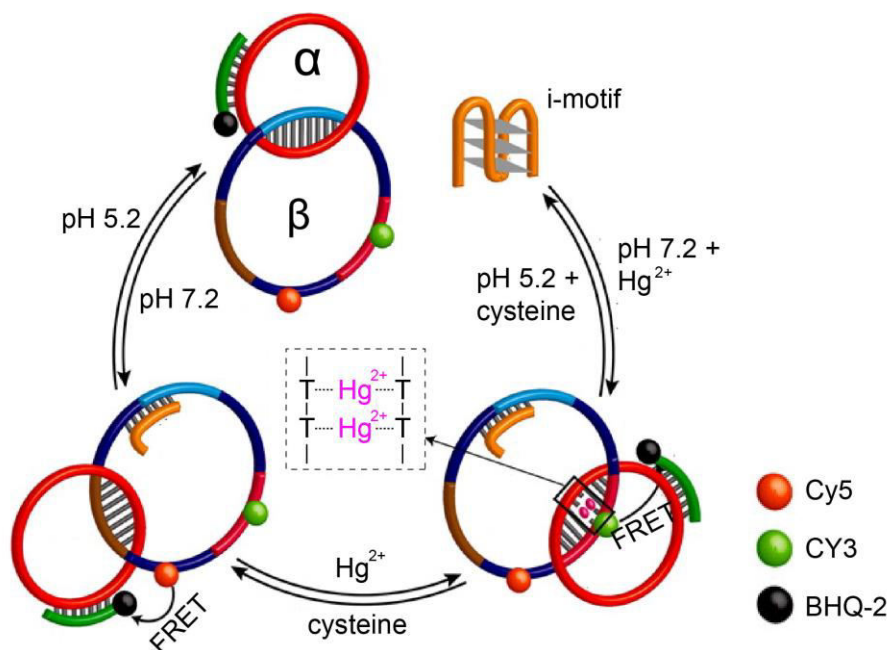


Figure 2.30. A) Three-dimensional model of a rotaxane with ring stoppers. The macrocycle dethreads over the ring stopper in a reverse slippage mechanism. B) Kinetics of the macrocycle dethreading for ring-stoppered rotaxanes with different macrocycle and stopper sizes. The images were taken and slightly modified from reference<sup>82</sup>.

Following the same threading principle, Willner *et al.* synthesized various interlocked architectures, consisting either of ss DNA, of partially ds DNA or of DNA- gold nanoparticle hybrids. Thus, catenanes consisting of two, three<sup>87</sup> and even five rings<sup>88</sup> were successfully synthesized as well as a rotaxane structure with gold nanoparticles as stoppers attached to a DNA axle.<sup>89</sup> Upon adjusting the pH or addition of diverse stimuli like mercury ions ( $\text{Hg}^{2+}$ ), cysteine and fuel ODNs<sup>45,87</sup> it was possible to switch between different stations in these catenane and rotaxane structures. FRET measurements were performed in order to distinguish between the different positions of the macrocycles.



The system shown in Figure 2.31 displays a [2]pseudocatenane in which one of the rings (ring  $\beta$ ) features three different stations. One of the stations can reversibly be blocked by an i-motif encoding sequence complementary to that station upon pH adjustment. The second station is only accessible if  $\text{Hg}^{2+}$  ions are present, upon formation of thymine- $\text{Hg}^{2+}$ -thymine bridges that stabilize the duplex formation at this position. If the latter two stations are blocked, only the third station is accessible directing the shuttle ring (ring  $\alpha$ ) towards this position of the ring  $\beta$ . Thus, these triggers allow directing the ring in a controlled fashion to each of the stations. Furthermore, by hybridizing “blocker strands” on the pathways of ring  $\alpha$ , it was possible to induce a directed rotary motion of that ring around ring  $\beta$ .



**Figure 2.31.** A ss DNA [2]pseudocatenane, with three stations on ring  $\beta$  between which ring  $\alpha$  can be translocated. In the absence of  $\text{Hg}^{2+}$ , at pH 5.2 only the brown station is accessible for ring  $\alpha$ , since an i-motif encoding ODN is blocking the blue station and the red station is only accessible in the presence of mercury upon formation of thymine- $\text{Hg}^{2+}$ -thymine bridges. Either by adjusting the pH or by the addition of mercury ions or cysteine, ring  $\alpha$  can be directed towards any of the three stations. The location of ring  $\alpha$  could be determined by FRET measurements, since the system was decorated with different fluorophore and quencher labels. The image was taken and slightly modified from reference <sup>45</sup>.

Taking advantage of the toe-hold mechanism, it was possible to translocate the macrocycle in the gold nanoparticle stoppered rotaxane from one station towards the other. The macrocycle translocation was monitored by FQ experiments.<sup>89</sup>

---

Another threading mechanism was utilized by Heckel *et al.* in order to assemble a DNA [2]pseudocatenane consisting of ds DNA rings, similar to the ones used by Famulok *et al.* for the rotaxane synthesis. Here, the DNA fragment of one ring is modified with dervan-type polyamides, which bind to a specific DNA sequence of the second ring. Ring closing upon addition of the corresponding ODNs based on Watson Crick base pairing and subsequent enzymatic ligation yielded the pseudocatenane.<sup>90</sup> Note that under native conditions this interlocked structure is trapped in the stalled state.

Due to the intuitive design, following the fundamental Watson Crick base pairing rules and the possibility to switch DNA hybridization reversibly on and off by means of various stimuli, these DNA based interlocked architectures might serve as ideal frameworks for further developments in the field of dynamic DNA nanotechnology. The easiness to chemically modify DNA with a broad variety of bioactive molecules and the fact that DNA represents a water soluble and stable substrate strengthens these expectations.

### 3 Aims of this Project

Famulok *et al.* reported the assembly of shape persistent ds DNA rings of distinct sizes (105 bp, 126 bp and 168 bp). These rings could be decorated with diverse modifications, like polyamides or RNA kissing loops,<sup>84</sup> which enable the assembly of two or more rings into dimers and polymeric aggregates.<sup>91</sup> Besides, it was possible to thread such ring on a DNA axle that was equipped with circular DNA stoppers in order to form a ds DNA pseudorotaxane, which could be converted into a rotaxane by adding release ODNs.

The overall goal of this project was to generate functional devices like switches, nanomechanical machines or computing units made of interlocked DNA architectures. In the following, the structuring of this goal into different approaches is given.

Chapter 4.1 elucidates how a DNA rotaxane is manipulated in a way that a reversible pseudorotaxane to rotaxane conversion can be achieved (see Figure 3.1). The pseudorotaxane has entirely different properties than the rotaxane, as in the latter, the threaded macrocycle can perform translational and rotational movement along the axle, whereas in the pseudorotaxane, the macrocycle is stalled on the axle. To extend the scope of this system, different switching strategies are explored in order to achieve efficient pseudorotaxane/rotaxane conversion, by means of toe-hold, pH and light triggered mechanisms.

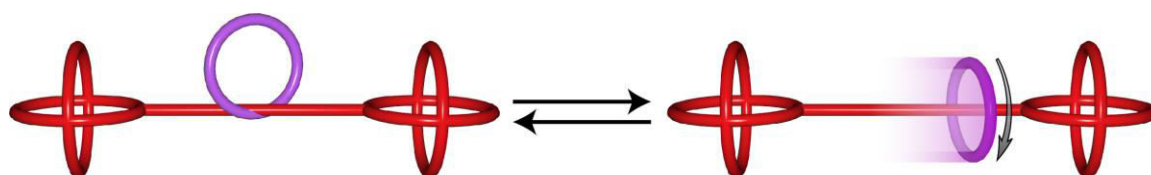


**Figure 3.1.** Scheme of the reversible switching of the macrocycle mobility in a rotaxane.

In chapter 4.2 it is shown that the possibility to switch the macrocycle between a stalled and a mobile state allows switching the macrocycle from one position towards the other. For this purpose, non-symmetric rotaxanes with two stations on the axle and two docking sites in the macrocycle should be assembled (see Figure 3.2). Toe-hold and light switching mechanisms were intended to trigger the accessibility of both stations. By

---

blockade of the station with the stalled macrocycle, the macrocycle should be released into a mobile state, and subsequently dock to the other station. This shuttling process should be determined by AFM since the non-symmetrical nature of the rotaxane enables the discrimination of the macrocycle location, near one or the other stopper.

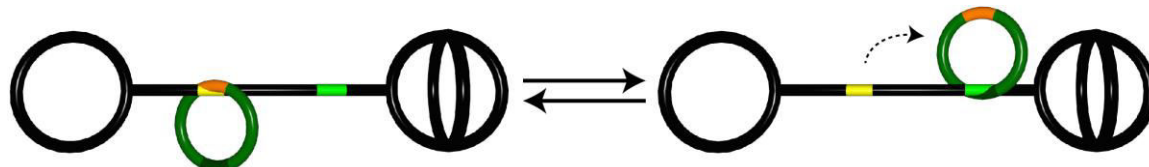


**Figure 3.2.** Scheme of the directed macrocycle translocation in a molecular shuttle based on a rotaxane.

In a follow-up study (see chapter 4.3), a similar system with two threaded macrocycles should be assembled, with the aim that the first macrocycle can be piloted from one station towards the other and thereby displace the second macrocycle. Therefore a [3]pseudorotaxane should be assembled, with a small macrocycle located on the first station, and a bigger shuttle-ring, capable to access both stations, on the second station (see Figure 3.3). By blocking the single stranded gap region of the shuttle-ring capable to bind on the first station, the release of the shuttle-ring would result in dethreading of the latter and the formation of a [2]pseudorotaxane with the small macrocycle threaded. Without blockade of the shuttle-ring, the release would lead to translocation to the first station and thereby replacement of the smaller macrocycle. Subsequent dethreading of the latter would result in a [2]pseudorotaxane with the bigger ring threaded. By carefully triggering of the [3]pseudorotaxane, this system should be able to perform AND logic operations. The system was meant to be analyzed by gel electrophoresis and AFM. Furthermore, the [3]pseudorotaxane should be decorated with a fluorophore/quencher pair in order to have a change in fluorescence emission as output for the logic operation.

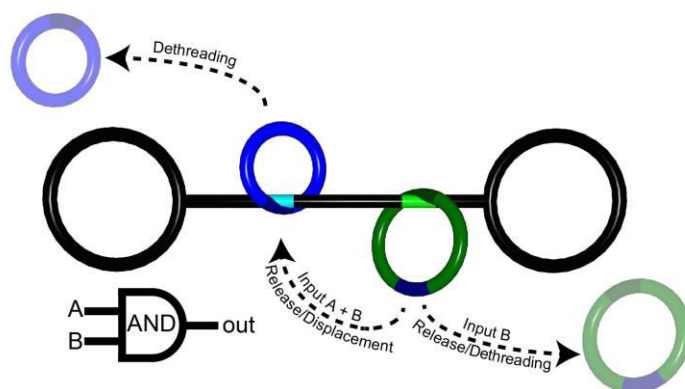


**Figure 3.3.** Scheme of the controlled release of the macrocycles in a [3]pseudorotaxane. This process performs a logic AND operation.

Additionally to the experiments based on rotaxane systems, another aim of this study was to explore a new class of interlocked ds DNA architectures, namely ds DNA catenanes, which is elucidated in chapter 4.4. Catenanes consist of two or more rings interlocked to each other. ss DNA catenanes were already described by Willner *et al.* and proved to be interesting scaffolds for dynamic processes. One ds DNA pseudocatenane was presented by Heckel *et al.*, in which both rings were linked together *via* polyamide-DNA interactions. Since the ss DNA catenanes lack rigidity and the polyamide-based catenane does not exist in a free mobile conformation under native conditions, the assembly and characterization of ds DNA catenanes with structurally stable rings and the possibility to reversibly switch from pseudocatenane- to catenane-state is a desirable goal. ds DNA [2]- and [3]catenanes should be designed, assembled and characterized by means of gel electrophoresis and AFM (see Figure 3.4). The reversible pseudocatenane to catenane switch should be performed and validated by gel electrophoresis and by FQ experiments. In collaboration with Dr. T. Li a [3]catenane system, which can serve as a device capable to reversibly activate and deactivate a DNAzyme, should be analyzed (see Figure 3.4). Therefore, the three different conformations in which the system can be converted (pseudocatenane, catenane and a condensed tetracyclic structure) should be visualized/monitored *via* AFM and FQ measurements.

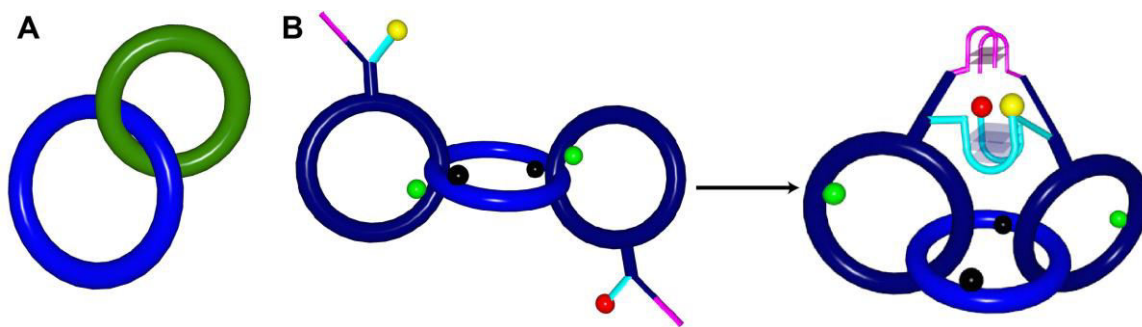


Figure 3.4. Three-dimensional representation of a non-symmetric [2]pseudocatenane (A) and scheme of how the switching of a [3]pseudocatenane into [3]catenane can promote the formation of a tetracyclic structure with an active DNAzyme (B).

---

## 4 Results

### 4.1 Switching of Macrocycle Mobility in an Interlocked DNA Architecture\*

The purpose of the present work was to introduce diverse functionality into interlocked architectures. The first step for this purpose was the introduction of a switch into a rotaxane structure. A rotaxane consists of a macrocycle (from here on termed as ring) threaded on the axle of a dumbbell shaped molecule. This ring can move unhindered translational and rotationally along the axle. The bulky stoppers located at the ends of the axle prevent it from dethreading. In a pseudorotaxane, the ring is immobilized on the axle. The switch should provide the possibility to switch in a reversible fashion between the stalled and mobile state of the ring (see Figure 3.1). First, the assembly of the rotaxane will be described, followed by an introduction to the three different switching mechanisms used in this study together with the results of the switching experiments within the rotaxane system.

#### 4.1.1 Assembly and Characterization of DNA Rotaxanes for Switching Applications

The design of the rotaxane was adapted from the work by Famulok *et al.* (see 2.7).<sup>82</sup> The assembly scheme is given in Figure 4.1.A. The first step is the threading of the ring on the axle, which is driven by the interaction between the complementary ss gap regions of the ring and axle. In the second step, the spherical stoppers are added and subsequently, hybridize with their sticky-ends to the sticky-ends of the axle followed by enzymatic ligation resulting in the pseudorotaxane structure. Addition of the RO releases the ring from the axle and the rotaxane structure is formed. Rotaxanes with less bulky ring stoppers, which were also used in this study, are assembled similarly. The secondary structure of the axle and the ring is given in Figure 4.1.B. For further switching

---

\* Parts of this chapter were taken and adapted from: Lohmann, F.; Ackermann, D.; Famulok, M. *J. Am. Chem. Soc.* **2012**, *134*, 11884-11887.





Indeed, AFM images of the purified ring stopper were taken. Therefore, the structure was immobilized on a mica surface and analyzed either with intermittent contact mode in air (AC mode) or with contact mode in liquid (Hyperdrive™ mode) (Figure 4.2.B). In both images the circular shape of the structure can be clearly observed. Nevertheless, the image taken in Hyperdrive™ mode provides better quality, which allows the resolution not only of the circular shape but also of the sticky-end of the ring stopper.

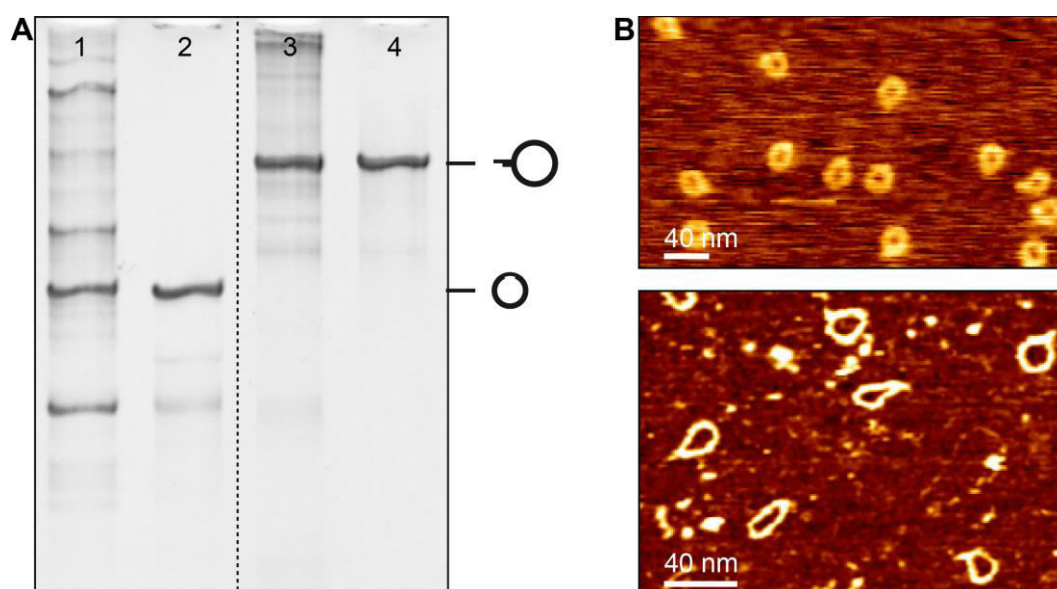


**Figure 4.2.** A) Analytical PAGE image of the crude and HPLC purified 126 bp gap ring (lanes 1 and 2) and 168 bp ring stopper (lanes 3 and 4). The uncropped PAGE image is given in Supporting Figure 1.A B) AFM images of the 168 bp ring stopper. The upper image was taken with intermittent contact mode in air, the lower image was taken with contact mode in liquid. The larger area AFM image is given in Supporting Figure 1.B.

The spherical stoppers consist of two 168 bp rings (SSt-ring1 and SSt-ring2) linked together *via* two Holliday four-way junctions. The synthesis was adapted from reference<sup>85</sup>. First, both rings were assembled and ligated as described above, analyzed by PAGE (see Figure 4.3.A) and then used for the spherical stopper assembly without further purification. Since SSt-ring1 encodes two single stranded regions for hybridization with four sticky-ends of SSt-ring2, the spherical stopper self-assembles after mixing both rings. WAX HPLC of the assembled and ligated product yielded the pure stopper, which was analyzed by agarose gel electrophoresis (see Figure 4.3.B).

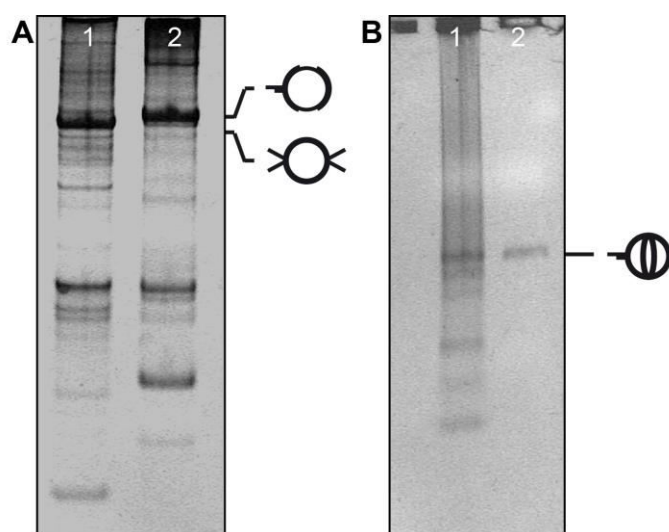


**Figure 4.3.** A) Analytical PAGE image of the SSt-ring1 and SSt-ring2. B) Analytical agarose gel image of the crude and purified spherical stopper.

The assembly of the rotaxane structure was performed as described above. After threading of the ring at low temperature, the stoppers were annealed and ligated. The products of the pseudorotaxane assembly with ring- and spherical-stoppers were analyzed by agarose gel electrophoresis. Addition of the RO to the pseudorotaxane with ring stoppers leads to the release of the ring and dethreading, since the ring stoppers allow slippage of the ring over time (see chapter 2.7). Hence, only pseudorotaxane could be analyzed by gel. As a reference, the dumbbell structure without the ring threaded was assembled and loaded on the gel (see Figure 4.4.A). Figure 4.4.B shows the analytical agarose gel image of the pseudorotaxane with spherical stoppers before and after addition of the RO. The RO releases the ring whereas the bulky stoppers prevent dethreading. Hence, a stable rotaxane structure is formed. The formation of the rotaxane from the pseudorotaxane results in a faster electrophoretic mobility, which is explained by the higher flexibility of the system when the ring is released.

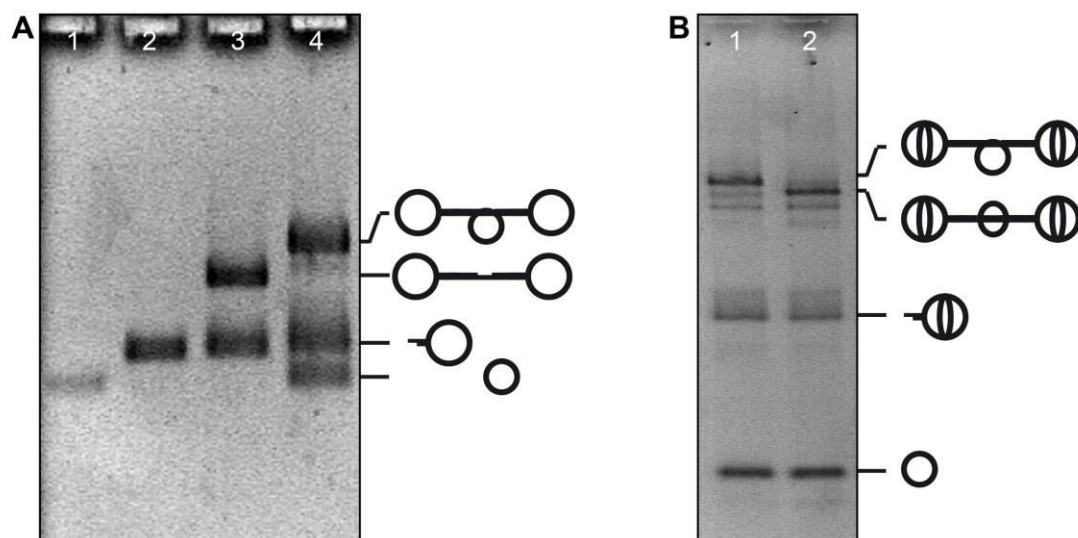


**Figure 4.4.** A) Analytical agarose gel image of the 126 bp gap ring (lane 1), the ring stopper (lane 2), the dumbbell structure with ring stoppers (lane 3) and the pseudorotaxane with ring stoppers (lane 4). B) Analytical agarose gel image of the pseudorotaxane with spherical stoppers before (lane 1) and after (lane 2) addition of RO.

The pseudorotaxane with spherical stoppers was purified by WAX HPLC. As evident from the HPLC chromatogram (see Figure 4.5.A) the pseudorotaxane can be isolated out of the reaction mixture and represents the major product. In order to confirm the shape of the pseudorotaxane, AFM imaging of this sample was performed. The image of a pseudorotaxane recorded with Hyperdrive™ mode unequivocally confirms the predicted structure containing two spherical stoppers at the end of an axle with a ring threaded (see Figure 4.5.B).

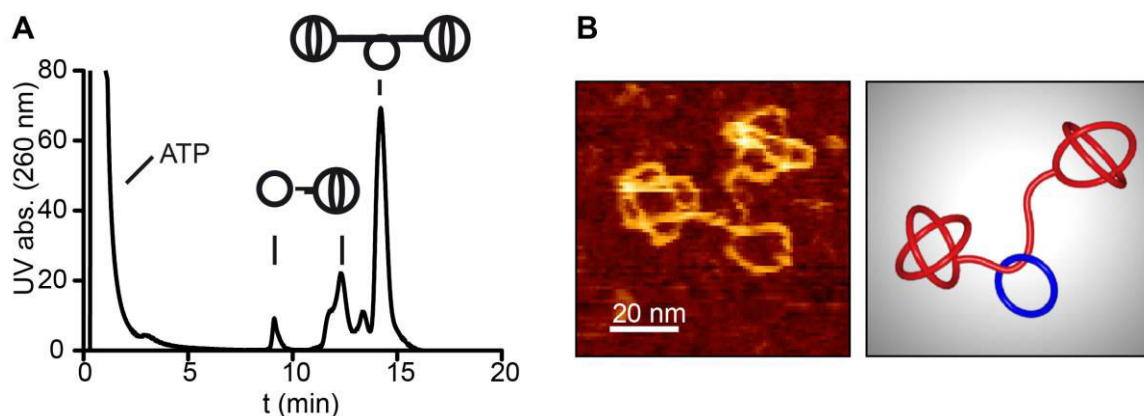


Figure 4.5. A) HPLC chromatogram of the pseudorotaxane with spherical stoppers. The precursor peaks (gap ring and stopper), the product peak (pseudorotaxane) as well as the ATP peak (resulting from the ligation buffer) are indicated. B) AFM image of a pseudorotaxane taken with contact mode in liquid (left) and a 3D representation of how the pseudorotaxane arranges on the mica surface (right). The AFM image was provided by Dr. D. Ackermann.<sup>92</sup>

#### 4.1.2 Toe-hold Switch

Nanoassemblies might be used for a broad variety of applications. Hence, the triggering of those might meet diverse requirements. Several switching mechanisms have been developed in the field of DNA nanotechnology and all of them have their pros and cons (see Table 2.1). In order to fulfill diverse requirements three different switching mechanisms have been used in this study to trigger the interlocked DNA assemblies: the toe-hold mechanism (see chapter 2.2.6.1), the pH based mechanism (see chapter 2.2.6.2) and the light switch (see chapter 2.2.6.3). In the following the results of the switching experiments using these three mechanisms to trigger the motion of the threaded ring of the DNA rotaxanes will be presented.

In order to integrate the toe-hold switch into the rotaxane system, the RO used for the release of the threaded ring was modified with a seven nucleotides long toe-hold. With the use of an ODN entirely complementary to the toe-hold RO the latter can be displaced from the axle. The sequences of the rotaxane axle, the toe-hold RO (TH-RO1) and of the complementary ODN (cODN1) are shown in Figure 4.6.A. The free energy of a duplex of the TH-RO1 and the twelve bases of the axle to which it is complementary was calculated to be approx. -20 kcal/mol whereas the free energy of the waste duplex was approx. -30 kcal/mol (the values were calculated using the nearest-neighbor empirical parameters and 50 mM Na<sup>+</sup> and 20 mM Mg<sup>2+</sup> concentrations with the open access DNA

analysis program available on [www.nupak.org](http://www.nupak.org))<sup>93-94</sup>. To prove that the decrease in free energy of approx. 10 kcal/mol is sufficient to provoke quantitative strand displacement, a hybridization experiment was performed. Two samples were prepared, the axle alone and the axle after addition of TH-RO1. From the second sample an aliquot was taken before an excess of cODN1 was added (third sample).

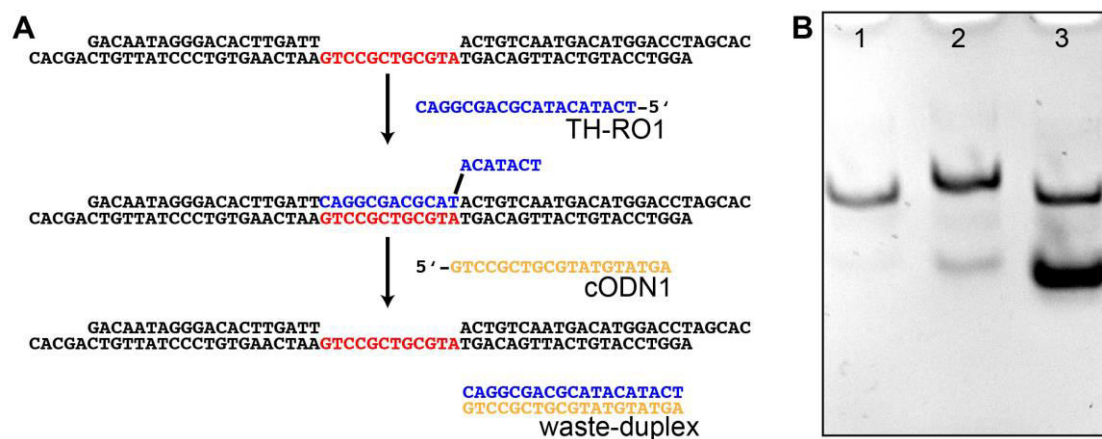


Figure 4.6. A) Sequences of the rotaxane axle together with or without TH-RO1 and cODN1. B) Analytical PAGE image of the axle (lane 1), the axle after addition of TH-RO1 (lane 2) and after subsequent addition of excess cODN1 (lane 3).

All three samples were analyzed by PAGE (see Figure 4.6.B). While the axle alone and the axle after addition of TH-RO1 and cODN1 show the same electrophoretic mobility on the gel, the axle with the TH-RO1 exhibits a lower electrophoretic mobility due to the higher mass of the formed complex. The excess of cODN1 leads to an additional band with a high electrophoretic mobility. The presented PAGE image demonstrates the capability to remove the RO from the axle simply by adding fuel DNA.

#### 4.1.2.1 Switching of Macrocycle Mobility *via* Toe-hold Mechanism

The DNA fuel mediated strand displacement reaction was utilized to reversibly switch the mobility of the threaded ring in the rotaxane from a stalled state (pseudorotaxane) into a mobile state (rotaxane) in which the ring can move unhindered along the axle. The concept for the reversible ring displacement is illustrated in Figure 4.7. Starting from the pseudorotaxane with the ring hybridized to the gap of the axle (light green), TH-RO1 (dark green) was added. As described above, the RO releases the ring into a mobile state (see chapter 4.1.1). In order to switch back to the stalled state, cODN1 was added.

---

Consequently cODN1 and TH-RO1 form a thermodynamic stable waste duplex thereby releasing the gap of the axle. This finally allows the hybridization of the ring to the axle.

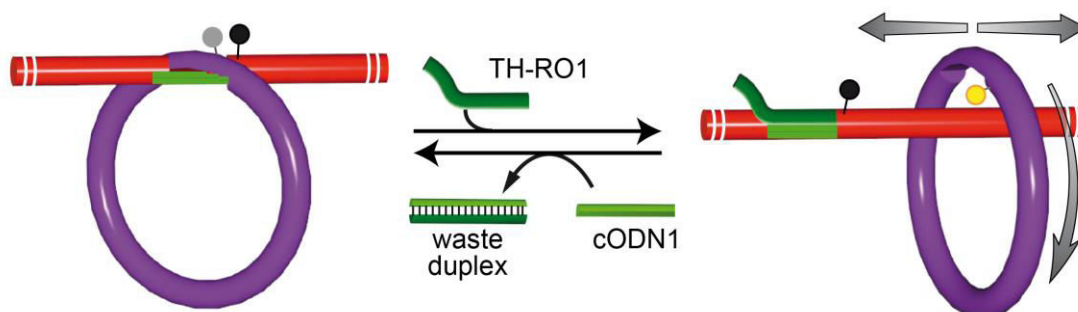


**Figure 4.7.** Scheme for the DNA fuel induced reversible ring displacement. Upon addition of TH-RO1, the macrocycle is released and moves unhindered along the axle. Addition of cODN, complementary to TH-RO1 replaces the later, resulting in the fixation of the macrocycle on the axle. The grey/yellow sphere represents a Cy3 label, the black sphere a BHQ-2 label. The stoppers are not shown. The image was taken and slightly modified from reference <sup>95</sup>.

The pseudorotaxane/rotaxane switching experiments were performed with a non-purified pseudorotaxane sample, which was assembled as described above (see chapter 4.1.1). The aim was to illustrate whether the pseudorotaxane or the rotaxane state is formed after subsequent switching events. Hence, electrophoretic mobility assays were performed. Pseudorotaxane and rotaxane (ring released with unmodified RO) were loaded on the gel as reference, taking into account that the rotaxane has a higher electrophoretic mobility. The switching was performed as follows. First, TH-RO1 was added to the pseudorotaxane to trigger the release of the ring. Then, cODN1 was added, which should lead back to pseudorotaxane with the stalled ring. Such switching cycle was performed twice and an aliquot of each state was loaded on the gel. As evident from the gel image shown in Figure 4.8.A the band corresponding to the interlocked assembly shifts towards higher electrophoretic mobility after addition of RO and TH-RO1 respectively, while the electrophoretic mobility is lower in the case of the pseudorotaxane and after addition of cODN1. Additionally it is obvious that the shifting occurs almost quantitatively; indicating that the implementation of a toe-hold to the RO allows highly efficient pseudorotaxane/rotaxane switching.

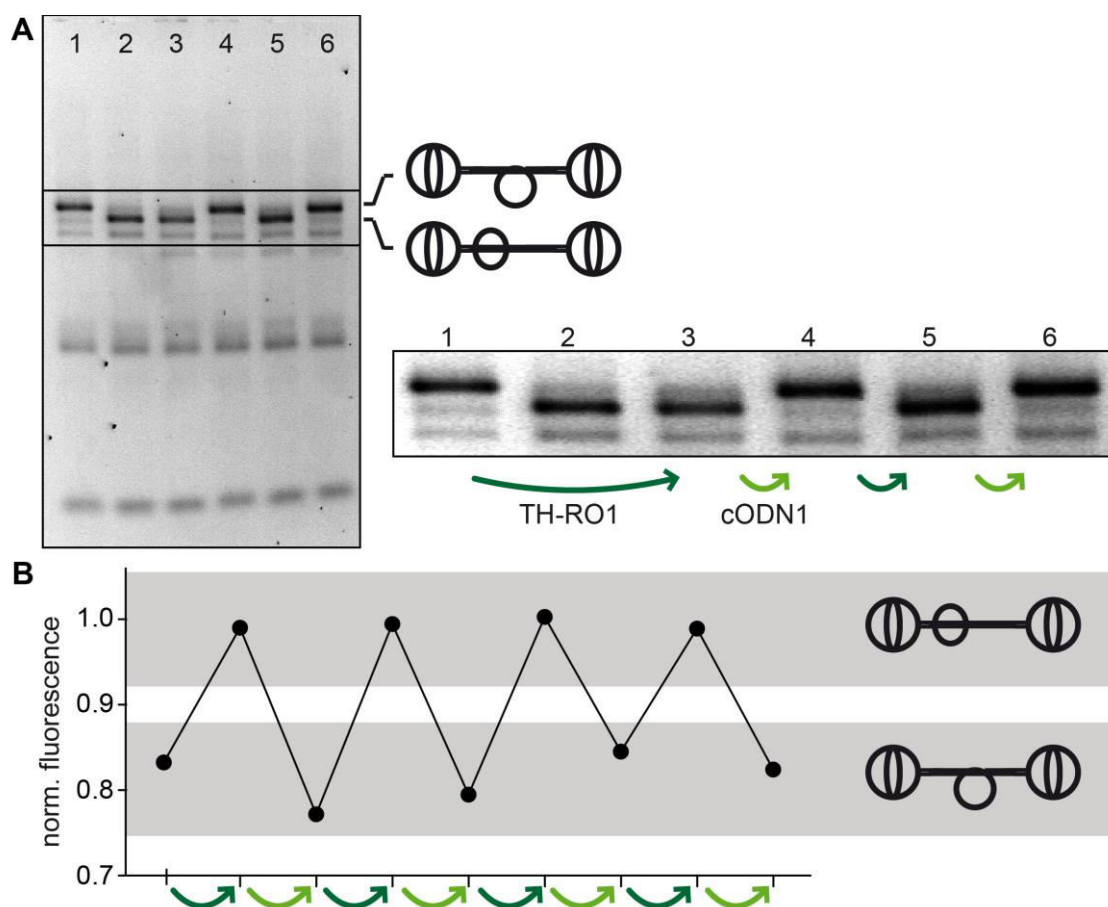


**Figure 4.8.** A) Analytical agarose gel image of the pseudorotaxane/rotaxane switching. Pseudorotaxane (lane 1) and rotaxane (lane 2) were loaded as references. Lanes 3-6 represent the pseudorotaxane sample after consecutive addition of TH-RO1 (lane 3/5) and cODN1 (lane 4/6). A detailed view of the gel is shown on the right. B) Results of the FQ experiment using the Cy3/BHQ-2 labeled pseudorotaxane sample. Starting from the pseudorotaxane TH-RO1 and cODN1 were added consecutively and fluorescence emission was measured. The images were taken and slightly modified from reference<sup>95</sup>.

Furthermore, with the intention to find out whether the switching can be performed for more than two cycles, fluorescence quenching (FQ) experiments were performed. Labeling of the ring and the axle with a fluorophore (Cy3) and a quencher (BHQ-2) as illustrated in Figure 4.7 allows to determine whether the ring is hybridized to the axle or not. Since the fluorophore/quencher pair is in close proximity when the ring is hybridized on the axle, a decrease of the fluorescence intensity is consequently observed. Conversely, they are separated when the ring is released, which results in an increase of fluorescence. The switching was performed as before, but now, four cycles of switching were performed and fluorescence emission was measured to distinguish between the pseudorotaxane- and rotaxane-state. Figure 4.8.B illustrates that

---

pseudorotaxane/rotaxane switching can be performed for up to four cycles without no evident fatigue.

### **4.1.3 pH Switch**

To introduce this switching mechanism into the rotaxane structure, an i-motif sequence was encoded into the gap of the axle. At neutral pH the ring should hybridize to the gap as described before, but at acidic pH the gap converts into the i-motif and thereby releases the ring (the switching principle is depicted in Figure 4.10, the sequences used to assemble the axle and an i-motif test-ODN are given in Figure 4.9.A). The pH induced switch was tested with a preliminary fluorescence polarization (FP) assay before applying it to the rotaxane system. With this method it is possible to differentiate between a big fluorescent molecule (high FP) and a smaller fluorescent molecule (low FP). For this experiment, a dumbbell containing the i-motif sequence encoded in the gap of the axle was assembled. The rhodamine green labeled i-motif test-ODN was added at a neutral pH, and since this ODN consists of a sequence partially complementary to the gap of the axle, both form a duplex (see Figure 4.9.B). Note that the sequence used for the i-motif test-ODN will later be used for the gap of the ring predestined to thread on the axle.



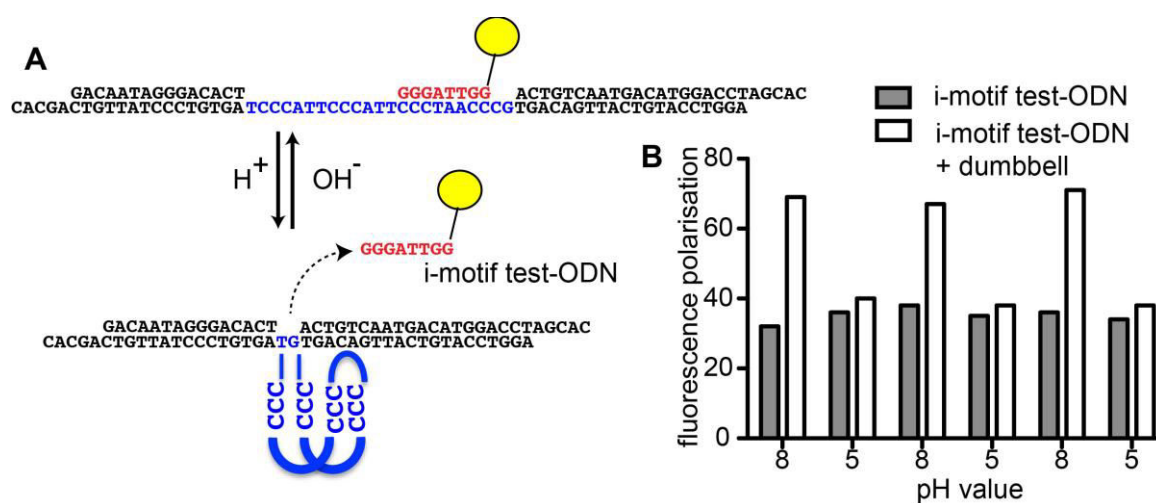


**Figure 4.9.** A) Sequences of the rotaxane axle with the i-motif test-ODN used for the FP assay. The yellow sphere represents a rhodamine green label. B) Result of the FP assay. Fluorescence polarization of the dumbbell together with the i-motif test-ODN after subsequent pH adjustments to pH 8 and 5 was measured. At pH 8, the i-motif test-ODN hybridizes on the gap of the dumbbell resulting in high FP, at pH 5 the gap of the axle forms the i-motif, leading to the release of the i-motif test-ODN and subsequent decrease in FP.

After measuring the FP, the pH was adjusted towards acidic and the FP was measured again. At low pH, the axle should form the i-motif quadruplex structure and thereby release the i-motif test-ODN resulting in a lower FP. As a reference, the i-motif test-ODN alone was also measured at the corresponding pH. The result presented in Figure 4.9.B corroborates this hypothesis as the mixture of dumbbell and i-motif test-ODN shows a higher FP at pH 8 than the mixture at pH 5 or the i-motif test-ODN alone. Besides, repetitive switching can be performed with this system. This result proves the potential use of the pH induced switch for the pseudorotaxane/rotaxane switch.

#### 4.1.3.1 Switching of Macrocycle Mobility *via* pH Adjustment

Encouraged by these results, a ring-stoppered pseudorotaxane with the i-motif sequence encoded in the gap of the axle was assembled (see Figure 4.11.B, for details of the secondary structure and for DNA sequences see Supporting Table 1 and Supporting Table 2). Using this pseudorotaxane, a dethreading experiment was performed. According to the mechanism shown in Figure 4.10, the ring of the pseudorotaxane should be released and subsequently dethreaded when the pH is adjusted towards acidic (see Figure 4.11.A).

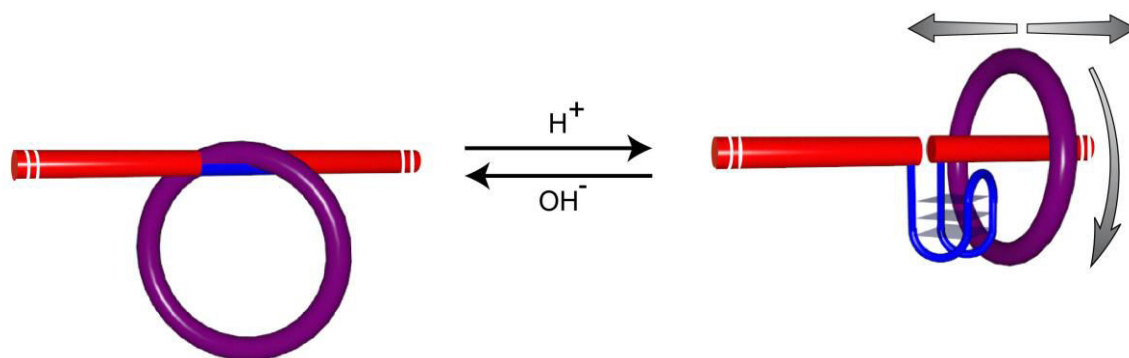


**Figure 4.10.** Scheme of the pH induced reversible ring displacement. At neutral pH, the macrocycle is threaded on the i-motif encoding ss gap region of the axle. Upon changing the pH towards acidic, the i-motif is formed and thereby the macrocycle is released. Addition of base reverts this process. The stoppers are not shown.

In order to perform a pH induced pseudorotaxane/rotaxane switch, the buffer of the pseudorotaxane was exchanged first from ligase buffer to Tris-Acetate (TA) buffer at pH8 and then to TA buffer at pH 5. After incubation, aliquots of the samples in the different buffers were analyzed by agarose gel electrophoresis, together with a dumbbell sample as reference (see Figure 4.11.B). The gel image clearly shows a dominant band with higher electrophoretic mobility for the dumbbell sample and with lower electrophoretic mobility for the pseudorotaxane sample in ligase buffer and TA buffer at pH 8, as expected. In the case of the pseudorotaxane sample at pH 5, an increase of the dumbbell-band (higher electrophoretic mobility) accompanied with a decrease of the pseudorotaxane-band (lower electrophoretic mobility) was expected, due to ring release and subsequent dethreading. Indeed, a slight increase of the dumbbell band can be observed; nevertheless, this increase is marginal, indicating a low switching efficiency. A possible explanation for this poor efficiency could be that the i-motif is less stable than the DNA duplex formed by the ring and the axle in this interlocked structure. Despite this result, Dr. T. Li successfully utilized a bimolecular i-motif sequence to trigger a different interlocked DNA architecture (see chapter 4.4.3).

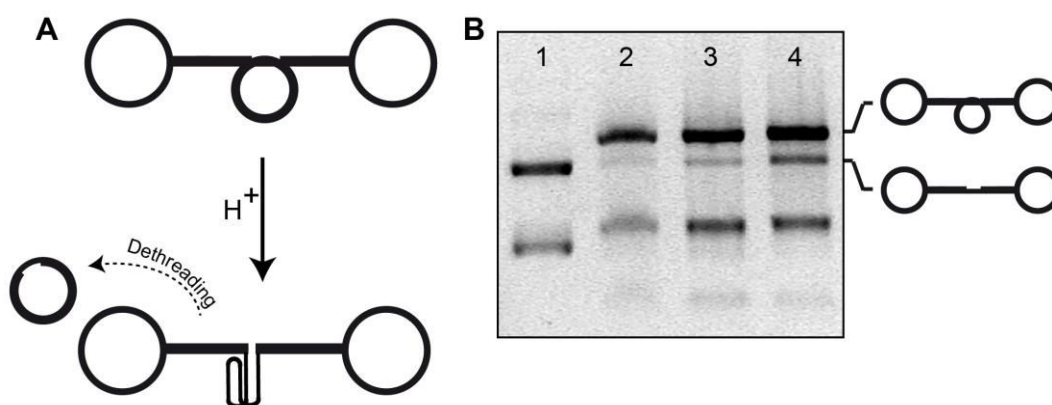


Figure 4.11. A) Scheme of the pH induced dethreading experiment. B) Analytical agarose gel image of the dumbbell (lane 1) and the pseudorotaxane containing the i-motif sequence in ligase buffer (lane 2), in TA buffer at pH 8 (lane 3) and in TA buffer at pH 5 (lane 4).

#### 4.1.4 Light switch

The light induced switch is an elegant way to switch DNA hybridization on and off, and present several advantages with respect to other switching methods (see Table 2.1) e.g. it is non-invasive, produces no pollution of the system and no additional fuel materials are consumed. Thus, it can be considered a “clean” switch with low fatigue.

##### 4.1.4.1 Synthesis and Characterization of Light Sensitive ODNs

In this study, two different azobenzene derivatives were introduced into DNA in order to obtain light sensitive ODNs, the AB and the DMAB. In both cases, the first step in order to obtain light sensitive ODNs is the synthesis of a DMT-protected azobenzene-phosphoramidite, required for solid phase DNA synthesis. In these molecules, the azobenzene is linked to a threoninol moiety, which carries a phosphoramidite and a DMT-group. The synthetic route for the DMAB phosphoramidite was adapted and slightly modified from Asanuma *et al.*<sup>28</sup> and is depicted in Figure 4.12. Starting from ethyl 4-nitrobenzoate, the nitro-group was reduced to a nitroso group *via* two steps in a one-pot reaction. In the first step, zinc was used to reduce the nitro to an amino group in ammonium chloride/water solution. In the second step, the oxidation to the nitroso-group was mediated by iron(III)chloride in an ethanol/water mixture. An azocoupling of the ethyl 4-nitrosobenzoate with 2,6-dimethylaniline in glacial acid under  $H_2O$  elimination followed by hydrolysis of the ester group with sodium hydroxide resulted in

the 4-carboxy-2',6'-dimethylazobenzene. In the next step, the HBTU activated carboxyl group was coupled to the amino group of D-threoninol *via* amide bond formation. The primary hydroxyl group of the threoninol moiety was protected with DMT. The reaction was carried out in pyridine by adding DMT-Cl under anhydrous conditions. In the last step, the DMAB phosphoramidite was formed by coupling of 2-cyanoethyl-N,N-diisopropylphosphoramidite to the secondary hydroxyl group of the threoninol moiety in dimethylformamide supplemented with diisopropylethylamine under anhydrous conditions. All intermediates were purified and subsequently analyzed by NMR.

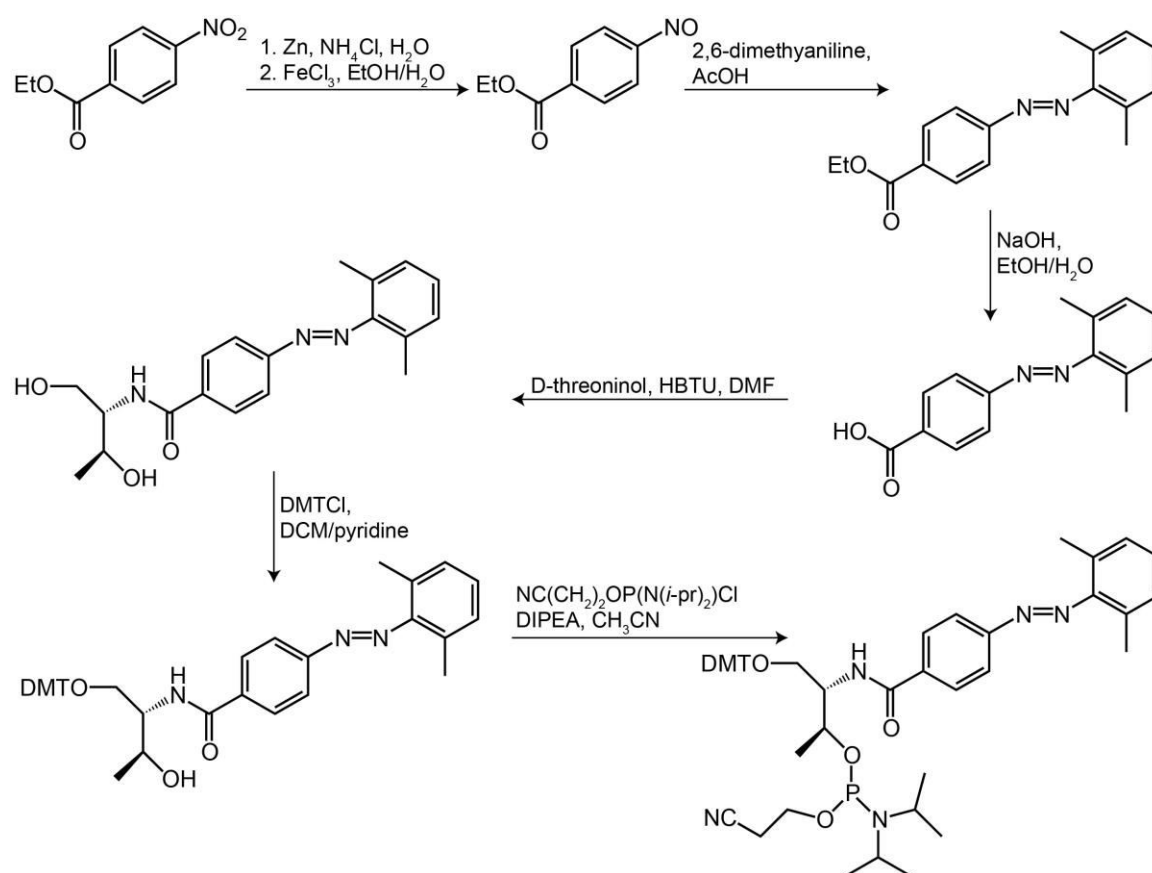


**Figure 4.12.** Synthesis route for the synthesis of the DMT protected DMAB phosphoramidite.

The resulting orange compound was used as a precursor for further DNA synthesis. The synthesis of the azobenzene phosphoramidite was performed similarly, starting with the commercially available 4-carboxyazobenzene and performing the last three steps beforehand described.

Following the same principle as presented for the toe-hold mediated pseudorotaxane/rotaxane switch (see chapter 4.1.2), the idea now was to modify the RO, responsible for the ring release in the pseudorotaxane system with azobenzene moieties, so that this azobenzene-release oligo (AB-RO) can be activated/deactivated by irradiation with light of specific wavelength. The switching principle is depicted in Figure 4.17 and will be explained in detail later. Before switching experiments with the pseudorotaxane system were performed, different AB-ROs and dimethylazobenzene ROs (DMAB-ROs) were synthesized and their switching capability was evaluated.

With the different azobenzene phosphoramidites in hand, AB and DMAB modified ODNs were synthesized by using an automated solid phase DNA synthesizer. First, six different AB modified ROs were synthesized (see Figure 4.13.C) and tested, but since the final results (see Figure 4.19) were not entirely satisfying, a DMAB-RO was synthesized (see Figure 4.13.C) and used for further experiments. After solid phase synthesis, the DNA was cleaved from the solid support and all protecting groups were removed. Then the crude products were analyzed and purified by means of reverse phase HPLC (see Figure 4.13.A and B). The concentration was calculated from the UV absorption at 260 nm. For the DMAB5-RO, mass analysis was performed for its unequivocal characterization (see Figure 4.13.D).

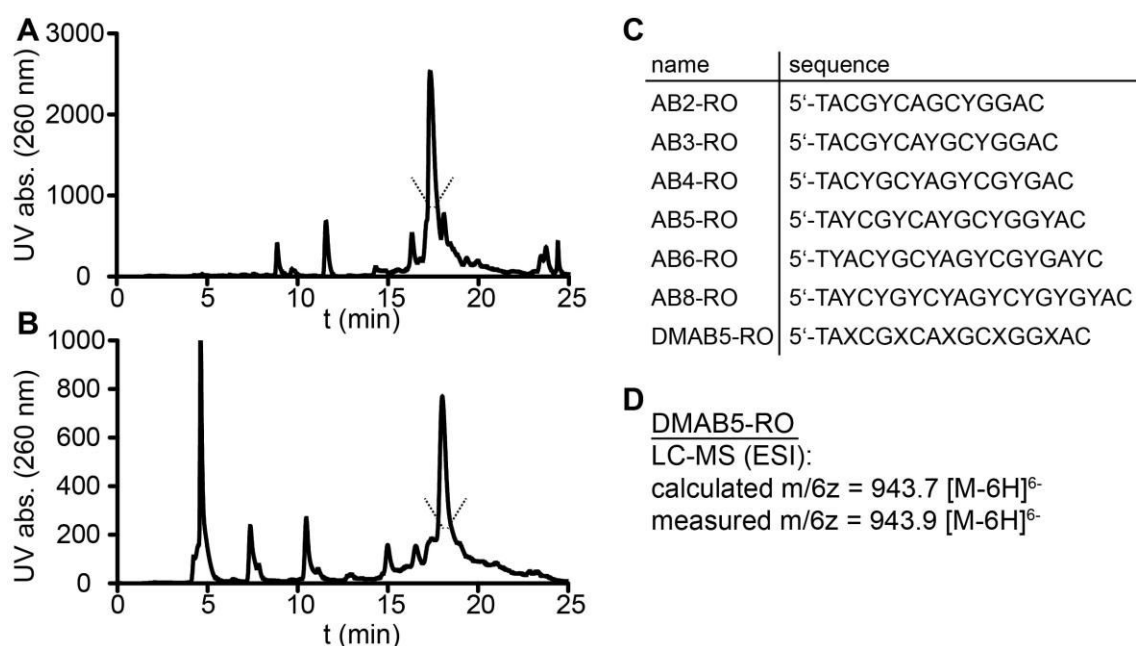


**Figure 4.13.** A) HPLC chromatogram of the AB2-RO. B) HPLC chromatogram of the DMAB5-RO. C) Table with the names and sequences of all modified AB- and DMAB-ROs used in this study. The number in the name represents the amount of AB- or DMAB-moieties incorporated. The Y represents one AB modification, the X one DMAB modification. D) Calculated and measured mass of the DMAB5-RO.

A convenient method to prove whether the AB (or DMAB) is isomerized into the *trans*- or the *cis*-form, respectively, is to measure its UV/vis-absorption spectrum. In the *trans* form, the absorption at 340 nm is increased while the absorption at 450 nm is decreased in comparison to the *cis* form. In order to establish an efficient and reversible switching mechanism, the reversible *trans* to *cis* isomerization was tested. Therefore, the DMAB5-RO was irradiated alternately with vis- and UV light. After each irradiation event the UV/vis spectrum of the DMAB5-RO was measured in order to assess its isomeric conformation. Figure 4.14.A shows the UV/vis-absorption spectrum of the DMAB5-RO after vis- (blue) and UV-irradiation (purple). The change in absorption at 340 nm can be clearly observed, indicating the possibility to trigger the modified ODN with light. The light switching was performed 14 times and the change in absorption at 340 nm after every irradiation event was measured (see Figure 4.14.B), the result proves robust switching reversibility.

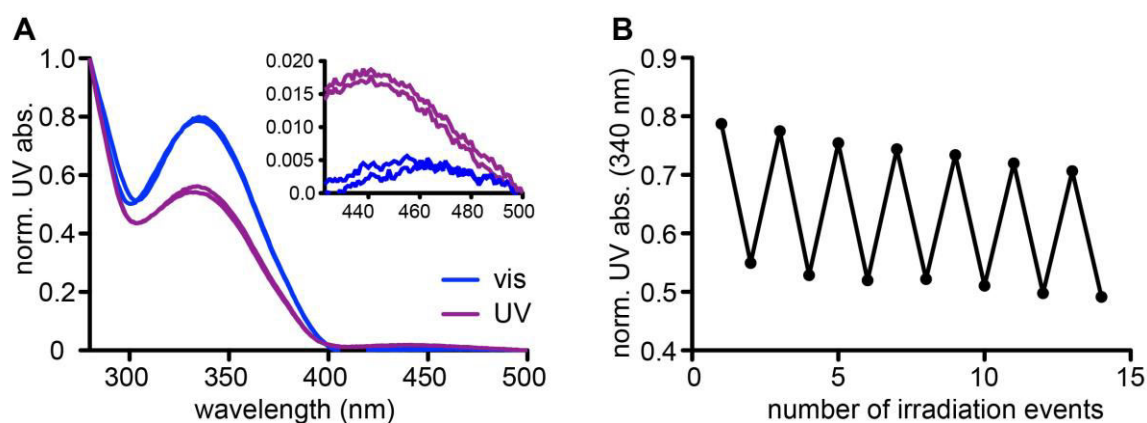


**Figure 4.14.** A) UV/vis-absorption spectra of the DMAB5-RO after two cycles of UV- (purple) or vis-irradiation (blue). The increase in absorption at 340 nm after vis irradiation is caused by the *cis* to *trans* isomerization. B) UV absorption at 340 nm of the DMAB5-RO measured after UV- or vis-irradiation (14 irradiation events).

As mentioned above, the *cis* to *trans* isomerization is not only light induced but also thermally. Since the latter decreases the selectivity and applicability of the switch, a thermally stable azoswitch is desired. Thus, it is crucial to assess the thermal stability of these molecular triggers, in order to improve and tune their switching ability. Therefore, lifetime measurements of the AB2-RO and the DMAB5-RO were performed as follows. First the UV/vis absorption of the corresponding ODN was measured after vis irradiation. Then, the sample was irradiated with UV and a kinetic analysis of its absorption spectra was performed at different temperatures (25 and 60 °C, respectively). An increase in absorption at 340 nm allowed monitoring the thermal *cis* to *trans* isomerization. As evident from Figure 4.15, at 25 °C the UV absorption at 340 nm of the *cis* species (after UV irradiation) only marginally increases in the case of the AB, and remains unaffected in the case of the DMAB even after 12 h. After 4 h incubation at 60 °C the absorbance of the *cis* species of the AB was almost the same as for the *trans* species (after vis irradiation), thus, thermal *cis* to *trans* isomerization occurred. However, this effect was not observed for the DMAB. Even after 24 h at 60 °C almost no increase of absorption was detected. This result is in agreement with published data, which described a higher thermal stability of the DMAB in comparison with the AB.<sup>29</sup> The thermal stability of the *cis* species of both tested ODNs was high at 25 °C, the temperature at which most experiments of this study were performed.

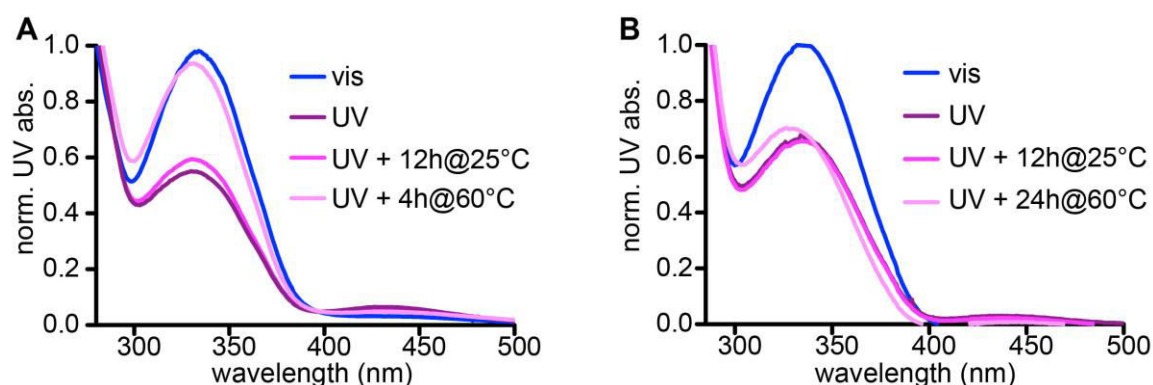


Figure 4.15. A) Lifetime measurements of the AB modified ODN AB2-RO. UV/vis absorption spectra was measured before and after irradiation with UV light. The increase of absorption at 340 nm over time at different Temperature was detected. B) Lifetime measurements of the DMAB modified ODN DMAB5-RO. O. Wolters performed the measurements under the author's supervision as part of her diploma-thesis.

#### 4.1.4.2 Switching DNA Hybridization with Light

Before the AB- or the DMAB-ROs were applied to the pseudorotaxane system, the switching of DNA hybridization was preliminarily tested. The switching principle is shown in Figure 4.16.A. Since the RO sequence remained unaltered compared with the toe-hold switched system, only the photo switchable molecular modifications were introduced and thus, the basic design of the rotaxane remained unchanged. The sequences used to assemble the axle together with a light switch test-ODN are given in Figure 4.16.A. The light switch test-ODN contains the sequence, which is encoded in the ring to thread on the axle. The light switch test-ODN was used to prove the feasibility of the modified ROs in terms of activation/deactivation by means of vis/UV irradiation in an FQ experiment. Therefore, the light switch test-ODN was labeled with a fluorophore (Cy3) and the axle with a quencher (BHQ-2). When this ODN is hybridized on the axle the fluorescence of Cy3 is quenched and thus, displacement of the light switch test-ODN leads to an increase of fluorescence. The experiment was performed as follows: first the AB modified RO was irradiated with UV light, added to the preassembled axle and the fluorescence of the sample was measured. Then, the system was irradiated with vis light before measuring the fluorescence again. Such switching cycle (UV- and vis- irradiation) and the corresponding fluorescence measurement were performed three times. The increase/decrease in fluorescence after vis/UV irradiation provides a quantitative



method to assess the switching efficiency. The AB modified RO in *trans* form should replace the light switch test-ODN whereas in *cis* form, dehybridization of the RO should occur, followed by rehybridization of the light switch test-ODN and subsequent fluorescence quenching. This experiment was performed with different AB-ROs. The best result in terms of efficiency and reversibility was achieved with the AB6-RO, which was then used for further experiments (see Figure 4.19).

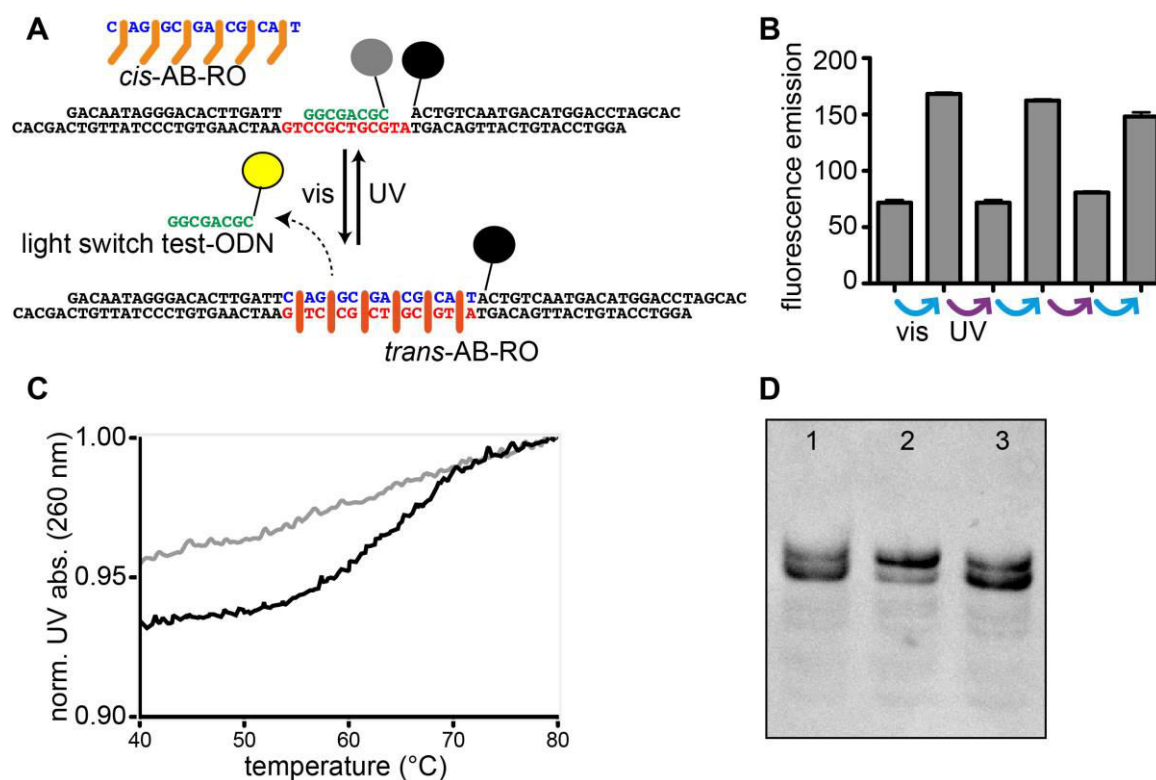


**Figure 4.16.** A) Sequences of the axle, the light switch test-ODN and the AB6-RO. The orange kinked bar represents *cis*-AB, the red bar *trans*-AB. B) Result of the FQ experiment. The fluorescence emission of the system as depicted in Figure 4.16.A before and after subsequent irradiation with vis- and UV-light was measured. The blue arrow represents vis irradiation, the purple arrow UV irradiation. The image was taken and slightly modified from reference<sup>95</sup>. C) DNA melting curves of the DNA duplex of DMAB5-RO and its complementary ODN before (black) and after (grey) irradiation with UV light. D) Analytical PAGE image of the axle together with the DMAB5-RO after UV irradiation (lane 1), subsequent vis- (lane 2) and UV- irradiation (lane 3).

As mentioned above, the results for pseudorotaxane/rotaxane switching with the AB6-RO were not entirely satisfactory: Consequently, DMAB-RO was also evaluated for these switching experiments. Based on the information gained from the FQ experiment with the AB-ROs, the DMAB5-RO containing five DMAB modifications was synthesized and used for further experiments. Note that the DMAB is known to have improved switching

---

properties compared with AB; hence, five DMAB modifications instead of six were considered to be sufficient. The hybridization/dehybridization of the DMAB5-RO with its complementary ODN was examined by means of DNA melting experiments and gel-shift assays. The melting curve of the mixture between the DMAB5-RO and its complementary ODN was measured before and after irradiation with UV light. The corresponding melting curves are presented in Figure 4.16.C. Before UV irradiation, the curve reveals the typical shape for the melting of a DNA duplex, in contrast to the curve measured after UV irradiation. Similar results were found by Asanuma *et al.* for other DMAB modified ODNs. They concluded from this result that in *cis* form no DNA duplex is formed at all. For the gel-shift assays, the DMAB5-RO was irradiated with UV light and mixed with the axle of the dumbbell. An aliquot was taken before irradiating the sample with vis light. After taking another aliquot, the sample was irradiated with UV light. All three aliquots were analyzed by PAGE. A shift to lower electrophoretic mobility was expected after vis irradiation, where hybridization should occur. In the case of UV irradiation, no hybridization of the DMAB5-RO with the axle was expected, thus no gel-shift was observed. The gel image shown in Figure 4.16.D demonstrates the on/off switch of this DNA hybridization by light irradiation.

#### **4.1.4.3 Switching of Macrocycle Mobility *via* Light irradiation**

The concept for the light induced reversible ring displacement is illustrated in Figure 4.17. On the left side, the azobenzene modified RO exists in the *cis* form and is thereby inactivated. Thus, the ring remains stalled on the axle. Irradiation with vis light isomerizes the AB- or DMAB-moieties into the *trans* form, thereby allowing the RO to hybridize on the gap of the axle. Consequently, the ring is released resulting in the rotaxane state with the mobile ring. UV light irradiation reverts this process.

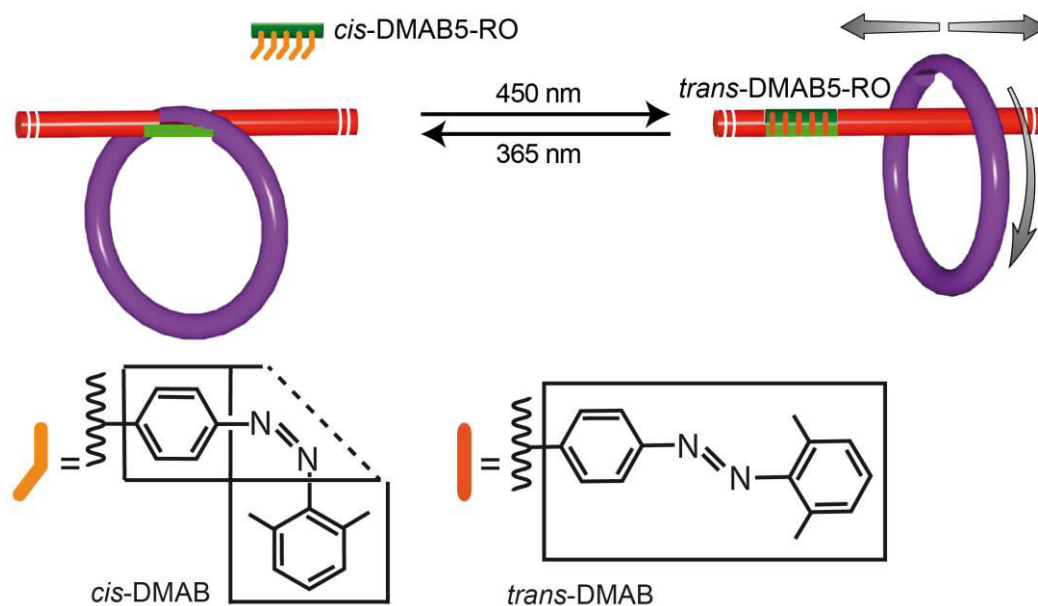


**Figure 4.17.** Scheme of the light induced reversible ring displacement using the DMAB5-RO. When the DMAB moieties are isomerized into the *cis* form, the DMAB5-RO is inactive and the macrocycle is stalled on the axle. Irradiation at 450 nm isomerizes the DMAB moieties into the *trans* form and activates the DMAB5-RO that thereby releases the macrocycle. Irradiation at 365 nm reverts this process. The image was taken and slightly modified from reference <sup>95</sup>.

The first experiment with the rotaxane system performed with a light sensitive RO was a dethreading experiment. A pseudorotaxane with ring stoppers, containing a fluorophore/quencher pair on the ring and the axle was assembled. To this sample, the AB6-RO was added either in its *cis*- or its *trans* form. In the case of the *trans*-AB6-RO, ring displacement and dethreading is expected whereas the inactivated *cis*-AB6-RO should not affect the system (see Figure 4.18.A). The ring replacement was followed by gel electrophoresis and FQ experiments. Therefore, the pseudorotaxane was analyzed on agarose gel before and after addition of the AB6-RO in the *cis*- and the *trans* form. An increase of the dumbbell band was only observed for the pseudorotaxane sample together with the AB6-RO in the *trans* form, indicating the successful deactivation/activation of the modified RO. For the FQ experiment, the fluorescence of the pseudorotaxane was measured before and after addition of the *cis*-AB6-RO. Next, fluorescence was measured after the sample was irradiated with vis light, isomerizing the AB into its *trans* form. Again, the increase in fluorescence only with the AB6-RO in *trans* form indicates successful deactivation/activation of the modified RO.

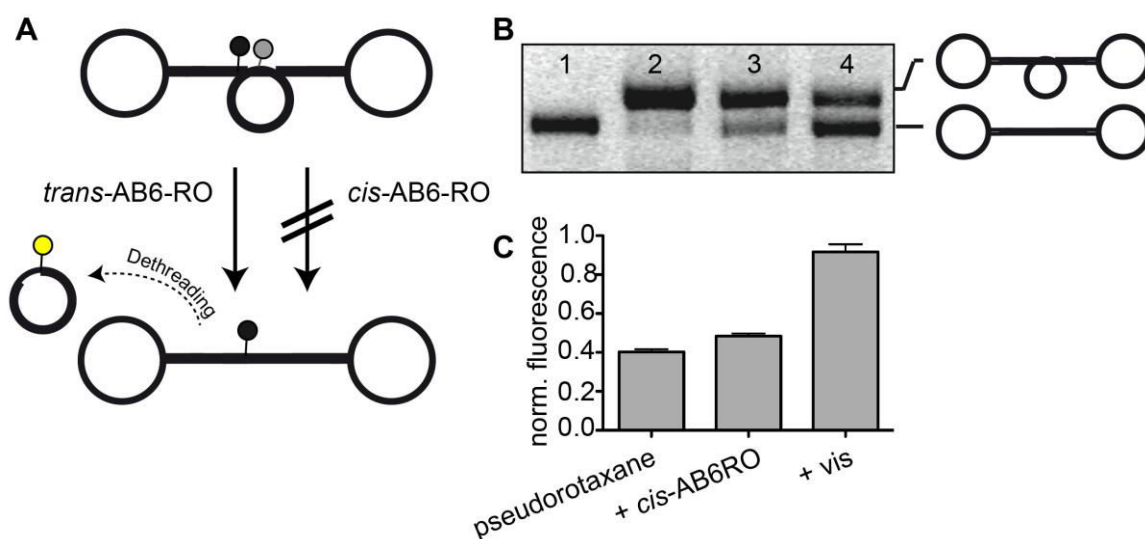
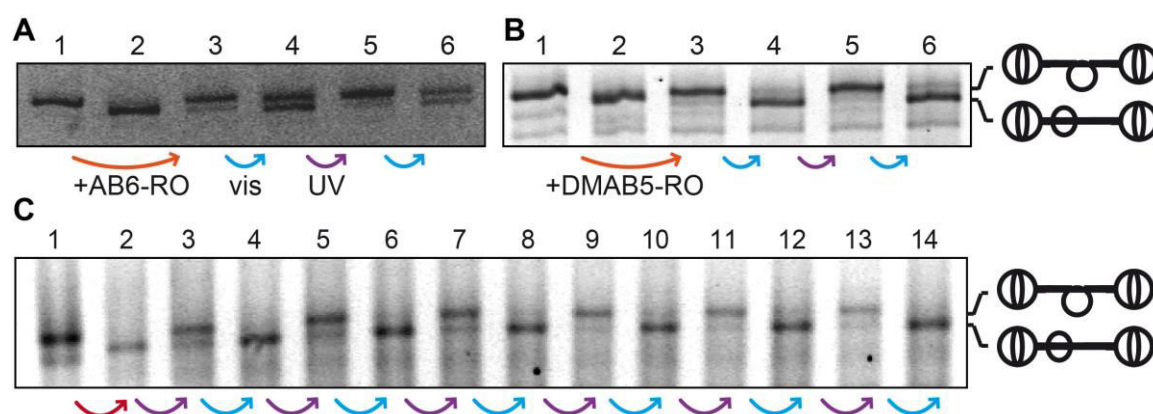


Figure 4.18. A) Scheme of the light induced dethreading experiment using *cis*- or *trans* AB6-RO. The grey/yellow sphere represents a Cy3 label, the black sphere a BHQ-2 label. For more details, see text. B) Analytical agarose gel image of the dumbbell (lane 1), the pseudorotaxane sample (lane 2), the pseudorotaxane sample after addition of the *cis*-AB6-RO (lane 3) and after subsequent irradiation with vis light (lane 4). The uncropped agarose gel image is given in Supporting Figure 2. C) Results of the FQ experiment using the Cy3/BHQ-2 labeled pseudorotaxane. The fluorescence was measured before and after addition of the *cis*-AB6-RO and after subsequent vis irradiation. The image was taken and slightly modified from reference<sup>95</sup>.

Following, the light induced reversible pseudorotaxane/rotaxane switch was performed. Therefore, the pseudorotaxane with spherical stoppers was assembled, so dethreading was prevented. The AB6-RO or the DMAB5-RO was irradiated with UV light in order to isomerize the AB- or DMAB-moieties into the *cis* form and then added to the pseudorotaxane sample. Subsequent irradiation with vis- and UV-light of the sample was performed, which should activate/deactivate the RO accordingly. After each switching event, an aliquot was taken. All aliquots together with a pseudorotaxane and a rotaxane sample as references were analyzed by agarose gel electrophoresis. Figure 4.19.A illustrates the result of the switching experiment performed with the AB6-RO. After addition of the inactivated *cis*-RO, nearly no rotaxane band appears whereas the pseudorotaxane band remained, indicating successful light induced deactivation of the RO. After irradiation with vis light, the intensity of the pseudorotaxane band decreased while the rotaxane band increased. This can be explained by the light induced activation of the RO and subsequent ring release. The switching was repeatable for one more cycle. Hence, the pseudorotaxane/rotaxane switch can be triggered by light using the

AB6-RO, but the switch is not performed in a quantitative fashion. Owing this, the switching experiment was repeated with the DMAB5-RO, since DMAB is known to have better switching qualities. The result in Figure 4.19.B unambiguously shows that by using the DMAB5-RO a quantitative reversible light switching was achieved. Since the light triggered mechanism does not lead to the accumulation of waste, a low fatigue of the switch is expected. To prove whether it is possible to switch quantitatively from stalled ring to mobile ring over more than two cycles, 12 switching events were carried out with the same sample. After each switching event an aliquot was taken and all aliquots were analyzed by gel electrophoresis. Figure 4.19.C proves a robust reversibility of the system over all switching events.



**Figure 4.19.** A) Analytical agarose gel image of the pseudorotaxane/rotaxane switching. Pseudorotaxane (lane 1) and rotaxane (lane 2) were loaded as references. The pseudorotaxane sample after addition of *cis*-AB6-RO (lane 3) and subsequent irradiation with vis- (lane 4/6) and UV light (lane 5) respectively. B) Pseudorotaxane (lane 1) and rotaxane (lane 2) were loaded as references. The pseudorotaxane sample after addition of *cis*-DMAB5-RO (lane 3) and subsequent irradiation with vis- (lane 4/6) and UV light (lane 5) respectively. C) Extended gel-shift assay of the switch, starting from the pseudorotaxane (lane 1) *trans*-DMAB5-RO was added. Twelve light switching events were performed. The blue arrow represents vis irradiation, the purple arrow UV irradiation, the orange arrow addition of *cis*-RO, and the red arrow addition of *trans*-RO. The uncropped agarose gel images are given in Supporting Figure 3.A-C. The images were taken and slightly modified from reference<sup>95</sup>.

Furthermore, FQ experiments of the switch were performed. Unfortunately, a strong quenching of the fluorophore (Cy3) after addition of the DMAB5-RO to the pseudorotaxane sample was observed (see Figure 4.20.B). This was also previously observed when only a Cy3 labeled ring instead of the whole rotaxane system was present (see Figure 4.20.A). Moreover, it was shown that the isomeric form of the DMAB

has influence on the degree of fluorescence quenching. Due to these findings, no further FQ experiments with this system were performed.

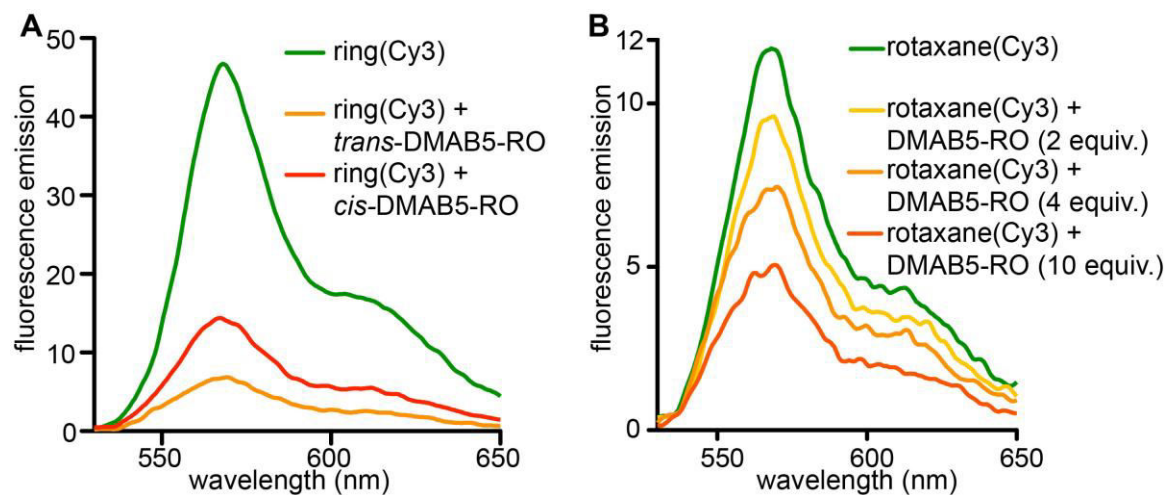


Figure 4.20. A) Fluorescence emission spectra of Cy3 labeled ring before (green) and after addition of *trans*-DMAB5-RO (orange). Subsequently the sample was irradiated with UV light and the fluorescence spectrum was measured again (red). B) Fluorescence spectra of Cy3 labeled pseudorotaxane sample before (green) and after addition of different amounts of *trans*-DMAB5-RO (yellow, orange, red). The images were taken and slightly modified from reference<sup>95</sup>.

#### 4.2 A Molecular Shuttle Based on a ds DNA Rotaxane\*

The aim of this part of the work was to construct a shuttle system in which a shuttle-ring can be reversibly translocated from one station to another station in a controllable fashion. The principle of a rotaxane based shuttle system is given in Figure 3.2. Molecular shuttles have been already reported in supramolecular chemistry and are of interest for nanotechnology in order to fabricate nanoscale electronic devices and machinery. In biology, biochemical functions depend on transport systems, e.g. kinesin proteins moving along microtubule filament;<sup>96</sup> shuttle systems might be capable of mimicking such transport systems.

\* Parts of this chapter were taken and adapted from: Lohmann, F.; Weigandt, J.; Valero, J.; Famulok, M. *Angew. Chem. Int. Ed.* **2014**, *53*, 10372-10376.

#### 4.2.1 Assembly and Characterization of a non-Symmetric Shuttle System Containing one Ring- and one Spherical-stopper

The assembly scheme of such structure is given in Figure 4.21.A and the secondary structures of all components used for the assemblies, in Figure 4.22. The assembly is performed similarly to the assembly presented for the rotaxane above. Conversely, here the axle contains two single stranded regions, namely station 1 and station 2. Station 1 can be blocked by the DMAB5-RO whereas station 2 contains DMAB modifications directly inserted into the axle. When the system is irradiated with vis light, the DMAB modifications are isomerized into the *trans* form and thereby station 1 is blocked by the DMAB5-RO while station 2 is free for hybridization. Addition of the shuttle-ring, containing two ss gap regions complementary to the two stations of the axle, results in the axle with the shuttle-ring threaded on station 2. In order to differentiate between the two states of the system with the shuttle-ring on station 1 or 2, two different stoppers were used: a ring stopper and a spherical stopper. For this purpose, the axle is equipped with two different sticky-ends, complementary to the sticky-ends either of the ring or the spherical stopper. Hybridization and subsequent ligation of both stoppers to the axle results in the formation of the shuttle system. The assembly and characterization was performed as described above (see chapter 4.1.1). The analytical agarose gel of the precursors, the dumbbell structure, the crude, and HPLC purified shuttle system (see Figure 4.23.A) clearly show the formation of the pseudorotaxane. By using AFM, it was possible to unambiguously prove that the shuttle-ring is located on station 2, near the ring stopper (see Figure 4.23.B, upper panel). In order to prove the accessibility of station 1, a second assembly was performed, without DMAB5-RO and threading of the shuttle-ring after irradiation of the axle with UV light, thus leading to the blockade of station 2 and the release of station 1. The resulting product was again analyzed by AFM, allowing the unequivocal localization of the shuttle-ring on station 1, near the spherical stopper (see Figure 4.23.B, lower panel).

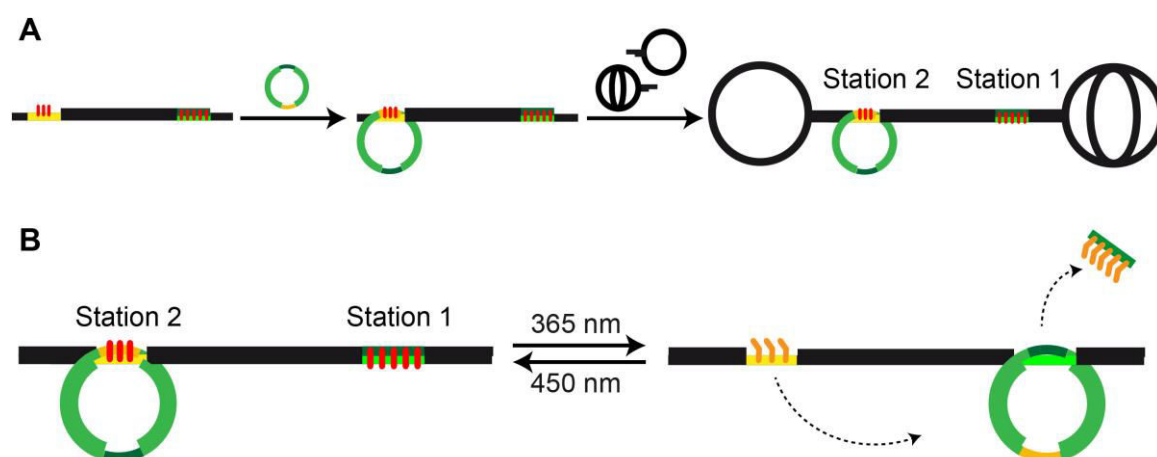


Figure 4.21. A) Scheme of the assembly of the non-symmetric pseudorotaxane which is used as a light switchable shuttle system. B) Principle of the light triggering for the shuttle system. When the DMAB moieties are isomerized into the *trans* form, station 1 is blocked by the DMAB5-RO and the shuttle-ring hybridizes to station 2. Irradiation at 365 nm isomerizes the DMAB into the *cis* form, resulting in a blocked station 2 and an unblocked station 1 and thereby a translocation of the shuttle-ring to that station. Irradiation at 450 nm reverts this process. The stoppers are not shown. The images were taken and slightly modified from reference <sup>97</sup>.

The switching principle for the light triggered shuttle system is given in Figure 4.21.B. Starting with the shuttle-ring on station 2, the system is exposed to UV light resulting in *trans* to *cis* isomerization of the DMABs, thus releasing the DMAB5-RO from station 1 and the shuttle-ring from station 2. Subsequently, the shuttle-ring moves unhindered along the axle until it hybridizes to station 1. Irradiation with vis light reverts this process.



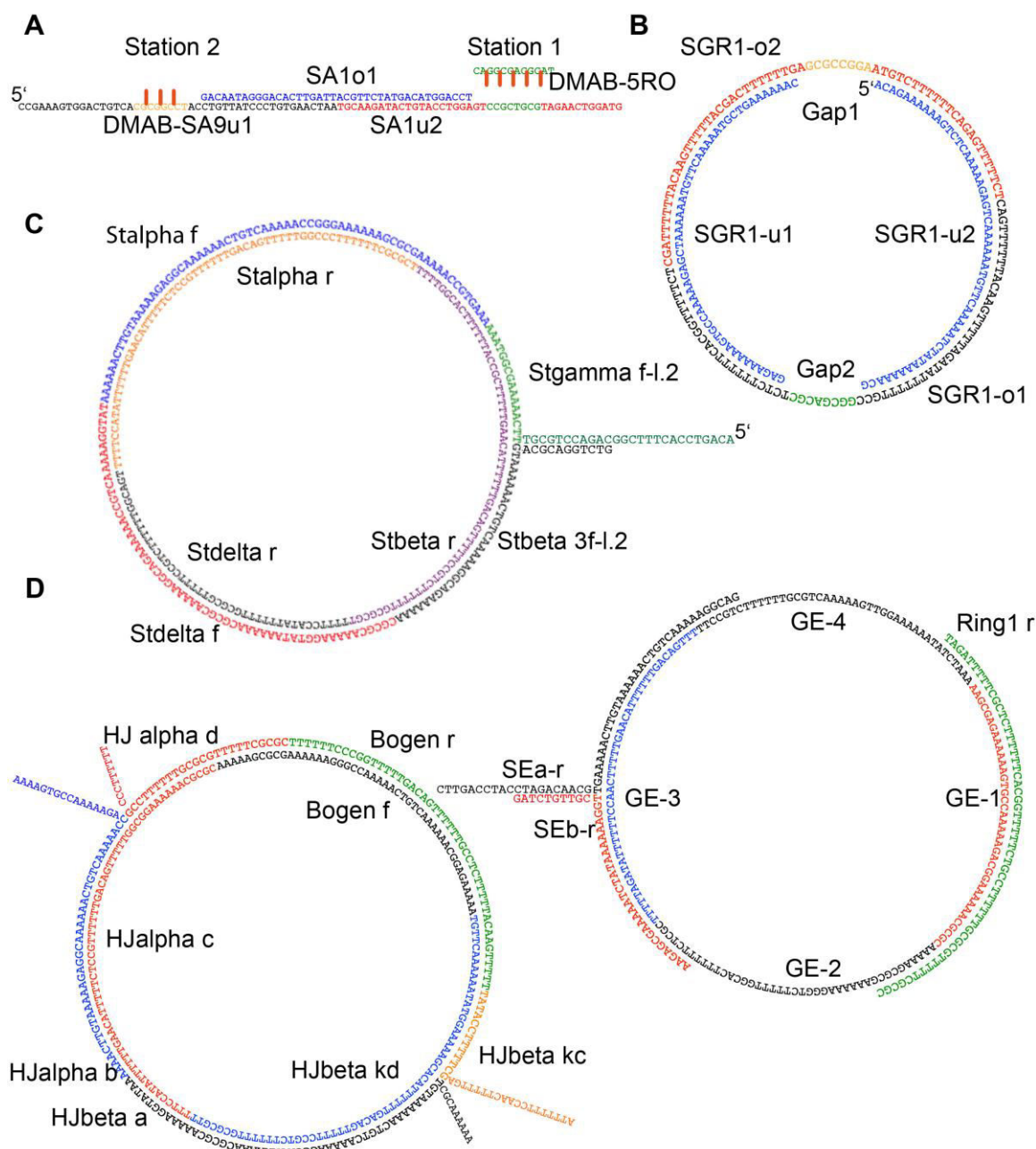


Figure 4.22. Secondary structures of the axle with the DMAB5-RO (A), the shuttle-ring (B) the ring stopper (C) and the SSt-ring1 and SSt-ring2 (D) which were used to assemble the shuttle system. The sequences of the structures can be found in Supporting Table 2.

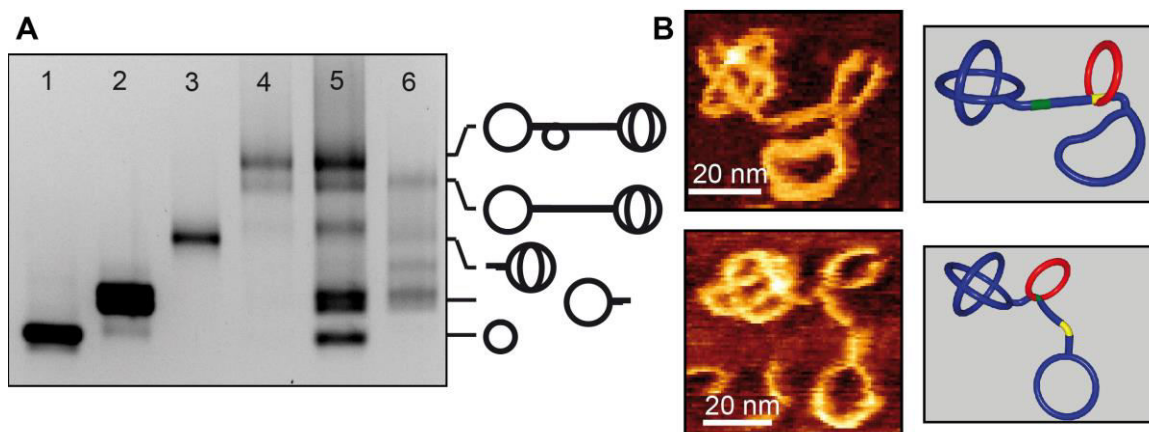
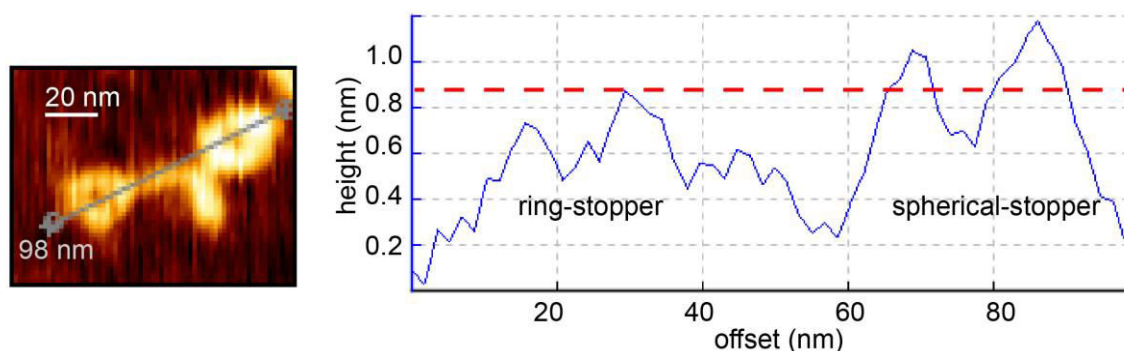


Figure 4.23. A) Analytical agarose gel image of the shuttle-ring (lane 1) the ring stopper (lane 2), the spherical stopper (lane 3) the HPLC purified non-symmetric pseudorotaxane which was used as shuttle system (lane 4), the crude non-symmetric pseudorotaxane (lane 5) and the non-symmetric dumbbell. B) AFM image of the non-symmetric shuttle system with the shuttle-ring on station 2 (near the ring stopper) (upper panel) and on station 1 (near the spherical stopper) (lower panel) together with the 3D representations of how the pseudorotaxanes arrange on the mica surface (right). The images were taken with contact mode in liquid. The images were taken and slightly modified from reference<sup>97</sup>.

#### 4.2.2 Light Induced Translocation of a Shuttle-ring in a ds DNA Rotaxane

To determine the efficiency of the shuttle-ring translocation, statistical analysis of the different states was performed by using AFM images, taken from the corresponding samples. Due to their three-dimensional shape, the spherical stoppers have a higher profile when adsorbed on mica surface and thus exhibit a brighter color in the AFM images taken with AC-mode. An AFM image of one pseudorotaxane structure with the shuttle-ring on station 1 together with its height profile is given in Figure 4.24. Although the exact shape of the spherical stopper is not clearly visible, it is possible to distinguish between the ring stopper and the spherical stopper by their height profile.



**Figure 4.24.** Height profile (right) of an AFM image (left) of a non-symmetric pseudorotaxane with the macrocycle near the spherical stopper. The ring stopper shows a lower height than the spherical stopper. The image was taken and slightly modified from reference <sup>97</sup>.

Using this feature, it was possible to analyze the shuttle system before and after translocation of the shuttle-ring from station 2 to station 1 and back. The experiment was performed as illustrated in Figure 4.25.A. First, AFM images of the shuttle system before switching, with the shuttle-ring located on station 2, were taken. After irradiation with UV light with the purpose to translocate the shuttle-ring to station 1, an aliquot was taken and the remaining sample was irradiated with vis light. This returns the shuttle-ring back to station 2. Finally, AFM images of the sample after every irradiation event were taken. The intact pseudorotaxane structures of all images were counted, and the percentage of structures with the shuttle-ring on the correct position compared with shuttle-rings on the wrong position, was determined. In some cases, the position of the shuttle-ring could not be precisely determined and therefore, in these cases the rotaxane was not evaluated. The images in Figure 4.25.B,C and D represent cuttings from the images, which were obtained without irradiation and after UV- sequential vis-irradiation, respectively. The images obviously display the shuttle-ring in most cases on the correct position, either near the ring stopper (see Figure 4.25.B and D) or near the spherical stopper (see Figure 4.25.C).

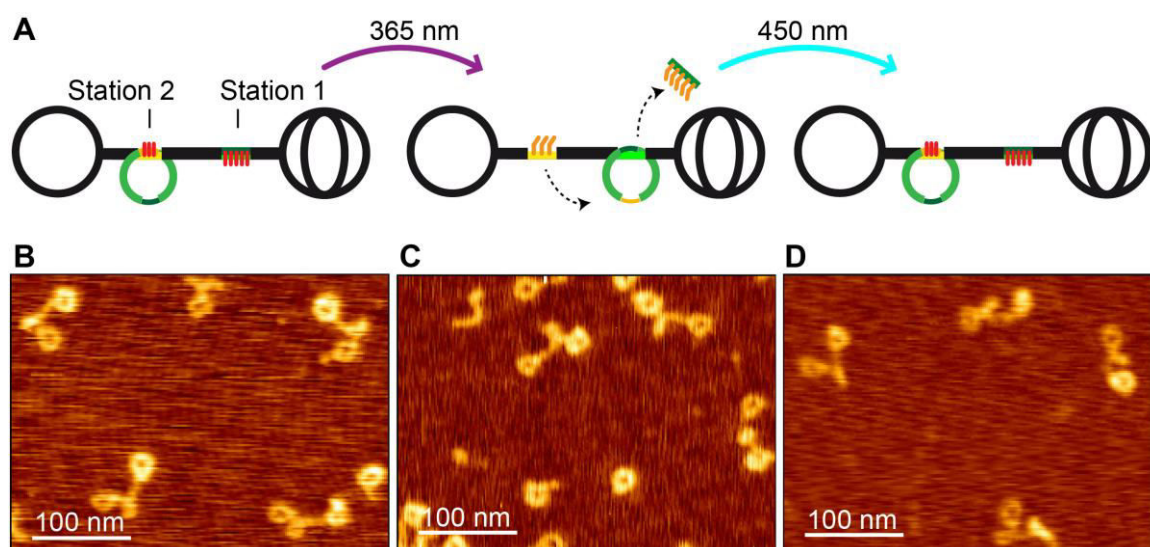


Figure 4.25. A) Illustration of the light triggering of the shuttle-ring from station 2 to station 1 and back. B) AFM image of the shuttle system with the shuttle-ring on station 2. C) AFM image of the shuttle system after irradiation with UV light. D) AFM image of the shuttle-system after sequential irradiation with UV- and vis light. The images were taken with intermittent contact mode in air. The larger area AFM images are given in Supporting Figure 4, Supporting Figure 5 and Supporting Figure 6. The images were taken and slightly modified from reference <sup>57</sup>.

The statistical numbers obtained from the evaluation of all AFM images given in Table 4.1 confirmed this finding. For larger area AFM images used for statistical analysis see Supporting Figure 4, Supporting Figure 5 and Supporting Figure 6. With this experiment, it was possible to demonstrate the successful light triggered translocation of a shuttle-ring within a DNA pseudorotaxane system.

irradiation	% of ring on station 2	% of ring on station 1
no	95	5
UV	23	76
UV + vis	97	3

Table 4.1. Percentages of pseudorotaxane structures with the shuttle-ring on station 2 or station 1 before and after irradiation events. The percentages were calculated from the ratio of structures with the ring on the corresponding position. The structures were visualized with AFM.

#### 4.2.3 Toe-hold Induced Translocation of a Shuttle-ring in a ds DNA Rotaxane Containing one Ring- and one Origami-stopper

The scope of the shuttle system was meant to be extended by using an alternative switching mechanism and also by the use of a new stopper species based on the origami technique. As already mentioned, depending on the application, the toe-hold

---

mechanism has advantages towards the light induced switch and *vice versa* (see Table 2.1). For instance, in this system the shuttle-ring translocation from one station towards the other was performed using the toe-hold mechanism. The origami technique is a very efficient and widely spread methodology used to assemble highly adaptable structures of almost any shape in a straightforward fashion. Hence, the use of an origami stopper in the pseudorotaxane assembly might significantly increase both the accessibility and applicability of the system.

#### **4.2.3.1 Assembly and Characterization of a Shuttle System Containing one Ring- and one Origami-stopper**

In order to replace the spherical stopper with a novel stopper, the origami technique introduced by Yan *et al.* was used.<sup>42</sup> In this case, the origami is assembled from several ss DNA fragments without using a long template strand (cf. chapter 2.3). A rectangular shaped origami<sup>42</sup> was slightly modified to contain a stem region with a sticky-end pointing towards one side of the rectangle (see Figure 4.26). The sticky-end was further used to attach the origami stopper to the axle of the pseudorotaxane. Furthermore, the dimensions of the origami (width 28.0 nm, length 48.0 nm) were chosen to prevent dethreading of the interlocked ring (diameter 13.6 nm). After the origami stopper was synthesized, the axle with the threaded ring was added, together with the ring stopper and thereby the pseudorotaxane was formed (see Figure 4.26). Ligation linked the stoppers covalently to the axle.

The origami stopper, synthesized by annealing the 97 ODNs required, was purified by Freeze 'N Squeeze extraction from agarose gels. The crude and pure origami stopper was further analyzed by agarose gel electrophoresis (see Figure 4.27.A). The gel image clearly shows one dominant band in both cases, representing the origami assembly. After purification, the broad band corresponding with the unreacted ss ODNs disappeared. The purified sample was then analyzed by AFM. The obtained image unequivocally indicates the formation of the rectangular shaped origami (see Figure 4.27.B). By measuring the width and length of several intact structures it was possible to corroborate that the obtained structures reveal the expected size (see Figure 4.27.C).

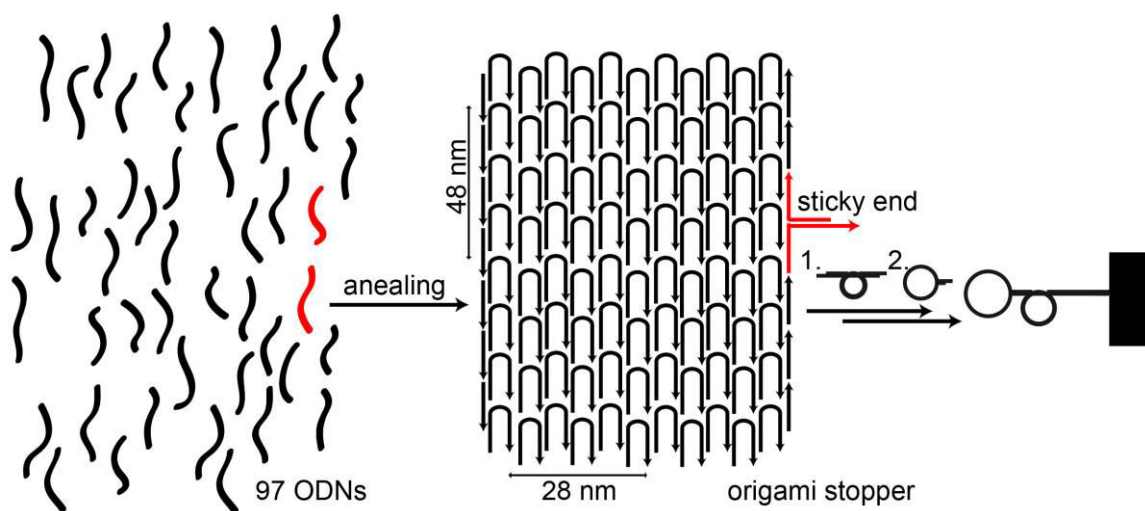


Figure 4.26. Scheme of the origami stopper assembly followed by the pseudorotaxane assembly.

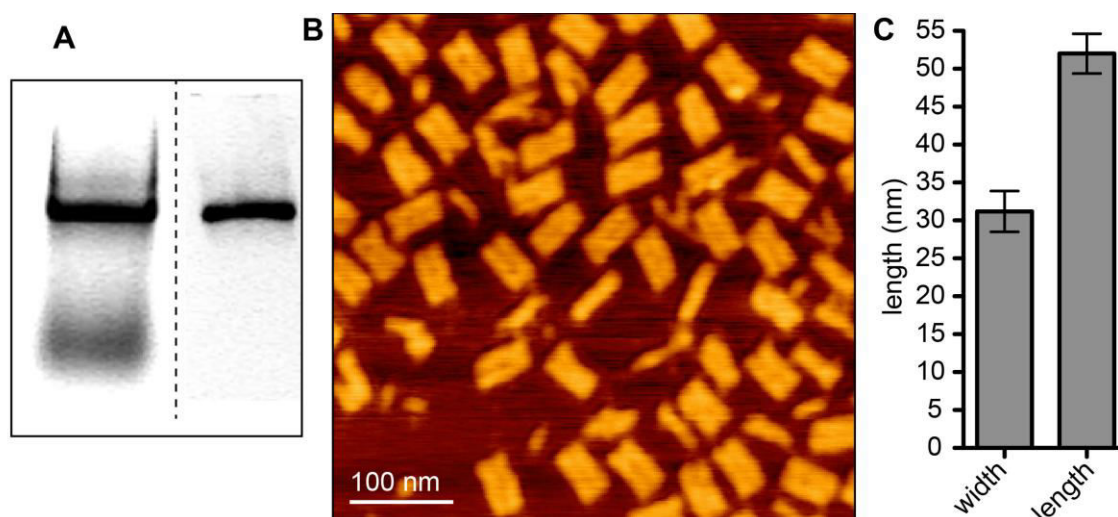


Figure 4.27. A) Analytical agarose gel image of the crude (left lane) and the Freeze 'N Squeeze purified origami stopper. The uncropped agarose gel images are given in Supporting Figure 7.A,B. B) AFM image of the purified origami stopper. The image was taken with intermitted contact mode in air. The larger area AFM image is given in Supporting Figure 7.C. C) Statistics for the width and length measurements of the origami stopper.

As explained above, this origami stopper was used to assemble the pseudorotaxane. The analytical agarose gel of the precursors, the dumbbell structure, and the crude pseudorotaxane (see Figure 4.28.A) clearly shows the formation of the pseudorotaxane. By using AFM, it was possible to unambiguously confirm the predicted structure of the rotaxane with one origami stopper and one ring stopper (see Figure 4.28.B). As shown before, the position of the shuttle-ring (near the ring stopper) can be determined by means of AFM.

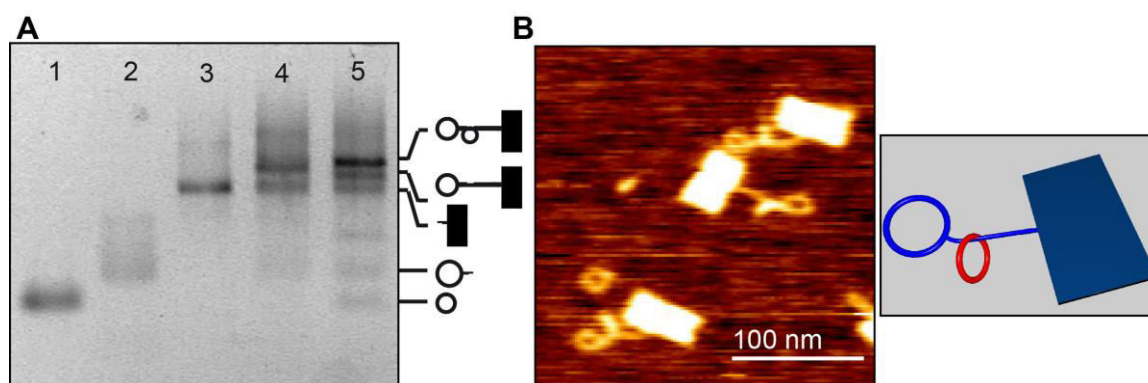
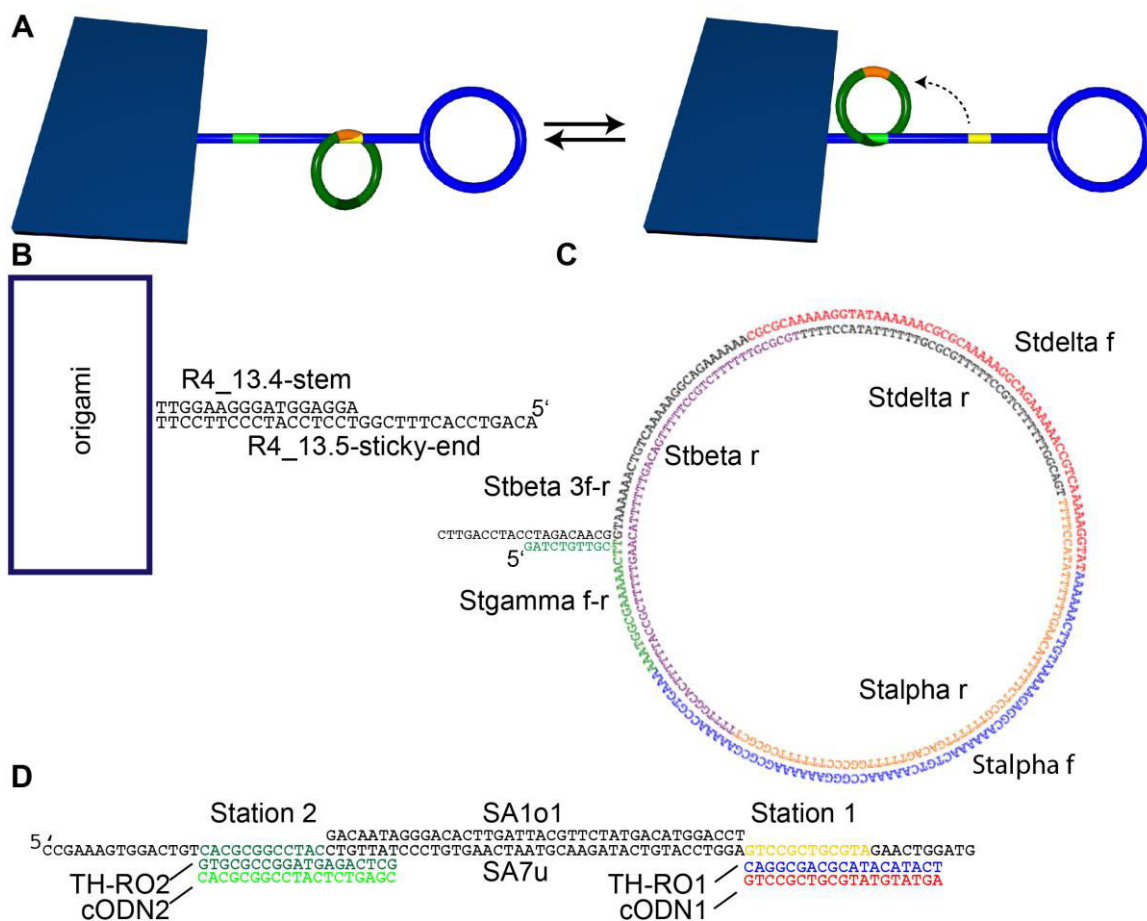


Figure 4.28. A) Analytical agarose gel image of the shuttle-ring (lane 1), the ring stopper (lane 2), the origami stopper (lane 3) the dumbbell structure with both ring- and origami-stoppers (lane 4) and the crude pseudorotaxane with both ring- and origami-stoppers (lane 5). B) AFM image of pseudorotaxane with one ring- and one origami-stopper (shuttle-ring on station 1 near the ring stopper) (left) together with the 3D representations of how the pseudorotaxane arranges on the mica surface (right). The image was taken with intermitted contact mode in air. The larger area AFM image is given in Figure 4.31.

These results exhibit the possibility to introduce origami based components into the interlocked DNA architectures. This feature might be of interest, when the system is meant to be modified with other bioactive molecules, like enzymes or DNA- and RNA-motifs.

#### 4.2.3.2 Toe-hold Induced Translocation of a Shuttle-ring in a ds DNA Rotaxane

The principle of the origami stopper containing shuttle system is illustrated in Figure 4.29, together with the sequence of the origami stem/sticky-end region and secondary structures of the ring stopper, the axle with the respective TH-ROs and cODNs used to trigger the shuttle.



**Figure 4.29.** A) Scheme of the shuttle-ring translocation in a rotaxane based shuttle system containing one ring- and one origami-stopper. B) Secondary structures of the stem/sticky-end region of the origami stopper (B) the ring stopper (right) (C) and the axle with the TH-ROs and cODNs used to trigger the shuttle system (D). The sequences of the structures can be found in Supporting Table 2 and Supporting Table 3.

The switching concept is elucidated in Figure 4.30.A. In the assembly of the pseudorotaxane, station 2 is blocked by the TH-RO2 (dark green), leading to the hybridization of the shuttle-ring on station 1 (Figure 4.30.A, left). Sequential addition of cODN2 (light green) and TH-RO1 (blue), first, releases station 2 and secondly, replaces the shuttle-ring from station 1, thus leading to the free movement of the ring along the axle. This intermediate rotaxane state is subsequently transformed into the pseudorotaxane due to hybridization of the shuttle-ring on station 2. Addition of cODN1 and TH-RO2 reverts this process. In a preliminary experiment using a pseudorotaxane with two spherical stoppers, the rotaxane intermediate of the shuttle switch could be detected and characterized. Since the spherical stoppers efficiently prevent dethreading of the interlocked ring, it was possible to preserve the rotaxane state while switching the



shuttle-ring from station 1 to station 2. The switching mechanism for this experiment, together with the result obtained from a gel-shift assay is given in Figure 4.30.B. Conversely to the switching mechanism explained in Figure 4.30.A, here the TH-RO1 is added first. Before adding the cODN2 to this intermediate, an aliquot was taken. With this experiment it is possible to trap the intermediate rotaxane state. Since the pseudorotaxane and the rotaxane exhibit a different gel electrophoretic mobility (see chapter 4.1.1), it is possible to differentiate between the pseudorotaxane states (with the shuttle-ring on station 1 or 2) and the rotaxane state (with the mobile shuttle-ring). The gel image of these three states (see Figure 4.30.B, left) indeed displays a shift of the band corresponding to the sample after addition of the TH-RO1, indicating the formation of the rotaxane.

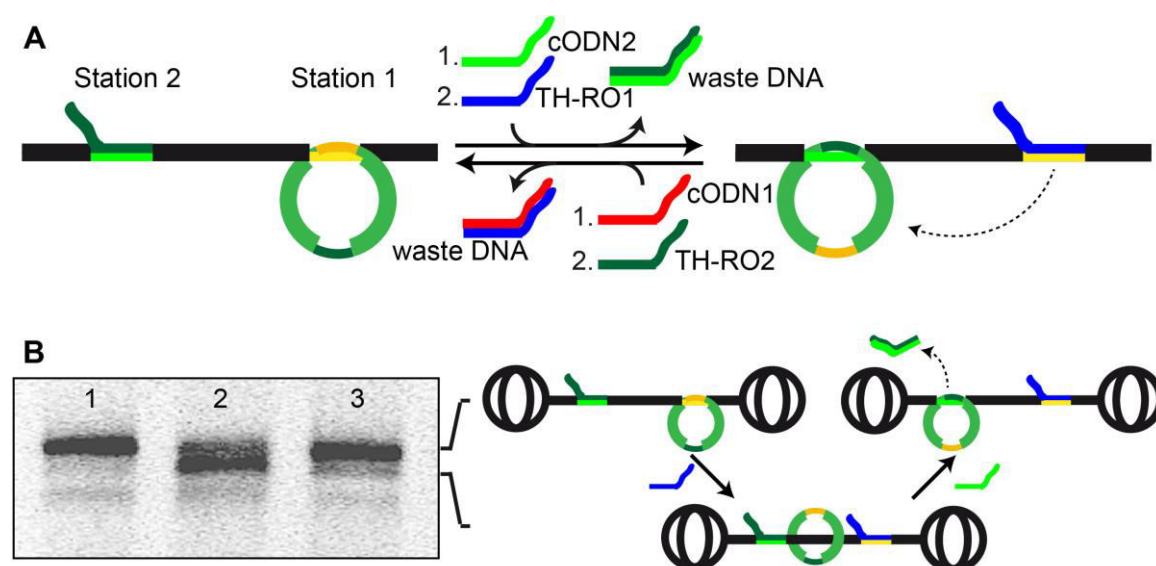


**Figure 4.30.** A) Principle of the toe-hold triggering for the shuttle system. Subsequent addition of cODN2 and TH-RO1 first unblocks station 2 and then releases the ring from station 1, which is subsequently translocated by Brownian motion to station 2. Addition of cODN1 and TH-RO2 reverts this process. B) Analytical agarose gel image displaying the pseudorotaxane states of a shuttle system containing two spherical stoppers with the shuttle-ring on station 1 and 2 (lanes 1 and 3) and the rotaxane state with the mobile shuttle-ring (lane 2). The uncropped agarose gel image is given in Supporting Figure 8. The switching principle of this experiment is depicted on the right.

Although it was possible to prove the existence of the intermediate rotaxane state with the presented gel-shift assay, it is not possible to differentiate between the different pseudorotaxane states with the shuttle-ring on station 1 or station 2. To overcome this limitation, the toe-hold mediated switch was performed with the non-symmetric shuttle

---

system containing one ring stopper and one origami stopper. With this system, it is possible to directly follow the translocation of the shuttle-ring by AFM, as shown for the light triggered shuttle system. Therefore, the sample with the shuttle-ring on station 1 (near the ring stopper) was examined by AFM. To the remaining sample, cODN2 and TH-RO1 were added successively, and analyzed by AFM. In all the intact structures displayed in Figure 4.31.A, which shows the AFM image of the sample before addition of the trigger ODNs, the shuttle-ring is located near the ring stopper as expected. The AFM image taken after addition of the trigger ODNs responsible to translocate the shuttle-ring to station 2 is shown in Figure 4.31.B. Here, in almost all the intact structures the shuttle-ring is located near the origami stopper in accordance with the design principle.

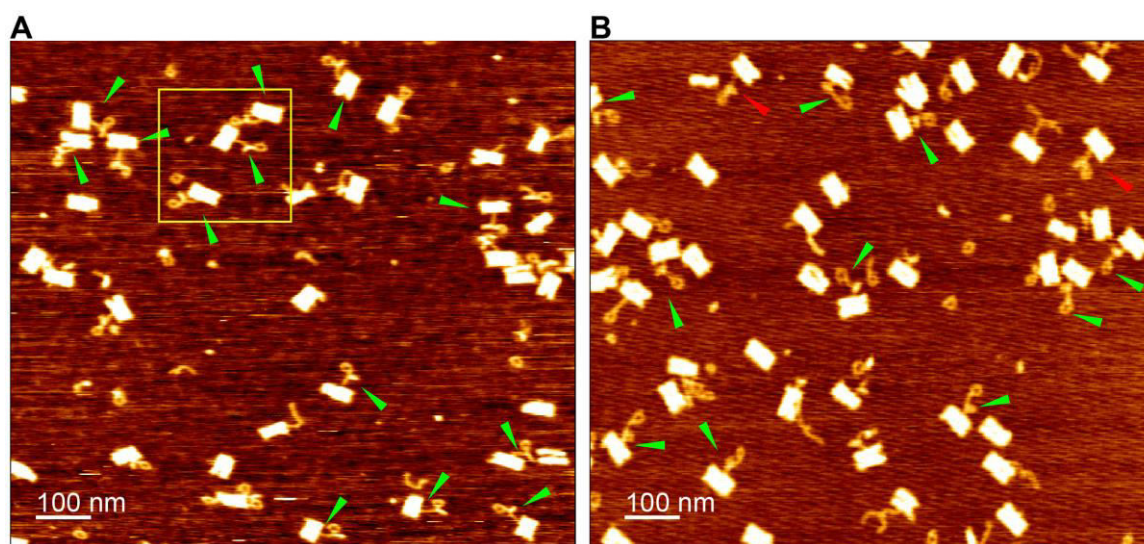


**Figure 4.31.** A) AFM image of the shuttle system with the shuttle-ring on station 1. B) AFM image of the shuttle system after sequential addition of cODN2 and TH-RO1. The intact structures with the shuttle-ring on the correct position are marked with a green arrow, the structures with the shuttle-ring on the wrong position with a red arrow. The images were taken with intermitted contact mode in air. The yellow frame marks the cropped area according to Figure 4.28.

The presented results prove the possibility to translocate a shuttle-ring in a DNA pseudorotaxane from one position towards the other not only by a light switching mechanism, but also by addition of distinct DNA fuel strands. This displays the versatility and possible adaptability of the presented shuttle system towards other complex nanoarchitectures and relevant applications.

### 4.3 Cascade Release Reaction in a [3]Pseudorotaxane Performing Logic AND Operation

Molecular shuttles are known to perform diverse functions in electrochemical, supramolecular and biological systems. In the following section, the shuttle-ring was utilized to induce a release of a second ring when translocated from one station towards the other. In a cascade like reaction, this leads to the subsequent dethreading of the second ring. Since this process is highly controllable, either one or the other ring can be dethreaded in this system. Thereby, the system can be operated as a logic AND gate.

#### 4.3.1 Assembly and Characterization of a [3]Pseudorotaxane

The assembly of the [3]pseudorotaxane was performed as presented in Figure 4.32 (for secondary structures see Figure 4.33). Starting from the axle with two ss gap regions, station 1 (green) and station 2 (blue), two different rings were threaded, a 105 bp ring with one ss gap region complementary to station 2 (called 1gap105bp-ring), and a 126 bp ring with one ss gap complementary to station 1. The 126 bp ring contains a second gap, complementary to station 2 (this ring is called 2gap126bp-ring), similarly to the shuttle-ring described in chapter 4.2. To direct the hybridization of this ring to the desired position, the gap responsible for hybridization with the other position was blocked by hybridization with a blocking-ODN (BO, orange). After both rings were threaded onto the axle, the ring stoppers were added and ligated.

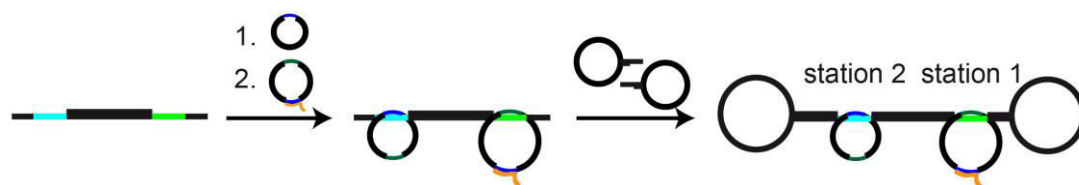


Figure 4.32. Scheme of the assembly of the [3]pseudorotaxane which functions in a cascade release reaction. In the first step, both rings are threaded on the corresponding gaps of the axle. In advance, the BO blocked the gap of the 2gap126bp-ring complementary to the blue gap of the axle. In the second step the stoppers hybridize to the ends of the axle and thereby the pseudorotaxane is formed. The image was taken and slightly modified from reference <sup>97</sup>.

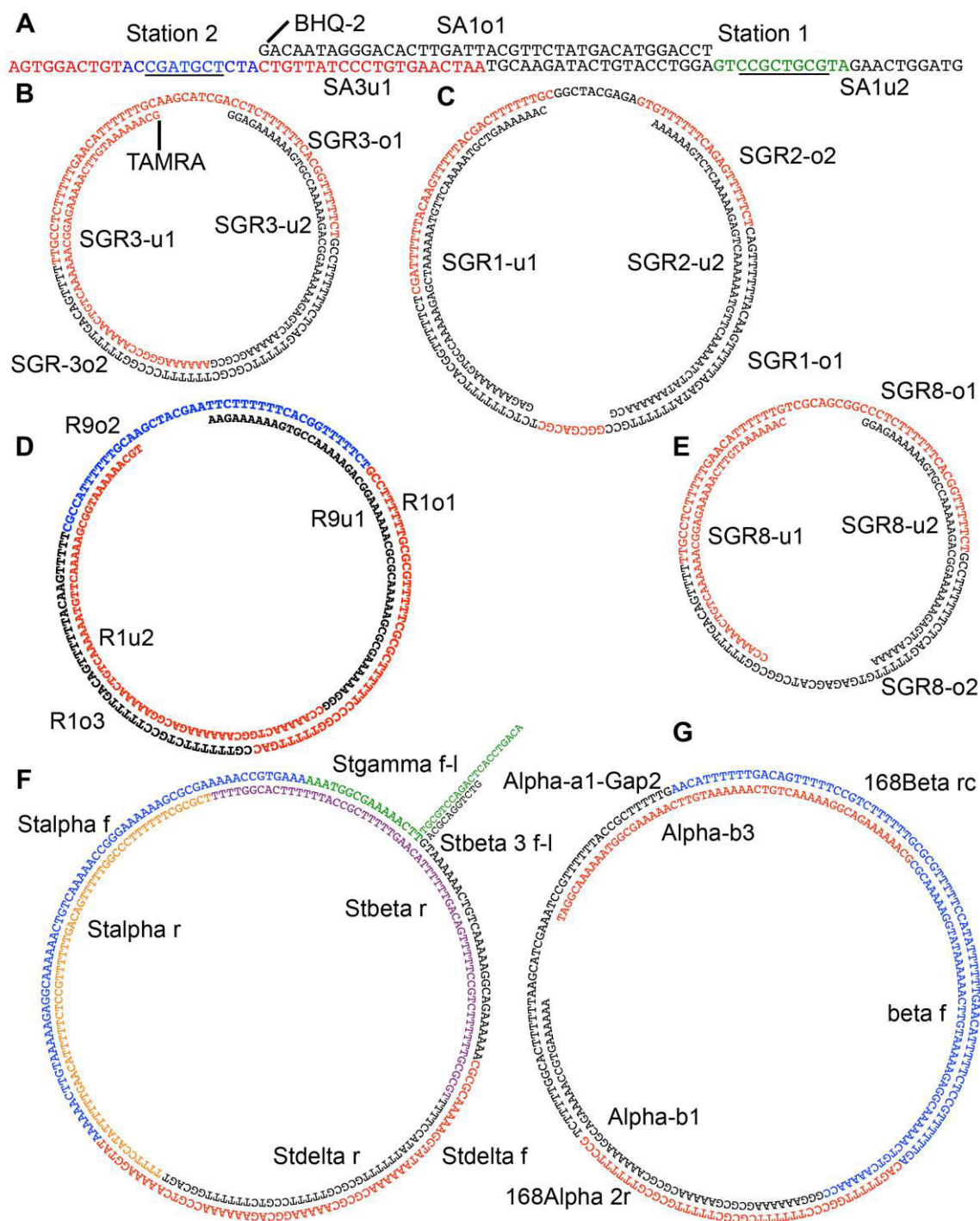
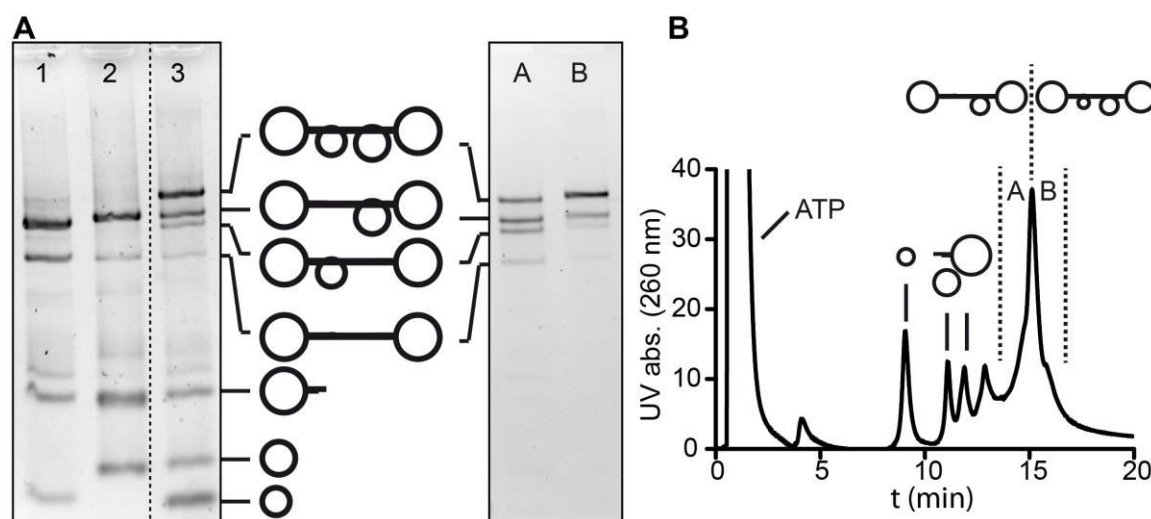


Figure 4.33. Secondary structures of the axle (the part where threading takes place is underlined) (A), the 1gap105bp-ring (B) the 2gap126bp-ring (C) the 1gap126bp-ring (D), the 2gap105bp-ring (E), the ring stopper (left) (F) and the 1gap168bp-ring (G) used to assemble the different [3]pseudorotaxanes. The ring stopper (right) is shown in Figure 4.29. For details of the secondary structures and for DNA sequences of all [3]pseudorotaxanes see Supporting Table 1 and Supporting Table 2.

Figure 4.34.A (left) shows the analytical agarose gel of the crude [3]pseudorotaxane. The [2]pseudorotaxanes with either a single 105 bp ring or 126 bp ring were also assembled

and used as references. Evidently, the [3]pseudorotaxane is the predominant specie although the corresponding [2]pseudorotaxane side-products are also formed. Purification of the crude product was performed by HPLC (see Figure 4.34.B). The [2]pseudorotaxane with the 126 bp ring and the [3]pseudorotaxane have similar retention times, hampering HPLC purification of the [3]pseudorotaxane. Nevertheless, separation of the product peak into two fractions (A and B) led to an enriched [3]pseudorotaxane sample (see Figure 4.34.A (right)). The level of purity of fraction B was sufficient to fully characterize the structure by AFM and for performing the subsequent switching experiments. Indeed, AFM imaging with Hyperdrive™ in liquid unequivocally confirms the predicted structure of the [3]pseudorotaxane (see Figure 4.35).



**Figure 4.34.** A) Left: Analytical agarose gel image of a [2]pseudorotaxane with the 1gap105bp-ring threaded (lane 1), with the 2gap126bp-ring threaded (lane 2) and the [3]pseudorotaxane with both rings threaded (lane 3). All pseudorotaxanes were assembled with ring stoppers. Right: Analytical agarose gel image of the fractions A and B from HPLC purification of the [3]pseudorotaxane sample, as shown in Figure 4.34.B. The uncropped agarose gel images are given in Supporting Figure 9. B) HPLC chromatogram of the [3]pseudorotaxane sample. The precursors and the product fractions A and B, which were analyzed by gel electrophoresis are indicated. The images were taken and slightly modified from reference<sup>97</sup>.

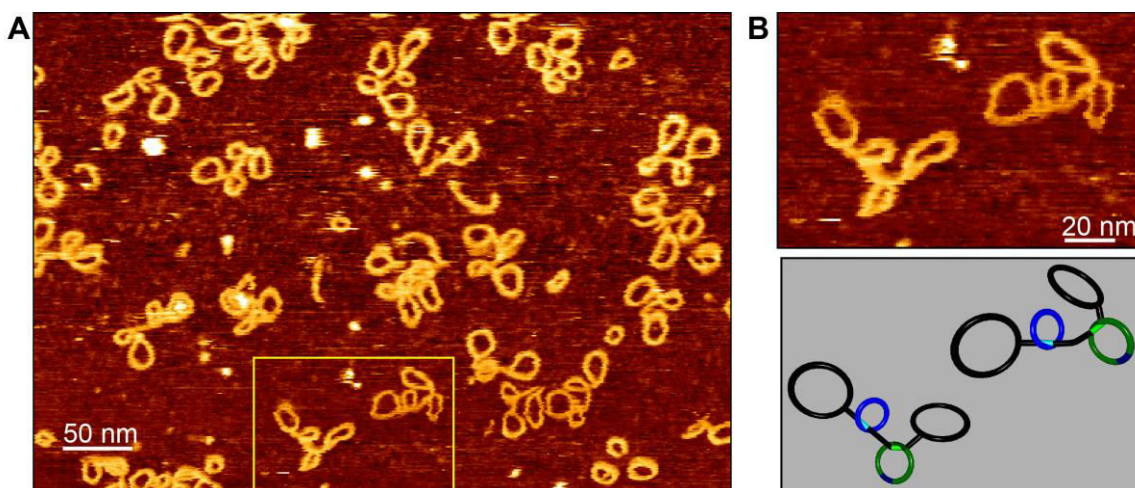


Figure 4.35 A) AFM image of a the [3]pseudorotaxane sample corresponding to fraction B from HPLC purification (see Figure 4.34.B). B) Cut-out of the presented AFM image together with the 3D representations of how the pseudorotaxanes arrange on the mica surface. The AFM image was taken with contact mode in liquid. The images were taken and slightly modified from reference <sup>97</sup>.

Apart from the mentioned structure containing the 1gap105bp-ring and the 2gap126bp-ring, [3]pseudorotaxanes with different ring sizes were assembled. It is known, that the dethreading time of the rings in rotaxanes with ring stoppers depend on the ring sizes. Hence, for possible future applications in which the dethreading should be performed in a time-controlled fashion, the ring sizes might become of great interest. Therefore, a [3]pseudorotaxane containing one 1gap126bp-ring and one 2gap105bp-ring as well as a [3]pseudorotaxane containing one 1gap168bp-ring and one 2gap126bp-ring were assembled (for secondary structures see Figure 4.33). The [3]pseudorotaxanes were further analyzed by agarose gel electrophoresis, together with the [2]pseudorotaxanes, containing only one 105 bp ring, one 126 bp ring or one 168 bp ring. The corresponding bands with the lowest electrophoretic mobility in the gel images given in Figure 4.36 prove the formation of the [3]pseudorotaxanes.

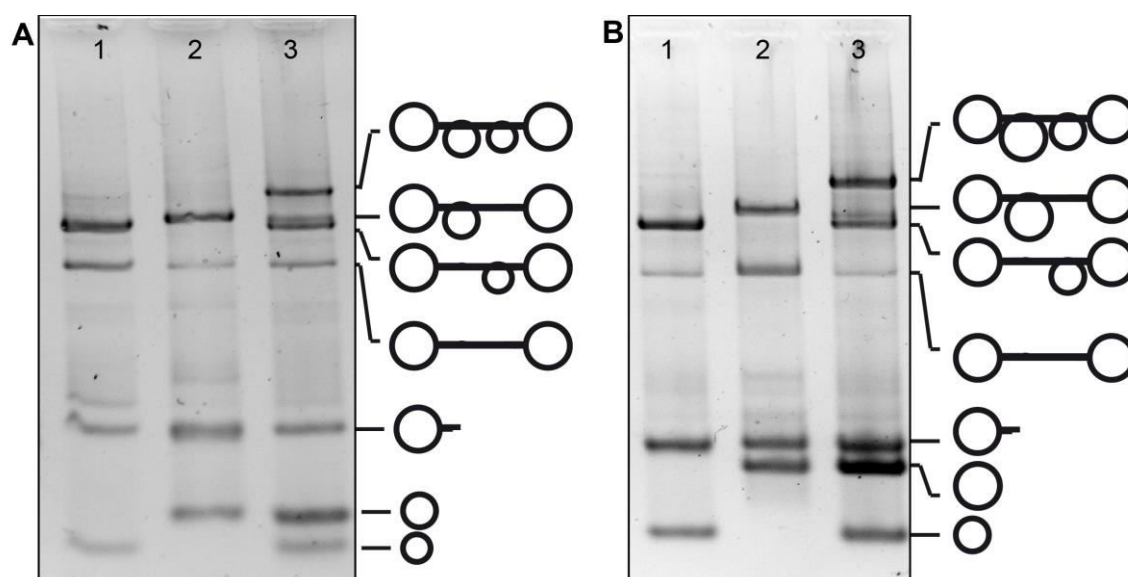


Figure 4.36. A) Analytical agarose gel image of a [2]pseudorotaxane with the 2gap105bp-ring threaded (lane 1), with the 1gap126bp-ring threaded (lane 2) and the [3]pseudorotaxane with both rings threaded (lane 3). B) Analytical agarose gel image of a [2]pseudorotaxane with the 2gap126bp-ring threaded (lane 1), with the 1gap168bp-ring threaded (lane 2) and the [3]pseudorotaxane with both rings threaded (lane 3). All pseudorotaxanes were assembled with ring stoppers. The images were taken and slightly modified from reference <sup>97</sup>.

#### 4.3.2 Input Dependent Cascade Release Reaction in a [3]Pseudorotaxane Performing AND Logic Operation \*

The directed shuttle-ring translocation, which can easily be triggered by addition of diverse inputs, was used to control the release of the threaded rings in the assembled [3]pseudorotaxane. This was achieved by the careful blocking and releasing of the ss gap regions in the assembly, which provoke the replacement of the corresponding rings.

\* Parts of this chapter were taken and adapted from: Lohmann, F.; Weigandt, J.; Valero, J.; Famulok, M. *Angew. Chem. Int. Ed.* **2014**, *53*, 10372-10376.

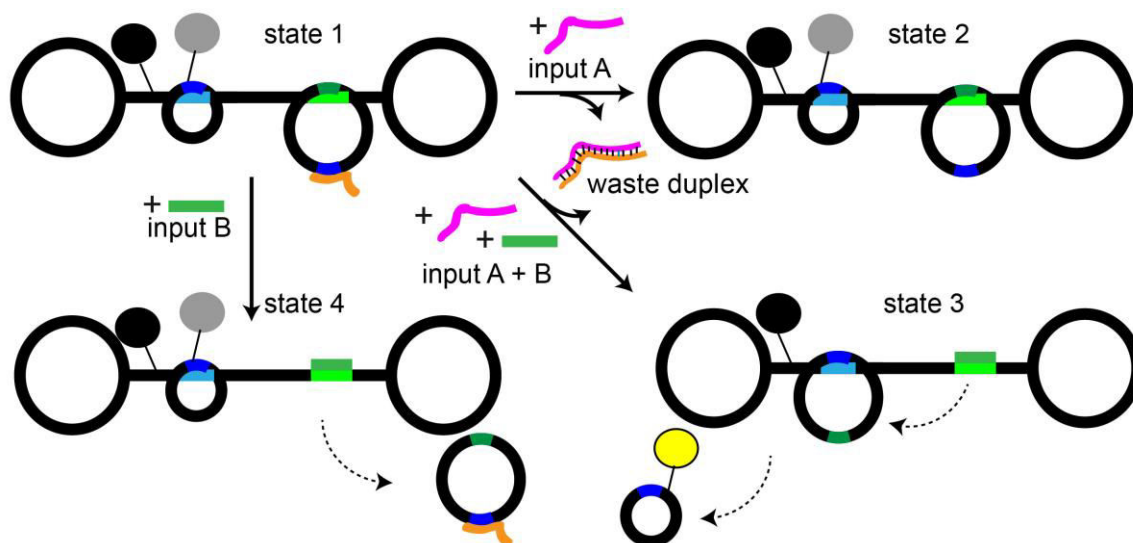


Figure 4.37. Switching scheme of the input A and B dependent triggering of the [3]pseudorotaxane. All four accessible states are depicted. Station 1 is depicted in green, station 2 in blue. Grey/yellow sphere represents a TAMRA label, the black sphere a BHQ-2 label. For clarity in this scheme, the ds nature of the system was not taken into account. For details of the switching mechanism, see text. The image was taken and slightly modified from reference <sup>97</sup>.

The [3]pseudorotaxane was designed so that the 2gap126bp-ring can shuttle from station 1 (green) to station 2 (blue). Therefore, the BO hybridized to the gap responsible for hybridization on station 2 in the 2gap126bp-ring can be removed before releasing the ring from station 1. This results in the free movement of this ring along the axle. Rather than dethreading, this ring docks on station 2 *via* hybridization of the unblocked gap of this station. Moreover, this gap sequence was designed to displace the 1gap105bp-ring when binding to station 2. Since the 1gap105bp-ring can form only seven base pairs with station 2, whereas the 2gap126bp-ring docks to this site through ten base pairs, binding of the latter is preferred. Apparently, the difference in free energy is sufficient for quantitative displacement of the smaller ring by the bigger one. Without any hybridization site available, the 105 bp ring dethreads from the axle.

The whole switching process is illustrated in Figure 4.37. Starting from the purified [3]pseudorotaxane (state 1) the system was triggered with two different input-ODNs: input A removes the BO from its complementary gap in the 2gap126bp-ring that now can hybridize to station 2. Input B releases the 2gap126bp-ring from station 1 (cf. RO in chapter 4.1.1, which has the same sequence as input B). Thus, upon addition of only input A, the 2gap126bp-ring remains bound to station 1 leaving the [3]pseudorotaxane



---

nearly unaltered (state 2). Addition of only input B releases the 2gap126bp-ring with the station 2-gap still blocked by the BO, and thus prevents it from displacing the 1gap105bp-ring. As a result, dethreading of the 2gap126bp-ring occurs, yielding a [2]pseudorotaxane with the 1gap105bp-ring bound to station 2 (state 4). When inputs A and B are added stepwise, the BO is removed from the 2gap126bp-ring, which is then released to freely move along the axle. Subsequently that ring hybridizes to station 2 in order to displace the 1gap105bp-ring, which then dethreads. This results in a [2]pseudorotaxane with the 2gap126bp-ring on station 2 (state 3).

The switching process was examined by different methods, including gel electrophoresis, AFM and FQ experiments. First, using the inputs A and B, the switching was performed as described above and the four resulting samples were analyzed by agarose gel electrophoresis. The lanes of the gel image shown in Figure 4.38.A represent the four possible states (1-4). Lane 1 corresponds to the sample without any input, while lane 2 represents the sample in presence of input A. Both lanes show predominantly the [3]pseudorotaxane and residual [2]pseudorotaxane from the purification. In lane 2, a small shift of the bands is observed due to the loss of the BO. In lane 3, displaying the sample after addition of inputs A and B, the main band corresponds to the [2]pseudorotaxane with the 2gap126bp-ring threaded. When only input B is added, as shown in lane 4, a [2]pseudorotaxane with the 1gap105bp-ring is formed. This leads to the dominant band, which is shifted towards higher electrophoretic mobility compared to the band of lane 3. These results clearly indicate that the assembled system is triggered in the predicted way and in a nearly quantitative fashion. To demonstrate that these bands correspond to the assigned [2]- or [3]pseudorotaxanes, the samples corresponding to the states 2-4 were analyzed by AFM. Representative AFM images are shown in Figure 4.38.B. Mainly [3]pseudorotaxanes are observed in state 2, whereas in states 3 and 4 the [2]pseudorotaxanes with only one ring threaded are the predominant species (note that the AFM image in Figure 4.35 corresponds to state 1). The AFM images thereby confirm the previously expressed assumption.

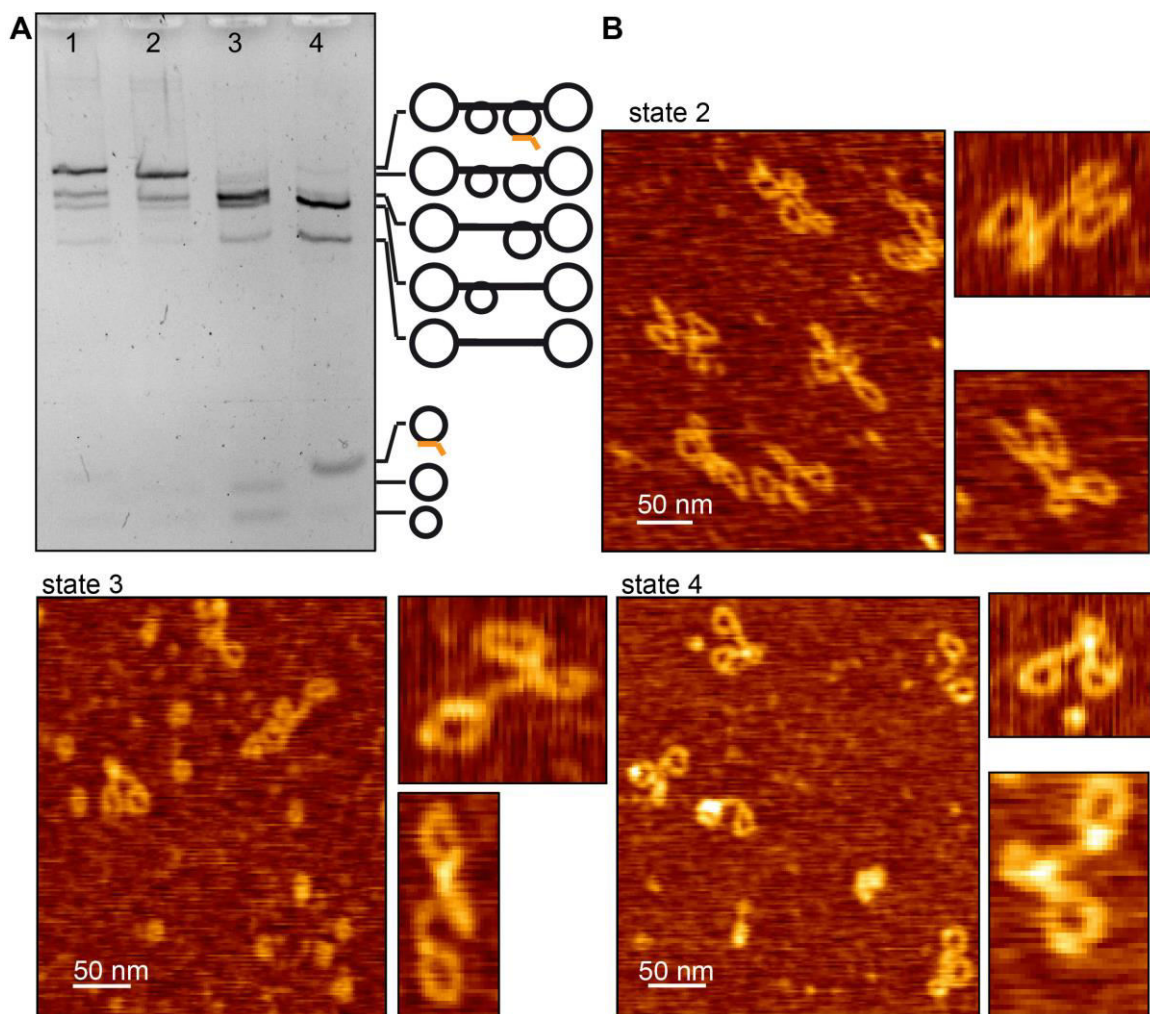


**Figure 4.38.** A) Analytical agarose gel image of the samples corresponding to the states 1-4 (lanes 1-4) obtained from the switching experiment with the [3]pseudorotaxane sample, as depicted in Figure 4.37. For more details, see text. B) AFM images of the samples corresponding to the states 2-4 obtained from the switching experiment with the [3]pseudorotaxane sample. The images were taken with intermittent contact mode in air. The images were taken and slightly modified from reference <sup>97</sup>.

To prove that the 1gap105bp-ring is released from the pseudorotaxane only in presence of the inputs A and B and to observe the switching process in real-time, FQ experiments were performed. Therefore, the 1gap105bp-ring was labeled with the fluorophore TAMRA and the axle with the quencher BHQ-2 (see Figure 4.33 and Figure 4.37). When the labeled ring is threaded on the axle, the TAMRA fluorescence is quenched due to its close proximity to BHQ-2, whereas the release of the ring will separate the fluorescence/quencher pair and lead to an increase of the fluorescence. After switching of the TAMRA/BHQ-2 labeled system in the same way as described before, the fluorescence spectra of all four states were measured. The fluorescence spectra are

given in Figure 4.39.A and as expected, only input A and B together lead to fluorescence increase due to the displacement of the TAMRA labeled ring by the 2gap126bp-ring. Considering the increase in fluorescence as output, and the addition of the trigger ODNs as input, this system represents a logic AND gate. The corresponding logic gate symbol and the table of truth are given in Figure 4.39.B.

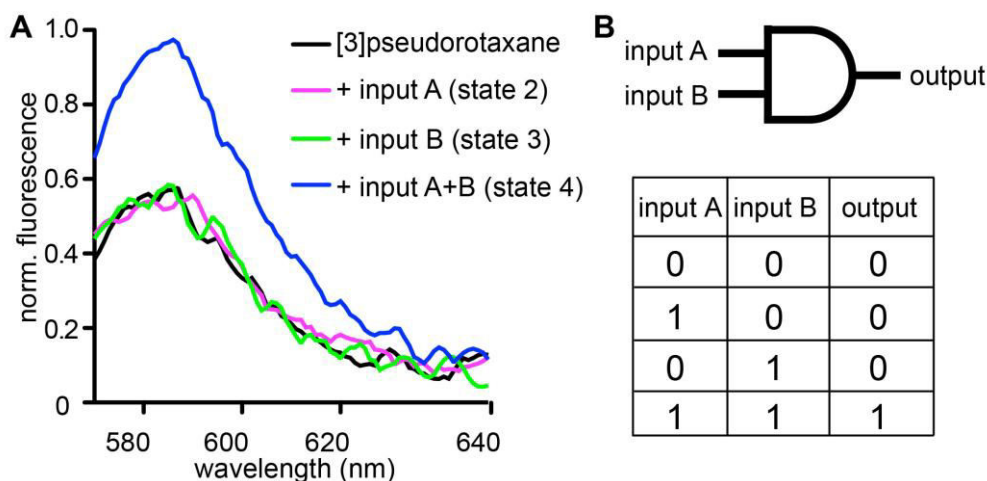


**Figure 4.39.** A) TAMRA fluorescence spectra recorded from the [3]pseudorotaxane before and after addition of the different inputs. The different colors of the spectra correspond to the states 1-4 from Figure 4.37. B) Logic gate symbol and the table of truth for a logic AND gate. The images were taken and slightly modified from reference <sup>97</sup>.

In a pilot study, the implementation of a light switchable input for this system was tested. This was achieved by replacing the input B by the light sensitive DMAB5-RO. Irradiation with vis- or UV light should activate or deactivate this light sensitive input B. In this way, light can be used as an input, instead of the external addition of ODNs. To prove the light induced activation/deactivation a switching experiment analogue to the already presented one (see Figure 4.37) was performed and the resulting samples were analyzed by agarose gel electrophoresis. The resulting gel image together with the switching scheme is given in Figure 4.40. Five samples were prepared. The [3]pseudorotaxane sample before (state 1) and after addition of the active *trans*-DMAB5-RO, which should yield in the [2]pseudorotaxane with the 1gap105bp-ring on station 2 (state 5). The [3]pseudorotaxane sample after addition of input A in order to replace the BO (state 2) and thereby allow the 2gap126bp-ring to hybridize with station 2 and additionally to this sample, either the inactive *cis*-DMAB5-RO (state 3) or the

active *trans*-DMAB5-RO (state 4) were added. Only in the latter case the formation of [2]pseudorotaxane out of the [3]pseudorotaxane was anticipated. In this system, the 2gap126bp-ring was expected to hybridize on station 2. As evident from the gel image (see Figure 4.40.A), in the case of the states 1-3 (lanes 1-3) the [3]pseudorotaxane band (lowest gel migration) remains nearly unchanged. However, in the case of state 4 (lane 4), the [2]pseudorotaxane band with the 2gap126bp-ring threaded (second lowest gel migration) and in case of state 5 (lane 5), the [2]pseudorotaxane band with the 1gap105bp-ring threaded (third lowest gel migration), represent the predominant species. These findings correlate with the switching mechanism presented in Figure 4.40.B.

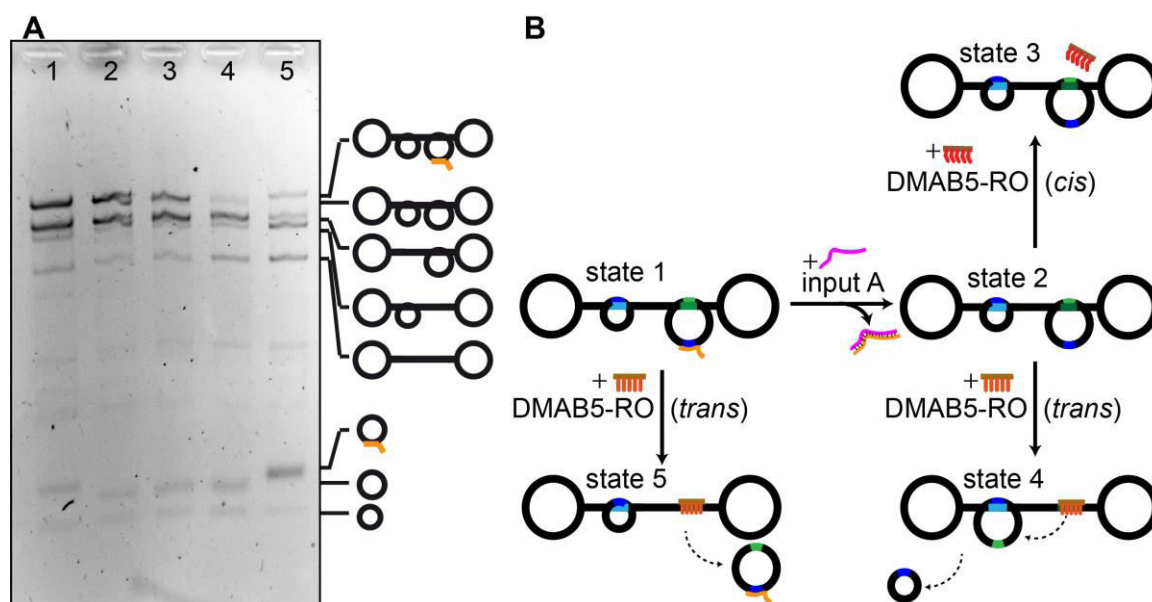


**Figure 4.40.** A) Analytical agarose gel image of the samples corresponding to the states 1-5 (lanes 1-5) received from the switching experiment with the [3]pseudorotaxane sample using the light sensitive input B (DMAB5-RO), as depicted in Figure 4.40.B. B) Switching scheme of the input A and light sensitive input B (DMAB5-RO) dependent triggering of the [3]pseudorotaxane. All five accessible states are depicted. For more details, see text. The images were taken and slightly modified from reference <sup>97</sup>.

Furthermore, for future applications requiring reversible switching mechanisms, the switching of a [3]pseudorotaxane with spherical stoppers was performed. The use of spherical stoppers prevents the threaded rings from dethreading when released from their hybridization sites and thereby allows resetting the system after replacing the smaller ring by the bigger one. In order to distinguish between the accessible states, [3]pseudorotaxane, [3]rotaxane with the mobile 2gap126bp-ring and [3]rotaxane with

the mobile 1gap105bp-ring, a gel-shift assay was performed, taking advantage of the higher electrophoretic mobility of the rotaxane compared with its homologues pseudorotaxane. It was assumed that the [3]rotaxane with the mobile 2gap126bp-ring exhibits a different electrophoretic mobility than the [3]rotaxane with the mobile 1gap105bp-ring. Figure 4.41.B shows the switching mechanism. Starting from the [3]pseudorotaxane, first the TH-RO1 was added, yielding the [3]rotaxane with the mobile 2gap126bp-ring. In this experiment, the TH-RO1 replaces the input B in order to make the ring release reversible (by addition of cODN1). Then the input A was added, releasing the BO which subsequently leads to the replacement of the smaller ring in order to generate the [3]rotaxane with the mobile 1gap105bp-ring. Addition of cODN1 and BO resets the system, resulting in the [3]pseudorotaxane. The gel image displaying the three states of the system and the sample after resetting is shown in Figure 4.41.A.

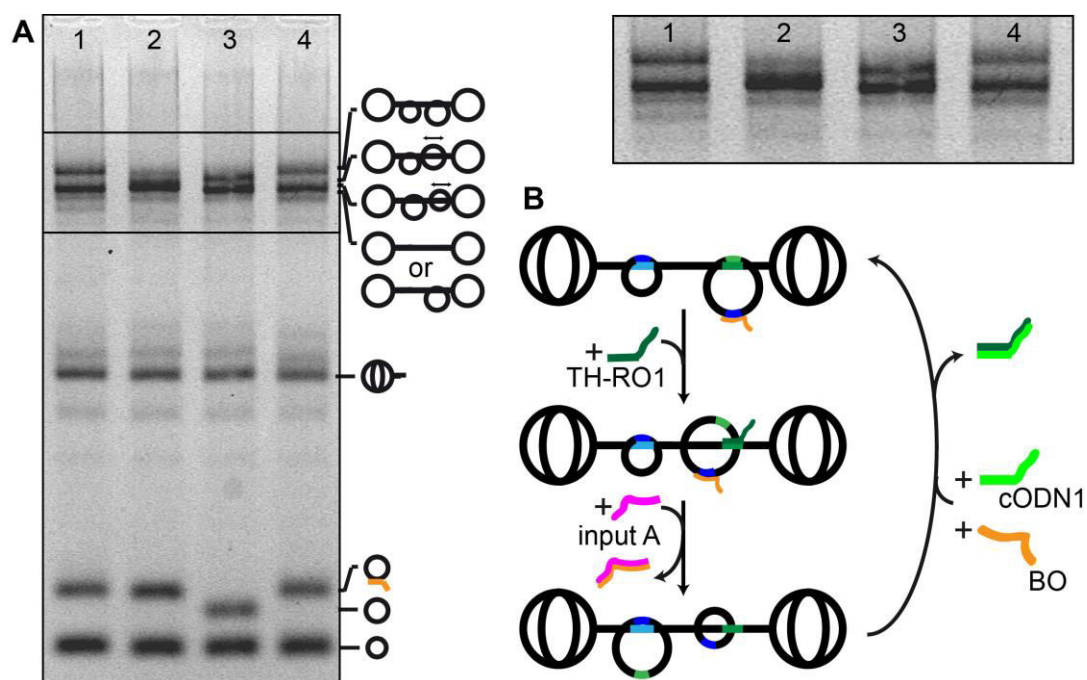


**Figure 4.41.** A) Analytical agarose gel image of the [3]pseudorotaxane sample (lane 1), the [3]rotaxane sample with the mobile 2gap126bp-ring (lane 2), the [3]rotaxane sample the with the mobile 1gap105bp-ring (lane 3) and the reset [3]pseudorotaxane (lane 4). The switching of the [3]pseudorotaxane was performed as shown in Figure 4.41.B. B. Scheme of the input A, TH-RO1, cODN1 and BO triggered reversible switching of the [3]pseudorotaxane with spherical stoppers.

Indeed, the [3]pseudorotaxane/rotaxane bands (lowest migrating band) of each state differ from the other, but the change in the electrophoretic mobility is marginal.

---

Nevertheless, this experiment opens the possibility to use the [3]pseudorotaxane switch as a reversible system although further investigation into this direction would be required in order to unambiguously identify the different states.

#### **4.4 Design, Assembly, Characterization and Triggering of ds DNA Catenanes\***

All results presented in the chapters 4.1, 4.2 and 4.3 are based on the principle design of the ds DNA rotaxanes as presented by Famulok *et al.*<sup>82</sup> The intrinsic properties of these structures exhibit diverse opportunities in order to incorporate function, which was successfully achieved in diverse cases, as presented above. In chapter 4.3.2 the dethreading of the threaded rings in the pseudorotaxane with ring stoppers is required for the function of the system. In other cases, especially in reversible operating systems, dethreading has to be suppressed by all means. In the rotaxane system, the use of spherical stoppers fulfills this requirement. The synthesis of such rotaxanes, which exhibit a highly complex shape, is demanding. For some applications, the use of rotaxane structures represents a drawback due to the lack in rigidity, especially in the part of the axle, as evident from Figure 4.5.B. To overcome this limitation, a new class of interlocked ds DNA nanoarchitectures was established. These architectures consist of at least two ds DNA rings interlocked to each other. Such structures are called catenanes. The design, assembly, characterization and triggering of ds DNA catenanes will be presented in the following chapters.

##### **4.4.1 Design, Assembly and Characterization of ds DNA Catenanes**

The scheme presented in Figure 4.42 illustrates how the assembly of a non-symmetric [2]catenane was performed. Starting from the ds DNA ring alpha, containing a ss gap region, a threading ODN was added. The threading ODN contains a complementary sequence towards the gap region and additionally two sticky-ends. After hybridization of the complementary sequence to the gap of ring alpha, the addition of the 3/4-ring beta,

---

\* Parts of this chapter were taken and adapted from: Lohmann, F.; Valero, J.; Famulok, M. *Chem. Commun.* **2014**, *50*, 6091-6093.

containing two sticky-ends complementary to the threading ODN, allowed closing the ring beta. Subsequently the catenane ROs (Cat-RO1 and Cat-RO2), entirely complementary to the gaps in ring alpha and ring beta were added and all nicks were ligated, yielding the catenane structure.

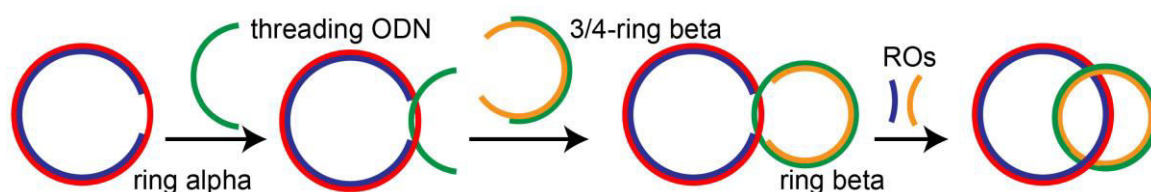


**Figure 4.42. Scheme of the assembly of the non-symmetric [2]catenane.** In the first step the threading ODN, with a complementary sequence towards the gap region of ring alpha hybridizes with this gap. In the second step the pseudocatenane is formed upon addition of the 3/4-ring beta and subsequent ring closing of ring beta. In the last step the ROs are added, releasing the rings from each other, which results in the catenane formation. The images were taken and slightly modified from reference<sup>98</sup>.

Using this straight forward methodology, symmetric catenanes containing two 126 bp or 168 bp rings and a non-symmetric catenane, containing one 126 bp ring and one 168 bp ring were assembled. The secondary structures of all of them are given in Figure 4.43. Following a similar synthesis strategy, it was also possible to assemble a [3]pseudocatenane consisting of three 126 bp rings. In the case of the [3]pseudocatenane, the synthesis started with the middle ring, which contains two ss gap regions for hybridization with two threading ODNs. Subsequent addition of the remaining parts of the outer rings and ligation, led to the final product. The secondary structure of this assembly is given in Figure 4.44.

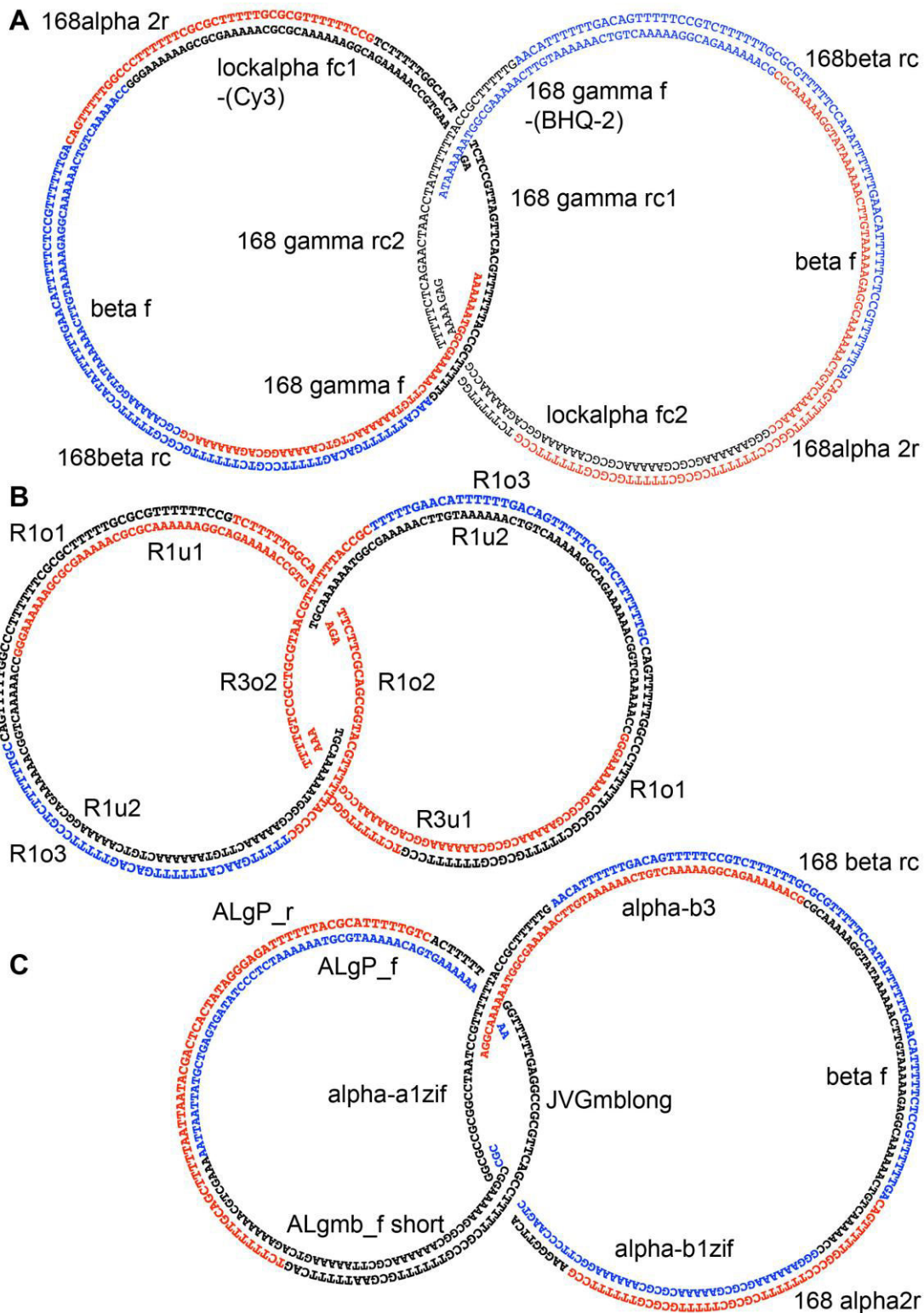
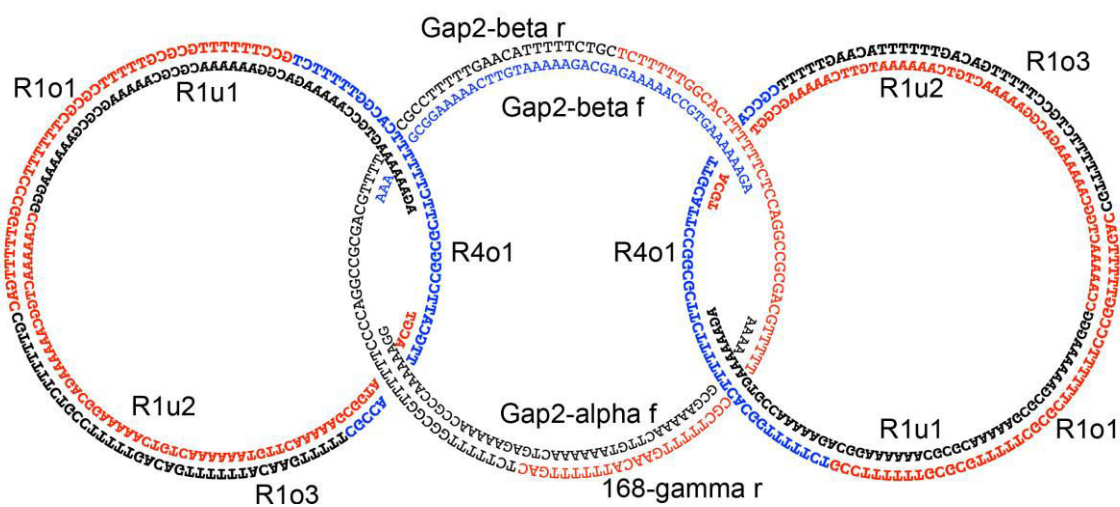


Figure 4.43. Secondary structures of the pseudocatenanes containing two 168 bp rings (A), two 126 bp rings (B) one 126 bp and one 168 bp ring (C). For details of the secondary structures and for DNA sequences of all [2]pseudocatenanes see Supporting Table 1 and Supporting Table 2.





**Figure 4.44.** Secondary structures of the [3]pseudocatenane containing three 126 bp rings. For details of the secondary structures and for the DNA sequences see Supporting Table 1 and Supporting Table 2.

The formation of the pseudocatenane was firstly confirmed by agarose gel electrophoresis. As evident from Figure 4.45.A, the non-symmetric [2]pseudocatenane structure is formed predominantly (main band in lane 1). Also the pseudocatenane to catenane conversion could be followed by gel electrophoresis, since the catenane shows a slightly higher electrophoretic mobility than the pseudocatenane. The second lane in Figure 4.45.A represents the catenane after addition of the Cat-ROs. In a kinetic study, the pseudocatenane to catenane conversion in a [3]pseudocatenane structure could be followed by means of an FQ experiment. The fluorescence of a [3]pseudocatenane with quencher labels (BHQ-1) near the gaps of the middle ring and fluorescent labels (rhodamine green) near the gaps of the outer rings was measured before and after addition of the corresponding ROs (the sample was provided by Dr. T. Li). Figure 4.46 illustrates how the fluorescence increases over time, reaching its maximum after approx. 50 min. The increase in fluorescence results from the separation of the fluorophore/quencher pairs after the pseudocatenane to catenane conversion. The gel-shift assay together with the FQ experiment demonstrates the existence of a state with two freely moving but interlocked rings in the catenane assemblies after addition of the ROs.

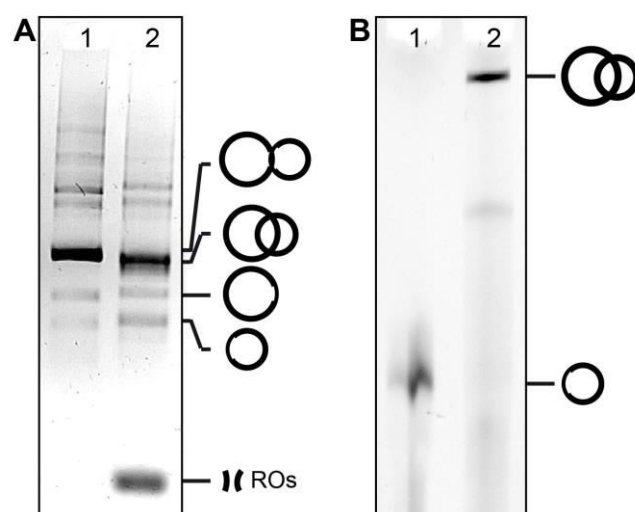


Figure 4.45. A) Analytical agarose gel image of the non-symmetric [2]pseudocatenane sample before (lane 1) and after (lane 2) addition of the ROs Cat-RO1 and Cat-RO2. B) Denaturing PAGE image of the 126 bp ring (lane 1) and the non-symmetric [2]catenane sample (this gel assay was performed by Dr. J. Valero). The images were taken and slightly modified from reference<sup>98</sup>.

To further prove the integrity of the catenane structure and to exclude that dethreading occurs after the ROs were added, the sample was examined on a denaturing gel (see Figure 4.45.B). The gel image doubtlessly shows that the catenane structure stays intact even under denaturing conditions, since almost no formation of single ring can be observed in the corresponding lane of the gel.

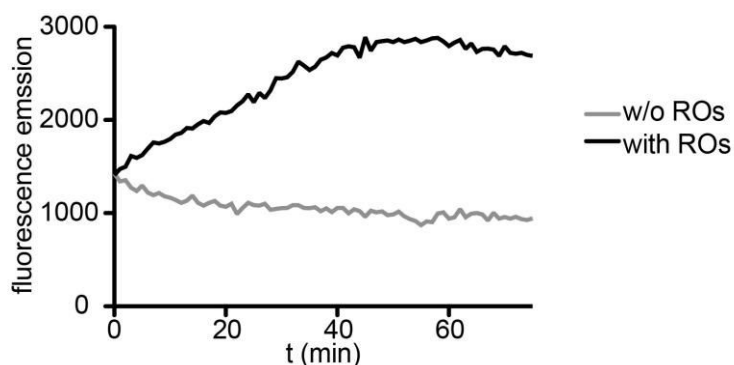
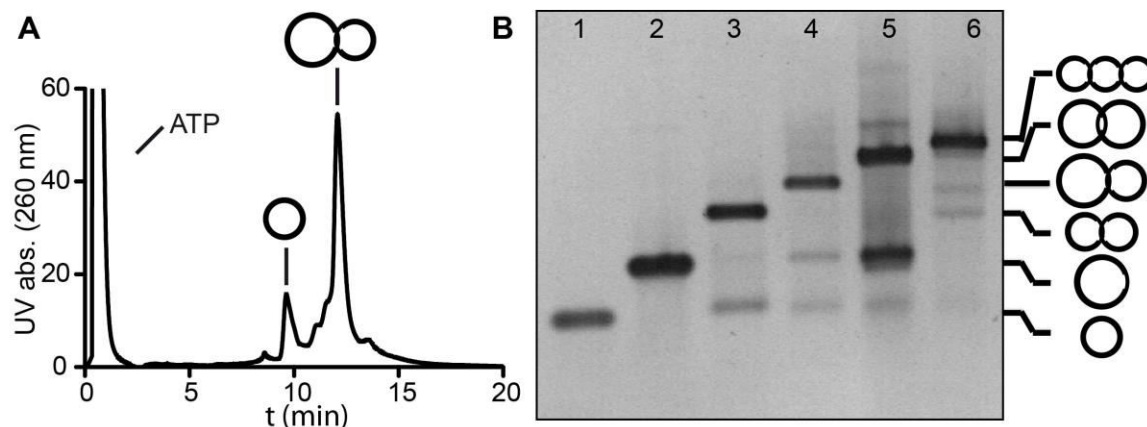


Figure 4.46. Fluorescence emission of a rhodamine green and BHQ-1 labeled [3]pseudocatenane sample with (black) and without addition of ROs (grey). The fluorescence was measured over a time period of 75 min. The [3]pseudocatenane sample was provided by Dr. T. Li. The images were taken and slightly modified from reference<sup>99</sup>.

The purification of all pseudocatenane assemblies was performed by HPLC. The chromatogram of the non-symmetric catenane shown in Figure 4.47.A exhibits one major signal, which corresponds to the catenane assembly. The separation of the

product fraction from the precursor ring leads to a highly pure catenane sample. Once the formation of all different pseudocatenane samples was analyzed by gel electrophoresis (see Figure 4.47.B), the robustness and rigidity of the HPLC purified non-symmetric catenane was examined by AFM.



**Figure 4.47.** A) HPLC chromatogram of the non-symmetric [2]pseudocatenane. The product peak as well as the precursor peak of the ring is indicated. B) Analytical agarose gel image of the 126 bp ring (lane 1) the 168 bp ring (lane 2), the [2]pseudocatenane containing two 126 bp rings (lane 3), the non-symmetric [2]pseudocatenane containing one 126 bp ring and one 168 bp ring (lane 4), the [2]pseudocatenane containing two 168 bp rings (lane 5) and the [3]pseudocatenane containing three 126 bp rings (lane 6). The images were taken and slightly modified from reference<sup>98</sup>.

The AFM image shown in Figure 4.48.A displays, that almost all structures remain intact after deposition on the mica surface and that almost no contamination is present. Furthermore, all catenanes exhibit a well-defined circular shape, confirming the rigid nature of the assemblies. Additionally, the [3]pseudocatenane sample was examined by AFM, confirming the formation of the three rings containing structure (see Figure 4.48.B). A [3]catenane sample delivered by Dr. T. Li was also analyzed by AFM, the high resolution images are shown in Figure 4.52.

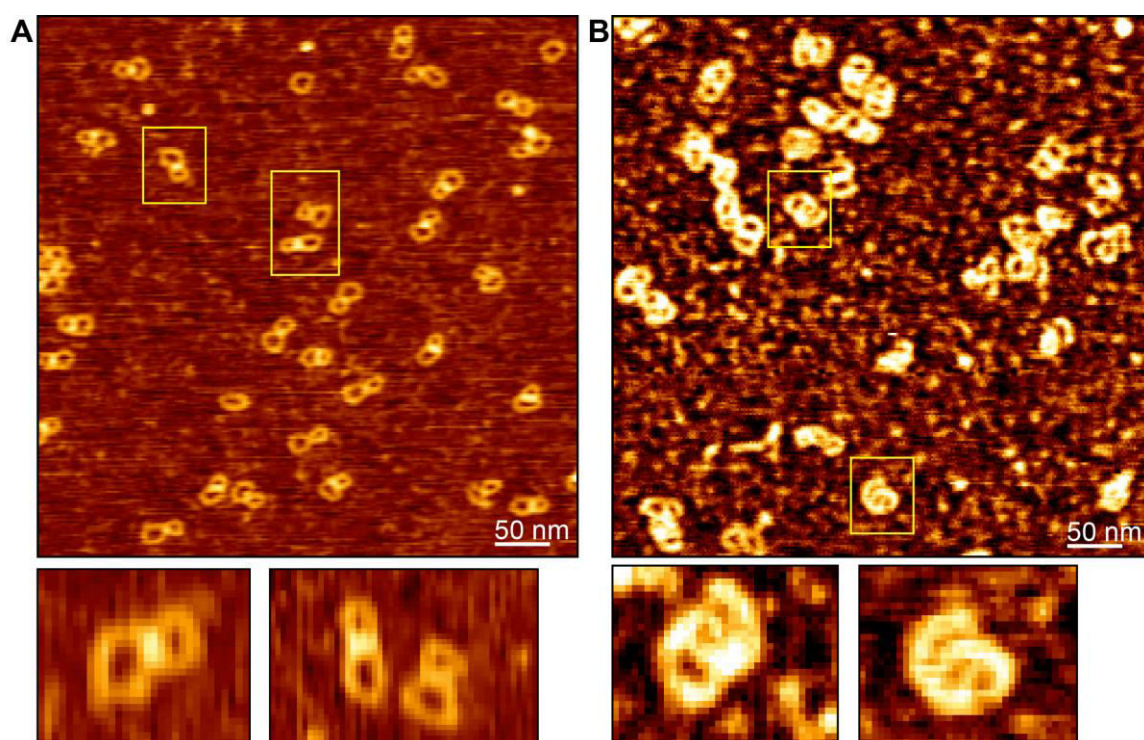


Figure 4.48. A) AFM image of the non-symmetric [2]catenane sample. Enlarged cutouts are shown below. B) AFM image of the [3]pseudocatenane sample. Enlarged cutouts are shown below. The images were taken with intermittent contact mode in air. The images were taken and slightly modified from reference <sup>98</sup>.

The AFM image of the non-symmetric [2]catenane was examined more in detail. In order to find whether the two rings of the catenane exhibit the sizes as calculated from the number of base pairs, the diameters of the rings were measured. The result of this cross section statistical analysis is given in Figure 4.49.B and the results fit well to the theoretically calculated diameters.

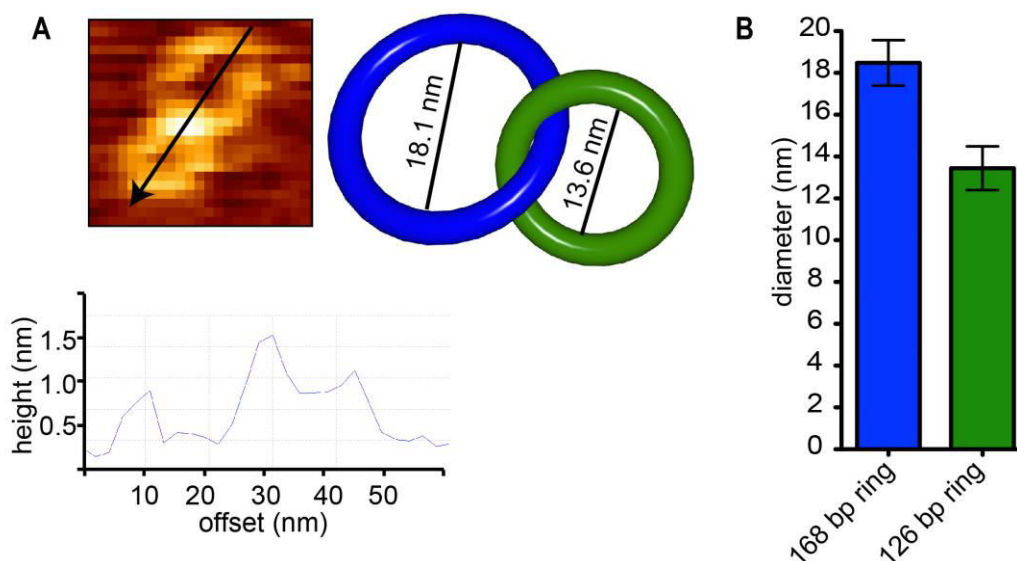


Figure 4.49. A) AFM image of one non-symmetric [2]catenane. The arrow indicates where the height profile (shown below) was measured. A 3D representation of the structure together with the theoretically calculated diameters of the corresponding rings is also shown (right). B) Result of the cross section statistical analysis. The found diameters correlate with the theoretical ones. The images were taken and slightly modified from reference <sup>98</sup>.

By the use of gel electrophoresis, HPLC, FQ experiments and AFM it was possible to show, that 1. the assembly of different types of ds DNA pseudocatenanes can be performed in a straightforward manner with relatively high yields, 2. the samples are accessible highly pure, 3. the structures can exist in a stalled pseudocatenane state and a mobile catenane state and 4. the catenanes exhibit a well-defined and rigid shape exhibiting ring diameters in agreement with the theoretical ones. The applicability of this new class of interlocked DNA architectures towards dynamic processes was further tested in a proof of concept switching experiment, which will be highlighted in the following section.

#### 4.4.2 Triggering of ds DNA Catenanes

Since the on/off switching of the mobility of the rings towards each other is of particular interest in order to introduce functionality into interlocked structures (cf. chapters 4.1, 4.2 and 4.3), a pseudocatenane/catenane switch was implemented into the catenane system containing two 168 bp rings. The switch was triggered by a toe-hold mechanism, similar to the pseudorotaxane/rotaxane switch presented in chapter 4.1.2. The switching principle is shown in Figure 4.50.C. Starting from the pseudocatenane, the Cat-TH-RO

(green) was added, an RO releasing the rings from each other equipped with a toe-hold, resulting in the catenane state with mobile rings. Addition of the Cat-cODN (magenta), entirely complementary to the Cat-TH-RO, led to the formation of a waste-duplex and release of the gap in the catenane ring. Subsequently, hybridization of the catenane gaps occurred, leading back to the pseudocatenane state. As shown before, in the case of the rotaxane switch (see chapter 4.1.2.1), the mobile to stalled conversion was followed by means of FQ experiments and a gel-shift assay. Due to the fluorophore and quencher labels on the catenane rings, the fluorescence emission should be reduced in the pseudocatenane state while it should increase in the catenane state. Measurement of the fluorescence after consecutive switching events resulted in the data presented in Figure 4.50.A.

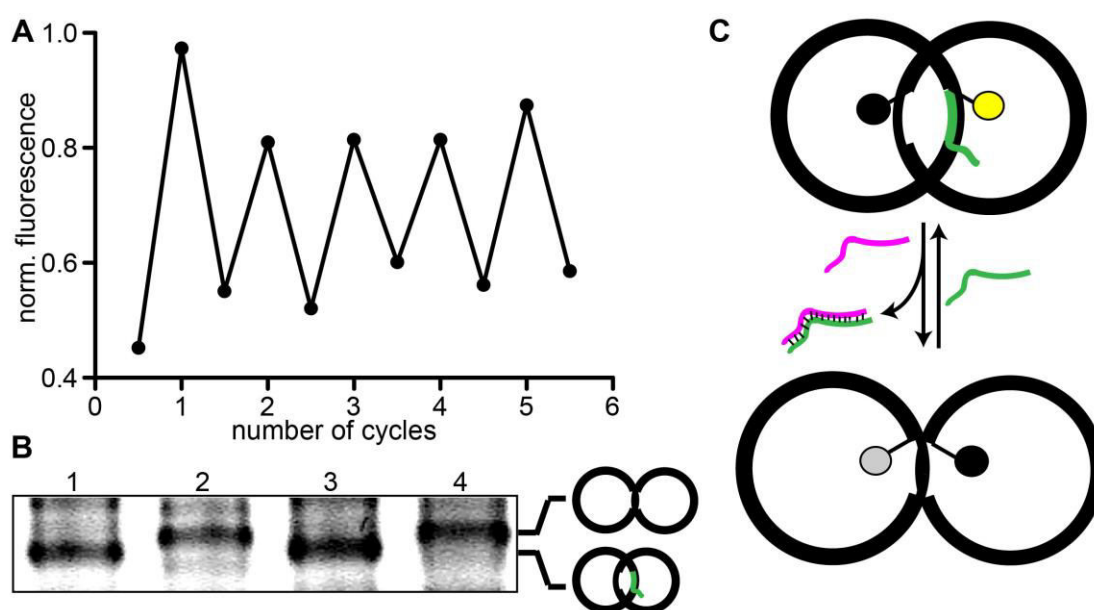


Figure 4.50. A) Results of the FQ experiment using the Cy3/BHQ-2 labeled [2]pseudocatenane containing two 168 bp rings. Starting from the pseudocatenane, Cat-TH-RO and Cat-cODN were added consecutively and fluorescence emission was measured. B) Analytical agarose gel image of the pseudocatenane/catenane switching. Lanes 1-4 represent the catenane sample after consecutive addition of Cat-cODN (lane 2/4) and Cat-TH-RO (lane 1/3). The uncropped agarose gel image is given in Supporting Figure 10. C) Schematic of the DNA fuel induced reversible ring release. Grey/yellow spheres represent a Cy3 label, the black sphere a BHQ-2 label. The images were taken and slightly modified from reference<sup>98</sup>.

The high fluorescence intensity after switching into the catenane state and *vice versa*, unambiguously proves the successful pseudocatenane/catenane switching over ten switching events. To identify whether the switch occurs quantitatively, four samples

---

after consecutive switching events were analyzed by gel electrophoresis. Since the corresponding bands in the gel image of Figure 4.50.B entirely switch from the catenane band (higher electrophoretic mobility) to the pseudocatenane band (lower electrophoretic mobility) after Cat-cODN addition and *vice versa* after Cat-TH-RO addition, quantitative switching can be assumed.

The presented study demonstrates the potential of such catenane structures for the implementation of higher functionalities. Indeed, in collaboration with Dr. T. Li it was possible to introduce a bimolecular DNAzyme into a [3]catenane, in a way, that the activity of this DNAzyme can be switched on and off in a highly controlled fashion.

#### 4.4.3 A [3]Catenane as Framework for a Controllable DNAzyme

In order to build a highly controllable logic circuit, with which the triggering of the activity of a DNAzyme can be achieved, a [3]catenane with several modifications was assembled. The principal design and the switching cycle of this catenane are shown in Figure 4.51.A. Since Dr. T. Li performed the synthesis and most of the switching experiments, no details of the design (secondary structures), of the synthesis and of the switching experiments will be shown in this thesis. Nevertheless, in order to clarify the functionality of this system, a short introduction will be given. The [3]pseudocatenane contains two heads on the outer rings, each equipped with a bimolecular DNAzyme sequence and a bimolecular i-motif sequence. When both bimolecular i-motif sequences are in close proximity and the pH is lowered towards acidic, the i-motif is formed. Only when the i-motif is formed and potassium is present, the two bimolecular DNAzyme sequences are able to assemble to the active DNAzyme. Since the formation of the i-motif cannot occur in the pseudocatenane state, due to the separation of both bimolecular i-motif sequences by the rigid middle ring, not only the addition of protons, but also the addition of the ROs is required to form the i-motif and consequently the DNAzyme.

The required pseudocatenane to catenane conversion was followed *via* the FQ experiment presented in chapter 4.4.2. The i-motif formation can be visualized by a FRET signal mediated by fluorescence labels on the end of the i-motif sequences (experiment

performed by Dr. T. Li, data not shown). The active DNAzyme is able to reduce 3,3',5,5'-tetramethylbenzidine (TMB) in the presence of hemin and H<sub>2</sub>O<sub>2</sub> into a colored product. Hence, the activity of the DNAzyme can be followed by the increase of UV absorption. The data presented in Figure 4.51.B proves that the DNAzyme is only active when ROs and protons were added (experiment performed by Dr. T. Li).

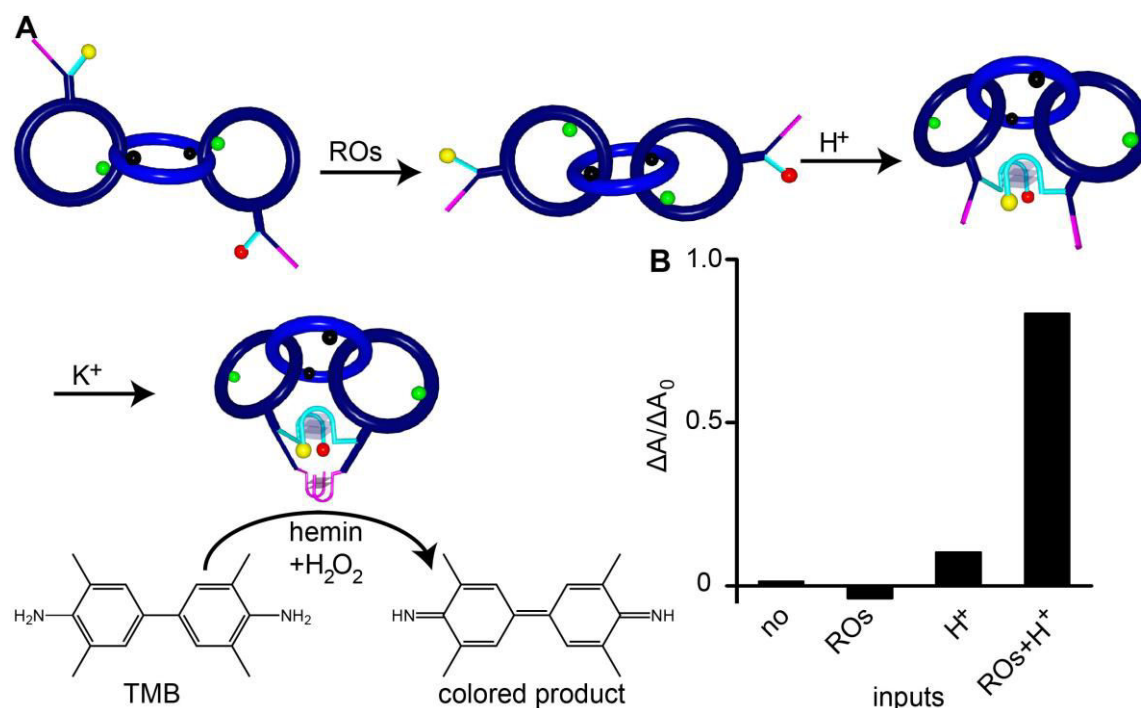


**Figure 4.51.** A) Scheme of the multi fuel induced switching of the [3]pseudocatenane, which is equipped with bimolecular i-motif (light blue) and bimolecular DNAzyme (magenta) sequences at the outer rings. Addition of the corresponding ROs converts the pseudocatenane to the catenane structure; subsequent addition of protons induces i-motif formation of the bimolecular i-motif sequences and thereby the formation of a condensed tetracyclic structure. Finally, the addition of potassium results in the formation of the DNAzyme out of the bimolecular DNAzyme sequences. Thereby, the DNAzyme activity is initiated, catalyzing the reduction of TMB to a colored product. Green spheres represent rhodamine green labels, black spheres BHQ-1 labels, the yellow sphere a Cy3 label and the red sphere a Cy5 label. B) The increase in absorption by the colored product from the TMB reduction reaction was measured, before and after addition of the ROs, the protons or both in the presence of potassium. The experiment was performed by Dr. T. Li. The images were taken and slightly modified from reference<sup>99</sup>.

The main contribution to this project within this thesis was to visualize the different states of the system by means of AFM, in order to have a direct proof of the formation of the predicted conformation. This is of particular interest, since the spatial separation of the outer rings in the case of the pseudocatenane state is essential for the operation of the system. Therefore, high resolution AFM images in Hyperdrive™ mode of the pseudocatenane before and after addition of the ROs were taken (see Figure 4.52).



While all structures in the pseudocatenane state exhibit a linear conformation, the structures in the catenane state display irregular conformations as expected, since the rings can now move unhindered towards each other. Note that even the heads of the outer rings can be observed in the AFM images. After addition of ROs, the pH was adjusted towards acidic and the sample was again analyzed *via* AFM. The resulting images depicted in Figure 4.52 now show structures with an entirely changed shape. The three rings of the catenane are still visible, but now, the two outer rings are connected to each other. This is in agreement with the predicted i-motif formation, which causes the structural rearrangement into the tetracyclic structure, and thereby proves the possibility to trigger the [3]catenane in the desired way.

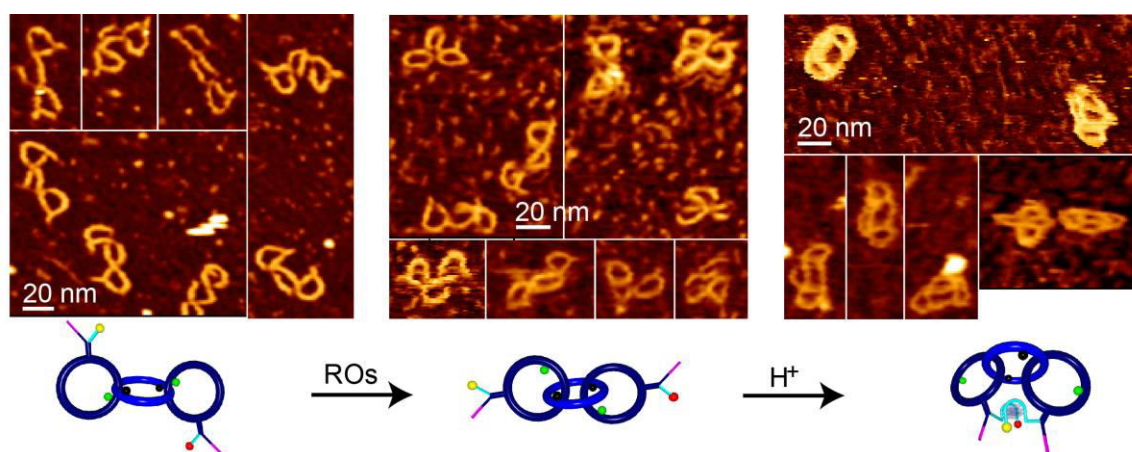


**Figure 4.52.** AFM images of a the [3]pseudocatenane sample before and after addition of the ROs and subsequent addition of protons. The reaction scheme and 3D representations of the corresponding structures are shown below. The images were taken with contact mode in liquid. The larger area AFM images are given in Supporting Figure 11. The images were taken and slightly modified from reference<sup>99</sup>

This controllable DNAzyme is based on the design of the beforehand presented [3]pseudocatenane (cf. chapter 4.4.1). This shows that these assemblies can be utilized to build up complex DNA nanomachineries, capable to catalyze chemical reactions in a highly controllable fashion.

---

## 5 Discussion and Outlook

In nature, complex protein systems such as enzymes are found. These systems can be considered as nanomachines that perform a large variety of biological functions upon triggering with external stimuli. The efficiency of these machineries is remarkable, and over the last decades has inspired the rational design of several artificial nanomachines. As pointed out in the introduction, DNA is an optimal material for the assembly of nanoscale objects, including complex structures, nanomechanical devices and computing systems. The principle of the assembly is usually based on fundamental Watson-Crick base pairing. The versatility and applicability of DNA based devices is enhanced by the easiness to chemically modify DNA with a broad range of bioactive molecules and the relatively high stability of DNA together with its solubility in aqueous solutions. Indeed, DNA is one of the most promising materials for the bottom-up assembly of functional nanosystems.

On the other hand, supramolecular chemists reported the synthesis of systems consisting of one, two or more interlocked molecules, which can move free relative to each other without losing their mechanical bond. Those interlocked molecules feature interesting properties for the use as molecular machinery, sensors and logic gates.

Recently, the assembly of interlocked systems made out of DNA has been reported. In particular, Famulok *et al.* presented a ds DNA rotaxane containing a macrocycle with free mobility along and around the axle. Depending on the stoppers used for the assembly, dethreading of the macrocycle could be favored or prevented. Heckel *et al.* reported the assembly of a ds DNA [2]pseudocatenane in which both rings are held together by polyamides. Willner *et al.* reported the assembly of various ss DNA catenanes consisting of two, three or five macrocycles, as well as a DNA/gold-nanoparticle hybrid rotaxane structure. The latter structures feature different switchable stations, thus a macrocycle can be piloted towards the desired station.

In this study, a ds DNA rotaxane was modified to promote the switching of the threaded macrocycle from a stalled state (pseudorotaxane) into a mobile state (rotaxane) in which

translational and rotational movement along and around the axle occurs unhindered. The switch can either be performed by the addition of fuel ODNs or by irradiation with light of specific wavelength. For both stimuli, a high reversibility of the switch was observed, proving the robustness of both, the rotaxane system and the switching mechanisms. Notably, the irradiation with light and the consequent isomerization of five azobenzene moieties induces the mobility of a stalled macrocycle with the weight of approx. 70 kDa. Then, Brownian motion powers the movement of the macrocycle. Since the rotaxane is entirely double stranded, in contrast with the systems presented by Willner *et al.*, no undesired interactions between unpaired bases or the formation of secondary structures hampers the mobility of the macrocycle. The structural differences between the pseudorotaxane and the rotaxane are reflected in a change of the electrophoretic mobility. By introducing fluorophore/quencher pairs to the system, a change of fluorescence emission could be detected after macrocycle mobility switching. This switch could serve as a nanosensor, responsive towards the mentioned stimuli. In this study, the switch was implemented into a more sophisticated system, namely a molecular shuttle. In this shuttle, the macrocycle can be reversibly directed from one station towards another station, again *via* addition of fuel ODNs or by irradiation with light. The driving force in order to move the macrocycle along the 20 nm long track is again Brownian motion. The applied stimuli are required to release the macrocycle and block one station or the other, respectively. The ds nature of the system and the resulting rigidity is the key in order to detect the macrocycle position. Therefore, the shuttle system features two different stoppers, thus allowing the direct and unambiguous determination of the position of the macrocycle near one or the other stopper by AFM. In this context, a novel stopper was designed and successfully synthesized by using the origami technique. Due to its modularity, this stopper can easily be altered and adapted to all kinds of requirements. The macrocycle in this shuttle system can be easily modified with diverse cargoes or bioactive components, as already presented in previous studies, which increases the scope of applications for this system (*vide infra*). The molecular shuttle mimics transport systems in living cells and its

---

realization is thereby one step further towards a nano machine, which imitates the efficiency of enzymes.

The enormous capability to store information and the programmability of DNA hybridization due to the base pairing rules led to a promising field within DNA nanotechnology, namely DNA computing. Logic gates are essential in order to build logic circuits and logical operators and within this context, the rotaxane-based shuttle was used to build a logic AND gate. Therefore, a [3]pseudorotaxane with a smaller and a bigger macrocycle threaded on the axle was designed and assembled. The design of this system allows the controlled release/dethreading of each macrocycle by addition of ODN inputs A and B, respectively. Addition of input B leads to dethreading of the big macrocycle, input A causes no dethreading of any macrocycle. Only the addition of input A and B leads to the dethreading of the small macrocycle, in a cascade-like reaction. First the big macrocycle is released, which then replaces the smaller macrocycle. The labeling of the small macrocycle and its station with a fluorophore/quencher pair allows detecting the dethreading of the small macrocycle by means of an increase in fluorescence emission (output). This logic AND gate operates nearly quantitatively, and no increase in fluorescence can be observed when only input A or B is added. Here, the characterization of the different accessible states was carried out by gel electrophoresis and AFM, which is only possible when the released ring dethreads. Therefore, a rotaxane with ring stoppers, which allows the dethreading of the macrocycle, was used. This prototype of logic gate can be further altered and improved. The use of spherical stoppers enables the assembly of a system in which no dethreading can occur. This could be used to fabricate a resettable and reversible logic gate, until now barely found in literature. The implementation of light sensitive inputs was tested, leading to the conclusion that such reversible logic gates might even be triggered by light instead of the addition of fuel ODNs, which further increases the applications and advantages of this logic gate system.

Apart from the work performed with the systems based on ds DNA rotaxanes, a new class of interlocked ds DNA assemblies has been established in this study. By using the same threading principle as for the rotaxane and the same macrocycle design, yielding

rigid rings of defined sizes, symmetric and non-symmetric ds DNA [2]catenanes and [3]catenanes were assembled and characterized by gel electrophoresis and AFM. These catenanes not only proved to have well defined circular shapes, but also were assembled with good yields and a high degree of purity. In switching experiments, with which the mobility of the rings can be induced or hampered, similar to the ones performed with the rotaxane system, the catenanes worked efficiently and therefore commend themselves for use in dynamic DNA nanotechnology. Indeed, in collaboration with Dr. T. Li, a [3]catenane system was used as the scaffold for a device capable to reversibly trigger the activity of a DNAzyme. Initially, the system has to exist in a linear pseudocatenane state in which the outer rings are separated. These rings are modified with a bimolecular DNAzyme. Only when all three rings can move unhindered relative to each other in the catenane state, the bimolecular split DNAzyme can be joined together, resulting in a condensed tetracyclic structure with the active DNAzyme. Switching back to the pseudocatenane state deactivates the DNAzyme. Part of this study was the determination of the three different states of the system *via* AFM and FQ experiments. The rigidity of the DNA rings in the presented system allowed the unambiguous detection of the different conformations of the catenane. Indeed, this is an essential requirement of the system, since the spatial separation of the two bimolecular DNAzyme parts in the pseudocatenane state leads to the deactivation of the DNAzyme itself.

The results of this study corroborate the presumption that DNA nanotechnology, combined with the unique properties of interlocked systems, may enable the fabrication of attractive and interesting nanodevices of diverse functionality. The contemporary research in the field of dynamic DNA nanotechnology will benefit from the possibility of utilizing interlocked DNA assemblies as scaffolds to fabricate sophisticated machinery.

Church *et al.* impressively demonstrated how a logic gated driven DNA container is capable to deliver drugs upon response to cellular stimuli (see chapter 2.5). Similarly, the systems presented in this thesis are highly modularly and can be potentially used and modified for a wide range of future applications. For instance, the macrocycle of the shuttle system as well as the origami stopper can easily be decorated with bioactive

---

molecules. One idea is, to attach two different enzymes to the macrocycle and the stopper. Enzyme A produces a substrate, which enzyme B requires for its activity. When both enzymes are spatially separated (macrocycle stalled on the station far from the corresponding stopper) only enzyme A is active, whereas in the case of close proximity of the enzymes (macrocycle stalled on the station near the corresponding stopper), also enzyme B is active. If the product of enzyme B is a drug, one could imagine a system that releases a specific drug exactly at the position where it is needed (e.g. in tumor cells). This controlled release might be triggered externally *via* light irradiation. Since the active mobile components of these structures are hold together *via* mechanical bonds, the possibility of disassembly at low concentrations (e.g. in the blood stream), which can cause a disfunction of the system, is very unlikely.

Another topic deals with DNA computing. The [3]catenane system presented above (see chapter 4.4.3) serves not only as a trigger for DNAzyme activity, but also as a reversible logic circuit. Interlocked architectures are ideal candidates for such approach, since the different components are tightly linked together. Additionally, it was shown that reversible switching within these systems could efficiently be achieved by diverse stimuli. Like the catenane system, the [3]pseudorotaxane architecture has proven its applicability for a logic operation, and by applying the mentioned modifications, like spherical stoppers and light sensitive inputs, this system could advance the research on DNA logic operators.

## 6 Materials and Methods

### 6.1 Materials and Reagents

<b>Materials and Reagents</b>	<b>Distributor (specification)</b>
Chemicals	Alfa Aesar, Sigma Aldrich, Fluka, VWR
Solvents	Alfa Aesar, Sigma Aldrich, Fluka
Water	usually ultra pure water was used
Columns and reagents for DNA synthesis	J.T. Baker, Proligo Reagents
ODNs	Metabion, Ella Biotech
T4-DNA Ligase/Buffer	Fermentas (5 U/ $\mu$ l)
Agarose High Resolution	ROTH
Acrylamide	30 % Acrylamide/Bisacrylamide 37.5:1
Centrifugal filter (30 kDa cutoff)	Amicon, Millipore
Freeze 'N Squeeze spin column	BioRad
Reverse phase C18 HPLC column	Macherey-Nagel (Nucleosil 100-5 C18)
WAX HPLC column (TSKgel)	TOSOH (DEAE-NPR 4.6 mm x 35 mm)
ACTA AFM probes	JPK
Ultra Short Cantilever AFM probes	NanoWorld
Mica	Plano (muscovite grade)

### 6.2 Buffer Systems

1x DNA storage buffer	10 mM Tris-HCl, 50 mM NaCl, 10 mM MgCl <sub>2</sub> at pH 7.5
1x Ligase buffer	40 mM Tris-HCl, 10 mM MgCl <sub>2</sub> , 10 mM DTT, 5 mM ATP at pH 7.8
1x Seeman buffer	40 mM Tris-HCl, 20 mM AcOH, 12 mM MgCl <sub>2</sub> , 2.5 EDTA at pH 7.8

---

1x TA buffer	40 mM Tris-AcOH, 50 mM NaCl at pH 5 or 8
1x origami buffer	5 mM Tris-HCl, 1 mM EDTA at pH 7.9
WAX A buffer	20 mM Tris-HCl at pH 9
WAX B buffer	20 mM Tris-HCl, 1 M NaCl at pH 9
TEAAc buffer	100 mM triethylammonium acetate
1x TAE buffer	40 mM Tris-HCl, 20 mM AcOH, 1mM EDTA
6x loading buffer	H <sub>2</sub> O (70 %), glycerol (30 %), bromophenol blue, xylene cyanol

### 6.3 Equipment

<b>Equipment</b>	<b>Producer (specification)</b>
PAGE chamber/equipment	BioRad
Agarose gel chamber	Institute of Chemistry, University of Bonn
Gel documentation system	BioRad
Plate reader Enspire	Perkin Elmer
Plate reader Varioscan	Thermo Scientific
Plate reader Tecan Ultra	Tecan
UV/vis spectrometer	Perkin Elmer (Lambda 2s)
Temperature control of UV/vis spectrometer	PTP-1 peltier controlled thermostat
UV photometer	Thermo Spectronic (Bio Mate 3)
NMR spectrometer	Bruker (DP400)
HPLC	Agilent (1100 series)
LC-MS (ESI)	Agilent (1100 series), Bruker (EsquireHCT)
AFM	JPK (NanoWizard 3)
Light source (UV/vis)	Institute of Chemistry, University of Bonn
DNA/RNA synthesizer	Applied Biosystems (ABi 3400)



---

Centrifuge	Eppendorf (5804R, 5810R, 5417C)
Vacuum centrifuge	Eppendorf (Concentrator 5301)
Thermo-Mixer	Eppendorf (Comfort)
Block heater	Stuart Scientific
Ultra pure water system	Barnstead (Easy Pure UV/UF)
Scale	Sartorius (BL1500S, BD211D)
Pipettes	Eppendorf (Research Plus)
pH meter	IonoLab

## 6.4 Methods

### 6.4.1 UV Absorption Spectroscopy

Due to the aromatic purine and pyrimidine nucleobases, DNA shows a maximum absorption at 260 nm. This can be used to determine the concentration of a DNA sample. By measuring the optical density (OD) in a photometer of a sample containing DNA with unknown concentration ( $c$ ),  $c$  can be calculated with the Lambert-Beer law:

$$OD = c \cdot \epsilon \cdot L$$

where  $\epsilon$  is the extinction coefficient of the DNA species in the sample and  $L$  the optical path length, which was 1 cm for the used quartz cuvette. If the DNA sequence is known, as it is the case for chemically synthesized ODNs,  $\epsilon$  can easily be calculated from the sum of the  $\epsilon$  values of each nucleotide of the ODN. The  $\epsilon$  of adenine is 15300 l/mol\*cm, of cytosine 7400 l/mol\*cm, of thymine 9000 l/mol\*cm and of guanine 11700 l/mol\*cm. By measuring a serial dilution of a sample containing azobenzene coupled to threoninol in a known concentration,  $\epsilon$  for azobenzene or dimethylazobenzene moiety was found to be 6000 l/mol\*cm. In order to determine the concentrations of DNA assemblies (rings, stoppers, dumbbells, rotaxanes and origami) the  $\epsilon$  values for each assembly was calculated with the following equation and are given in Supporting Table 4:

$$\epsilon = 20 \cdot MW$$

---

where MW is the molecular weight of the assembly, which can easily be calculated from the sum of the MWs of the nucleotides. The equation results from the averaged assumption of an OD value of 1 for a solution containing 50 µg/ml ds DNA and upon transforming of Lambert-Beer law and integration of the MW.

#### **6.4.2 Absorption Spectroscopy of *cis/trans*-DMAB5-RO**

In order to distinguish between the *cis*- and the *trans* form of azobenzene modified DNA, UV/vis spectra of the corresponding compounds were measured. For reversible photo switching experiments, 5 µM solution of DMAB5-RO in water was photo isomerized *via* irradiation at 450 nm (*vide infra*) into the *trans* form and the absorption was measured with a Perkin Elmer Lambda 2S UV/vis spectrometer from 280 to 500 nm. Subsequently, the sample was irradiated at 365 nm in order to isomerize the DMAB moieties into the *cis* form and the absorption spectrum was measured again. Alternate irradiation with vis/UV light and measuring of the absorption spectra was carried out in order to prove reversibility of the switching.

#### **6.4.3 Absorption Spectroscopy of AB and DMAB Modified DNA after Thermally Induced *cis* to *trans* Isomerization**

In order to examine the thermally induced *cis* to *trans* isomerization of AB and DMAB modified ODNs, the corresponding samples (AB2-RO and DMAB5-RO) (10 µM) in TA buffer containing additionally 50 mM NaCl at pH 7 were photo isomerized *via* irradiation at 450 nm into the *trans* form and absorption was measured with a Perkin Elmer Lambda 2S UV/vis spectrometer from 280 to 500 nm. After irradiation at 365 nm in order to isomerize the AB/DMAB moieties into the *cis* form, the absorption of the sample was measured. Following, the samples were protected from light, incubated at either 25 or 60 °C, and the absorption spectra were measured after 4 h, 12 h and 24 h respectively.

#### **6.4.4 DNA Melting Experiment**

For the DNA melting experiment, a solution of 1 µM DMAB5-RO and its complementary ODN in DNA storage buffer was heated from 25 °C to 90 °C while the change in the

absorption at 260 nm was measured with a Perkin Elmer Lambda S2 UV/vis spectrometer, equipped with a PTP-1 peltier controlled thermostat system. The sample was measured in a 1 ml quartz cuvette and degassed prior measurement *via* heating to 95 °C for 5 min.

## 6.5 Gel Electrophoresis

Precursors and final products as well as switching products of pseudorotaxane/rotaxane conversion were separated and analyzed *via* gel electrophoresis. Axles and rings were analyzed *via* native polyacrylamide gel electrophoresis (PAGE) whereas larger assemblies like spherical stoppers, origami and rotaxanes were analyzed *via* agarose gel electrophoresis.

### 6.5.1 Native Polyacrylamide Gel Electrophoresis (PAGE)

PAGE gels were always poured from 6 ml of a 6 % acrylamide solution containing 1x TAE buffer. The polymerization was induced by addition of 25  $\mu$ l of APS and 5  $\mu$ l of TEMED. The samples were mixed with 1/6 of the volume of 6x loading buffer prior loading the gel. The electrophoretic separation was carried out with 200 V at room temperature (approx. 20 °C) over 20 min. The gels were post-stained with ethidium bromide for 10 min before DNA assemblies/fragments were visualized and photographed in a transilluminator (360 nm) with integrated camera.

### 6.5.2 Agarose Gel Electrophoresis

Agarose gels were prepared with 1.5-3.6 % (w/v) of agarose in 0.5x TAE buffer (for analysis of origami structures, the TAE buffer contained 10 mM MgCl<sub>2</sub>). In order to dissolve the agarose, the mixture was carefully heated in a microwave oven before pouring the gel. The samples were mixed with 1/6 of the volume of 6x loading buffer prior loading the gel. The electrophoretic separation was carried out with 80-200 V at 4 °C or room temperature (approx. 20 °C) over 20-120 min (details are noted in the corresponding chapters). The gels were post-stained with ethidium bromide for 10 min and destained for 30 min in water before DNA assemblies/fragments were visualized and photographed with a transilluminator (360 nm) with integrated camera.

---

## 6.6 High Performance Liquid Chromatography (HPLC)

Purification and analysis of synthesized ODNs and DNA assemblies were performed with HPLC. While ODNs were separated from byproducts and contaminations on a reverse phase column, DNA assemblies were separated from byproducts and contaminations on a weak anion exchange (WAX) column. All separations were performed on a HPLC system with quaternary pump and automated injector from Agilent connected to a UV spectrometer. Fractions were detected by UV absorption at 260 nm and collected manually.

### 6.6.1 Reverse Phase HPLC

Deprotected ODNs were purified on a C-18 reverse phase column with a solvent gradient, using solvent A (TEAAc buffer) and solvent B (acetonitrile). The gradient was solvent A/solvent B → 100 % to 70 % in 25 min. The product fraction was collected, dried with a vacuum concentrator and dissolved in water. The concentration was determined *via* UV absorption measurement (*vide supra*).

### 6.6.2 Weak Anion Exchange HPLC

DNA assemblies (except DNA origami) were purified on a WAX column with a solvent gradient, using WAX-A and WAX-B buffer. The gradient for all structures except for the [3]pseudorotaxane was WAX A/WAX B → 65 % to 45 % in 20 min, for the [3]pseudorotaxane in 30 min. The collected product fraction was concentrated with centrifugal filters, washed twice with DNA storage buffer and eluted in DNA storage buffer. The concentration was determined *via* UV absorption measurement (*vide supra*).

## 6.7 Fluorescence Measurements

### 6.7.1 Fluorescence Quenching Experiments

In the case of the Cy3/BHQ-2 labeled assemblies, the samples were excited at 550 nm and fluorescence was measured five times at 570 nm for 500 ms in a Varioscan plate reader. In the case of the TAMRA/BHQ-2 labeled assembly, the sample was excited at 550 nm and fluorescence spectra were measured between 570 nm and 650 nm in an

Enspire plate reader. In the case of the Rhodamine green/BHQ-1 labeled assembly, the sample was excited at 500 nm and fluorescence was measured at 534 nm in an Enspire plate reader.

### **6.7.2 Fluorescence Polarization (FP) Experiments**

The Rhodamine green labeled sample was excited at 550 nm and the fluorescence polarization was measured in a Tecan plate reader.

## **6.8 Atomic Force Microscopy (AFM)**

The direct visualization of DNA nanoassemblies was performed with the atomic force microscope Nanowizard 3 (JPK instruments). Two different modes were utilized. The intermittent contact mode in air (AC mode) and the contact mode in liquid (Hyperdrive™ mode). The AC mode allows scanning larger regions in shorter periods of time but with lower resolution in comparison with the Hyperdrive™ mode, which gives high-resolution images but with lower scanning speed. The data was processed using the JPK processing software.

### **6.8.1 Intermittent Contact Mode (AC Mode)**

The samples were measured on freshly cleaved mica surface. Therefore, the upper layer of the mica was removed with a cellotape. A circle of 3 mm diameter was drawn on the mica, using a water-resistant marker, and 3  $\mu$ l of polyethylenimine was pipetted inside the circle. After incubation for 1 min at RT, the mica was rinsed four times with 200  $\mu$ l water and dried under air stream. Following, 3  $\mu$ l of the sample (3-5 nM concentration dissolved in 1x Seeman buffer) was pipetted in the circle and incubated for 1 min at RT. The mica was rinsed four times with 200  $\mu$ l water and dried under air stream. Then, the sample was ready to analyze by AFM using the JPK software and ACTA probes (silicon tips).

### **6.8.2 Contact Mode in Liquid (Hyperdrive™ Mode)**

The mica was prepared similar as for the AC mode measurements, but polyornithine was used instead of polyethylenimine. 3  $\mu$ l of the sample (3-10 nM concentration dissolved

---

in 1x Seeman buffer) was pipetted in the circle and incubated for 1 min at RT. The mica was rinsed once with 200  $\mu$ l water placed in the AFM and immediately covered with 400  $\mu$ l water. In some cases, 0.2 x Seeman buffer was used instead of water, in order to keep the structures intact immobilized on the mica. For the [3]catenane sample, a customized TA buffer either at pH 5 or 8 was used instead of the Seeman buffer (*vide infra*). Once the mica was covered with liquid, the sample was ready to analyze by AFM using the JPK software and Ultra Short Cantilever probes (high dense carbon tips).

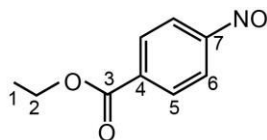
### 6.9 Photo Induced Isomerization of AB and DMAB

The irradiation of the samples was carried out in glass cuvettes with an in house fabricated light source. The light source is equipped with two LED (Nichia Corporation), which irradiate at 365 nm and 450 nm, respectively. Additionally, the light source is equipped with a Peltier module for temperature control. Unless otherwise noted, *trans* to *cis* isomerization was achieved by irradiating 10 min at 365 nm at 25 °C, and *cis* to *trans* isomerization by irradiating 2 min at 450 nm at 25 °C.

### 6.10 Synthesis of AB and DMAB Phosphoramidite

The synthesis of the AB phosphoramidite was performed as described in the diploma thesis: F. Lohmann, *Entwicklung und Steuerung einer lichtschtbaren DNA-Nanoarchitektur, University of Bonn 2010*. The author performed the first four synthetic steps towards the DMAB phosphoramidite, whereas O. Wolters as part of her diploma thesis performed the whole synthesis under the author's supervision. The experimental data was provided by O. Wolters.<sup>100</sup> NMR spectra of intermediates and the final DMAB phosphoramidite product are given in chapter 7.3. Both, the synthesis of AB and DMAB phosphoramidite was adapted and slightly modified from references<sup>25,28</sup>.

### 6.10.1 Synthesis of Ethyl-4-nitrobenzoate



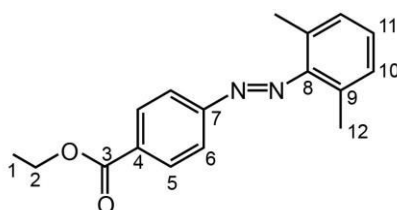
Ethyl-4-nitrobenzoate (9.8 g, 50 mmol), dissolved in 120 ml 2-methoxyethanol was mixed with a solution of ammoniumchloride (7.2 g, 145 mmol) in 30 ml distilled water and stirred at 30 °C for 10 min. Zinc powder (7.0 g, 150 mmol) was added over 30 min while the temperature was kept lower than 30 °C with a water bath before the solution was stirred for 24 h at RT. The solid residue was removed *via* vacuum filtration, and the solution was cooled to 0 °C with an ice bath. A solution of iron(III)chloride-hexahydrate (35.5 g, 127 mmol) in 200 ml distilled water and 30 ml of ethanol was cooled to 0 °C and added dropwise over 30 min to the filtrate. After stirring for 1 h at 0 °C, 170 ml of distilled water was added. The aqueous part was removed by filtration and precipitate was dissolved in 170 ml of dichloromethane. The organic layer was washed with 100 ml of distilled water and 100 ml of brine, before drying with magnesium sulfate. The solvent was removed under reduced pressure and the yellow, solid product was purified by recrystallization from a water/ethanol mixture (1:4) and dried under reduced pressure. The yield was 69.5 % (6.2 g).

$^1\text{H-NMR}$ : (300 MHz,  $\text{CDCl}_3$ )  $\delta$  [ppm] = 8.27-8.31 (2 H, dt,  $^4J_{\text{HH}} = 1.92$  Hz,  $^3J_{\text{HH}} = 6.84$  Hz,  $\text{H}_5$ ), 7.90-7.95 (2 H, dt,  $^4J_{\text{HH}} = 1.89$  Hz,  $^3J_{\text{HH}} = 6.78$  Hz,  $\text{H}_6$ ), 4.40-4.47 (2 H, q,  $^3J_{\text{HH}} = 7.14$  Hz,  $\text{H}_2$ ), 1.40-1.45 (3 H, t,  $^3J_{\text{HH}} = 7.11$  Hz,  $\text{H}_1$ ).

$^{13}\text{C-NMR}$ : (75 MHz,  $\text{CDCl}_3$ )  $\delta$  [ppm] = 165.4 ( $\text{C}_7$ ), 164.6 ( $\text{C}_3$ ), 135.7 ( $\text{C}_4$ ), 131.1 ( $\text{C}_5$ ), 120.5 ( $\text{C}_6$ ), 62.0 ( $\text{C}_2$ ), 14.4 ( $\text{C}_1$ ).

Mass spectrum (EI):  $m/z$  (%): 179.0 (100).

### 6.10.2 Synthesis of Ethyl-2',6'-dimethylazobenzene-4-carboxylate



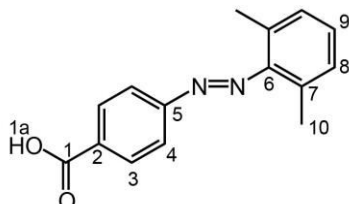
To a solution of ethyl-4-nitrosobenzoate (5.0 g, 27.9 mmol) in 300 ml glacial acetic acid, 2,6-dimethylaniline (4.5 g, 36.9 mmol) was added and stirred at RT for 16 h in the dark. Subsequently, the solution was mixed with 300 ml distilled water and the pH was adjusted to 7 with hydrogen carbonate. The product was extracted four times from the solution with 250 ml ethyl acetate. The organic layer was washed with 800 ml saturated solution of NaHCO<sub>3</sub>, 800 ml of brine and dried with magnesium sulfate. The solvents were removed under reduced pressure and the red, oily product was purified *via* column chromatography (stationary phase: silica; eluent: cyclohexane/ethyl acetate = 50/1). The solvents were removed under reduced pressure. The yield was 20 % (1.6 g).

<sup>1</sup>H-NMR: (300 MHz, CDCl<sub>3</sub>) δ [ppm] = 8.19-8.23 (2 H, dt, <sup>3</sup>J<sub>HH</sub> = 8.60 Hz, <sup>4</sup>J<sub>HH</sub> = 1.71 Hz, H<sub>5</sub>), 7.90-7.95 (2 H, dt, <sup>3</sup>J<sub>HH</sub> = 8.70 Hz, <sup>4</sup>J<sub>HH</sub> = 1.71 Hz, H<sub>6</sub>), 7.12-7.21 (3 H, m, H<sub>10</sub>, H<sub>11</sub>), 4.40-4.47 (2 H, q, <sup>3</sup>J<sub>HH</sub> = 7.11 Hz, H<sub>2</sub>), 2.41 (6 H, s, H<sub>12</sub>), 1.41-1.46 (3 H, t, <sup>3</sup>J<sub>HH</sub> = 7.11 Hz, H<sub>1</sub>).

<sup>13</sup>C-NMR: (75 MHz, CDCl<sub>3</sub>) δ [ppm] = 166.2 (C<sub>3</sub>), 155.3 (C<sub>7</sub>), 151.1 (C<sub>8</sub>), 132.3 (C<sub>4</sub>), 131.5 (C<sub>9</sub>), 130.7 (C<sub>5</sub>), 129.4 (C<sub>10</sub>), 129.0 (C<sub>11</sub>), 122.3 (C<sub>6</sub>), 61.4 (C<sub>2</sub>), 19.3 (C<sub>12</sub>), 14.5 (C<sub>1</sub>).

Mass spectrum (EI): m/z (%): 281.1 (50) [M]<sup>+</sup>.

### 6.10.3 Synthesis of 4-Carboxy-2',6'-dimethylazobenzene



To a solution of ethyl-2',6'-dimethylazobenzene-4-carboxylate (1.5 g, 5.3 mmol) in 60 ml ethanol, 16 ml of 2 M solution of sodium hydroxide was added. The mixture was stirred at RT for 16 h in the dark. 30 ml of 1 M solution of hydrochloric acid was added in order



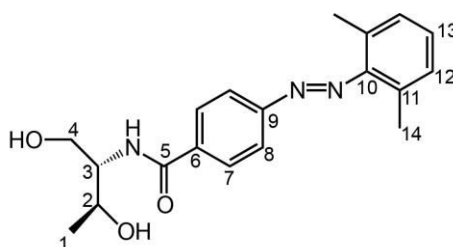
to adjust the pH to slightly acidic before the product was extracted two times from the solution with 350 ml ethyl acetate. The organic layer was washed twice with 200 ml distilled water and 200 ml of brine and dried with magnesium sulfate. The solvents were removed under reduced pressure yielding 95 % (1.4 g) of the red solid product.

$^1\text{H-NMR}$ : (300 MHz,  $\text{CDCl}_3$ )  $\delta$  [ppm] = 13.24 (1 H, s,  $\text{H}_{1a}$ ) 8.13-8.17 (2 H, dt,  $^3J_{\text{HH}} = 8.16$  Hz,  $\text{H}_3$ ), 7.90-7.94 (2 H, dt,  $^3J_{\text{HH}} = 8.49$  Hz,  $\text{H}_4$ ), 7.18-7.27 (3 H, m,  $\text{H}_8, \text{H}_9$ ), 2.34 (6 H, s,  $\text{H}_{10}$ ).

$^{13}\text{C-NMR}$ : (75 MHz,  $\text{CDCl}_3$ )  $\delta$  [ppm] = 166.7 ( $\text{C}_1$ ), 154.6 ( $\text{C}_5$ ), 150.3 ( $\text{C}_6$ ), 132.8 ( $\text{C}_2$ ), 130.8 ( $\text{C}_7$ ), 130.6 ( $\text{C}_3$ ), 129.3 ( $\text{C}_8$ ), 128.1 ( $\text{C}_9$ ), 122.1 ( $\text{C}_4$ ), 18.7 ( $\text{C}_{10}$ ).

Mass spectrum (EI):  $m/z$  (%): 254.1 (38)  $[\text{M}]^+$ .

#### 6.10.4 Synthesis of 4-Carboxy-2',6'-dimethylazobenzene-D-threoninol



To a solution of 4-carboxy-2',6'-dimethylazobenzene (1.2 g, 4.7 mmol) in 30 ml DMF, D-threoninol (0.5 g, 4.9 mmol) was added. A solution of HBTU (1.9 g, 4.9 mmol) in 20 ml DMF was added dropwise, the solution was stirred at RT for 16 h in the dark. The precipitate was removed by filtration and the filtrate was dried under reduced pressure. The product was purified *via* column chromatography (stationary phase: silica; eluent: ethyl acetate/methanol = 40:1). The solvents were removed under reduced pressure. The yield was 60 % (1.0 g).

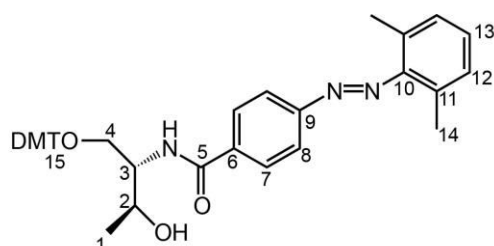
$^1\text{H-NMR}$ : (300 MHz,  $d_6$ -DMSO)  $\delta$  [ppm] = 8.07-8.10 (2 H, d,  $^3J_{\text{HH}} = 8.43$  Hz,  $\text{H}_7$ ) 7.90-7.92 (2 H, d,  $^3J_{\text{HH}} = 8.43$  Hz,  $\text{H}_8$ ), 7.18-7.26 (3 H, m,  $\text{H}_{12}, \text{H}_{13}$ ), 4.62-4.67 (1 H, m,  $\text{H}_2$ ), 3.86-3.96 (1 H, m,  $\text{H}_3$ ), 3.50-3.67 (2 H, m,  $\text{H}_4$ ), 2.33 (6 H, s,  $\text{H}_{14}$ ), 1.08-1.10 (3 H, d,  $^3J_{\text{HH}} = 6.21$  Hz,  $\text{H}_1$ ).

---

$^{13}\text{C}$ -NMR: (75 MHz,  $d_6$ -DMSO)  $\delta$  [ppm] = 165.9 ( $\text{C}_5$ ), 162.3 ( $\text{C}_4$  or  $\text{C}_{11}$ ), 153.6 ( $\text{C}_6$ ), 150.5 ( $\text{C}_{10}$ ), 137.0 ( $\text{C}_9$ ), 130.6 ( $\text{C}_{13}$ ), 129.3 ( $\text{C}_{12}$ ), 121.9 ( $\text{C}_8$ ), 64.9 ( $\text{C}_2$ ), 60.5 ( $\text{C}_4$  or  $\text{C}_{11}$ ), 56.9 ( $\text{C}_3$ ), 20.3 ( $\text{C}_1$ ), 18.6 ( $\text{C}_{14}$ ).

Mass spectrum (EI):  $m/z$  (%): 364.2 (100)  $[\text{M}+\text{Na}^+]^+$ , 342.2 (31)  $[\text{M}+\text{H}^+]^+$ .

#### 6.10.5 Synthesis of DMT Protected 4-Carboxy-2',6'-dimethylazobenzene-D-threoninol



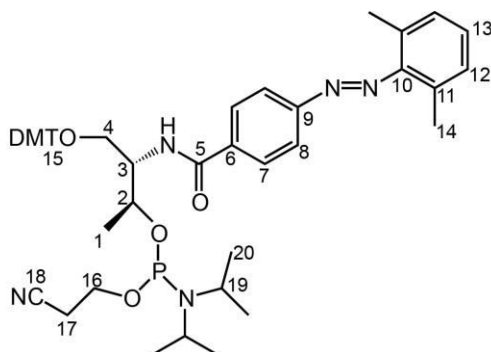
To a solution of 4-carboxy-2',6'-dimethylazobenzene-D-threoninol (0.50 g, 1.46 mmol) and 4-(dimethylamino)-pyridine (0.01 g, 0.07 mmol) in 10 ml pyridine, at 0 °C under argon, a solution of 4,4'-dimethoxytritylchloride (0.52 g, 1.53 mmol) in dichloromethane was added over 30 min. The mixture was stirred for 24 h at RT and the product was purified *via* column chromatography (stationary phase: silica; eluent: cyclohexane/ethyl acetate/triethylamine = 50:50:3). The solvents were removed under reduced pressure, yielding 35 % (0.33 g) of a red foam.

$^1\text{H}$ -NMR: (300 MHz,  $d_6$ -DMSO)  $\delta$  [ppm] = 7.95 (4 H, s,  $\text{H}_7$ ,  $\text{H}_8$ ) 6.77-7.45 (16 H, m,  $\text{H}_{12}$ ,  $\text{H}_{13}$ ,  $\text{H}_{15}$ ), 4.08-4.25 (2 H, m,  $\text{H}_2$ ,  $\text{H}_3$ ), 3.76-3.77 (6 H, d,  $^4J_{\text{HH}} = 2.44$  Hz,  $\text{H}_3\text{C-O-DMT}$ ), 3.35-3.53 (2 H, m,  $\text{H}_4$ ), 2.40 (6 H, s,  $\text{H}_{14}$ ), 1.20-1.23 (3 H, d,  $^3J_{\text{HH}} = 8.48$  Hz,  $\text{H}_1$ ).

$^{13}\text{C}$ -NMR: (75 MHz,  $d_6$ -DMSO)  $\delta$  [ppm] = 167.1 ( $\text{C}_5$ ), 159.2 ( $\text{C}_{11}$ ), 154.9 ( $\text{C}_6$ ), 151.4 ( $\text{C}_{10}$ ), 145.1 ( $\text{C}_9$ ), 136.8 ( $\text{C}_{15}$ ), 135.9 ( $\text{C}_{15}$ ), 131.8 ( $\text{C}_{15}$ ), 130.3 ( $\text{C}_{13}$ ), 129.6 ( $\text{C}_{12}$ ), 129.2 ( $\text{C}_{15}$ ), 128.7 ( $\text{C}_{15}$ ), 128.4 ( $\text{C}_{15}$ ), 127.3 ( $\text{C}_{15}$ ), 122.9 ( $\text{C}_7$ ), 120.8 ( $\text{C}_8$ ), 113.6 ( $\text{C}_{15}$ ), 87.0 ( $\text{C}_{15}$ ), 68.6 ( $\text{C}_2$ ), 65.0 ( $\text{C}_4$ ), 55.6 ( $\text{C}_3$ ), 38.8 ( $\text{H}_3\text{C-O-DMT}$ ), 19.3 ( $\text{C}_{14}$ ), 17.9 ( $\text{C}_1$ ).

Mass spectrum (EI):  $m/z$  (%): 666.3 (100)  $[\text{M}+\text{Na}^+]^+$ .

### 6.10.6 Synthesis of DMT Protected 4-Carboxy-2',6'-dimethylazobenzene-D-threoninol-phosphoramidite



To a solution of DMT protected 4-carboxy-2',6'-dimethylazobenzene-D-threoninol (0.30 g, 0.47 mmol) in 5 ml dichloromethane, at 0 °C under argon, diisopropylamine (0.07 g, 0.51 mmol) was added and the mixture was stirred for 15 min at 0 °C before 2-cyanoethyl-N,N-diisopropylchlorophosphoramidite (0.12 g, 0.51 mmol) was added dropwise. The mixture was stirred for 10 min at 0 °C, then allowed to warm to RT and stirred for one hour. The solvents were removed under reduced pressure and the product was purified *via* column chromatography (stationary phase: silica; eluent: cyclohexane/ethyl acetate/triethylamine = 60:40:3). The solvents were removed under reduced pressure. The product was obtained as a red foam in a 72 % yield (0.28 g).

$^1\text{H-NMR}$ : (300 MHz,  $d_6$ -DMSO)  $\delta$  [ppm] = 7.91-7.93 (4 H, m, H<sub>7</sub>, H<sub>8</sub>), 6.79-7.47 (16 H, m, H<sub>12</sub>, H<sub>13</sub>, H<sub>15</sub>), 4.33-4.49 (2 H, m, H<sub>2</sub>, H<sub>3</sub>), 3.67-3.85 (8 H, m, H<sub>15</sub>, H<sub>20</sub>), 3.48-3.61 (2 H, m, H<sub>4</sub>), 2.39 (6 H, s, H<sub>14</sub>), 1.13-1.17 (12 H, m, H<sub>20</sub>), 1.01-1.03 (3 H, d,  $^3J_{\text{HH}} = 9.04$  Hz, H<sub>1</sub>).

$^{13}\text{C-NMR}$ : (75 MHz,  $d_6$ -DMSO)  $\delta$  [ppm] = 166.5 (C<sub>5</sub>), 159.0 (C<sub>15</sub>), 154.8 (C<sub>9</sub>), 151.4 (C<sub>10</sub>), 145.4 (C<sub>15</sub>), 137.0 (C<sub>6</sub>), 136.4 (C<sub>15</sub>), 131.8 (C<sub>11</sub>), 127.1-130.5 (C<sub>15</sub>, C<sub>12</sub>, C<sub>13</sub>, C<sub>7</sub>, C<sub>8</sub>), 122.9 (C<sub>15</sub>, C<sub>12</sub>, C<sub>13</sub>, C<sub>7</sub>, C<sub>8</sub>), 120.8 (C<sub>18</sub>), 113.5 (C<sub>15</sub>), 86.5 (C<sub>15</sub>), 63.3 (C<sub>4</sub>), 58.9 (C<sub>2</sub>, C<sub>3</sub>), 58.6 (C<sub>2</sub>, C<sub>3</sub>), 55.6 (C<sub>16</sub>), 43.5 - 43.7 (C<sub>19</sub>), 24.6 - 25.1 (C<sub>20</sub>), 20.8 (C<sub>17</sub>), 19.3 (C<sub>1</sub>), 18.0 (C<sub>14</sub>).

$^{31}\text{P-NMR}$ : (162 MHz,  $\text{CD}_2\text{Cl}_2$ )  $\delta$  [ppm] = 149.2 (s), 148.5 (s).

Mass spectrum (EI):  $m/z$  (%): 866.4 (100)  $[\text{M}+\text{Na}]^{+\bullet}$ .

---

### 6.11 Synthesis of AB and DMAB Modified ODNs

Solid phase synthesis using the phosphoramidite method of AB and DMAB modified ODNs was performed with a DNA/RNA synthesizer from Applied Biosystems. For the synthesis of the corresponding ODN low volume columns with the first DMT protected deoxynucleotide coupled to the solid support (controlled pore glass (CPG)) were used. The coupling time for A, T, G and C was 1 min, whereas for AB and DMAB was 5 min. 3 % trichloroacetic acid in dichloromethane was used as detritylation reagent. The coupling was achieved with 0.1 M phosphoramidite solution in acetonitrile together with the activator solution containing 0.25 M 5-(ethylthio)-1H-tetrazole in acetonitrile. The capping was achieved with acetic anhydride (10 %) and 2,6-lutidine (10 %) in THF (80 %) (capping solution 1) and with 1-methylimidazole (16 %) in THF (84 %) (capping solution 2). For the oxidation, a solution of iodine (0.02 mM, 3 %) in pyridine (20 %), water (2 %) and THF (75 %) was used. The synthesis cycle ended with “trityl-off” including the detritylation of the final nucleotide.

The cleavage from the solid support and the deprotection of the nucleobases and the phosphate was achieved with the Ammonia-Methylamine method (AMA method). Therefore, the solid support was transferred from the column to a micro test tube (1.5 ml), 400 µl of aqueous ammonia (25 %) and 400 µl of aqueous methylamine (40 %) were added and the mixture was heated to 55 °C for 30 min. After removing the precipitate, the solvent was removed in a vacuum concentrator. The remaining crude product was purified by HPLC (*vide supra*).

### 6.12 Assembly of DNA Nanostructures

The rotaxanes and catenanes were synthesized from the macrocycles, stoppers and axles, which were preliminarily assembled and purified. Supporting Table 1 gives a summary of all assembled structures together with their constituent ODNs. Supporting Table 2 and Supporting Table 3 display all ODN sequences used for the assemblies. The ODNs used for the synthesis were HPLC purified, dissolved and diluted to 100 µM solutions in water.

### 6.12.1 Assembly of Macrocycles and Ring Stoppers

The ODNs for the corresponding macrocycle or ring stopper (16  $\mu$ l each) were mixed in a PCR tube with 1M sodium chloride solution (16  $\mu$ l) in 1x ligase buffer in order to achieve a total volume of 400  $\mu$ l with a final ODN concentration of 4  $\mu$ M. Annealing was achieved by heating the sample to 60 °C and subsequent cooling to 15 °C over 75 min in a thermo cycler. Then, ligase (4  $\mu$ l) was added and ligated for at least 12 h at 15 °C. The raw product was analyzed *via* PAGE, purified by WAX HPLC, concentrated with centrifugal filters and concentration was determined by UV measurement at 260 nm. After PAGE analysis of the purified product, it was used for further synthesis.

### 6.12.2 Assembly of Spherical Stopper

The SSt-ring1 and SSt-ring2 were synthesized as described for the macrocycle and mixed without purification. After annealing for 15 min at 15 °C, 4  $\mu$ l of ligase were added and ligated for at least 12 h at 15 °C. The crude was analyzed *via* agarose gel electrophoresis, purified by WAX HPLC, concentrated with centrifugal filters and concentration was determined by UV measurement at 260 nm (*vide supra*). After analysis of the purified product *via* agarose gel electrophoresis (2 % w/v, 200 V, 20 min, RT), it was used for further synthesis.

### 6.12.3 Assembly of Origami Stopper

In order to synthesize the origami stopper, the corresponding ODNs (2  $\mu$ l) were mixed with 1M MgCl<sub>2</sub> (18.5  $\mu$ l) in 1x origami buffer to a total volume of 1000  $\mu$ l with a final ODN concentration of 200 nM. The solution was heated to 95 °C for 5 min, cooled to 60 °C over 145 min (1 °C/5 min) and then to 15 °C over 450 min (1 °C/10 min). The crude product was analyzed *via* agarose gel electrophoresis (1.5 % w/v, 80 V, 60 min, 4 °C). The gel and running buffer contained additionally 10 mM MgCl<sub>2</sub>). The origami solution was purified by gel extraction, using the “Freeze ‘N Squeeze” method. Therefore, the sample was mixed with loading buffer, and the product was separated from unreacted ss ODNs and side products by agarose gel electrophoresis (1.5 % w/v, 80 V, 60 min, 4 °C). The gel was post stained with ethidium bromide, and after visualization under UV and gel

---

excision of the corresponding band, the gel was cut into small pieces, transferred into Quantum Prep™ Freeze 'N Squeeze DNA gel extraction spin column and frozen at - 80 °C for 5 min. The spin column was centrifuged (squeezed) at 5000 g for 10 min at RT. Thereby, the agarose debris is retained in the filter, while the DNA containing buffer is recovered in the bottom of the tube. The freezing and squeezing was repeated three times. The recovered DNA containing buffer was concentrated, using centrifugal filters and concentration was determined by UV measurement at 260 nm. After analysis of the purified product *via* agarose gel electrophoresis (1.5 % w/v, 80 V, 60 min, 4 °C), it was further used in following synthetic steps. In order to properly characterize the origami stopper, AFM images in AC mode of the purified sample were taken and the length and width of 20 intact structures were measured and statistically evaluated (see Figure 4.27).

#### 6.12.4 Assembly of [2]Rotaxane

The ODNs for the corresponding axle (2 µl) were mixed in 1x DNA storage to a total volume of 100 µl with a final ODN concentration of 2 µM. After 10 min of incubation at RT, the axle was mixed with 1.5 equiv. of macrocycle in 1x ligase buffer containing additionally 20 mM MgCl<sub>2</sub>. Threading was achieved after incubation at 15 °C over 12 h. Following, 2.5 equiv. of ring-, spherical- or origami-stopper (or 1.25 equiv. of the left and right stopper in the non-symmetric rotaxane) were added. After incubation at 15 °C over 10 min, ligase (1/100 v/v) was added and ligated for at least 12 h at 15 °C. The [2]pseudorotaxanes featuring two gap regions were prepared similarly, but before adding the macrocycle, either 5 equiv. of TH-RO2 or 5 equiv. of DMAB5-RO (irradiated with vis light) were added to the axle. The resulting pseudorotaxane sample was either purified *via* WAX HPLC or Freeze 'N Squeeze (in the case of the origami stopper containing pseudorotaxane) or used without further purification. After analysis of the product *via* agarose gel electrophoresis (2.4 % w/v, 180 V, 120 min, 4 °C for ring- and spherical-stoppered pseudorotaxane), (1.5 % w/v, 100 V, 60 min, 4 °C for origami-stoppered rotaxane) (see Figure 4.4, Figure 4.23 and Figure 4.28), it was used for further experiments. The shape of the non-symmetric pseudorotaxanes (with ring- and origami-stopper or with ring- and spherical-stopper) was further confirmed by AFM images taken in AC mode and in Hyperdrive™ mode (see Figure 4.28 and Figure 4.23).

The pseudorotaxane to rotaxane conversion was achieved by addition of 10 equiv. of the corresponding ROs and incubation at RT for at least 10 min.

#### 6.12.5 Assembly of [3]Pseudorotaxane

The ODNs for the corresponding axle (2  $\mu$ l) were mixed in 1x DNA storage buffer to a total volume of 100  $\mu$ l with a final ODN concentration of 2  $\mu$ M. After 10 min of incubation at RT, the axle was mixed with 2 equiv. of the macrocycle featuring only one gap in 1x ligase buffer containing additionally 20 mM MgCl<sub>2</sub>. Threading was achieved by incubation at 4 °C for 12 h. In parallel, 1 equiv. of the macrocycle featuring two gaps was mixed with 1.5 equiv. of BO and incubated at 4 °C for 12 h. Then, this macrocycle was added to the axle with the first macrocycle threaded and the sample was incubated for 2 h at 4 °C before 1.25 equiv. of the left and right stopper were added. After incubation at 4 °C over 10 min, ligase (1/100 v/v) was added and ligated for at least 12 h at 15 °C. The resulting pseudorotaxane sample was purified by WAX HPLC or used without further purification. After analysis of the product *via* agarose gel electrophoresis (3.2 % w/v, 200 V, 80 min, 4 °C), it was used for further experiments. The shape of the [3]pseudorotaxane was further confirmed by AFM imaging of the sample using Hyperdrive™ mode (see Figure 4.34, Figure 4.35 and Figure 4.36).

#### 6.12.6 Assembly of [2]Catenane

The 3/4-ring beta, containing all ODNs of ring beta except the threading ODN, was synthesized and purified as described for the macrocycles. 1 equiv. of ring alpha was mixed with 1.1 equiv. of the threading ODN in 1x ligase buffer supplemented with additional 50 mM NaCl and 10 mM MgCl<sub>2</sub>. Threading was achieved after incubation at 15 °C over 3 h. Following, 1.1 equiv. of 3/4-ring beta was added and the sample was incubated at 15 °C over 10 min before ligase (1/100 v/v) was added and ligated for at least 12 h at 15 °C. The resulting pseudocatenane sample was purified *via* WAX HPLC or used without further purification. After analysis of the product by agarose gel electrophoresis (2 % w/v, 200 V, 30 min, 4 °C) (see Figure 4.47), it was used for further experiments. The pseudocatenane to catenane conversion was achieved by addition of 10 equiv. of the corresponding ROs and subsequent ligation. The conversion was

---

followed by agarose gel electrophoresis (2 % w/v, 200 V, 20 min, RT) (see Figure 4.45). The shape of the non-symmetric catenane was further confirmed by AFM imaging using AC mode (see Figure 4.48). In order to properly characterize the shape of the catenane, the diameter of 25 structures were measured and statistically evaluated (see Figure 4.49).

### 6.12.7 Assembly of [3]Pseudocatenane

The [3]pseudocatenane was synthesized similarly to the [2]pseudocatenane. First, 1 equiv. of the middle ring featuring two gaps was incubated with 3 equiv. of the threading ODN in 1x ligase buffer supplemented with additional 50 mM NaCl and 10 mM MgCl<sub>2</sub>. Following, 3 equiv. of the 3/4-outer rings were added and the sample was incubated at 15 °C over 10 min before ligase (1/100 v/v) was added and ligated for at least 12 h at 15 °C. The resulting pseudorotaxane sample was purified *via* WAX HPLC. The shape of the [3]catenane was further confirmed by AFM imaging in AC mode (see Figure 4.48).

The [3]catenane used to control a DNAzyme was synthesized with a slightly modified protocol by Dr. T. Li, as described in: Li, T.; Lohmann, F.; Famulok, M. *Nat. commun.* **2014**, *5*, 4940.

## 6.13 Switching of Macrocycle Mobility

### 6.13.1 Toe-hold Mechanism

The preliminary hybridization experiment corresponding to Figure 4.6 was performed as follows. The axle was prepared as described for the rotaxane synthesis, an aliquot was taken and then 10 equiv. TH-RO1 were added. After taking another aliquot, 15 equiv. of cODN1 were added. All aliquots were incubated for 30 min at RT and analyzed *via* PAGE.

For the “switching of macrocycle mobility experiment” corresponding to Figure 4.8, the pseudorotaxane sample in DNA storage buffer was treated alternating with the TH-RO1 and cODN1 always with 5 equiv. excess with regard to the pseudorotaxane. After each addition, the sample was incubated at RT for 30 min. and an aliquot was taken. After



two switching cycles, all aliquots were incubated at RT for 12 h and analyzed *via* agarose gel electrophoresis (2.4 % w/v, 180 V, 2 h, 4 °C).

For the fluorescence quenching experiment, the fluorescence of the pseudorotaxane sample was measured. Then, the sample was treated alternating with TH-RO1 and cODN1. In the first switching cycle, 2.5 equiv. of TH-RO1 and 5 equiv. of cODN1 were added. The amount of TH-RO1 and cODN1 was gradually increased to a final of 20 equiv. for the TH-RO1 and 22.5 equiv. for the cODN1. After each addition of the corresponding ODN, the sample was incubated 30 min at RT and the fluorescence was measured.

### 6.13.2 pH Induced Mechanism

For the FP experiment corresponding to Figure 4.9, the dumbbell featuring the i-motif encoding sequence in the gap and the i-motif test-ODN were prepared in 0.1  $\mu\text{M}$  concentration in 100  $\mu\text{l}$  TA buffer at pH 8. As a reference, the i-motif test-ODN alone was prepared in the same buffer. FP of both samples was measured before the pH was adjusted to ca. 5, by adding 1  $\mu\text{l}$  of 1M hydrochloric acid. The FP was measured and the pH was adjusted to ca. 8 by adding 1  $\mu\text{l}$  of 1M sodium hydroxide. FP was measured and the switching cycle was repeated twice.

The dethreading experiment corresponding to Figure 4.11 was performed as follows. The dumbbell and the ring-stoppered pseudorotaxane featuring the i-motif encoding sequence were prepared. An aliquot of the pseudorotaxane was taken and the buffer of the remaining sample was changed into TA buffer at pH 8 with centrifugal filters (as described above). Then, another aliquot was taken and the buffer of the remaining sample was exchanged into TA buffer at pH 5 with centrifugal filters. All aliquots were incubated 12 h at RT and analyzed by agarose gel electrophoresis (2 % w/v, 200 V, 20 min, RT).

### 6.13.3 Light Switching Mechanism

The preliminary hybridization experiment corresponding to Figure 4.16 was performed as follows. The BHQ-2 containing axle was prepared as described for the rotaxane synthesis and mixed with 1 equiv. of the light switch test-ODN and 1 equiv. of AB6-RO in

---

DNA storage buffer (200  $\mu$ l of 1  $\mu$ M axle). The AB6-RO was preliminary irradiated with UV light at 50 °C for 5 min. After 5 min incubation at 40 °C, the fluorescence was measured at 40 °C, then, the sample was irradiated with vis light at 50 °C for 2 min and fluorescence was measured at 40 °C. Subsequently, the sample was irradiated with UV light at 50 °C for 5 min and fluorescence was measured at 40 °C. Three more switching events were performed and in each step, the fluorescence was monitored.

For the preliminary hybridization experiment corresponding to Figure 4.16, the axle was prepared as described for the rotaxane synthesis and mixed with DMAB5-RO, which was irradiated with UV light prior to use. An aliquot was taken and the remaining sample was irradiated with vis light. After taking another aliquot, the remaining sample was irradiated with UV light. All aliquots were incubated for 10 min at RT and analyzed by PAGE.

The dethreading experiment corresponding to Figure 4.18 was performed as follows. The dumbbell and the ring-stoppered pseudorotaxane were prepared. An aliquot of the pseudorotaxane was taken before 10 equiv. of AB6-RO (irradiated with UV light for 5 min at 40 °C prior to use) were added. Another aliquot was taken before the remaining sample was irradiated with vis light for 2 min at 40 °C. All aliquots were incubated 12 h at RT and analyzed by agarose gel electrophoresis (2 % w/v, 180 V, 30 min, RT). For the corresponding FQ experiment (see Figure 4.18), the fluorescence of purified Cy3/BHQ-2 labeled pseudorotaxane with ring stoppers was measured at 30 °C. Then, 2.5 equiv. of AB6-RO (previously irradiated with UV light for 5 min at 40 °C) were added and the fluorescence was measured again at 30 °C. Then, the sample was irradiated with vis light at 40 °C for 2 min and fluorescence was measured at 30 °C.

For the switching of macrocycle mobility experiment corresponding to Figure 4.19, pseudorotaxane and rotaxane samples in DNA storage buffer were prepared. An aliquot of the pseudorotaxane sample was taken before 10 equiv. of AB6-RO or DMAB5-RO (irradiated with UV light for 5 min at 40 °C prior to use in the case of Figure 4.19 A and B, or with vis light for 2 min at 40 °C in the case of Figure 4.19 C) were added. After taking an aliquot, which was immediately cooled to 4 °C, the remaining sample was irradiated with vis light (or UV light for the latter case respectively). An aliquot was taken,

immediately cooled to 4 °C and the sample was irradiated with UV or vis light, respectively. This switching cycle was repeated up to six times. All aliquots were analyzed by agarose gel electrophoresis (2.4 % w/v, 180 V, 2 h, 4 °C).

## **6.14 Translocation of a Shuttle-ring**

### **6.14.1 Light Induced Translocation**

The purified pseudorotaxane sample with two gaps, one blocked by the DMAB5-RO and the other modified with three DMAB moieties (the sample was irradiated with vis light during the synthesis) was diluted to 4 nM in 1x Seeman buffer and an aliquot was taken. The remaining sample was irradiated with UV light and an aliquot was taken and cooled immediately to 4 °C before the sample was irradiated with vis light. All three samples were analyzed by AFM in AC mode. Several images (1  $\mu\text{m}^2$ ) of each aliquot were taken and all the intact structures were counted (minimum 40 structures). The percentage of structures with the shuttle-ring on the correct position compared with the shuttle-ring on the wrong position was determined (see Table 4.1 and Supporting Figure 4, Supporting Figure 5 and Supporting Figure 6). In some cases, the position of the shuttle-ring could not be clearly determined and therefore, those structures were not evaluated.

AFM images in Hyperdrive™ mode were taken of the pseudorotaxane sample before irradiation (shuttle-ring on station 2) and another pseudorotaxane sample with the shuttle-ring on station 1 was also analyzed by AFM in Hyperdrive™ mode (see Figure 4.23). Therefore, the axle was irradiated with UV light and no DMAB5-RO was added before the shuttle-ring was threaded on the axle.

### **6.14.2 Toe-hold Mechanism Induced Translocation**

For the preliminary experiment with the pseudorotaxane with two spherical stoppers corresponding to Figure 4.30, the axle was mixed with 1 equiv. of TH-RO2 before threading the shuttle-ring. Then, the spherical stoppers were added in order to form a [2]pseudorotaxane with two spherical stoppers and the shuttle-ring located on station 1. An aliquot of the sample was taken prior to the addition of 5 equiv. of TH-RO1 and 5

---

equiv. of TH-RO2 were added, respectively. Another aliquot was taken and the remaining sample was treated with 10 equiv. of cODN2. The samples were incubated for 12 h at RT and analyzed by agarose gel electrophoresis (2.4 % w/v, 180 V, 2 h, 4 °C).

The shuttle-ring translocation in the pseudorotaxane with one ring- and one origami-stopper was performed with a Freeze 'N Squeeze purified pseudorotaxane sample with the shuttle-ring on station 1, diluted to a concentration of 4 nM in 1x Seeman buffer. An aliquot was taken before the remaining sample was treated with 5 equiv. of cODN2, incubated for 30 min at RT, then treated with 5 equiv. of TH-RO1 and incubated for 30 min at RT. Both samples were analyzed *via* AFM in AC mode (see Figure 4.31).

### **6.15 Input Dependent Cascade Release Reaction in a [3]Pseudorotaxane**

The HPLC purified [3]pseudorotaxane sample (50 nM) in 1x DNA storage buffer containing additionally 10 mM MgCl<sub>2</sub> was divided in 4 aliquots. In the first aliquot no input was added, whereas for the other three aliquots, addition of 10 equiv. of input A, 50 equiv. of input B and sequential addition of input A (10 equiv.) and B (50 equiv.), was performed respectively. The samples were incubated 1 h at RT after addition of each input. For analysis on agarose gel (3.2% w/v, 200 V, 80 min, 4 °C), all four aliquots were diluted to 4 µl in DNA storage buffer, whereas for AFM imaging in AC mode, the samples were diluted to a 3 nM concentration in 1x Seeman buffer (see Figure 4.38).

The FQ experiment corresponding to Figure 4.39 was performed as follows. HPLC purified TAM/BHQ-2 labeled [3]pseudorotaxane sample in 1x DNA storage buffer was divided into two fractions (60 µl and 60 nM) and then, fluorescence of both was measured. 10 equiv. of input A were added to one fraction, whereas the same volume of 1x DNA storage buffer was added to the other fraction. Then, fluorescence was measured again before and after addition of 100 equiv. of input B to both fractions.

For the triggering of the [3]pseudorotaxane with the light sensitive input B corresponding to Figure 4.40, HPLC purified [3]pseudorotaxane sample (approx. 40 nM) in 1x DNA storage buffer containing additionally 10 mM MgCl<sub>2</sub> was prepared. Two aliquots were taken, to one of which 100 equiv. of DMAB5-RO (previously irradiated with vis light) were added. The remaining sample was treated with 10 equiv. of input A,

incubated for 1 h at RT, an aliquot was taken and the remaining sample was split in two. The first halve was treated with 100 equiv. of DMAB5-RO which was irradiated with UV light prior to use (5min at 40 °C); the other halve was treated with 100 equiv. of DMAB5-RO which was irradiated with vis light prior to use. All samples were shielded from light, incubated for 1 h at RT and analyzed by agarose gel electrophoresis (3.2% w/v, 200 V, 80 min, 4 °C).

The preliminary experiment for a reversible triggering of a [3]pseudorotaxane with spherical stoppers corresponding to Figure 4.41 was performed with unpurified [3]pseudorotaxane sample. The assembly was similar to the [3]pseudorotaxane with ring stoppers, with the difference that the ring stoppers were replaced by spherical stoppers. An aliquot of the 60 nM sample was taken; the remaining sample was treated with 10 equiv. of TH-RO1 before taking another aliquot. Then, 10 equiv. of input A was added and an aliquot was taken. To the remaining sample, 20 equiv. of BO and 20 equiv. of cODN1 were added. All samples were incubated for 1 h at RT and analyzed by agarose gel electrophoresis (2.4 % w/v, 180 V, 120 min, 4 °C).

### 6.16 Pseudocatenane to Catenane Conversion

The conversion from [3]pseudocatenane to [3]catenane was performed with a 100 nM HPLC purified rhodamine green/BHQ-1 labeled sample (provided by Dr. T. Li) in TA buffer containing additionally 20 mM MgCl<sub>2</sub>. The sample was divided into two fractions; one was treated with 10 equiv. of the corresponding ROs and the other with the same volume of water. Kinetic fluorescence measurements were performed before and after addition of the ROs over 80 min (measuring every minute) (see Figure 4.46).

The reversible [2]pseudocatenane to the [2]catenane conversion experiment corresponding to Figure 4.50 was performed with Cy3/BHQ-2 labeled catenane sample consisting of two 168 bp macrocycles in DNA storage buffer containing additionally 10 mM MgCl<sub>2</sub>. For the FQ experiment, the fluorescence of the pseudocatenane sample was measured. Then, Cat-TH-RO and Cat-cODN were sequentially added to the sample. In the first switching cycle, 2 equiv. of Cat-TH-RO and 4 equiv. of Cat-cODN were added. The amount of Cat-TH-RO and Cat-cODN was gradually increased to a final of 20 equiv.

---

for the Cat-TH-RO and 22 equiv. for the Cat-cODN. After each addition of the corresponding ODN, the sample was incubated 30 min at RT and the fluorescence was measured.

For the gel-shift assay, the sample was treated with 5 equiv. of Cat-TH-RO, incubated for 30 min at RT and an aliquot was taken before 10 equiv. of Cat-cODN were added. After 30 min of incubation at RT, another aliquot was taken and then, 10 equiv. of Cat-TH-RO were added. After 30 min of incubation at RT, an aliquot was taken and 10 equiv. of Cat-cODN were added. After 30 min incubation at RT, all aliquots were analyzed *via* agarose gel electrophoresis (2.4 % w/v, 160 V, 90 min, RT).

### **6.17 AFM Study with [3]Pseudocatenane, [3]Catenane and the Tetracyclic Structure**

The AFM images were taken with HPLC purified samples in TA buffer containing additionally 12.5 mM MgCl<sub>2</sub> and 2.5 mM EDTA. The samples were prepared by Dr. T. Li either containing [3]pseudocatenane, [3]pseudocatenane together with the corresponding ROs in order to release the rings, both at pH 8, and the [3]pseudocatenane containing the corresponding ROs at pH 5, in order to form the tetracyclic structure. The samples were diluted in the TA buffer either at pH 8 or 5 to a final concentration of 10 nM, directly before measuring. After adsorption of the structures on mica, the mica was rinsed and then covered with 400 µl of TA buffer containing 2.5 mM MgCl<sub>2</sub> and 0.5 mM EDTA at pH 8 or 5. The sample was immediately analyzed in AFM using the JPK software (see Figure 4.52).

### **6.18 Three-Dimensional Models**

The three-dimensional models of the rotaxane and catenane structures were generated with the *Cheetah 3D* software.

---

## 7 Appendix

### 7.1 List of Abbreviations

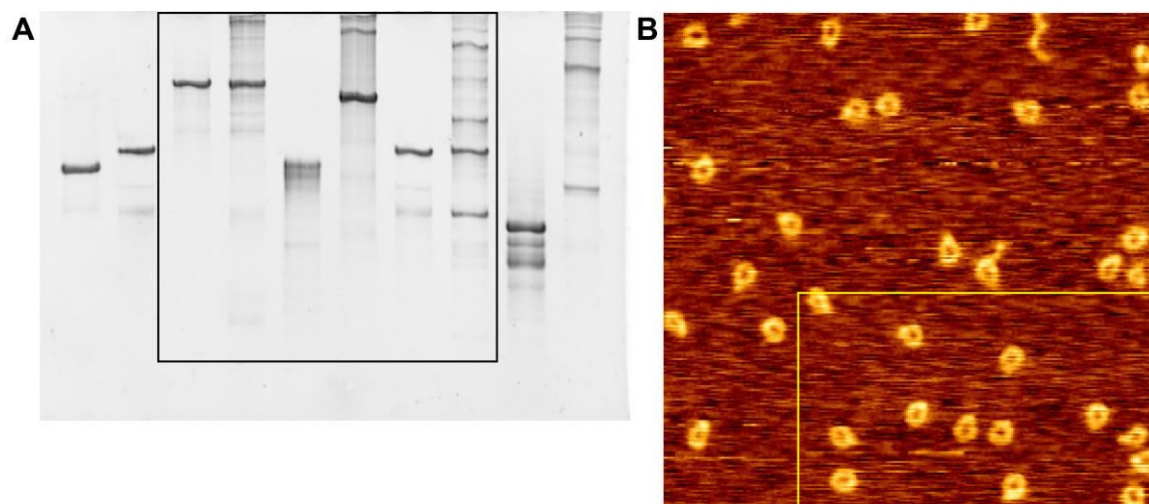
3D	three-dimensional
A	adenine
AB	azobenzene
AMA	Ammonia-Methylamine (method)
BHQ-2	black hole quencher 2
bp	base pairs
C	cytosine
C <sup>+</sup>	protonated cytosine
CPG	controlled pore glass
Cy3	cyanine 3
DMAB	dimethylazobenzene
DMT	dimethoxytrityl group
DNA	Deoxyribonucleic acid
ds	double stranded
FP	fluorescence polarization
FQ	fluorescence quenching
FRET	Förster Resonance Energy Transfer
G	guanine
HPLC	High Performance Liquid Chromatography
MW	molecular weight
N	randomized deoxynucleotide

---

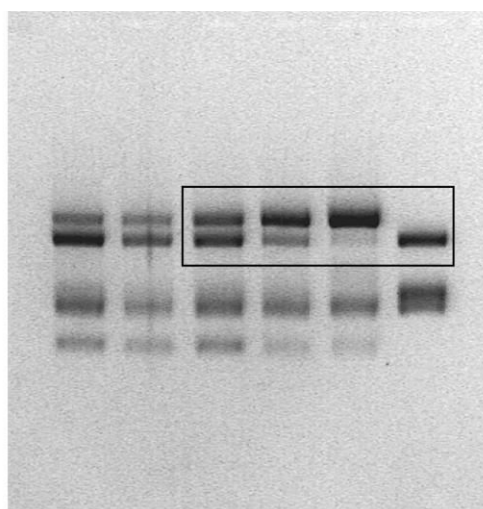
NMR	nuclear magnetic resonance spectroscopy
OD	optical density
ODN	oligodeoxynucleotides
PAGE	polyacrylamide gel electrophoresis
PCR	polymerase chain reaction
RNA	ribonucleic acid
RO	release oligodeoxynucleotide
RT	room temperature (approx. 20 °C)
ss	single stranded
T	thymine
TA buffer	Tris Acetate buffer
TMB	3,3',5,5'-tetramethylbenzidine
UV	ultraviolet (here always 365 nm)
vis light	visible light (here always 450 nm)
WAX	weak anion exchange



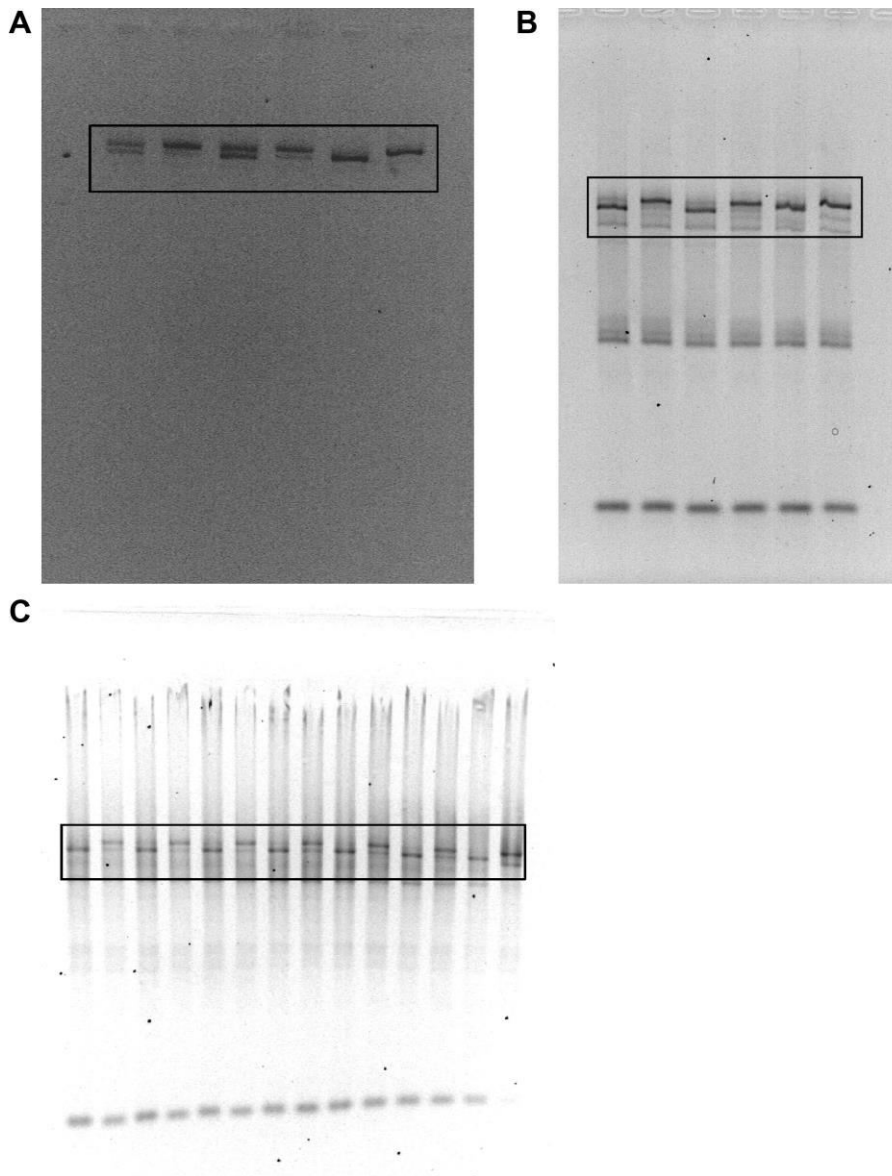
## 7.2 Supplementary Data



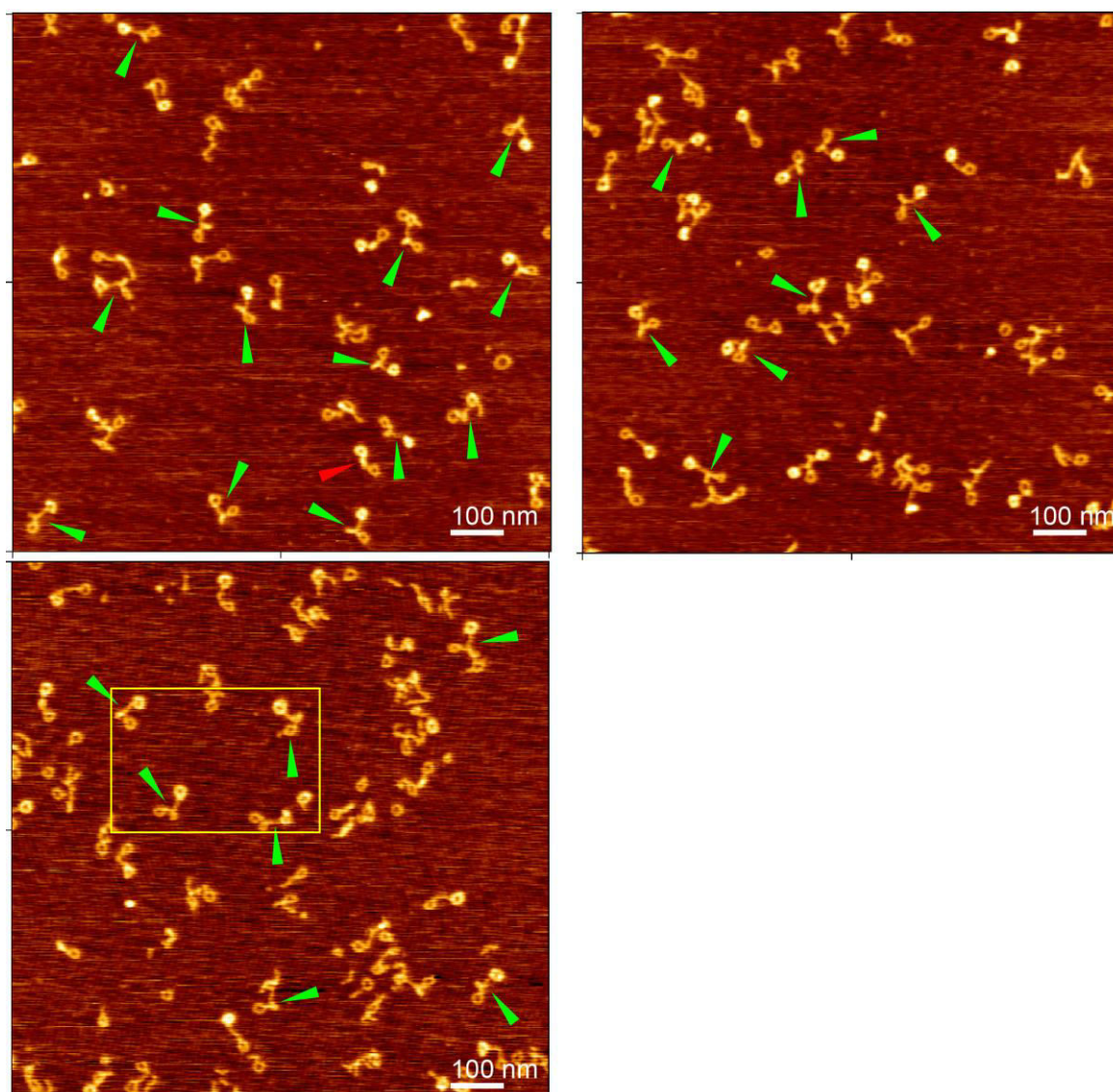
Supporting Figure 1. A) Uncropped PAGE image according to Figure 4.2.A. The black frame marks the cropped area. B) Larger area AFM image according to Figure 4.2.B. The yellow frame marks the cropped area.



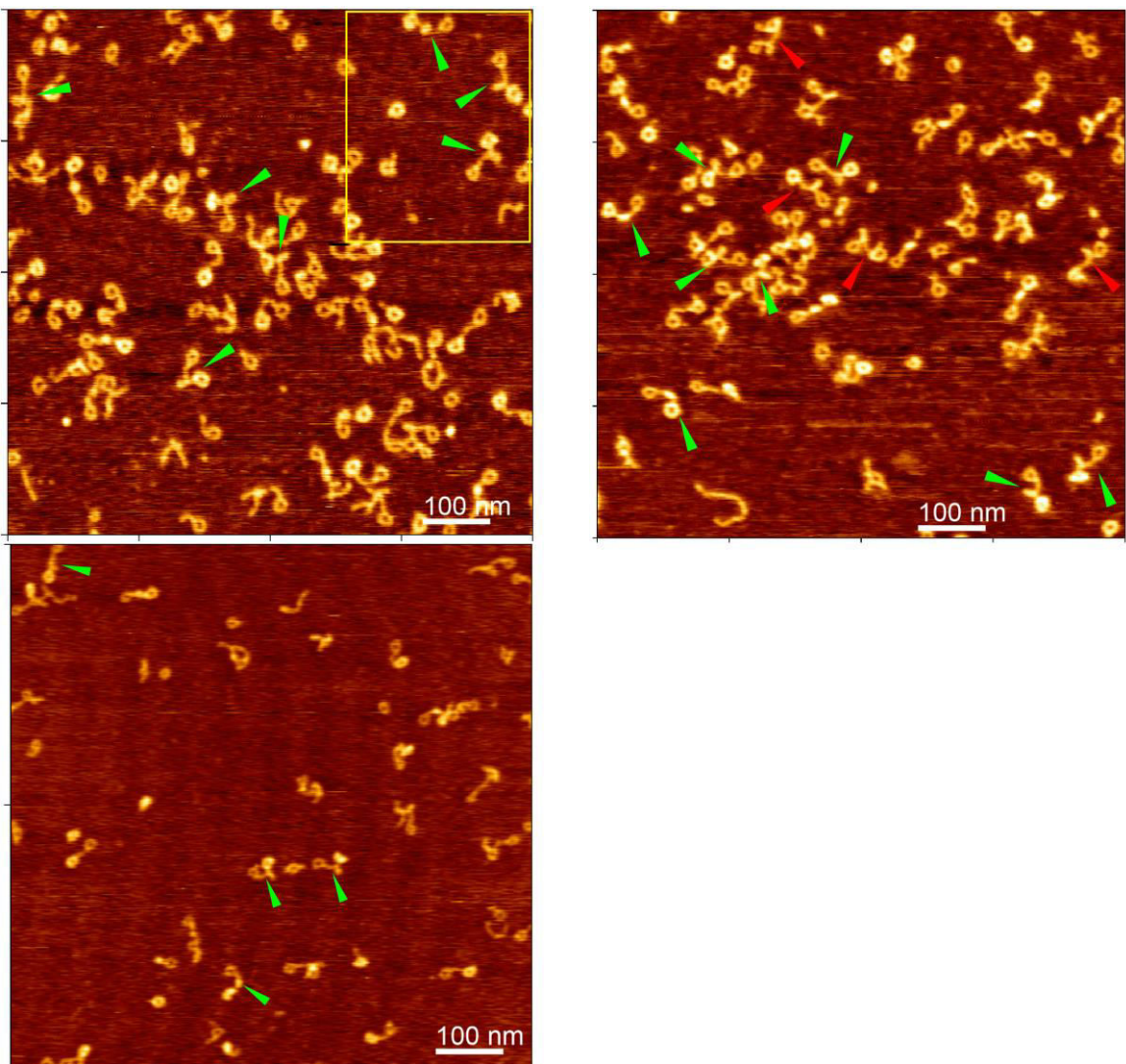
Supporting Figure 2. Uncropped agarose gel image according to Figure 4.18.B. The black frame marks the cropped area.



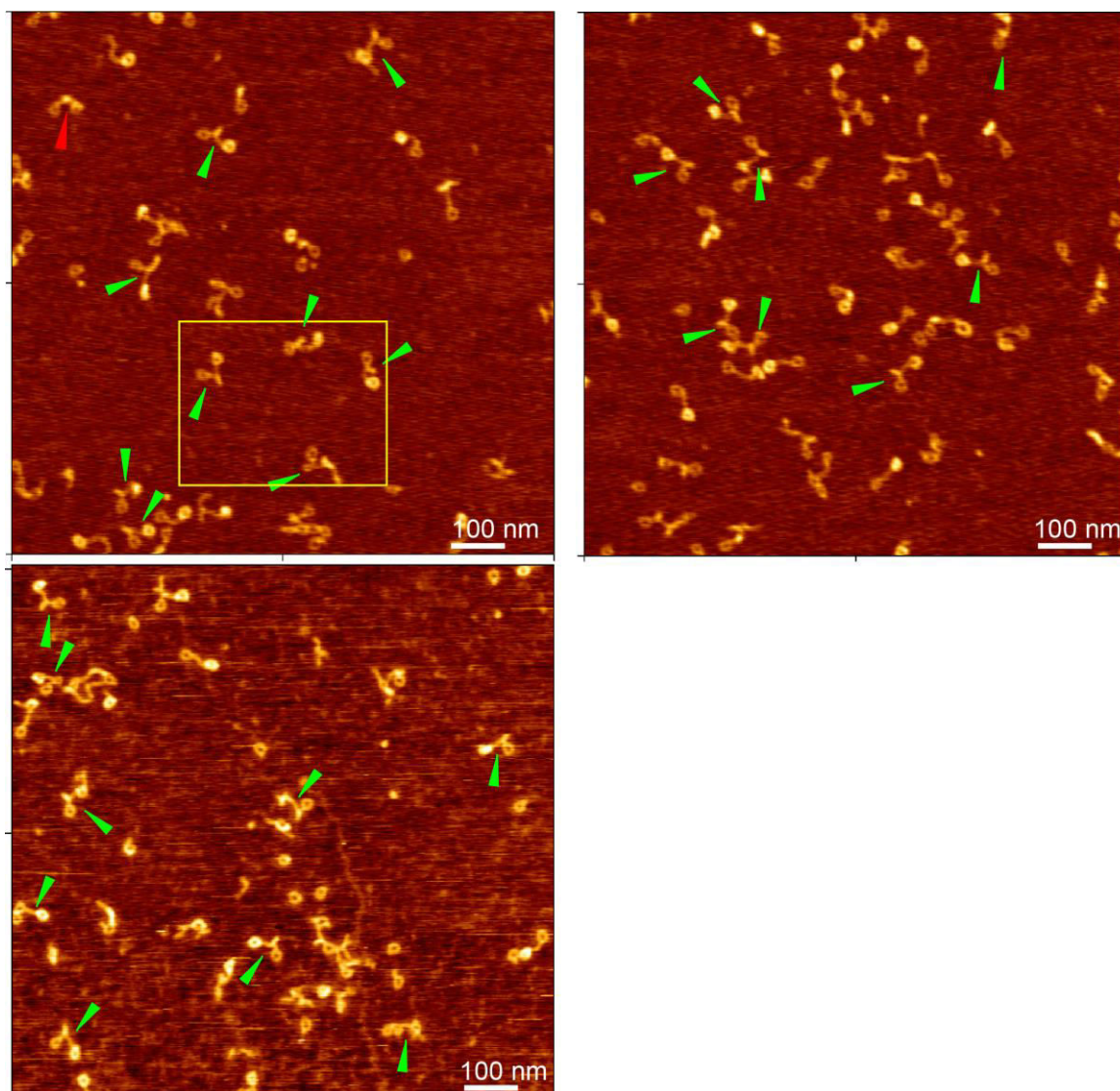
Supporting Figure 3. A-C) Uncropped agarose gel images according to Figure 4.19.A-C. The black frames mark the cropped areas.



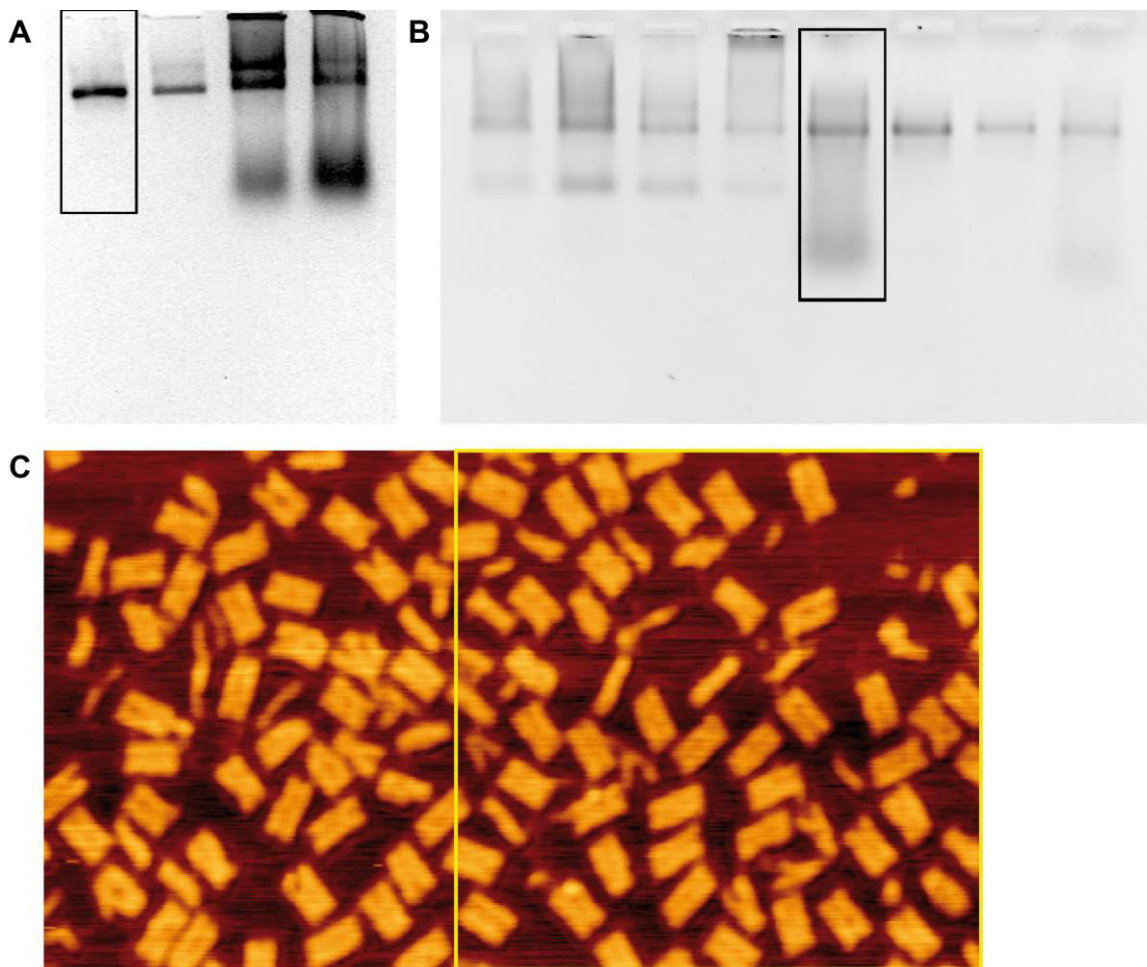
**Supporting Figure 4.** Larger area AFM images of the light switchable shuttle system with the shuttle-ring on station 2. The yellow frame marks the cropped area according to Figure 4.25.B. The images were taken with intermitted contact mode in air.



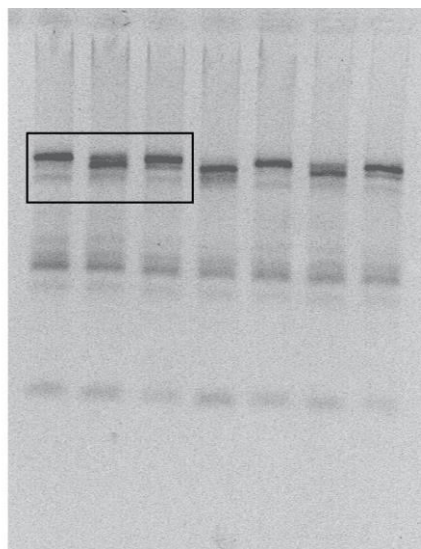
Supporting Figure 5. Larger area AFM images of the light switchable shuttle system after irradiation with UV light. The yellow frame marks the cropped area according to Figure 4.25.C. The images were taken with intermitted contact mode in air.



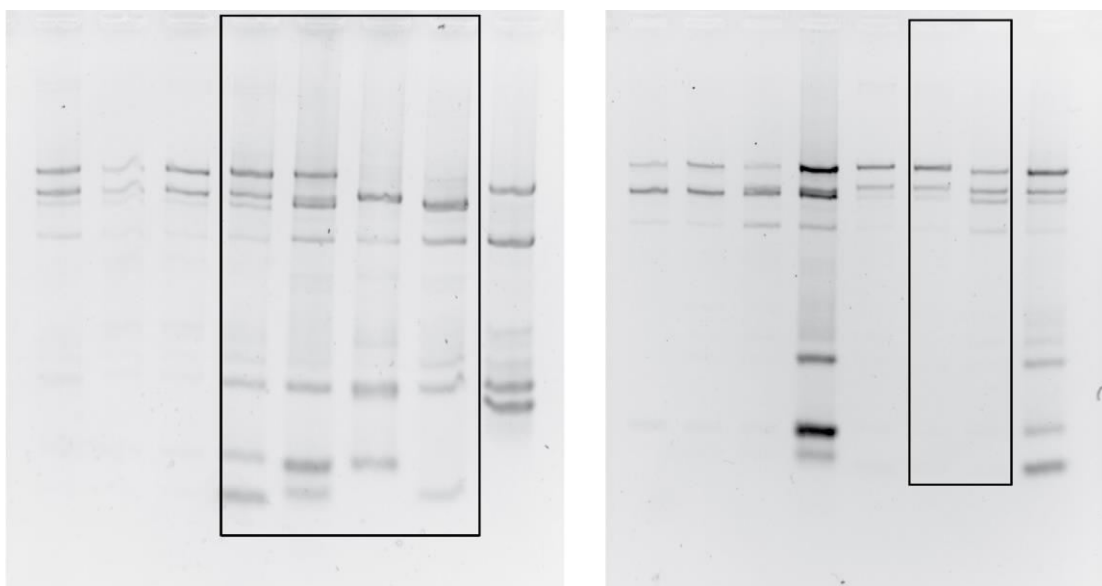
Supporting Figure 6. Larger area AFM images of the light switchable shuttle system after sequential irradiation with UV- and vis light. The yellow frame marks the cropped area according to Figure 4.25.D. The images were taken with intermitted contact mode in air.



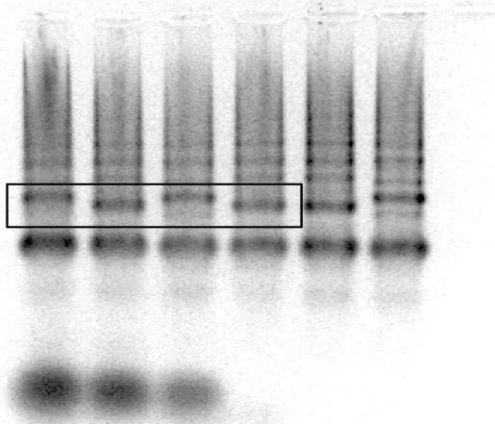
Supporting Figure 7.A,B) Uncropped agarose gel images according to Figure 4.27.A. The black frames mark the cropped areas. C) Larger area AFM image according to Figure 4.27.B. The yellow frame marks the cropped area.



Supporting Figure 8. Uncropped agarose gel image according to Figure 4.30.B. The black frame marks the cropped area.

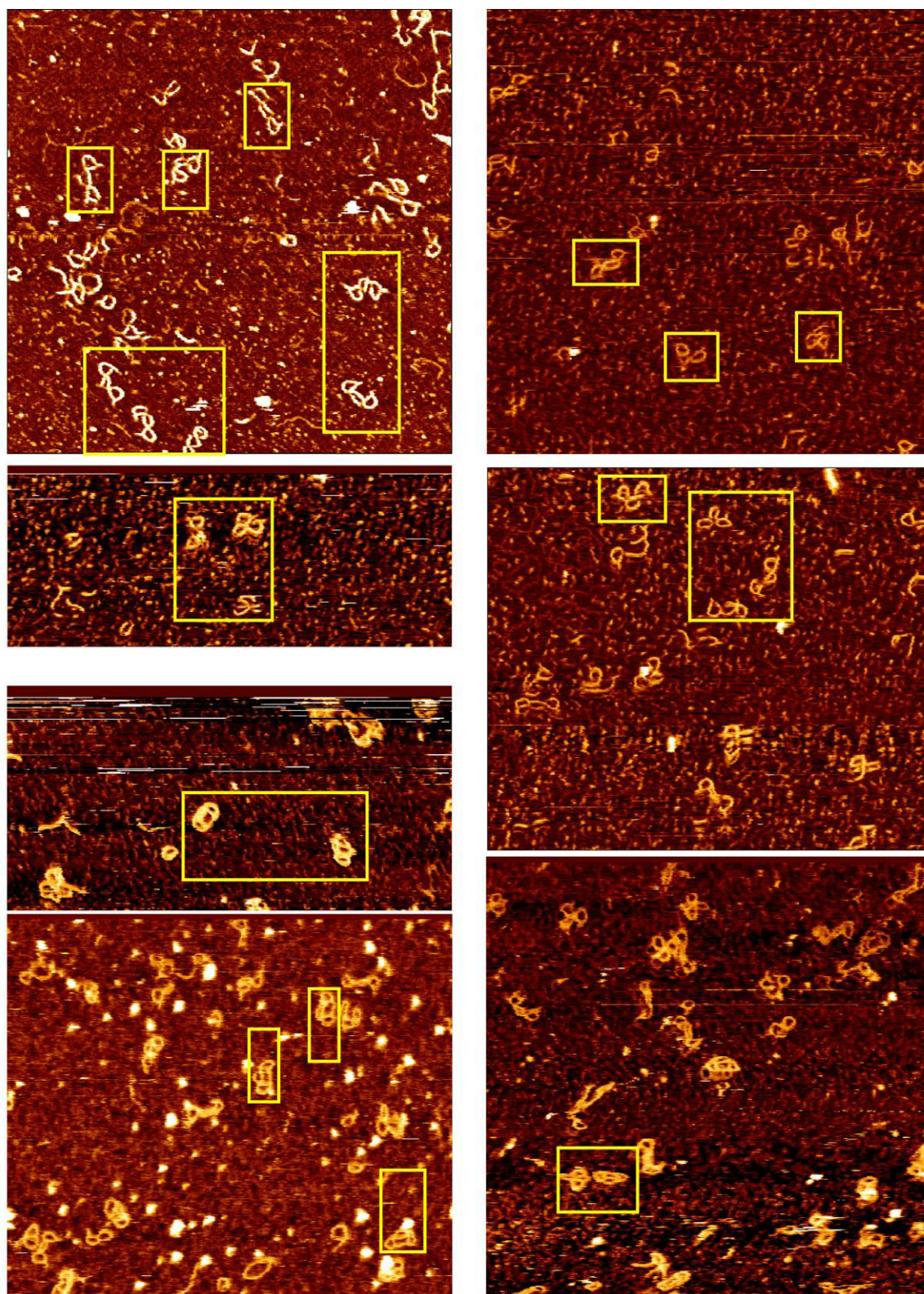


Supporting Figure 9. Uncropped agarose gel images according to Figure 4.34.A. The black frames mark the cropped areas.



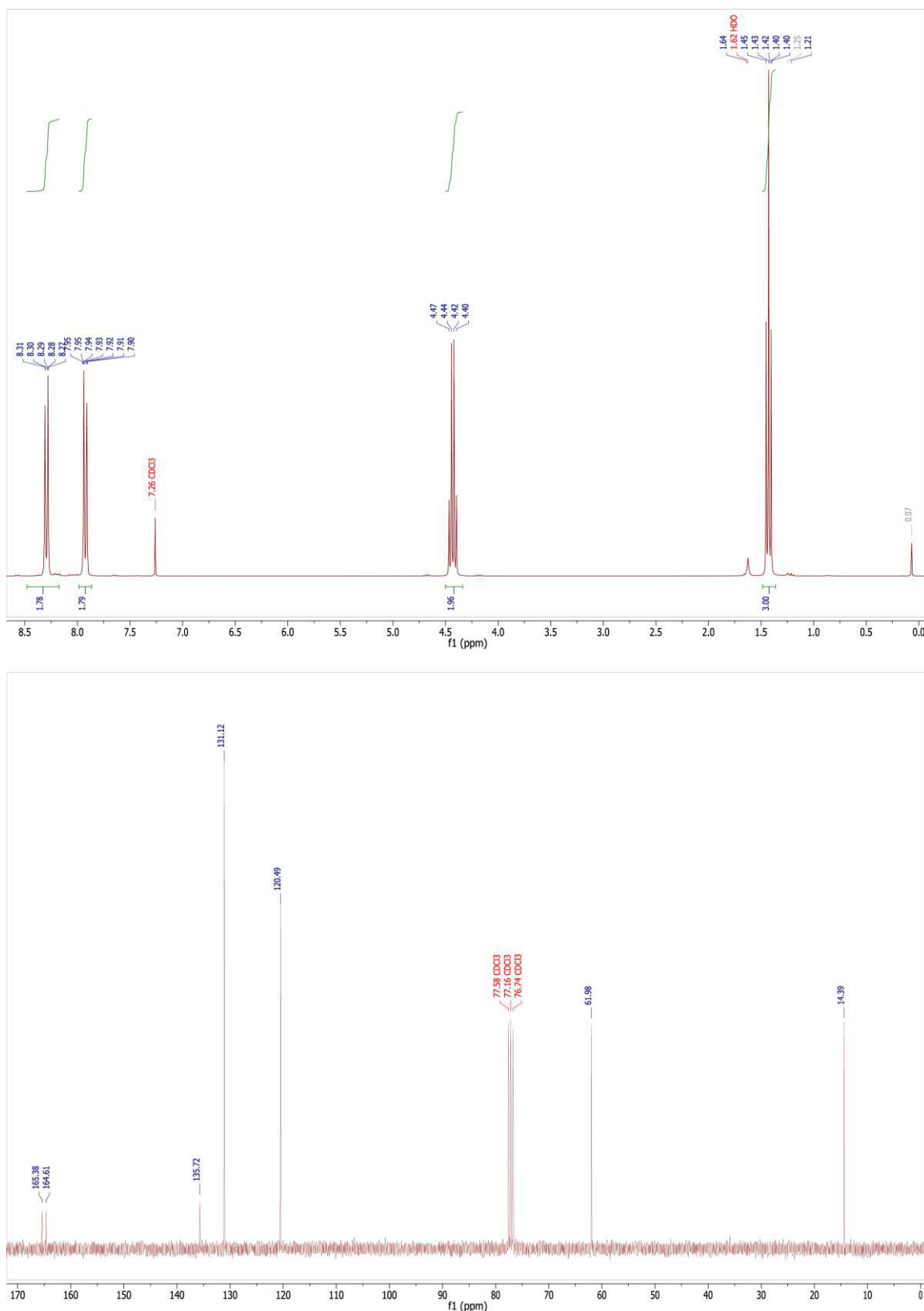
**Supporting Figure 10. Uncropped agarose gel image according to Figure 4.50.B. The black frame marks the cropped area.**



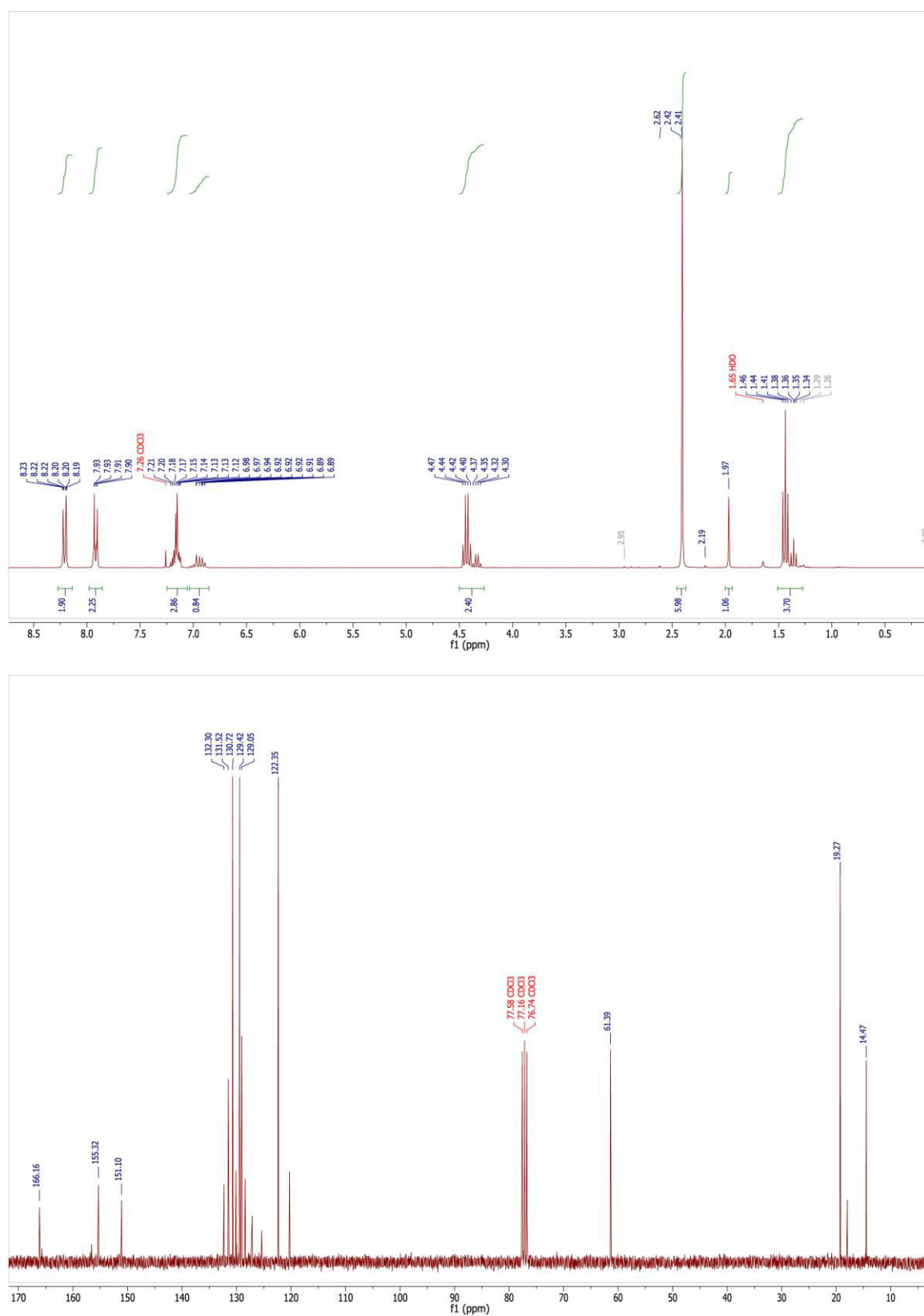


Supporting Figure 11. Larger area AFM images according to Figure 4.52. The yellow frames mark the cropped areas.

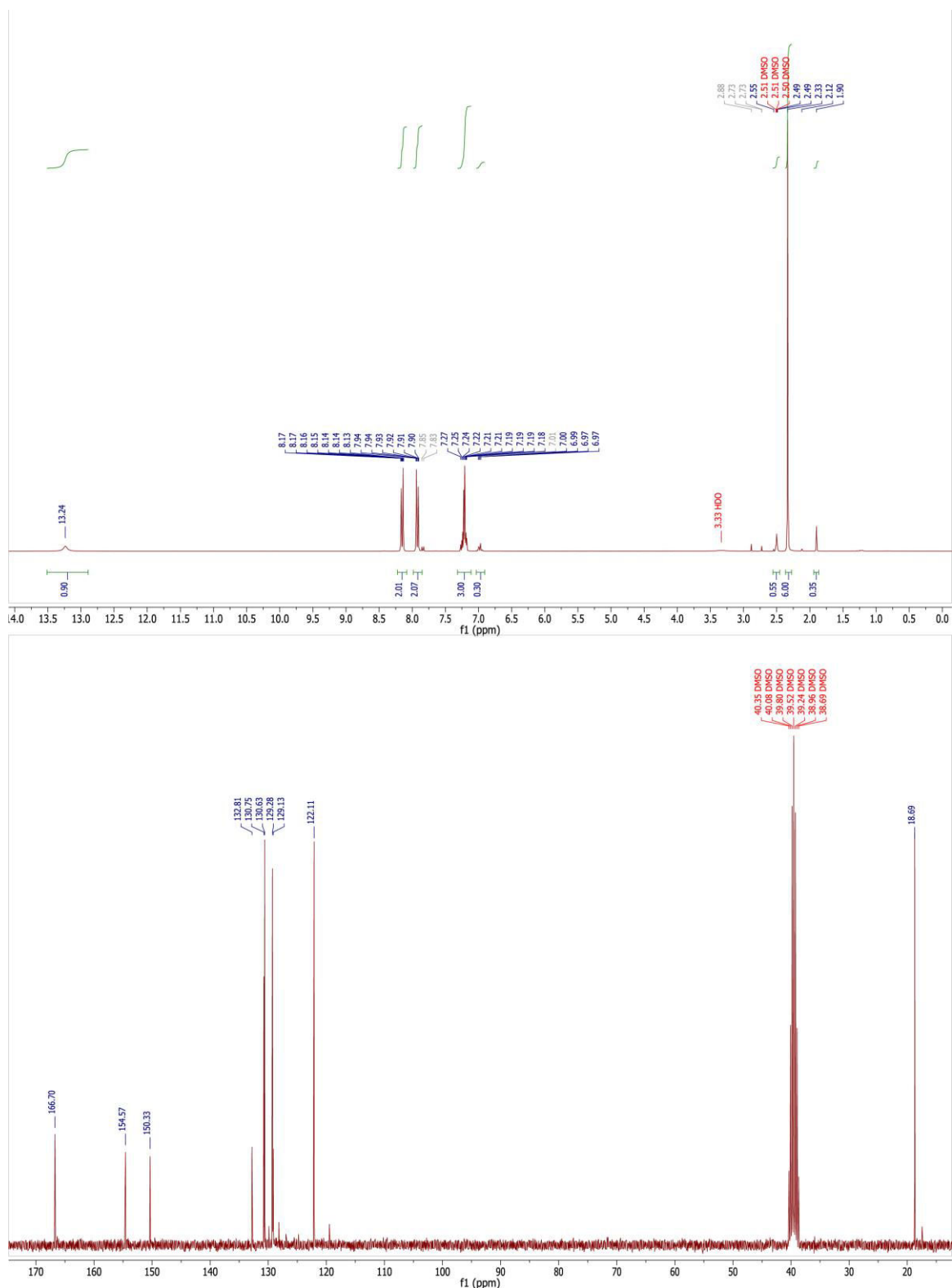
### 7.3 NMR Spectra



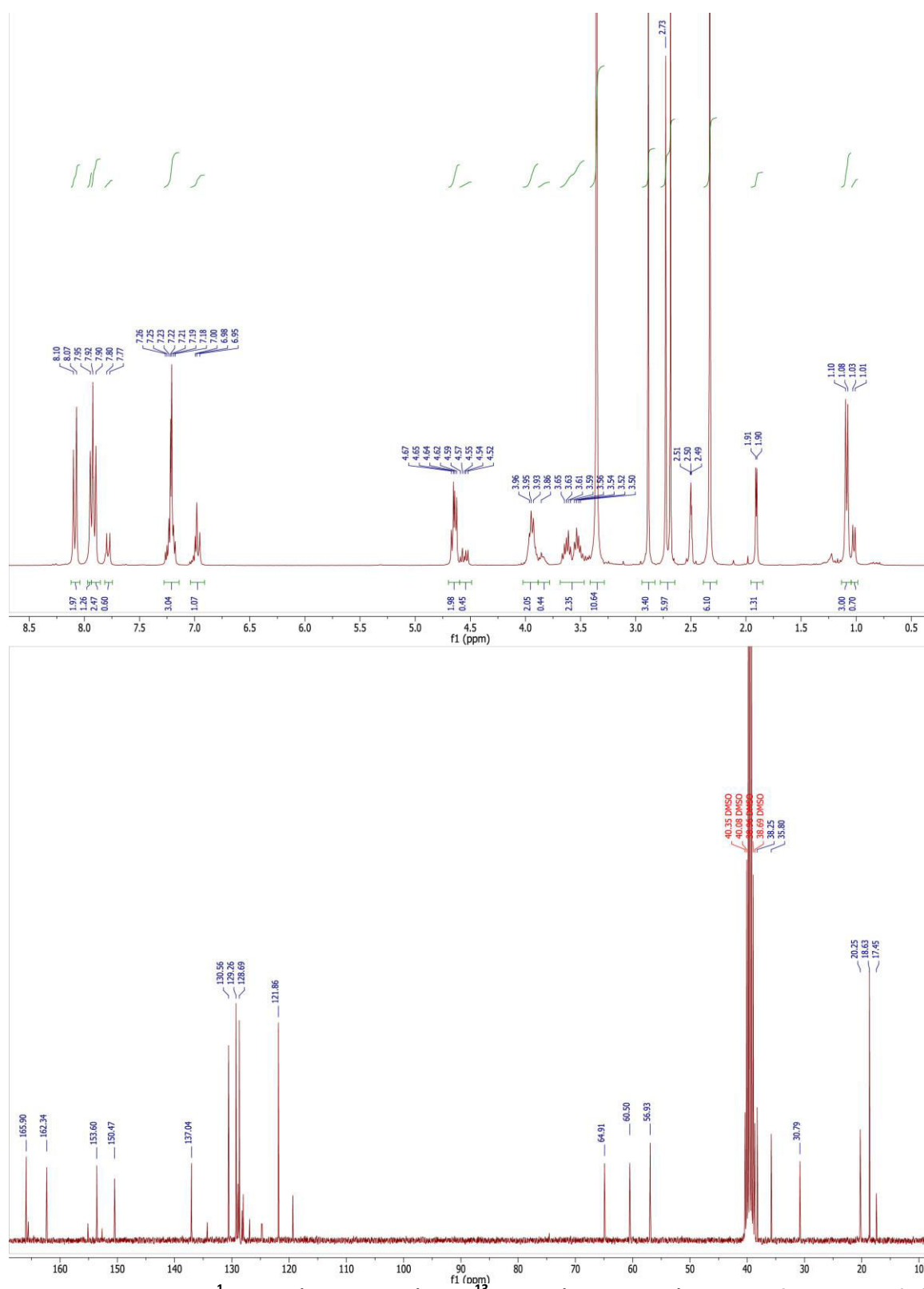
Supporting Figure 12.  $^1\text{H-NMR}$  (upper panel) and  $^{13}\text{C-NMR}$  (lower panel) spectra of ethyl-4-nitrosobenzoate. The image was taken and slightly modified from reference <sup>100</sup>.



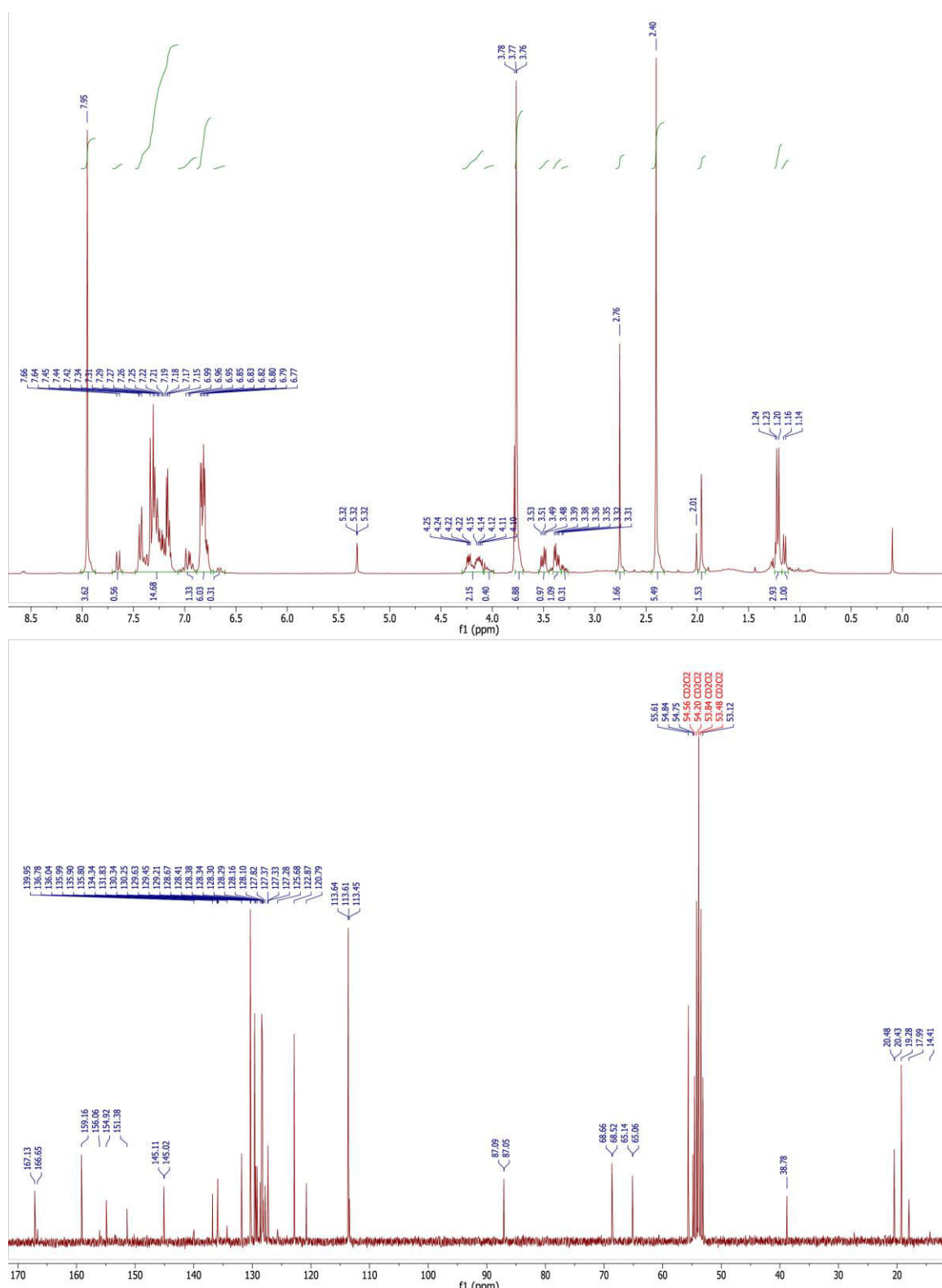
Supporting Figure 13.  $^1\text{H-NMR}$  (upper panel) and  $^{13}\text{C-NMR}$  (lower panel) spectra of ethyl-2',6'-dimethylazobenzene-4-carboxylate. The image was taken and slightly modified from reference <sup>100</sup>.



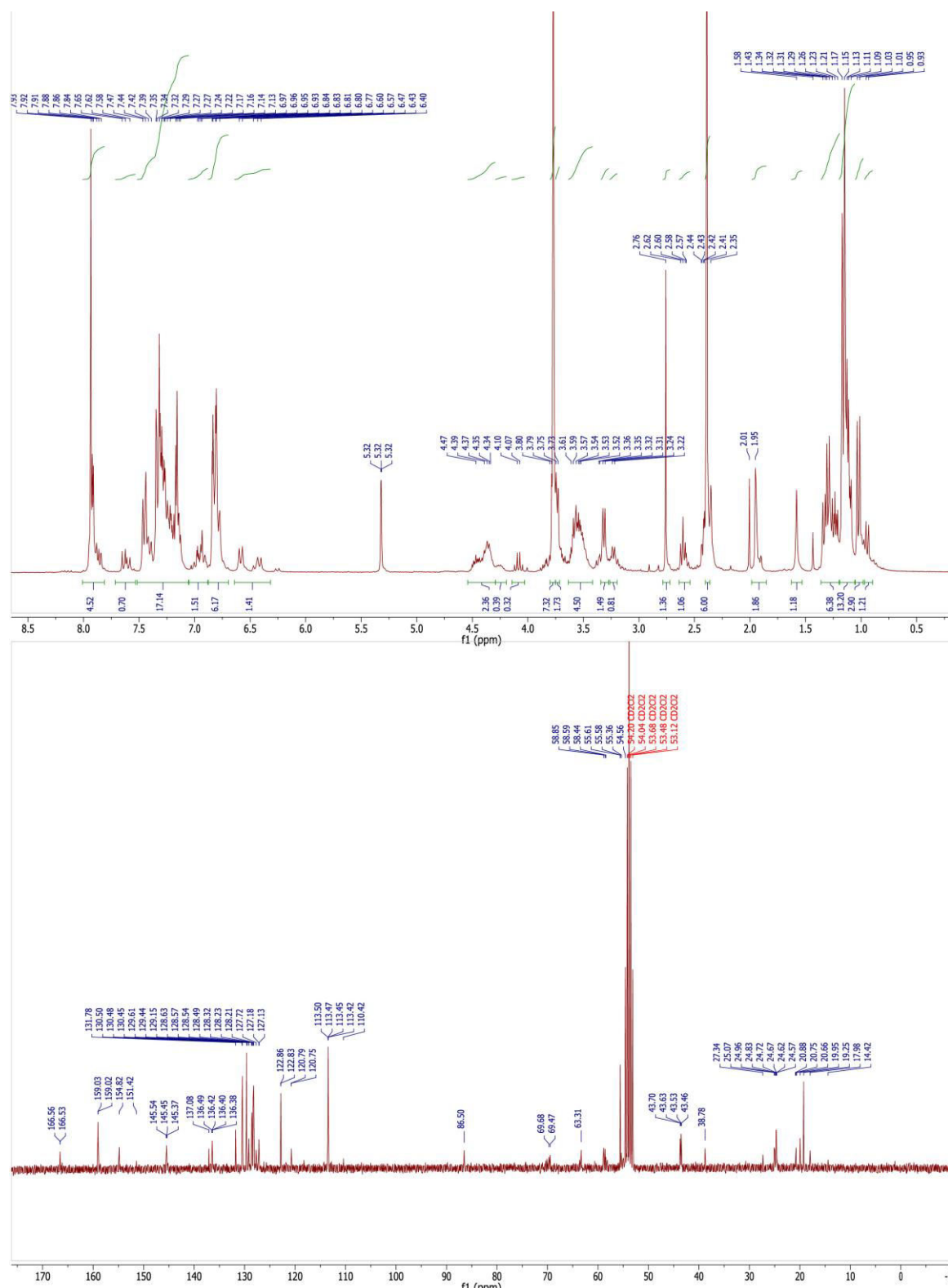
Supporting Figure 14.  $^1\text{H-NMR}$  (upper panel) and  $^{13}\text{C-NMR}$  (lower panel) spectra of 4-carboxy-2',6'-dimethylazobenzene. The image was taken and slightly modified from reference <sup>100</sup>.



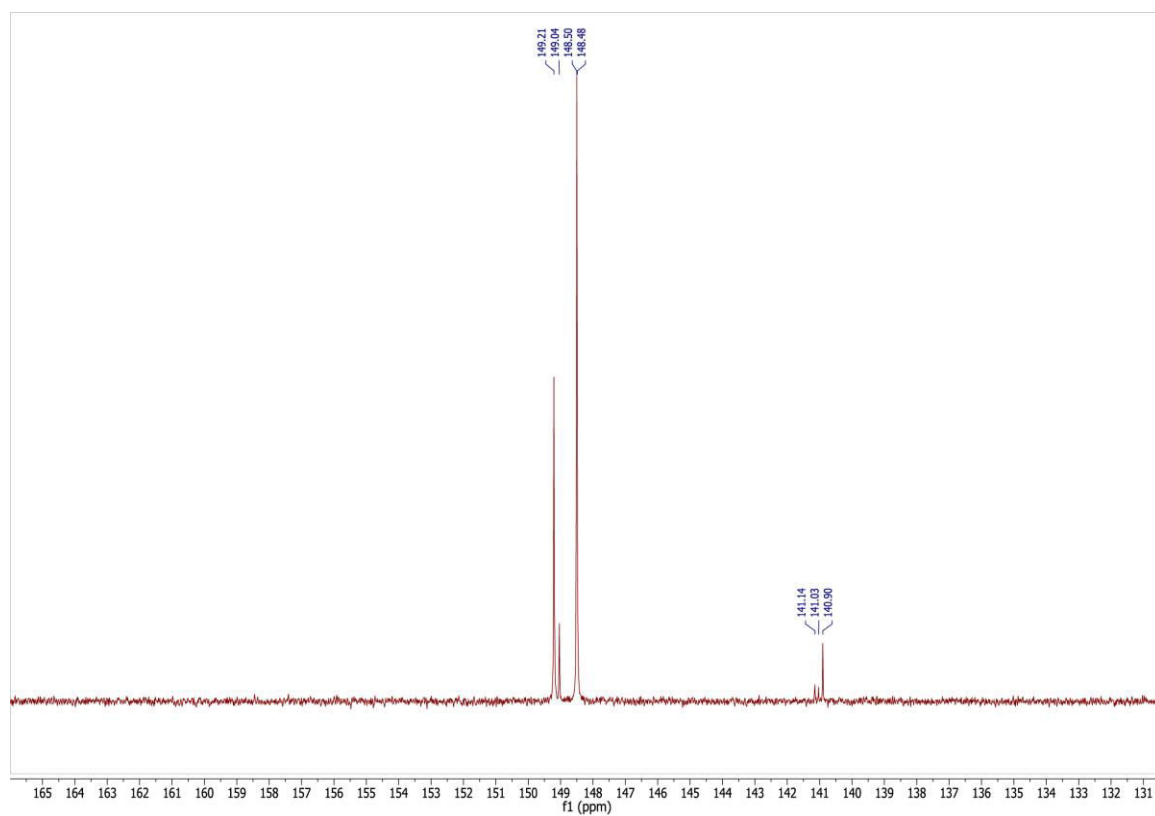
Supporting Figure 15.  $^1\text{H-NMR}$  (upper panel) and  $^{13}\text{C-NMR}$  (lower panel) spectra of 4-carboxy-2',6'-dimethylazobenzene-D-threoninol. The image was taken and slightly modified from reference <sup>100</sup>.



Supporting Figure 16.  $^1\text{H-NMR}$  (upper panel) and  $^{13}\text{C-NMR}$  (lower panel) spectra of DMT protected 4-carboxy-2',6'-dimethylazobenzene-D-threoninol. The image was taken and slightly modified from reference <sup>100</sup>.



Supporting Figure 17.  $^1\text{H-NMR}$  (upper panel) and  $^{13}\text{C-NMR}$  (lower panel) spectra of DMT protected 4-carboxy-2',6'-dimethylazobenzene-D-threoninol-phosphoramidite. The image was taken and slightly modified from reference <sup>100</sup>.



Supporting Figure 18.  $^{31}\text{P}$ -NMR spectra of DMT protected 4-carboxy-2',6'-dimethylazobenzene-D-threosinol-phosphoramidite. The image was taken and slightly modified from reference<sup>100</sup>.



## 7.4 Tables

### Pseudorotaxane used for toe-hold switch (chapter 4.1.2.1)

Axle	EFCT-1, EFCT-2-(BHQ-2), A1u1
Macrocycle	R1u1-(Cy3), R1u2, R1o1-2, R1o2, R1o3
Spherical Stopper:	
SSt-ring1	Ring1 r, RingSE a, RingSE b, GE-1, GE-2, GE-3, GE-4
SSt-ring-2	HJalpha b, HJalpha c, HJalpha d, HJbeta a, HJbeta kc, HJbeta kd, Bogen f, Borgen r
ROs	RO, TH-RO1, cODN1

### Pseudorotaxane used for pH switch (chapter 4.1.3.1)

Axle	A2o2, EFCT-2, A2u2
Macrocycle	R1u1, R1u2, R1o1-2, i-motif-R1o2, R1o3
Ring stopper	Stalpha f, Stalpha r, Stbeta3 f, Stbeta r, Stgamma f, Stdelta f, Stdelta r

### Pseudorotaxane used for light switch (either with ring- or spherical stopper) (chapter 4.1.4.3)

Axle, macrocycle, spherical stopper	same ODNs as for the pseudorotaxane used for toe-hold switch (chapter 4.1.2.1)
Ring stopper	same ODNs as for the pseudorotaxane used for pH switch (chapter 4.1.3.1)
ROs	RO, AB6-RO, DMAB5-RO

### Pseudorotaxane shuttle (with one ring- and one spherical-stopper) (chapter 4.2.1)

Axle	DMAB3-SA9u1, SA1u2, SA1o1
Macrocycle	SGR1-u1, SGR1-u2, SGR1-o1, SGR1-o2
Ring stopper (left)	Stalpha f, Stalpha r, Stbeta 3 f-l.2, Stbeta r, Stgamma f-l.2, Stdelta f, Stdelta r
Spherical Stopper (right):	
SSt-ring1	Ring1 r, SEa-r, SEb-r, GE-1, GE-2, GE-3, GE-4
SSt-ring2	same ODNs as for the pseudorotaxane used for toe-hold switch (chapter 4.1.2.1)
ROs	DMAB5-RO

### Pseudorotaxane shuttle (with one ring- and one origami-stopper) (chapter 4.2.3)

Axle	SA7u, SA1o1
Macrocycle	same ODNs as for the pseudorotaxane shuttle (chapter 4.2.1)

---

Ring stopper (right)	Stalpha f, Stalpha r, Stbeta3 f-r, Stbeta r, Stgamma f-r, Stdelta f, Stdelta r
Origami stopper	97 ODNs (see Supporting Table 3)
ROs	TH-RO1, cODN1, TH-RO2, cODN2
<b>Pseudorotaxane shuttle (with two spherical stoppers) (chapter 4.2.3.2)</b>	
Axle	SA2u1, SA1u2, SA1o1
Macrocycle	same ODNs as for the pseudorotaxane shuttle (chapter 4.2.1)
Spherical stopper (right)	same ODNs as for the pseudorotaxane shuttle (chapter 4.2.1)
Spherical stopper (left):	
SSt-ring1	Ring1 r, SEa-l, SEb-l, GE-1, GE-2, GE-3, GE-4
SSt-ring-2	same ODNs as for the pseudorotaxane used for toe-hold switch (chapter 4.1.2.1)
ROs	TH-RO1, cODN1, TH-RO2, cODN2
<b>[3]Pseudorotaxane (chapter 4.3.1)</b>	
Axle	SA3u1, SA1u2, SA1o1-(BHQ-2)
Rings	
1Gap105bp-ring	SGR3-u1-(TAMRA), SGR3-u2, SGR3-o1, SGR3-o2
2Gap126bp-ring	SGR1-u1, SGR2-u2, SGR1-o1, SGR2-o2
or rings	
1Gap126bp-ring	R9u1, R1u2, R1o1, R9o2, R1o3,
2Gap105bp-ring	SGR8-u1, SGR8-u2, SGR8-o1, SGR8-o2
or rings	
1Gap168bp-ring	Alpha-b1, beta f, Alpha-b3, 168Alpha 2r, 168Beta rc, Alpha-a1-Gap2
2Gap126bp-ring	SGR1-u1, SGR2-u2, SGR1-o1, SGR2-o2
Ring stopper (right)	same ODNs as for the pseudorotaxane shuttle (chapter 4.2.3)
Ring stopper (left)	Stalpha f, Stalpha r, Stbeta3 f-l, Stbeta r, Stgamma f-l, Stdelta f, Stdelta r
ROs, Inputs	Input A, Input B, BO, DMAB5-RO, TH-RO1, cODN1
<b>Pseudocatenane with two 168 bp macrocycles (chapter 4.4.1)</b>	
Ring alpha	168alpha 2r, 168beta rc, 168 gamma rc1, lockalpha fc1-(Cy3), beta f, 168 gamma f
Threading ODN	168 gamma rc2

3/4-ring beta	168beta rc, 168alpha 2r, 168 gamma f-(BHQ-2), beta f, lockalpha fc2
---------------	---

ROs	Cat-TH-RO, Cat-cODN
-----	---------------------

**Pseudocatenane with two 126 bp macrocycles (chapter 4.4.1)**

Ring alpha	R1o1, R1o2, R1o3, R1u1, R1u2
------------	------------------------------

Threading ODN	R3o2
---------------	------

3/4-ring beta	R1o1, R1o3, R3u1, R1u2
---------------	------------------------

**Pseudocatenane with one 126 bp and one 168 bp macrocycle (chapter 4.4.1)**

Ring alpha	168 beta rc, 168 alpha 2r, alpha-a1zif, alpha-b3, beta f, alpha-b1zif
------------	---

Threading ODN	JVGmblong
---------------	-----------

3/4-ring beta	ALgP_r, ALgP_f, ALgmb_f short
---------------	-------------------------------

ROs	Cat-RO1, Cat-RO2
-----	------------------

**[3]Pseudocatenane (chapter 4.4.1)**

Middle ring	Gap2-beta r, 168-gamma r, Gap2-beta f, Gap2-alpha f
-------------	---

Threading ODN	R4o1
---------------	------

3/4-outer rings	R1u1, R1u2, R1o1, R1o3
-----------------	------------------------

**[3]Pseudocatenane with DNAzymes (chapter 4.4.3), see:** Li, T.; Lohmann, F.; Famulok, M. *Nat. commun.* **2014**, *5*, 4940.

**Supporting Table 1. Summary of all DNA structures assembled in this study and their constituent ODNs.**

Name (number of nucleotides)	Sequence
<b>axle ODNs</b>	
EFCT-2 (25)	5'-phos-CACGATCCAGGTACAGTAACTGTCA
EFCT-2-BHQ-2 (25)	5'-phos-CACGATCCAGGTACAGTAACTGTCA-BHQ-2
EFCT-1 (20)	5'-TTAGTTCACAGGGATAACAG
A1u1 (57)	5'-phos-CACGACTGTTATCCCTGTGAACTAAGTCCGCTGCGTATGACAGTTACTGTACCTGGA
A2u (63)	5'-phos-CACGACTGTTATCCCTGTGATCCCTAACCCCTAACCCGTGACAGTTACTGTACCTGGA
A2o2 (15)	5'-TCACAGGGATAACAG
DMAB3-SA9u1 (47)	5'-phos-CCGAAAGTGGACTGTCACGXCGXGCXTACCTGTTATCCCTGTGAACTAA
SA1-o1 (40)	5'-TCCAGGTACAGTATCTTGCAATTAGTTCACAGGGATAACAG
SA1-o1-BHQ-2 (40)	5'-TCCAGGTACAGTATCTTGCAATTAGTTCACAGGGATAACAG-BHQ-2
SA1-u2 (42)	5'-phos-TGCAAGATACTGTACCTGGAGTCCGCTGCGTAGAACTGGATG
SA7u (89)	5'-phos-CCGAAAGTGGACTGTCACGCGGCCTACCTGTTATCCCTGTGAACTAATGCAAGATACTGTACCTGGAGTCCGCTGCGTAGAACTGGATG
SA2-u1 (42)	5'-phos-AGTGGACTGTCACGCGGCCTACCTGTTATCCCTGTGAACTAA
SA3-u1 (42)	5'-phos-AGTGGACTGTACCGATGCTCTACTGTTATCCCTGTGAACTAA
<b>macrocycle ODNs</b>	
R1o1 (43)	5'-phos-CAGTTTTTGGCCCTTTTTTCGCGCTTTTTTCGCGTTTTTTCCG
R1o2 (44)	5'-phos-TCTTTTTGGCACTTTTTTCTTCGAGCGGTACGTTTTTACC
R1o3 (39)	5'-phos-TTTTTGAACATTTTTTGACAGTTTTTCCGCTTTTTTGC
R1u1 (53)	5'-AGAAAAAAGTGCCAAAAAGACGGAAAAACGCGCAAAAAGCGCGAAAAAAGGG
R1u1-Cy3 (53)	5'-Cy3-AGAAAAAAGTGCCAAAAAGACGGAAAAACGCGCAAAAAGCGCGAAAAAAGGG
R1u2 (63)	5'-phos-CCAAAAACTGGCAAAAAAGACGGAAAAACTGTCAAAAAATGTTCAAAAAGCGGTAAAAAACGT
i-Motiv-R1o2 (44)	5'-phos-TCTTTTTGGCACTTTTTTCTTCGTTAGGGAACGTTTTTACC
SGR1-o1 (63)	5'-phos-TCTTTTTGGCACTTTTTTCTCTCGCAGCGGCCGTTTTTATAGATTTTTGAACATTTTTTAC
SGR1-o2 (63)	5'-phos-TCTTTTTGAGACTTTTTTCTGTAAGGCCGCGAGTTTTTTCAGCATTTTTGAACATTTTTTAC
SGR1-u1 (52)	5'-GAGAAAAAAGTGCCAAAAAGAGCTAAAAATGTTCAAAAATGCTGAAAAAC
SGR1-u2 (54)	5'-ACAGAAAAAAGTCTCAAAAAGAGTCAAAAATGTTCAAAAATCTATAAAAAACG
SGR2-o2 (63)	5'-phos-TCTTTTTGAGACTTTTTTGTGAGAGCATCGCGTTTTTTCAGCATTTTTGAACATTTTTTAC
SGR2-u2 (50)	5'-AAAAAAGTCTCAAAAAGAGTCAAAAATGTTCAAAAATCTATAAAAAACG
SGR3-o1 (56)	5'-phos-TTGCCTTTTTTGAACATTTTTTGTCAAGCATCGACCTTTTTTTCACGGTTTTTCT
SGR-3-o2 (49)	5'-phos-GCCTTTTTTCTCAGTTTTTTCGCGCTTTTTTCCCGTTTTTTCAGAGTTTT
SGR-3-u1 (50)	5'-GCAAAAAATGTTCAAAAAGAGGCAAAAAACTGTCAAAAACCGGGAAAAA
SGR-3-u2 (46)	5'-phos-GCGCGAAAAACTGAGAAAAAGGCAGAAAAACCGTGAAAAAAGAGG
SGR-3-u1-TAMRA (50)	5'-TAMRA-GCAAAAAATGTTCAAAAAGAGGCAAAAAACTGTCAAAAACCGGGAAAAA
R1o1 (43)	5'-phos-CAGTTTTTGGCCCTTTTTTCGCGCTTTTTTCGCGTTTTTTCCG
R9o2 (44)	5'-phos- TCTTTTTGGCACTTTTTTCTTAAGCATCGAACGTTTTTACC
R1o3 (39)	5'-phos-TTTTTGAACATTTTTTGACAGTTTTTCCGCTTTTTTGC
R9u1 (54)	5'-AAGAAAAAAGTGCCAAAAAGACGGAAAAACGCGCAAAAAGCGCGAAAAAAGGG
R1u2 (63)	5'-phos-CCAAAAACTGGCAAAAAAGACGGAAAAACTGTCAAAAAATGTTCAAAAAGCGGTAAAAAACGT
SGR8-o1 (56)	5'-phos-TTGCCTTTTTTGAACATTTTTTGTGAGAGCATCGGCGCTTTTTTTCACGGTTTTTCT
SGR8-o2 (49)	5'-phos-GCCTTTTTTCTCAGTTTTTGTGAGAGCATCGGCGTTTTTTCAGAGTTTT
SGR8-u1 (40)	5'-CAAAAATGTTCAAAAAGAGGCAAAAAACTGTCAAAAAC
SGR8-u2 (41)	5'-AAAAACTGAGAAAAAAGCAGAAAAACCGTGAAAAAAGAGG
Alpha-b1 (51)	5'-phos-AAAAAAGTGCCAAAAAGACGGAAAAACGCGCAAAAAGCGCGAAAAAAGGG
alpha-a1 Gap2 (50)	5'-phos-TCTTTTTGGCACTTTTTTAAAGCATCGAAATCCGTTTTTACC

168Beta rc (75)	5'-phos-AACATTTTTTGACAGTTTTTCCGTCTTTTTGCGCGTTTTTCCATATTTTTGAACATTTTTCTCCGTTTTTTGA
Beta f (52)	5'-phos-CCAAAACTGTCAAAAAACGGAGAAAAATGTTCAAAAAATATGGAAAAACGG
Alpha-b3 (55)	5'-phos-GCAAAAAAGACGGAAAAACTGTCAAAAAATGTTCAAAAAAGCGGTAAAAAACGGAT
168Alpha2 r (43)	5'-phos-CAGTTTTTGCCCTTTTTTCGCGCTTTTTGCGCGTTTTTTCCG
Lockalpha fc1	5'-AGAAAAAAGTGCCAAAAAGACGGAAAAAACGCGCAAAAAAGCGCGAAAAAAGGG
Lockalpha fc1-(Cy3)	5'-Cy3-AGAAAAAAGTGCCAAAAAGACGGAAAAAACGCGCAAAAAAGCGCGAAAAAAGGG
168gamma rc2	5'-phos-TCTTTTTGGCACTTTTTTCTCAGAACTAACCTATTTTTTACCGCTTTTTG
168gamma f	5'-phos-GCAAAAAAGACGGAAAAACTGTCAAAAAATGTTCAAAAAAGCGGTAAAAAATA
168gamma f-BHQ-2	5'-phos-GCAAAAAAGACGGAAAAACTGTCAAAAAATGTTCAAAAAAGCGGTAAAAAATA-BHQ-2
Lockalpha fc2	5'-GAGAAAAAAGTGCCAAAAAGACGGAAAAAACGCGCAAAAAAGCGCGAAAAAAGGG
168gamma rc1	5'-phos-TCTTTTTGGCACTTTTTTCTCCGTTAGTTCACGTTTTTACCGCTTTTTG
R3u1	5'-AAAAAAGTGCCAAAAAGACGGAAAAAACGCGCAAAAAAGCGCGAAAAAAGGG
R3o2	5'-phos-TCTTTTTGGCACTTTTTTGTCCGCTGCGTAACGTTTTTACCGC
Alfa-b1zif	5'-phos-CGCCACGCTGAACCTTCGGAAAAAACGCGCAAAAAAGCGCGAAAAAAGGG
Alfa-a1zif	5'-phos-AAGGGTTCAGCGTGGGCGCGCGCTAATCCGTTTTTACCGCTTTTTG
Alpha-b3	5'-phos-GCAAAAAAGACGGAAAAACTGTCAAAAAATGTTCAAAAAAGCGGTAAAAAACGGAT
JVgmblong	5'-phos-ACTTTTTTGTGGGTTTTTGAGGCCGCGTTCAGCCTTTTTTCGCCGTTTTTTCGCAATTTTTTCAG
ALgP_r	5'-phos- TCTTTTTTGCAGCTTTTTTAATTAATACGACTCACTATAGGGAGATTTTTTACGCATTTTTGTCT
ALGmb_f short	5'-phos-AAAGCTGCAAAAAAGACTGAAAAATTCGAAAAACGGCGAAAAAAGGG
ALgP_f	5'-phos-AACCCACAAAAAGTGACAAAAATGCGTAAAAAATCTCCATAGTGAGTCGTATTAATTA
R4o1	5'-phos-TCTTTTTGGCACTTTTTTCTTCGCGGCCCTTACGTTTTTACCGC
Gap2-beta r	5'-phos-TCTTTTTGGCGTTTTTCCCCAGGCCGCGACGTTTTTCCGCCTTTTTGAACATTTTTCTGC
Gap2-alpha f	5'-GGAAAAAACCGCCAAAAAGAGTCAAAAAATGTTCAAAAAAGCGGTAAAAA
Gap2-beta f (50)	5'-AGAAAAAAGTGCCAAAAAGACGAGAAAAATGTTCAAAAAAGCGCGAAAAA
168Gamma r	5'-phos-TCTTTTTGGCACTTTTTTCTCCAGGCCGCGACGTTTTTACCGCTTTTTGAACATTTTTTGAC
<b>ring stopper ODNs</b>	
Stalpha f (65)	5'-phos-AAAGTGCCAAAAAGCGCGAAAAAAGGGCCAAAAACTGTCAAAAAACGGAGAAAAATGTTCAAAA A
Stalpha r (63)	5'-phos-TTTTCCATATTTTTGAACATTTTTCTCCGTTTTTTGACAGTTTTTGGCCCTTTTTTCGCGCT
Stbeta3 f (49)	5'-phos-AAAAAAGACGGAAAAACTGTCAAAAAATGGGACACTGACGGATCCTCCA
Stbeta r (63)	5'-phos-TTTTGGCACTTTTTTACCGCTTTTTGAACATTTTTTACAGTTTTTCCGCTTTTTTTCGCGCT
Stgamma f (41)	5'-phos-TCGTGTGGAGGATCCGTCACTGTCTTCAAAAAAGCGGTAAA
Stdelta f (58)	5'-phos-ATATGGAAAAACTGCCAAAAAGACGGAAAAACGCGCAAAAAATATGGAAAAACGCGC
Stdelta r (42)	5'-phos-TTTTCCATATTTTTGCGCGTTTTTCCGCTTTTTTGGCAGT
Stgamma f-l.2 (42)	5'-ACAGTCCACTTTCGGCAGACCTGCGTTTTCAAAAAAGCGGTAAA
Stbeta-3f-l (40)	5'-phos-AAAAAAGACGGAAAAACTGTCAAAAAATGACGCAGGTCTG
Stbeta-3f-r (49)	5'-phos-AAAAAAGACGGAAAAACTGTCAAAAAATGGCAACAGATCCATCCAGTTC
Stgamma f-r (26)	5'-phos-GATCTGTTGCTTCAAAAAAGCGGTAAA
Stgamma f-l (37)	5'-ACAGTCCACTCAGACCTGCGTTTTCAAAAAAGCGGTAAA
<b>spherical stopper ODNs</b>	
HJalpha b (53)	5'-phos-AAAAGTGCCAAAAAGACCAAAAAACTGTCAAAAAACGGAGAAAAATGTTCAAAA
HJalpha c (61)	5'-phos-TTTCCATATTTTTGAACATTTTTCTCCGTTTTTTGACAGTTTTTGGCGAAAAAACGCGC
HJalpha d (33)	5'-phos-CGCGCTTTTTGCGCGTTTTTCCGCCCTTTTTT
HJbeta a (56)	5'-phos-AATATGGAAAAACGCGCAAAAAAGACGGAAAAACTGTCAAAAAATGTCGCAAAAA
HJbeta kc (32)	5'-phos-ATTTTTTCCAACTTTTTGAGCTTTTTTCCATAT
HJbeta kd (60)	5'-phos-TGTTCAAAAAATATGGAAAAAGCACATTTTTTACAGTTTTTCCGCTTTTTTTCGCGCTT
Ring1 r (56)	5'-phos-CGCGCTTTTTGCGCGTTTTTCCGCTTTTTTGGCACTTTTTTCTCGCTTTTTAGAT

---

RingSE a (54)	5'-phos-GACGGAAAACTGTCAAAAAATGTTCAAAAAGTGCAGCACCTCACGTCTCATGG
RingSE b (52)	5'-phos-TCGTGCCATGAGACGTGAGGTGCTGCTGGAAAAATATCTAAAAAGCGAGAA
Bogen f (47)	5'-phos-AAAAAGCGCGAAAAAAGGGCCAAAAACTGTCAAAAAACGGAGAAAAA
Bogen r (47)	5'-phos-TTTTTGAACATTTTTCTCCGTTTTTTGACAGTTTTTTGGCCCTTTTTT
GE-1 (39)	5'-phos-AAGCGAGAAAAAAGTGCCAAAAAGACGGAAAAACGCGC
GE-2 (42)	5'-phos-AAAAAGCGCGAAAAAAGGGTCTTTTTGGCACTTTTTTCTCGC
GE-3 (45)	5'-phos-TTTTTAGATATTTTTTCCAACTTTTTGAACATTTTTTGACAGTTT
GE-4 (42)	5'-phos-TTCCGTCTTTTTTGCCTCAAAAAGTTGGAAAAATATCTAAA
SEa-r (53)	5'-phos-GACGGAAAACTGTCAAAAAATGTTCAAAAAGTGCACAGATCCATCCAGTTC
SEb-r (36)	5'-phos-GATCTGTTGCTGAAAAAATATCTAAAAAGCGAGAA
SEb-l (47)	5'-ACAGTCCACTCAGACCTGCGTTGGAAAAAATATCTAAAAAGCGAGAA
SEa-l (44)	5'-phos-GACGGAAAACTGTCAAAAAATGTTCAAAAAGTACGCAGGTCTG

#### ROs and Test-ODNs

RO (12)	5'-TACGCAGCGGAC
TH-RO1 (19)	5'-TCATACATACGCAGCGGAC
cODN1 (19)	5'-GTCCGCTGCGTATGTATGA
TH-RO2	5'-GCTCAGAGTAGGCCGCGTG
cODN2	5'-CACGCGGCCTACTCTGAGC
AB2-RO (12)	5'-TACGYCAGCYGGAC
AB3-RO (12)	5'-TACGYCAYGCGYGGAC
AB4-RO (12)	5'-TACYGICYAGYCGYGAC
AB5-RO (12)	5'-TAYCGYCYGCGYGGYAC
AB6-RO (12)	5'-TYACYGICYAGYCGYGAYC
AB8-RO (12)	5'-TAYCYGYCYAGYCYGYGYAC
DMAB5-RO (12)	5'-TAXCGXCAXGCXGGXAC
i-Motiv test-ODN (8)	5'-Rhodamine Green-GGTTAGGG
light switch test-ODN (8)	5'-Cy3-CGCAGCGG
input A (24)	5'-GGACGAGTCTGTGAGAGCATCGGC
input B (= RO) (12)	5'-TACGCAGCGGAC
BO (24)	5'-GCCGATGCTCTCACAGACTCGTCC
Cat-RO1	5'-phos-TAGGCCGCGG
Cat-RO2	5'-phos-TGAACGCGGCCTCAAA

**Supporting Table 2. Names and sequences of all ODNs used in this study (except for origami stopper, see Supporting Table 3). The Y represents one AB modification, the X one DMAB modification, phos stands for 5'-phosphorylation, Cy3, TAMRA, Rhodamine Green and BHQ-2 indicate the corresponding fluorophore and quencher labels.**

Name	Sequence
R4_13.1	5'-CCCGAAGTACCTCTGCAGGAT
R4_13.2	5'-CGTTACCAGGCTACGATGAGT
R4_13.3	5'-CTGTCCCACTCTCCTTCAAAT
R4_13.6	5'-CATTGCACTGCTCTACCCTTT
R4_13.7	5'-CTTCATCGACCTGTTTAGGTT
R_25.1	5'-GCCGATACAGATACATACTGA
R_25.2	5'-GACCCAGATGATTATACTAAA
R_25.3	5'-GACATCTGTGAGGGTCTTGTA
R_25.4	5'-GTCCACGCTGACTCGCAAATA

---

R\_25.5 5'-GGCGAGCCGGAATTGTTACGA  
R\_25.6 5'-GAGCTAGGCGAGCTACCCAGA  
R\_25.7 5'-GATAGCCGGGACAGTTTGCTA  
R4\_14.8 5'-CTGCACCAGCTTTTTTTTTTTTTTTTTTTTTTAAACCTAAACA  
R4\_16.8 5'-CCCTCAGCACTTTTTTTTTTTTTTTTTTTTTTATAAGACACA  
R4\_18.8 5'-CTATACGGCCTTTTTTTTTTTTTTTTTTTTTTAGGTGGCGCA  
R4\_20.8 5'-CACCAACGGCTTTTTTTTTTTTTTTTTTTTTTAAATTATATA  
R4\_22.8 5'-CAGGAGAACCTTTTTTTTTTTTTTTTTTTTTTAGGACCCTTA  
R4\_24.8 5'-CCCGGCTATCTTTTTTTTTTTTTTTTTTTTTTACTGTCTAAA  
R\_24.1 5'-TTTTTTTTTTTTCAGTATGTATGGGCAGGCATGTTTTTTTTTT  
R\_24.2 5'-CTGTATCGGCTTTAGTATAATGTATAGTCTTGAAGTTAGCAA  
R\_24.3 5'-CATCTGGGTCTACAAGACCCTGGATGCGCGTGAGCGTCCTGA  
R\_24.4 5'-CACAGATGTCTATTTGCGAGTGCAGCTTACGAATAAACGGA  
R\_24.5 5'-CAGCGTGGACTCGTAACAATTGTGCATTACGATAGACCATA  
R\_24.6 5'-CCGGCTCGCCTCTGGGTAGCTGTATTACCGAGAGTCTACCGA  
R\_24.7 5'-CGCCTAGCTCTAGCAAAGTGTGGAGACTCTTGATAGCATAAA  
R\_23.1 5'-CATGCCTGCCCTTGCTAACTTGCCGTCAGAGAACAACAACA  
R\_23.2 5'-CAAGACTATACTCAGGACGCTGGCACTTCCGACCTCAATGTA  
R\_23.3 5'-CACGCGCATCCTCCGTTTATTGCCATGGTAGACAATCATGGA  
R\_23.4 5'-CGTAAAGCTGCTATGGTCTATGCCGACTAAGACTCGTGAGCA  
R\_23.5 5'-CGTGAATGCACTCGGTAGACTGGCGCTTGCGAACTATCGGCA  
R\_23.6 5'-CTCGGTAATACTTTATGCTATGCGTCACCAGAACCTGATACA  
R\_23.7 5'-CAAGAGTCTCCTTTAGACAGTGGTTCTCTGACGAATTAGAA  
R\_22.1 5'-TTTTTTTTTTTGTGTTTGTGGCAAAGCAAGTTTTTTTTTT  
R\_22.2 5'-CTCTGACGGCTACATTGAGGTGCGGTGATTGATCGTTAGGA  
R\_22.3 5'-CGGAAGTGCCCTCCATGATTGTGCCGTCCCAAGAGGCTTTGCA  
R\_22.4 5'-CTACCATGGCTGCTCAGAGTGTCTAATTGGAATTTCCAAA  
R\_22.5 5'-CTTAGTCGGCTGCCGATAGTTGATGGCCAAGATCTAAATTA  
R\_22.6 5'-CGCAAGCGCCTGTATCAGGTTGATAACCAGGGATTTGGATAA  
R\_22.7 5'-CTGGTGACGCTTCTAATTCGTGAGGACAATAGAAGGATAGGA  
R\_21.1 5'-CTTGCTTTGCCTCCTAACGATGACTTAAGCGAAGCAAGGTAA  
R\_21.2 5'-CAATACACCGCTGCAAGACCTGGGCTAGGGATTAGCGCCAA  
R\_21.3 5'-CTTGGGACGGCTTTGAAAATTGAAGGCTTAGACATGCAGCTA  
R\_21.4 5'-CCAATTAGGACTAATTTAGATGTGGAGCCCGAAGAATTAACA  
R\_21.5 5'-CTTTGGCCATCTTATCCAAATGATAACAGAGAAGCACTTACA  
R\_21.6 5'-CCCTGGTTATCTCCTATCCTTGTCGCACGGGACCTACTACCA  
R\_21.7 5'-CTATTGTCCTCTAAGGGTCCTGCCGTTGGTGATCTAATTGTA  
R\_20.1 5'-TTTTTTTTTTTTTACCTTGCTTGATCATCTCAGTTTTTTTTTT  
R\_20.2 5'-CGCTTAAGTCTTGGCGCTAATGGCGGGAAGGGATTGTTTGA  
R\_20.3 5'-CCCTAGGCCCTAGCTGCATGTGACTAGCCAGGAGCCGCCTAA  
R\_20.4 5'-CTAAGCCTTCTGTTAATTCTTGCTCCACGTAGATTAACAATA  
R\_20.5 5'-CGGGCTCCACTGTAAGTCTTGGTAATGTCAGATCCCTAATA  
R\_20.6 5'-CTCTGTTATCTGGTAGTAGGTGAAACGCCTAGAGGATTGTGA  
R\_20.7 5'-CCCGTGCGACTACAATTAGATGGCACCTTAAGAAGGACATAA  
R\_19.1 5'-CTGAGATGATCTCAAACGAATGAAGCGAACGATAGTCTGGAA  
R\_19.2 5'-CCCTTCCCGCCTTAGGGCGCTGGTAAGGGTGACGGCCAGCA  
R\_19.3 5'-CCTGGCTAGTCTATTGTTAATGTGTGAGGCGATTGGCAGAAA

---

R_19.4	5'-CTACGTGGAGCTATTAGGGATGGCAGGTTAGAACTCTGACA
R_19.5	5'-CTGACATTACCTCACAAATCCTGGTATCGTCGACGATCGGTCA
R_19.6	5'-CTAGGCGTTTCTTATGTCCTTGCAGGCGAAGACCACGCCTTA
R_19.7	5'-CTTAAGGTGCCTATATAATTTGGCCGTATAGAGACATGGTAA
R_18.7	5'-CTTCGCCTGCTTACCATGTCTGTGACAGCTGGACTGAACATA
R_18.1	5'-TTTTTTTTTTTTCCAGACTATGGTACCCAAAGTTTTTTTTTT
R_18.2	5'-CGTTCGCTTCTGCTGGGCCGTGCGGACATGCGAACCCGTCTA
R_18.3	5'-CACCCCTTACCTTTCTGCCAATGACGTCCTTAGACTTTCTGGA
R_18.4	5'-CGCCTCACACTGTCAGAGTTTGTATGCATTTGATGAATTGGA
R_18.5	5'-CTAACCTGCCTGACCGATCGTACTCTAAGTGACTAAACAAA
R_18.6	5'-CGACGATACCTAAGGCGTGGTGTACATGAGAGACCGGGCCCA
R_17.1	5'-CTTTGGGTACCTAGACGGGTTGTATGTCTTGATGATGGGCCA
R_17.2	5'-CGCATGTCCGCTCCAGAAAGTGGTGGTCTAGAATACAGAATA
R_17.3	5'-CTAAGGACGTCTCCAATTCATGCCACAAGGGATAAAGAAAGA
R_17.4	5'-CAAATGCATACTTTGTTTGTAGTGGGTTCCGGTGAGACCTCCTTA
R_17.5	5'-CACTTAGAGTCTGGGCCCGGTAAGTTCAGGAGCGAGCGGAA
R_17.6	5'-CTCTCATGTACTATGTTTCAGTGGTCACTCAGATCGGGATCAA
R_17.7	5'-CCAGCTGTCACCTGCGCCACCTGTGCTGAGGGAATGGATGGAA
R_16.1	5'-TTTTTTTTTTTTGGCCCATCATGGCTTGCCAGTTTTTTTTTT
R_16.2	5'-CAAGACATACTATTCTGTATTGGGACCGCACGATCGCAATAA
R_16.3	5'-CTAGACCACCTCTTTCTTTATGGCCGCCCGCGACTGCGCGTA
R_16.4	5'-CCCTTGTGGCTAAGGAGGTCTGTACAAGATAGATAATTGAAA
R_16.5	5'-CACCGAACCCCTCCGCTCGCTGGACGGTTTGAACCGGTGCA
R_16.6	5'-CCTGAAGTTCTTGATCCCGATGTTGGGACATGAAACGTAGGA
R_16.7	5'-CTGAGTGACCTTCCATCCATTGAACGCGCTGGAAAGACTCCA
R_15.1	5'-CTGGGCAAGCCTTATTGCGATGTGCGATCGGATCAAGTAACA
R_15.2	5'-CGTGCGGTCCCTACGCGCAGTGTGGCAGCGAGACATATCAA
R_15.3	5'-CGCGGGCCGCTTTCAATTATGACCCTTCTGAAGGCCCTGAA
R_15.4	5'-CTATCTTGTACTGCACCGGTTGCGGCGCTCGACAGTTACACA
R_15.5	5'-CCAAACCGTCCCTCCTACGTTTGTAGCCTCCTGAAATAGCCGCA
R_15.6	5'-CATGTCCCAACTGGAGTCTTTGTCGTCCCAGAAGCGGTTGGA
R_15.7	5'-CCAGCGGTTCTGTGTCTTATGCTGGTGCAGATGACGTGCCA
R_14.2	5'-CCGATGCGACTTGATATGTCTGCCTGGTAACGATCCTGCAGA
R_14.3	5'-CGCTGCCAGCTTCAGGGCCTTGTAGTGGGACAGACTCATCGTA
R_14.4	5'-CAGAAGGGTCTGTGTAAGTGTGCAATATAATGATTTGAAGGA
R_14.5	5'-CGAGCGCCGCTGCGGCTATTTGGGCATGCACGACCCTCAGGA
R_14.6	5'-CAGGAGGCTCTCCAACCGCTTGCAGTGAATGAAGTTTGGGA
R_14.7	5'-CTGGGACGACTGGCACGTCATGGTGCATGAAGAAAGGGTAGA
R_14.1	5'-TTTTTTTTTTTGTACTTGATGGTACTTCGGGTTTTTTTTTT
R4_13.4-Stem	5'-CATTATATTGCTCCTGAGGGTTTGAAGGGATGGAGGA
R4_13.5-Sticky-end	5'-ACAGTCCACTTTCGGTCTCCATCCCTTCCTTCGTGCATGCCCTCCCAAACCTT

**Supporting Table 3. Names and sequences of all ODNs used to assemble the origami stopper.**



---

Structure	Extinction coefficient $\epsilon$ [mol <sup>-1</sup> *cm <sup>-1</sup> ]
Macrocycles (105 bp)	1.24*10 <sup>6</sup>
Macrocycles (126 bp)	1.49*10 <sup>6</sup>
Macrocycles (168 bp)	1.99*10 <sup>6</sup>
Ring stopper	2.40*10 <sup>6</sup>
Spherical stopper	4.40*10 <sup>6</sup>
[2]Rotaxane (ring stopper)	6.80*10 <sup>6</sup>
[2]Rotaxane (ring- and spherical-stopper)	8.80*10 <sup>6</sup>
[2]Rotaxane (spherical stopper)	10.80*10 <sup>6</sup>
[3]Rotaxane (ring stopper, 105 and 126 bp macrocycle)	8.04*10 <sup>6</sup>
[2]Catenane (2x 126 bp macrocycle)	2.98*10 <sup>6</sup>
[2]Catenane (126 and 168 bp macrocycle)	3.48*10 <sup>6</sup>
[2]Catenane (2x 168 bp macrocycle)	3.98*10 <sup>6</sup>
[3]Catenane (3x 126 bp macrocycle)	4.47*10 <sup>6</sup>

**Supporting Table 4. DNA structures assembled in this study and their extinction coefficients  $\epsilon$ .**

---

## 7.5 Acknowledgements

Prof. Dr. M. Famulok danke ich für das Vertrauen und die Förderung meiner Fähigkeiten.

Prof. Dr. G. Mayer danke ich für die freundliche Übernahme des Zweitgutachtens.

Prof. Dr. S. Höger und Prof. Dr. G. Bendas danke ich für die freundliche Bereitschaft diese Arbeit zu begutachten.

Dr. Damian Ackermann und Dr. Julián Valero danke ich für die erhellende Betreuung.

Dr. Damian Ackermann, Dr. Julián Valero, Dr. Tao Li, Dr. Chia-Ling Chung, Daniel Keppner, Volker Adam und Johannes Weigand gilt mein Dank für unsere produktive Zusammenarbeit.

Dr. Julián Valero, Dr. Daniel Lohmann und Gillrich danke ich für Verbesserungsvorschläge und die ausführliche Diskussion des Manuskripts dieser Arbeit.

Dank Mo, Jeff, Ben, Falk, Alex, Jan, Daniel und Julián waren die Kaffee- und Mittags-Pausen stets äußerst amüsant.

Allen Mitarbeitern der AGs Mayer und Famulok danke ich für die sehr freundliche und kollegiale Arbeitsatmosphäre.

Meinen Eltern danke ich für die ausnahmslose Unterstützung in allen Belangen.

## 7.6 Curriculum Vitae Finn Lohmann

### Work Experience

---

Nov 2010 – Feb 2015	<b>Scientific Assistant</b> , Life and Medical Sciences Institute, Bonn
Aug 2003 – May 2004	<b>Internship</b> in Children's Home <i>Hogar Esperanza</i> , Viña del Mar, Chile

### Education

---

Nov 2010 – Today	<b>PhD in Chemistry</b> , under Supervision of Prof. Dr. M. Famulok, Life and Medical Sciences Institute, Bonn  PhD thesis: <i>Design, Assembly and Triggering of Interlocked DNA Nanoarchitectures</i>
Oct 2005 – July 2010	<b>Diploma in Chemistry</b> , Rheinische Friedrich-Wilhelms-Universität, Bonn Degree: Diploma (1.0)
Mar 2013 – Sep 2013	<b>Certificate in Business and Management</b> , Euro FH, Grade 2.3
Oct 2004 – Sept 2005	<b>Diploma in Chemistry</b> , Friedrich-Alexander Universität, Erlangen-Nürnberg
1995 – 2003	<b>Secondary School</b> , Windthorst-Gymnasium, Meppen Degree: Abitur
1999 – 2000	<b>Rotary Exchange Program</b> , Colegio Mochis, Los Mochis, Mexico

---

## 8 Literature

- (1) Feynman, R. *Engineering and Science* **1960**, *23*, 22-36.
- (2) Riedel, E. *Moderne Anorganische Chemie*; Walter de Gruyter: Berlin, 2007.
- (3) Sanchez, F.; Sobolev, K. *Constr. Build. Mater.* **2010**, *24*, 2060-2071.
- (4) Watson, J. D.; Crick, F. H. C. *Nature* **1953**, *171*, 737-738.
- (5) Seeman, N. C. *Annu. Rev. Biochem.* **2010**, *79*, 65-87.
- (6) Chargaff, E.; Lipshitz, R.; Green, C. J. *Biol. Chem.* **1952**, *195*, 155-160.
- (7) Holliday, R. *Genetics Research* **1964**, *5*, 282-304.
- (8) Liu, Y.; West, S. C. *Nat. Rev. Mol. Cell Bio.* **2004**, *5*, 937-944.
- (9) Seeman, N. C. *J. Theor. Biol.* **1982**, *99*, 237-247.
- (10) Heckel, A.; Famulok, M. *Biochimie* **2008**, *90*, 1096-1107.
- (11) Zadeh, J. N.; Steenberg, C. D.; Bois, J. S.; Wolfe, B. R.; Pierce, M. B.; Khan, A. R.; Dirks, R. M.; Pierce, N. A. *J. Comput. Chem.* **2011**, *32*, 170-173.
- (12) Hagerman, P. J. *Annual review of biophysics and biophysical chemistry* **1988**, *17*, 265-286.
- (13) Dlakic, M.; Harrington, R. E. *J. Biol. Chem.* **1995**, *270*, 29945-29952.
- (14) MacDonald, D.; Herbert, K.; Zhang, X.; Polgruto, T.; Lu, P. *J. Mol. Biol.* **2001**, *306*, 1081-1098.
- (15) Gehring, K.; Leroy, J.-L.; Gueron, M. *Nature* **1993**, *363*, 561-565.
- (16) Michelson, A. M.; Todd, A. R. *J. Chem. Soc.* **1955**, 2632-2638.
- (17) Matteucci, M. D.; Caruthers, M. H. *J. Am. Chem. Soc.* **1981**, *103*, 3185-3191.
- (18) Lakowicz, J. R. *Principles of Fluorescence Spectroscopy*; Springer, 2010.
- (19) Kröck, L.; Heckel, A. *Angew. Chem.* **2005**, *117*, 475-477.
- (20) Brieke, C.; Rohrbach, F.; Gottschalk, A.; Mayer, G.; Heckel, A. *Angew. Chem. Int. Ed.* **2012**, *51*, 8446-8476.
- (21) Heckel, A.; Mayer, G. *J. Am. Chem. Soc.* **2004**, *127*, 822-823.
- (22) Asanuma, H.; Takarada, T.; Yoshida, T.; Tamaru, D.; Liang, X.; Komiyama, M. *Angew. Chem.* **2001**, *113*, 2743-2745.
- (23) Mitscherlich, E. *Anna. Phys.* **1834**, *108*, 225-227.
- (24) Bandara, H. M. D.; Burdette, S. C. *Chem. Soc. Rev.* **2012**, *41*, 1809-1825.
- (25) Asanuma, H.; Liang, X.; Nishioka, H.; Matsunaga, D.; Liu, M.; Komiyama, M. *Nature protocols* **2007**, *2*, 203-212.

- 
- (26) Liang, X.; Mochizuki, T.; Asanuma, H. *Small* **2009**, *5*, 1761-1768.
- (27) Nishioka, H.; Liang, X.; Kashida, H.; Asanuma, H. *Chem. Commun.* **2007**, 4354-4356.
- (28) Asanuma, H.; Nishioka, H.; Ishikawa, T.; Liang, X. *Curr. Protoc. Nucleic. Acid. Chem.* **2011**, *Chapter 4*, Unit 4.45.41-18.
- (29) Nishioka, H.; Liang, X.; Asanuma, H. *Chemistry* **2010**, *16*, 2054-2062.
- (30) Zhang, D. Y.; Seelig, G. *Nat. Chem.* **2011**, *3*, 103-113.
- (31) Liu, D.; Balasubramanian, S. *Angew. Chem. Int. Ed.* **2003**, *42*, 5734-5736.
- (32) Rothmund, P. W. K. *Nature* **2006**, *440*, 297-302.
- (33) Chen, J.; Seeman, N. C. *Nature* **1991**, *350*, 631-633.
- (34) Mohammed, A. M.; Schulman, R. *Nano Lett.* **2013**, *13*, 4006-4013.
- (35) Zheng, J.; Birktoft, J. J.; Chen, Y.; Wang, T.; Sha, R.; Constantinou, P. E.; Ginell, S. L.; Mao, C.; Seeman, N. C. *Nature* **2009**, *461*, 74-77.
- (36) Bath, J.; Turberfield, A. J. *Nat. Nanotechnol.* **2007**, *2*, 275-284.
- (37) Ezziane, Z. *Nanotechnology* **2006**, *17*, R27.
- (38) Barbara, S.; Christof, M. N. *Angew. Chem.* **2012**, *124*, 60-69.
- (39) Goodman, R. P.; Schaap, I. A. T.; Tardin, C. F.; Erben, C. M.; Berry, R. M.; Schmidt, C. F.; Turberfield, A. J. *Science* **2005**, *310*, 1661-1665.
- (40) Andersen, E. S.; Dong, M.; Nielsen, M. M.; Jahn, K.; Subramani, R.; Mamdouh, W.; Golas, M. M.; Sander, B.; Stark, H.; Oliveira, C. L. P.; Pedersen, J. S.; Birkedal, V.; Besenbacher, F.; Gothelf, K. V.; Kjems, J. *Nature* **2009**, *459*, 73-76.
- (41) Topping, T.; Voigt, N. V.; Nangreave, J.; Yan, H.; Gothelf, K. V. *Chem. Soc. Rev.* **2011**, *40*, 5636-5646.
- (42) Wei, B.; Dai, M.; Yin, P. *Nature* **2012**, *485*, 623-626.
- (43) Wei, B.; Ong, L. L.; Chen, J.; Jaffe, A. S.; Yin, P. *Angew. Chem. Int. Ed.* **2014**, *53*, 7475-7479.
- (44) Seeman, N. C. *Trends Biochem. Sci.* **2005**, *30*, 119-125.
- (45) Lu, C.-H.; Cecconello, A.; Elbaz, J.; Credi, A.; Willner, I. *Nano Lett.* **2013**, *13*, 2303-2308.
- (46) Dittmer, W. U.; Reuter, A.; Simmel, F. C. *Angew. Chem. Int. Ed.* **2004**, *43*, 3550-3553.
- (47) Yurke, B.; Turberfield, A. J.; Mills, A. P.; Simmel, F. C.; Neumann, J. L. *Nature* **2000**, *406*, 605-608.
- (48) Wang, W.; Yang, Y.; Cheng, E.; Zhao, M.; Meng, H.; Liu, D.; Zhou, D. *Chem. Commun.* **2009**, 824-826.

- 
- (49) Liang, X.; Nishioka, H.; Takenaka, N.; Asanuma, H. *ChemBioChem* **2008**, *9*, 702-705.
- (50) Shin, J.-S.; Pierce, N. A. *J. Am. Chem. Soc.* **2004**, *126*, 10834-10835.
- (51) Bath, J.; Green, S. J.; Turberfield, A. J. *Angew. Chem.* **2005**, *117*, 4432-4435.
- (52) Liber, M.; Tomov, T. E.; Tsukanov, R.; Berger, Y.; Nir, E. *Small* **2015**, *11*, 568-575.
- (53) Yang, Y.; Endo, M.; Hidaka, K.; Sugiyama, H. *J. Am. Chem. Soc.* **2012**, *134*, 20645-20653.
- (54) Saccà, B.; Ishitsuka, Y.; Meyer, R.; Sprengel, A.; Schöneweiß, E.-C.; Nienhaus, G. U.; Niemeyer, C. M. *Angew. Chem. Int. Ed.* **2015**, n/a-n/a.
- (55) Goldman, N.; Bertone, P.; Chen, S.; Dessimoz, C.; LeProust, E. M.; Sipos, B.; Birney, E. *Nature* **2013**, *494*, 77-80.
- (56) Adleman, L. M. *Science* **1994**, *266*, 1021-1024.
- (57) Stojanovic, M. N.; Mitchell, T. E.; Stefanovic, D. *J. Am. Chem. Soc.* **2002**, *124*, 3555-3561.
- (58) Li, T.; Ackermann, D.; Hall, A. M.; Famulok, M. *J. Am. Chem. Soc.* **2012**, *134*, 3508-3516.
- (59) Prokup, A.; Hemphill, J.; Deiters, A. *J. Am. Chem. Soc.* **2012**, *134*, 3810-3815.
- (60) Baron, R.; Lioubashevski, O.; Katz, E.; Niazov, T.; Willner, I. *L. Phys. Chem. A* **2006**, *110*, 8548-8553.
- (61) Willner, I.; Shlyahovsky, B.; Zayats, M.; Willner, B. *Chem. Soc. Rev.* **2008**, *37*, 1153-1165.
- (62) Genot, A. J.; Bath, J.; Turberfield, A. J. *J. Am. Chem. Soc.* **2011**, *133*, 20080-20083.
- (63) Li, W.; Yang, Y.; Yan, H.; Liu, Y. *Nano Lett.* **2013**, *13*, 2980-2988.
- (64) Douglas, S. M.; Bachelet, I.; Church, G. M. *Science* **2012**, *335*, 831-834.
- (65) Famulok, M.; Mayer, G. *Chemistry & Biology* **2014**, *21*, 1055-1058.
- (66) Stoddart, J. F. *Chem. Soc. Rev.* **2009**, *38*, 1802-1820.
- (67) Jäger, R.; Vögtle, F. *Angew. Chem.* **1997**, *109*, 966-980.
- (68) Meyer, C. D.; Forgan, R. S.; Chichak, K. S.; Peters, A. J.; Tangchaivang, N.; Cave, G. W.; Khan, S. I.; Cantrill, S. J.; Stoddart, J. F. *Chemistry* **2010**, *16*, 12570-12581.
- (69) Reuter, C.; Mohry, A.; Sobanski, A.; Vogtle, F. *Chemistry* **2000**, *6*, 1674-1682.
- (70) Fang, L.; Hmadeh, M.; Wu, J.; Olson, M. A.; Spruell, J. M.; Trabolsi, A.; Yang, Y. W.; Elhabiri, M.; Albrecht-Gary, A. M.; Stoddart, J. F. *J. Am. Chem. Soc.* **2009**, *131*, 7126-7134.

- 
- (71) Frisch, H. L.; Wasserman, E. *J. Am. Chem. Soc.* **1961**, *83*, 3789-3795.
- (72) Aricó, F.; Badjic, J.; Cantrill, S.; Flood, A.; Leung, K. F.; Liu, Y.; Stoddart, J. F. In *Templates in Chemistry II*; Schalley, C., Vögtle, F., Dötz, K., Eds.; Springer Berlin Heidelberg: 2005; Vol. 249, p 203-259.
- (73) Schomburg, I. *Angew. Chem.* **2009**, *121*, 4719-4738.
- (74) Dietrich-Buchecker, C. O.; Sauvage, J. P.; Kern, J. M. *J. Am. Chem. Soc.* **1984**, *106*, 3043-3045.
- (75) Dietrich-Buchecker, C. O.; Sauvage, J. P.; Kintzinger, J. P. *Tetrahedron Lett.* **1983**, *24*, 5095-5098.
- (76) Schalley, C. A.; Beizai, K.; Vögtle, F. *Acc. Chem. Res.* **2001**, *34*, 465-476.
- (77) Bissell, R. A.; Cordova, E.; Kaifer, A. E.; Stoddart, J. F. *Nature* **1994**, *369*, 133-137.
- (78) Bruns, C. J.; Stoddart, J. F. *Acc. Chem. Res.* **2014**, *47*, 2186-2199.
- (79) Coutrot, F.; Romuald, C.; Busseron, E. *Org. Lett.* **2008**, *10*, 3741-3744.
- (80) Dawson, R. E.; Lincoln, S. F.; Easton, C. J. *Chem. Commun.* **2008**, 3980-3982.
- (81) Bruns, C. J.; Li, J.; Frasconi, M.; Schneebeli, S. T.; Lehl, J.; Jacquot de Rouville, H.-P.; Stupp, S. I.; Voth, G. A.; Stoddart, J. F. *Angew. Chem. Int. Ed.* **2014**, *53*, 1953-1958.
- (82) Ackermann, D.; Schmidt, T. L.; Hannam, J. S.; Purohit, C. S.; Heckel, A.; Famulok, M. *Nat. Nanotechnol.* **2010**, *5*, 436-442.
- (83) Rasched, G.; Ackermann, D.; Schmidt, T. L.; Broekmann, P.; Heckel, A.; Famulok, M. *Angew. Chem. Int. Ed.* **2008**, *47*, 967-970.
- (84) Mayer, G.; Ackermann, D.; Kuhn, N.; Famulok, M. *Angew. Chem.* **2008**, *120*, 985-987.
- (85) Ackermann, D.; Jester, S.-S.; Famulok, M. *Angew. Chem. Int. Ed.* **2012**, *51*, 6771-6775.
- (86) Shen, Z.; Yan, H.; Wang, T.; Seeman, N. C. *J. Am. Chem. Soc.* **2004**, *126*, 1666-1674.
- (87) Elbaz, J.; Wang, Z.-G.; Wang, F.; Willner, I. *Angew. Chem.* **2012**, *124*, 2399-2403.
- (88) Lu, C.-H.; Qi, X.-J.; Ceconello, A.; Jester, S.-S.; Famulok, M.; Willner, I. *Angew. Chem. Int. Ed.* **2014**, *53*, 7499-7503.
- (89) Ceconello, A.; Lu, C.-H.; Elbaz, J.; Willner, I. *Nano Lett.* **2013**, *13*, 6275-6280.
- (90) Schmidt, T. L.; Heckel, A. *Nano Lett.* **2011**, *11*, 1739-1742.
- (91) Ackermann, D.; Rasched, G.; Verma, S.; Schmidt, T. L.; Heckel, A.; Famulok, M. *Chem. Commun.* **2010**, *46*, 4154-4156.
- (92) Ackermann, D.; Famulok, M. *Nucleic Acids Res.* **2013**, *41*, 4729-4739.

- 
- (93) Koehler, R. T.; Peyret, N. *Bioinformatics* **2005**, *21*, 3333-3339.
- (94) SantaLucia, J. *Proc. Natl. Acad. Sci.* **1998**, *95*, 1460-1465.
- (95) Lohmann, F.; Ackermann, D.; Famulok, M. *J. Am. Chem. Soc.* **2012**, *134*, 11884-11887.
- (96) Vale, R. D. *Cell* **2003**, *112*, 467-480.
- (97) Lohmann, F.; Weigandt, J.; Valero, J.; Famulok, M. *Angew. Chem. Int. Ed.* **2014**, *53*, 10372-10376.
- (98) Lohmann, F.; Valero, J.; Famulok, M. *Chem. Commun.* **2014**, *50*, 6091-6093.
- (99) Li, T.; Lohmann, F.; Famulok, M. *Nat. Commun.* **2014**, *5*, 4940.
- (100) Wolters, O. *Diploma Thesis, University of Bonn*, **2012**.